Appendix B

Groundwater

B1 Water Quality
B2 Groundwater Model Report
B3 Geochemical Model Report
B4 Hollister Mine West Pit Shallow Groundwater Technical Memorandum

B1 Water Quality

Table B1-1 Nevada Water Quality Standards and Mine Wall Rock and Waste Rock Surface Area

Parameter[1] (mg/L)	Mine Wall Rock and Waste Rock Surface Area		Drinking Water Standards		Municipal or Domestic Supply	Drinking Water Standards		
	5.411 m^2/L	54.11 m^2/L	Primary	Secondary		Irrigation	Stock Water	Wildlife Propagation
Antimony	0.02222	0.1381	0.006	--		--	--	--
Arsenic	5.477×10^{-7}	4.100×10^{-6}	0.05	--	0.146	0.1	0.2	--
Barium	0.001997	6.134×10^{-4}	2.0	--	0.05	--	--	--
Beryllium	0.002037	0.01684	0.004	--	2.0	0.1	--	--
Boron	0.34651	2.516	--	--	0	0.75	5.0	--
Cadmium[3]	1.427×10^{-4}	0.001451	0.005	--	--	0.01	0.05	--
Chromium	0.2253	0.4303	0.1	--	0.005	0.1	1.0	--
Copper[3]	2.685×10^{-4}	2.880×10^{-4}	1.3	--	0.10	0.2	0.5	--
Iron	4.929×10^{-4}	5.948×10^{-4}	--	0.3 [0.6][5]	--	5.0	--	--
Lead[3]	9.402×10^{-7}	1.055×10^{-5}	0.05	--	--	5.0	0.1	--
Magnesium	0.004043	0.003428	--		0.05			
Manganese	3.004×10^{-8}	6.367×10^{-4}	--	0.05[0.1]	125/150	0.2	--	--
Mercury			0.002	--	--	--	0.01	--
Molybdenum			--	--	0.002			
Nickel[3]	0.02087	0.05370	0.1	--	--	0.2	--	--
Selenium	0.3231	0.08062	0.05	--	0.0134	0.002	0.05	--
Silver			0.05	--	0.05	--	--	--
Thallium	0.03141	0.3158	0.002	--	--	--	--	--
Zinc[3]	1.935×10^{-5}	0.05634	--	5.0	0.013	2.0	25.0	--
Cyanide (WAD)			--	--	--	--	--	--
Alkalinity			--	--	0.2	--		30-130
Chloride	30.17	75.12	--	250[400]	--	--	1,500	1,500
Color (PCU)			--	15	250[400]	--	--	--
Dissolved Oxygen			--	--	75	--	Aerobic	Aerobic
Fluoride	1.964	2.367	4.0	2.0	Aerobic	1.0	2.0	--
Nitrate as N	1.782	5.241	10	--	--	--	100	100
pH (SU)	10.24	10.32	--	6.5-8.5	10	4.5-9.0	5.0-9.0	7.0-9.2
Sulfate	1,602	2,277	--	250[500]	5.0-9.0	--	--	--

Table B1-1 Nevada Water Quality Standards and Mine Wall Rock and Waste Rock Surface Area

Parameter[1] (mg/L)	Mine Wall Rock and Waste Rock Surface Area		Drinking Water Standards		Municipal or Domestic Supply	Drinking Water Standards		
	5.411 m^2/L	54.11 m^2/L	Primary	Secondary		Irrigation	Stock Water	Wildlife Propagation
Temperature °C			--	--	250[500]	--	--	--
TDS	2,473	3,736	--	500[1,000]	--	--	3,000-7,000	--
TSS			--	--	500[1,000]	--	--	--
Turbidity (NTU)			--	--	--	--	--	--

[1] mg/L = milligrams per liter; PCU = photoelectric color units; SU = standard units; NTU = nephelometric turbidity units; TDS = total dissolved solids; TSS = total suspended solids; °C = degrees Celsius; WAD = weak acid dissociable.

[2] Dissolved fraction only.

[3] Parameter dependent on hardness; a hardness value of 175 mg/L was used to calculate the criteria for hardness-dependent metals in Maggie Creek and the Humboldt River.

[4] Numbers in brackets [ ] are mandatory secondary standards for public water systems.

[5] (w) refers to warm water and (c) is for cold water. No letter designation indicates criteria are common to both warm and cold water.

Source: Enchemica 2010; Nevada Administrative Code (NAC) 445.119; NAC 445A.144.

Table B1-2 Borehole Water Quality

Well ID	Unit Screened	Water Quality Summary	Comments
BH-1	Vinini	• TDS less than 500 mg/L • calcium-sodium Bicarbonate water • pH 7 – 8	
BH-2	Vinini	• TDS less than 500 mg/L • calcium-sodium bicarbonate water • pH 7 – 8	
BH-4	Vinini	• TDS less than 500 mg/L • calcium-sodium bicarbonate water • pH 7 – 8	
BH-7	Tertiary Volcanics	• TDS less than 200 mg/L • sulfate less than 100 mg/L • calcium-sodium bicarbonate water • pH 7 – 8	Background well: non-mineralized rock
BH-9	Tertiary Volcanics	• TDS less than 200 mg/L • sulfate less than 100 mg/L • calcium-sodium bicarbonate water • pH 7 – 8	Background well: non-mineralized rock
HP-1	Vinini	• TDS 250 mg/L • calcium-sodium bicarbonate water • pH 8.0 • arsenic 0.043 mg/L	Background well
HP-3	Tertiary Volcanics	• TDS 276 mg/L • calcium-sodium bicarbonate water • pH 7.4 • sulfate and bicarbonate less than 100 mg/L	Background well
HP-4	Vinini	• TDS 458 mg/L • calcium-magnesium sulfate water • pH 6.7 • sulfate 181 mg/L • arsenic 0.064 mg/L	Downgradient of West Pit
HP-5	Tertiary Fanglomerate	• TDS 256 mg/L • calcium-sodium bicarbonate water • pH 7.0 • sulfate less than 100 mg/L	Downgradient of West Pit
HP-6	Tertiary Volcanics	• TDS 304 mg/L • calcium-magnesium sulfate/bicarbonate water • pH 7.1 • sulfate 127 mg/L • bicarbonate 110 mg/L	Downgradient of West Pit

Table B1-2 Borehole Water Quality

Well ID	Unit Screened	Water Quality Summary	Comments
WW-0		• TDS 260 mg/L • calcium-sodium bicarbonate water • pH 7.9 • elevated iron and manganese	Background well: down gradient of West Pit
WW-1	Vinini	• TDS 300 – 400 mg/L • sulfate 140 – 160 mg/L • bicarbonate 60 – 50 mg/L • pH 6.5 – 8.0 • arsenic to 0.35 mg/L • iron to 180 mg/L with most in range of 1 – 7 mg/L	Downgradient of West Pit
WW-3	Tertiary Volcanics	• TDS 326 – 898 mg/L • sulfate 136 – 392 mg/L • calcium sulfate water • pH 6.8 – 7.6 • elevated iron	South of project
WW-4	Tertiary Volcanics and Vinini	• TDS 280 – 327 mg/L • calcium-sodium bicarbonate water • pH 7.6 – 8.1 • elevated iron and manganese • arsenic exceeds Nevada standards	Background well: upgradient of West Pit
WW-5	Tertiary Volcanics	• TDS 230 – 506 mg/L • sulfate 150 – 250 mg/L • pH 7.0 – 7.5 • arsenic .08 – .4 mg/L • iron 2 – 60 mg/L • manganese to 0.7 mg/L	
DGW-1R	Tertiary Volcanics	• TDS 11,000 – 15,000 mg/L • sulfate 5,5000 –10,000 mg/L • pH 3.5 • calcium-magnesium sulfate water • arsenic 2.0 – 4.5 mg/L • iron 750 – 1,150 mg/L • exceeds Nevada standards for aluminum, arsenic, cadmium, iron, manganese, nickel, thallium, zinc	
H6-224WW	Tertiary Volcanics	• TDS 800 – 1,100 mg/L • sulfate 500 – 900 mg/L • pH 4.0 – 6.7 • calcium-magnesium sulfate water • arsenic 0.053 – 0.067 mg/L • iron 1.45 – 17.9 mg/L • manganese 2.6 – 4.7 mg/L • fluoride to 2.5 mg/L	

Table B1-2 Borehole Water Quality

Well ID	Unit Screened	Water Quality Summary	Comments
H6-225WW	Tertiary Volcanics and Waste Rock	• TDS 1,000 – 1,300 mg/L • sulfate 380 – 480 mg/L • calcium-magnesium sulfate water • pH 5.5 – 6.5 • arsenic 0.16 – 1.72 mg/L • iron to 74 mg/L • manganese to 7.2 mg/L	
H6-226WW	Tertiary Volcanics	• TDS 690 – 1,100 mg/L • sulfate 270 – 720 mg/L • calcium-sodium-magnesium sulfate/bicarbonate water • pH 6.5 – 7.0 • mercury to 0.067 mg/L	
H6-227WW	Vinini	• TDS 8,000 – 12,000 mg/L • sulfate 5,300 – 10,000 mg/L • calcium-magnesium sulfate water • pH 2.6 – 2.8 • fluoride to 30 mg/L • aluminum 209 – 613 mg/L • arsenic .11 –.47 mg/L • iron 316 – 834 mg/L • manganese to 398 mg/L • thallium to 0.022 mg/L • mercury to 0.13 mg/L • exceedences of Nevada standards for copper, zinc, cadmium, and selenium	
H6-228WW	Waste Rock and Tertiary Volcanics	• TDS 1,000 – 5,400 mg/L • sulfate 1,000 – 3,800 mg/L • calcium-magnesium sulfate water • pH 6 – 8 • arsenic 0.05 – 0.62 • iron 1.2 – 8 1 mg/L • manganese 5.2 – 21.6 mg/L	
H6-229WW	Vinini	• TDS 31,000 – 39,000 mg/L • sulfate 20,000 – 28,000 mg/L • calcium-magnesium sulfate water • pH 2.9 • aluminum 1,950 – 2,470 mg/L • arsenic 0.34 – 0.84 mg/L • iron 2,930 – 3,650 mg/L • manganese 535 – 594 mg/L • exceeds Nevada standards for cadmium, nickel, selenium, thallium, and zinc	

Table B1-2 Borehole Water Quality

Well ID	Unit Screened	Water Quality Summary	Comments
H6-230WW	Waste Rock	• TDS 4,600 – 14,000 mg/L • sulfate 3,000 – 8,500 mg/L • calcium-magnesium sulfate water • pH 2.8 – 3.0 • aluminum 121 – 634 mg/L • arsenic 0.071 – 1.52 mg/L • iron 211 – 1,150 mg/L • manganese to 85 mg/L • exceeds Nevada standards for cadmium, nickel, and selenium	
H7-251WW	Tertiary Volcanics	• TDS 800 – 1,000 mg/L • sulfate 470 – 560 mg/L • calcium-magnesium/sodium sulfate water • pH 5.0 – 6.0 • arsenic 11.6 – 41 mg/L • iron 1.1 – 10 mg/L	
H7-252WW	Vinini	• TDS 5,900 – 8,200 mg/L • sulfate 5,600 – 7,500 mg/L • calcium-magnesium sulfate water • pH 2.8 – 3.7 • aluminum 260 – 436 mg/L • arsenic 0.17 – 0.309 mg/L • iron 220 – 604 mg/L • manganese 19 – 27 mg/L • exceeds Nevada standards for cadmium, nickel, and thallium	
H7-253WW	Vinini	• TDS 1,400 – 2,600 mg/L • sulfate 1,000 – 2,500 mg/L • calcium-magnesium sulfate water • pH 3.5 – 4.5 • aluminum to 130 mg/L • selenium to 0.17 mg/L	
H7-254WW	Vinini	• TDS 1,300 – 4,100 mg/L • sulfate 1,700 mg/L or greater • pH 2.8 – 4.1 • calcium-magnesium sulfate water • aluminum to 130 mg/L • arsenic 0.069 – 0.19 mg/L • iron 77 – 230 mg/L • manganese 6 – 60 mg/L • exceeds Nevada standard for cadmium, nickel, thallium, and mercury	

Table B1-2 Borehole Water Quality

Well ID	Unit Screened	Water Quality Summary	Comments
H7-255WW	Tertiary Volcanics	• TDS 310 – 450 mg/L • sulfate 120 – 195 mg/L • bicarbonate 130 – 160 mg/L • calcium-magnesium/sodium sulfate/bicarbonate water • pH 7.1 – 7.5 • arsenic 0.07 – 0.4 mg/L • iron 5.4 – 7.7 mg/L	Background well: sulfide rock
H7-256WW	Tertiary Volcanics	• TDS 260 – 380 mg/L • sulfate and bicarbonate less than 200 mg/L • calcium-sodium bicarbonate/sulfate water • pH 6.9 – 7.5 • arsenic 0.065 – 0.23 mg/L	Background well: sulfide rock
P-1	West Pit – in Tertiary Volcanics	• TDS 1,700 – 2,840 mg/L • sulfate 1,160 – 2,200 mg/L • fluoride 4.7 – 5.65 mg/L • calcium-magnesium sulfate water • pH 4.1 – 5.65 • aluminum 11 – 28 mg/L • arsenic 0.055 – 0.085 mg/L • iron 4.4 – 89 mg/L • manganese 9.4 – 12.6 mg/L • nickel 0.13 – 0.21 mg/L	
P-2	West Pit – in Tertiary Volcanics	• TDS 900 – 1,300 mg/L • sulfate 230 – 480 mg/L • calcium-sodium sulfate/bicarbonate water • pH 5.7 – 6.9 • iron 6.7 – 90 mg/L • mercury 0.021 – 0.062 mg/L	
HOL-MW-1	Tertiary Volcanics	• TDS 250 – 280 mg/L • calcium-sodium bicarbonate/sulfate water • bicarbonate and sulfate less than 100 mg/L • pH 7.2	Background well
W-E-1	Tertiary Volcanics	• TDS 380 – 530 • sodium bicarbonate/sulfate water • pH 6.4 – 7.5	
West Pond		• TDS 1,800 – 5,800 mg/L • sulfate 1,000 – 5,400 mg/L • calcium-magnesium sulfate water • pH 4.0 – 7.0	

Table B1-2 Borehole Water Quality

Well ID	Unit Screened	Water Quality Summary	Comments
MA-1 Seep		• TDS 1,100 – 1,360 mg/L • sulfate 410 – 619 mg/L • bicarbonate 180 – 239 mg/L • calcium-sodium sulfate/bicarbonate water • pH 7.7 – 8.2	

mg/L = milligrams per liter; TDS = total dissolved solids; TSS = total suspended solids.

Source: Brown and Caldwell 2003; Montgomery & Associates 2010a.

Table B1-3 MWMP Results (NDEP Profile I)

Rotating Extraction

Parameter Unit Standard	pH	Aluminum	Iron	Manganese	Arsenic	Antimony	Zinc	Copper
IH020 COMP	4.08	6.93	86.4	0.67	0.087	0.019	1.81	0.0249
IH209 (1016-26+1040-50)	3.93	27.4	40.8	9.95	0.233	0.011	3.12	0.369
IH157 (1016-1026)	6.42	0.146	0.066	0.103	0.037	0.034	0.0634	0.0096
IH208 (514-522)	4.18	32.6	18.2	0.411	-0.01	0.011	0.674	0.0292
IH208 (530-37, 547-56)	3.13	106	117	0.576	0.096	0.005	13	3.94
IH112 (308-318)	4.59	0.51	5.89	0.168	0.232	0.045	0.453	-0.003
IH059 (641-51, 651-61)	3.19	100	157	1.56	0.365	0.005	24.1	5.98
IH057 (528-538)	3.65	32.8	53.7	0.442	0.044	0.009	3.69	0.385
IH013 (700-710)	3.59	112	72.6	0.386	0.02	0.006	10.9	1.24
IH013 (690-700)	3.51	87.5	77.9	0.478	0.028	0.005	6.04	1.37
IH149 (128-138,181-186)	5.08	0.144	0.048	0.0053	0.013	0.003	0.0435	0.0084
IH149 198-206 OLD&NEW	6.21	0.193	0.249	0.0994	0.016	0.007	0.586	0.0528
IH070 695-705 OLD&NEW	5.75	-0.005	4.31	-0.0002	75	-0.005	-0.01	0.0577
IH083 587-596 OLD&NEW	5.75	0.343	0.00022	0.913	-0.04	0.037	0.01	210
IH083 596-605 OLD&NEW	3.35	70.7	148	0.0742	0.127	0.011	4.44	1.13

Column Extraction

Parameter Unit	pH	Aluminum	Iron	Manganese	Arsenic	Antimony	Zinc	Copper
PL-5	6.58	0.122	-0.02	-0.002	0.018	0.001	0.0059	-0.003
BH01 (740-)	4.33	1	2.44	1.57	0.024	0.006	0.116	0.113
BH01 (745-)	4.36	1.21	3.11	1.8	0.027	0.006	0.117	0.167
BH02 (650-)	3.19	2.91	6.51	1.9	0.056	0.003	1.2	0.915
BH02 (665-)	4.17	0.787	1.87	0.649	0.025	0.003	0.226	0.168
BH03	5.07	0.228	0.275	0.919	0.038	0.002	0.235	0.0555
BH04	4.52	0.646	5.63	3.88	0.014	-0.001	0.104	0.197
BH05	4.07	8.27	4.53	1.51	0.05	-0.002	1.91	0.656
BH06	5.72	0.937	0.032	0.392	0.039	0.027	0.141	0.0107
BH08 (945-)	6.34	-0.02	-0.02	1.74	-0.01	0.009	0.0137	0.0049
BH08 (950-)	6.21	-0.02	0.039	2.26	-0.01	0.012	0.0092	0.0048

Note: All parameters reported in milligrams per liter except pH, which is reported in standard units.
Source: Walker and Associates 2003.

Table B1-4 Modeled Aqueous Concentrations at the Project Boundary Using Initial Underground Workings Water

	Average Groundwater	Initial Underground Workings Water	Groundwater/ Underground Workings Water Mixture with Reaction	Groundwater/ Underground Workings Water Mixture with Reaction and Inorganic Carbon Diffusion	NDEP Profile I Reference Values
pH	7.96	10.24	8.37	7.91	6.5 to 8.5
log P_{CO2} (atm)	-3.13	-8.00	-3.91	-3.13	--
pe	-0.37	10.32	-4.18	-3.65	--
Eh (mvolts)	-21.65	610	-247	-216	--
Aluminum	0.050	0.216	0.0028	0.00096	0.2
Antimony	0.0094	0.0222	0.0132	0.0132	0.006
Arsenic	0.0121	5.48×10^{-7}	8.29×10^{-4}	0.0085	0.01
Barium	0.0830	0.00200	0.0100	0.0103	2.0
Beryllium	0.00	0.00204	0.00061	0.00061	0.004
Boron	0.11	0.346	0.177	0.177	--
Inorganic carbon[a]	69.8	1.49	32.8	68.5	--
Cadmium	0.00	1.43×10^{-4}	4.26×10^{-5}	4.26×10^{-5}	0.005
Calcium	25.0	639	197	208	--
Chloride	25.0	30.2	26.5	26.5	400
Chromium	0.00	0.225	8.97×10^{-5}	1.74×10^{-4}	0.1
Copper	0.00	2.68×10^{-4}	8.01×10^{-5}	8.01×10^{-5}	1
Fluoride	1.08	1.96	1.34	1.34	4
Iron	0.02	4.93×10^{-4}	1.10	1.10	0.6
Lead	0.00	9.40×10^{-7}	2.80×10^{-7}	2.80×10^{-7}	0.1
Magnesium	7.80	0.00404	5.48	5.48	150
Manganese	0.08	3.00×10^{-8}	0.056	0.056	0.1
Nickel	0.00	0.0209	0.0062	0.0062	0.1
Nitrogen	0.00	1.78	0.53	0.53	10
Potassium	2.53	43.5	14.7	14.7	--
Selenium	0.00	0.323	5.15×10^{-10}	1.46×10^{-9}	0.05
Silica	0.00	68.8	17.5	17.1	--
Sodium	30.0	56.8	38.0	38.0	--

Table B1-4 Modeled Aqueous Concentrations at the Project Boundary Using Initial Underground Workings Water

	Average Groundwater	Initial Underground Workings Water	Groundwater/ Underground Workings Water Mixture with Reaction	Groundwater/ Underground Workings Water Mixture with Reaction and Inorganic Carbon Diffusion	NDEP Profile I Reference Values
Sulfate	53.5	1,602	519	519	500
Sulfide	0.00	0.00	2.62×10^{-6}	6.76×10^{-7}	--
Thallium	0.0000	0.0314	0.0094	0.0094	0.002
Zinc	0.00	1.93×10^{-5}	5.77×10^{-6}	5.77×10^{-6}	5
TDS	215	2,446	854	901	1,000

[a] mg CO_3^{2-}/L

Notes:

All units mg/L unless otherwise noted
atm – atmospheres
mvolts – millivolts
TDS – total dissolved solids

Source: Brown and Caldwell 2012.

B2 Groundwater Model Report

FINAL

HOLLISTER MINE GROUNDWATER MODEL DEVELOPMENT AND DEWATERING SIMULATIONS

Prepared for

Rodeo Creek Gold Inc., Winnemucca, Nevada

October 28, 2010

FINAL

HOLLISTER MINE GROUNDWATER MODEL

Prepared for

Rodeo Creek Gold Inc., Winnemucca, Nevada

October 28, 2010

Brown AND Caldwell

3264 Goni Road, Suite 153

Carson City, NV, 89706-7925

TABLE OF CONTENTS

LIST OF FIGURES V

LIST OF TABLES VI

LIST OF ABBREVIATIONS VII

EXECUTIVE SUMMARY ES-1

1. INTRODUCTION 1-1
   1.1 Location 1-1
   1.2 Physical and Climatic Setting 1-2
   1.3 Project Background 1-2
   1.4 Project Approach 1-3

2. CONCEPTUAL MODEL 2-1
   2.1 Geologic Setting 2-1
   2.2 Conceptual Hydrogeologic Model 2-2

3. MODEL DEVELOPMENT 3-1
   3.1 Previous Groundwater Modeling 3-1
      3.1.1 Exploration Decline Modeling 3-1
      3.1.2 Drawdown Extents Modeling 3-1
   3.2 Screening-Level Model Development and Results 3-2
   3.3 Refined MODFLOW Model Development 3-2
      3.3.1 Approach 3-2
      3.3.2 Computer Code Description 3-4
      3.3.3 Units and Coordinate System 3-4
      3.3.4 Model Domain and Boundary Conditions 3-4
      3.3.5 Model Discretization and Layering 3-4
      3.3.6 Temporal Discretization and Initial Conditions 3-5
      3.3.7 Hydraulic Parameterization 3-5
      3.3.8 Wells and Mine Dewatering 3-6

4. MODEL CALIBRATION RESULTS AND SENSITIVITY ANALYSIS 4-1
   4.1 Calibration Approach 4-1
   4.2 Model Calibration 4-1
   4.3 Results 4-2
      4.3.1 Simulated Water Levels 4-2
      4.3.2 Simulated Water Budget 4-3
   4.4 Sensitivity Analysis 4-3

5. PREDICTIVE SIMULATIONS AND ANALYSIS 5-1
   5.1 Predictive Simulation Development 5-1
      5.1.1 Stress Periods and Initial Conditions 5-1

Use of contents on this sheet is subject to the limitations specified at the end of this document.

5.1.2 Simulated Dewatering 5-2
5.2 Results of Predictive Simulation 5-3
5.2.1 Predicted Drawdown and Cumulative Effects 5-3
5.2.2 Predicted Water Budget and Dewatering Rates 5-4
5.3 Water Level Recovery 5-5

6. NO ACTION ALTERNATIVE SIMULATION AND ANALYSIS 6-1
6.1 Development of No Action Alternative Simulation 6-1
6.2 Results of No Action Alternative Simulation 6-1

7. CONCLUSIONS 7-1

8. REFERENCES 8-1

FIGURES FIG-1

APPENDIX A: SUPPORTING GROUNDWATER MODEL INFORMATION ..... A

Use of contents on this sheet is subject to the limitations specified at the end of this document.
HollisterMineEIS_GWModelingReport_FINAL.docx

LIST OF FIGURES

Figure 1-1 Hollister Mine Location
Figure 1-2 Predicted Maximum Extent of the Cumulative 10-Foot Drawdown Contour from Carlin Trend Dewatering Operations
Figure 2-1 Location of the Little Antelope Creek Fault and the Hatter Graben
Figure 2-2 Cross-Section Showing Offset Across the Little Antelope Creek Fault
Figure 2-3 Hydrographs of Ordovician Vinini Aquifer and Tertiary Volcanoics Aquifer Monitor Wells
Figure 2-4 Locations of Ordovician Vinini Aquifer and Tertiary Volcanics Aquifer Monitor Wells
Figure 2-5 Regional Groundwater Elevation Contours
Figure 2-6 Tertiary Volcanics Aquifer Groundwater Elevation Contours
Figure 3-1 2002 Hydrogeologic Investigation Piezometer and Borehole Location Map
Figure 3-2 Model Domain and Boundary Conditions
Figure 3-3 Surface of Vinini Formation
Figure 3-4. Mine Workings with Theoretical Dewatering Locations
Figure 4-1 BH-01 Observed Versus Simulated Water Levels
Figure 4-2. BH-02 Observed Versus Simulated Water Levels
Figure 4-3 Steady-State Simulated Water Levels
Figure 4-4 Transient Water Levels – 2010
Figure 4-5 BH-01 Hydraulic Conductivity Sensitivity Plot
Figure 4-6 BH-02 Hydraulic Conductivity Sensitivity Plot
Figure 4-7 BH-01 Storage Values Sensitivity Plot
Figure 4-8 BH-02 Storage Values Sensitivity Plot
Figure 5-1 Drain Locations - Predictive Simulation
Figure 5-2 Simulated Maximum Extent of 10-Foot Drawdown (2070)
Figure 5-3 Hollister Mine Cross Sections - 2015
Figure 5-4 Hollister Mine Cross Sections - 2029
Figure 5-5 Hatter Expansion Area Cross Section - 2029, A-A'
Figure 5-6 Hatter Expansion Area Cross Section - 2029, B-B'
Figure 5-7 Simulated Water Level Drawdown and Recoveries
Figure 5-8 Simulated Mine Dewatering – Observed and Predicted Pumping Rates
Figure 5-9 Hollister Mine Workings Refilling Curve
Figure 5-10 Harter Expansion Area Refilling Curve
Figure 6-1 No Action Alternative Simulation - Maximum Extent of 10 Foot Drawdown (2020)
Figure 6-2 No Action Alternative Simulation - Hollister Mine Water Level Recovery

Use of contents on this sheet is subject to the limitations specified at the end of this document.
HollisterMineEIS_GWModelingReport_FINAL.docx

LIST OF TABLES

Table 3-1 Specifications of the Hollister Model 3-3
Table 4-1 Simulated Water budget....4-3
Table 5-1 Hollister Model Stress Period Setup 5-1
Table 5-2 Hollister Mine Drain Setup Schedule 5-2
Table 5-3 Simulated Water Budgets – Predictive Simulation....5-5
Table 5-4 Simulated Water Level Recovery Times 5-6

Use of contents on this sheet is subject to the limitations specified at the end of this document.

LIST OF ABBREVIATIONS

2-D	two-dimensional
3-D	three-dimensional
AFY	acre feet per year
amsl	above mean sea level
BLM	Bureau of Land Management
EIS	Environmental Impact Statement
ft/day	feet per day
GBG	Great Basin Gold
GHB	general head boundary condition
gpm	gallons per minute
HDB	Hollister Development Block
Hecla	Hecla Mining Company
RCG	Rodeo Creek Gold Inc.
RIB	rapid infiltration basin
USX	U.S. Steel Corporation

Use of contents on this sheet is subject to the limitations specified at the end of this document.

EXECUTIVE SUMMARY

The Hollister Mine Model (Hollister Model) and Final Hollister Mine Groundwater Modeling Report for Rodeo Creek Gold Inc. (RCG) has been prepared by Brown and Caldwell to document a numerical groundwater flow model developed to simulate mine dewatering and estimate the extent of groundwater drawdown that would result from current and future dewatering activities at the Hollister Mine and planned Hatter Expansion, which is sited approximately one mile to the east. RCG is in the process of permitting full-scale mining at the Hollister Mine, and the permitting process includes the preparation of an Environmental Impact Statement (EIS) by the United States Department of the Interior, Bureau of Land Management (BLM). Results of predictive groundwater flow model simulations are intended to support the EIS for the Hollister Mine.

Project Goals

As a part of the EIS process for permitting the Hollister Mine for full-scale production, groundwater modeling is required to estimate:

- the maximum areal extent of drawdown in the groundwater potentiometric surface resulting from dewatering of the Ordovician Vinini Formation-hosted aquifer;
- the timing of the occurrence of the maximum extent of drawdown;
- the post-mining rebound, or recovery, of the potentiometric surface;
- the relationship of the Hollister Mine-related groundwater drawdown to the hydrologic cumulative effects area created by major mine dewatering activities located to the southeast along the Carlin Trend; and
- future rates of groundwater pumping that will be necessary to achieve dewatered conditions in the underground workings.

Model simulations were used to compare the extent of the simulated 10-foot groundwater surface drawdown resulting from dewatering at the Hollister Mine with the cumulative drawdown prediction resulting from groundwater model simulations of combined dewatering efforts within the Carlin Trend by Barrick Goldstrike (BLM, 2008; Barrick, 2010). Additionally, a predictive simulation was performed for the Hollister Mine No Action Alternative scenario. This future scenario is defined as a continuation of underground test mining and exploration activities at current rates through the end of 2011, with groundwater recovery beginning in 2012.

Hydrogeologic Setting

The two hydrogeologic units of interest for development of the Hollister Mine are the 1) Vinini Formation and 2) overlying Tertiary volcanic rocks. The more permeable carbonate hydrogeologic units underlying the Vinini Formation are not included in this study because of the approximately 4,500-foot vertical separation between the planned lower-most extent of the Hollister Mine workings and the deeper carbonate units. The Vinini Formation is the unit that will be locally dewatered to accommodate subsurface mining activities at the Hollister Mine and Hatter Expansion. The shallower, Tertiary volcanic rock aquifer is separated from the Vinini in the vicinity of Hollister by low permeability clays, and hydrographs from monitor wells completed in both the Vinini Formation and the Tertiary volcanic rocks show that water levels have declined by up to 300 feet locally in the Vinini Formation as a result of dewatering at Hollister. Contrastingly, water levels in the Tertiary volcanic rocks have exhibited only minor seasonal fluctuation and no long-term changes.

Use of contents on this sheet is subject to the limitations specified at the end of this document.

Unconfined groundwater flow directions in the regional aquifer in the Vinini Formation have a resultant flow direction to the southwest in the Hollister area. This general direction of groundwater flow reflects the influence of a major regional recharge area along the Tuscarora Mountains located up-gradient, east and northeast, of Hollister (BLM, 2000a). The orientation of groundwater flow direction for the Tertiary aquifer differs from that of the regional aquifer, and is directed to the south-southeast. The absence of water level response in the Tertiary volcanic aquifer, despite significant dewatering in the Ordovician Vinini Formation in the vicinity of the Hollister Mine, combined with the divergent groundwater flow directions for both aquifers indicate that there is a general lack of hydraulic communication between the aquifers.

The hydrogeologic conceptualization, hydrogeologic data, and results from previous regional and local groundwater dewatering and drawdown modeling efforts and aquifer testing activities, were all used as a starting point in the development of the Hollister numerical groundwater model. A two-dimensional (2-D), simplified, screening-level model ("screening model") was developed using MODFLOW-2000 in order to assess the sufficiency of the model domain and any anticipated model boundary interference (Harbaugh et al., 2000). The screening model consists of a single layer composed of 750 rows by 740 columns with 100 foot by 100-foot spacings. The areal extent of the model domain totals approximately 200 square miles and was generally centered upon the Hollister Mine location.

Model Development

Initially, the simplified, two-dimensional screening model was set up to estimate regional groundwater gradients, elevations, and regional impact of 20 years (2010 to 2030) of ongoing and future mine dewatering and associated groundwater drawdown in the vicinity of the Hollister Mine. The results of this preliminary modeling were then used to refine the model domain extent, construction, and overall design for a more advanced and expanded flow model that is better suited to estimate impacts of proposed and future dewatering activities at the Hollister Mine and Hatter Expansion.

Following the review of the screening model results, a more sophisticated three-dimensional (3-D) numerical flow model ("Hollister Model") was constructed using MODFLOW-SURFACT to simulate previous mine dewatering activities and estimate future groundwater conditions and dewatering rates. The Hollister Model contains multiple aquifer layers bounded by three-dimensional surfaces (or geologic contacts), and it is primarily a tool to assess the regional impacts attributable solely to mine dewatering at the Hollister Mine and Hatter Expansion. It was not designed to reflect detailed hydrogeologic heterogeneity or to include other regional groundwater sources or sinks other than underflow within the Ordovician Vinini aquifer.

The full active model domain of the refined Hollister Model is approximately 590 square miles, is centered upon the location of the Hollister Mine workings, and extends approximately 11 miles away from the mine workings. Three active model layers represent the portions of the Vinini Formation at similar elevations to the various Hollister and Hatter mine workings. With the exception of a zone of low- permeability intrusive geologic features immediately east of the Hollister Mine, the Vinini Formation in the Hollister Model was simulated as a homogeneous medium with constant hydraulic properties.

Both steady-state and transient models were constructed and calibrated to reproduce past, observed groundwater conditions prior to performing predictive dewatering simulations to estimate future groundwater drawdown and recovery. In particular, the model was calibrated to adequately match water level measurements and declines observed at monitor well locations BH-01 and BH-02. The steady-state model generally approximates groundwater conditions in March 2005, prior to dewatering activities at the Hollister Mine. The transient model simulates dewatering activities at the Hollister Mine from March 2005 through December 2009, and total dewatering pumping was based upon recorded, historical inflow volumes to the mine decline. Simulated dewatering proceeded at the recorded locations, elevations, and rate of advance of the mine workings. The model-simulated water levels and water budget for the local Vinini Formation aquifer both matched observed and interpreted local and regional groundwater conditions by the end of 2009.

Use of contents on this sheet is subject to the limitations specified at the end of this document.
HollisterMineEIS_GWModelingReport_FINAL.docx

Additionally, a sensitivity analysis for the primary model inputs demonstrated the robustness of the model calibration and supported the estimated aquifer hydraulic parameters developed during model calibration.

Predictive Simulation

Following the successful calibration of the Hollister model, a predictive simulation was developed to estimate future groundwater drawdown and recovery associated with past and planned dewatering at the Hollister Mine and Hatter Expansion, per the project goals listed above. The predictive model simulation time period begins in January 2010 and continues through the year 2250. Future dewatering rates were estimated by the model based upon the specified elevations of planned future active mining activities and the calibrated model hydraulic parameters. Future water levels were allowed to decline to the prescribed elevations of future mine workings at both the Hollister Mine and Hatter Expansion coincident with the time when it is anticipated that they will be excavated and advanced. When mining and dewatering activities were anticipated to be complete in a given area, simulated dewatering pumping was turned off for that particular portion of the various mine workings.

Results

After completion of the predictive simulation, estimated future water levels, drawdown, dewatering rates, model water budgets, and water level recoveries were assessed at no greater than 10-year intervals. The simulated 10-foot drawdown was also superimposed upon the estimated maximum extent of cumulative dewatering impacts from the Barrick Goldstrike model (BLM, 2000b).

The simulated maximum extent of 10-foot drawdown that is attributable to past, current, and future dewatering activities at the Hollister Mine and Hatter Expansion has a radial extent of approximately 8 miles in every direction around the Hollister site and Hatter Expansion. The low conductivity intrusive zone, while significant to predicted drawdown and anticipated dewatering rates at the local scale of current and planned mine workings, did not significantly affect the shape or extent of the 10-foot contour. The maximum extent of 10-foot drawdown is predicted to occur in approximately 2070, or approximately 40 years after the cessation of dewatering at the Hollister Mine and Hatter Expansion. The estimated maximum extent of the 10-foot drawdown contour resulting from Hollister Mine and Hatter Extension overlaps the maximum extent of the cumulative 10-foot drawdown contour for pumping within the Carlin Trend by a maximum distance of approximately six miles directly southeast of the Hollister Mine.

Although the maximum 10-foot contours overlap, dewatering at mines in the Carlin Trend southeast of the Hollister Mine occurs primarily in the carbonate aquifer beneath the Vinini Formation. Elsewhere in the Carlin Trend, water levels in low permeability units overlying the deeper carbonates have declined at a lower rate or have remained relatively constant (Maurer, et. al, 1996); therefore, water level declines indicated by the Barrick groundwater model may be expressed at lesser magnitudes in the overlying, less permeable Vinini Formation. This indicated low level of communication between the Vinini Formation and underlying carbonate aquifer implies that the maximum extent of 10-foot drawdown predicted by the Hollister Model may not be directly summed with the drawdown from the Barrick Model to produce a revised cumulative extent of maximum impact.

The overall simulated water budget for the predictive simulation increased by approximately 300 AFY (or 190 gpm) from 2010 to 2030, in response to an estimated increase in dewatering pumping from approximately 420 gpm in 2010 to approximately 610 gpm by the planned end of mining activities in 2030. Additionally, by 2110, the total simulated water budget is within approximately 60 AFY of that for the steady-state simulation, indicating that regional groundwater flow conditions are no longer significantly influenced by dewatering at the Hollister Mine and Hatter Expansion. During the predictive simulation, estimated future average annual dewatering rates vary substantially in magnitude in response to mining activities and are almost always greater than those previously observed. This trend is due to the greater depth of additional mining at the Hollister

Use of contents on this sheet is subject to the limitations specified at the end of this document.
HollisterMineEIS_GWModelingReport_FINAL.docx

Mine and additional deep mining activities at the Hatter Expansion. Overall, future annualized dewatering estimates for full scale mining activities range from approximately 450 gpm to over 1,100 gpm; however, beyond year 2020, in response to an anticipated consistent, active mine working elevation at Hatter, estimated dewatering rates asymptotically decline and ultimately approach 600 gpm. These future dewatering estimates are dependent upon current understanding of hydrogeologic conditions at depth at both the Hollister and Hatter Expansion locations and are simulated using numerical, passive drain boundary conditions. Due to local variations in hydrogeologic conditions, lithology, and required dewatering techniques, actual pumping and dewatering rates may vary depending upon conditions encountered in the field.

Simulated Water level declines reach the planned depths of mine workings at the appropriate future times for both sites. The minimum, simulated water level elevation in the future is approximately 4,000 feet amsl and occurs at the Hatter Expansion by the year 2019, when the planned, maximum mine depth is reached. This corresponds to a maximum simulated drawdown of approximately 1,420 feet at Hatter. When simulated mine dewatering ceases in 2030, water levels rapidly recover and rebound and come within 100 feet of pre-dewatering conditions by 2050. The timing of water level recoveries for 95 percent and 99 percent of the total maximum simulated drawdown were evaluated. For the Hollister Mine, 95 percent and 99 percent water level recovery is estimated to occur at a maximum of approximately 40 and 130 years after the cessation of mining in 2030. For the Hatter Expansion, the same recovery percentages were met 35 and 88 years after the cessation of mining activities.

Modeling of future potential groundwater conditions under the No Action Alternative scenario was also performed. The No Action Alternative is defined as a continuation of underground test mining and exploration activities at current rates through the end of 2011, with groundwater recovery beginning in 2012. A predictive simulation of the No Action Alternative scenario with the Hollister Mine groundwater model estimates that the maximum extent of the 10-foot drawdown contour will extend radially approximately 2 to 2.5 miles from the Hollister Mine, with the maximum extent of impact occurring approximately between the years 2020 and 2025. Water levels rapidly rise following the simulated cessation of mining activities at the Hollister Mine, and are estimated to recover to 95 percent and 99 percent of pre-mining conditions by approximately 2023 and 2034, respectively.

Use of contents on this sheet is subject to the limitations specified at the end of this document.
HollisterMineEIS_GWModelingReport_FINAL.docx

1. INTRODUCTION

Brown and Caldwell has prepared this Final Hollister Mine Groundwater Modeling Report for Rodeo Creek Gold Inc. (RCG) to document a numerical groundwater flow model developed to simulate mine dewatering and estimate the extent of groundwater drawdown that would result from current and future dewatering activities at the Hollister Mine and planned Hatter Expansion area of the Hollister Mine, which would be connected via an underground drift to the Hollister Mine workings and is sited approximately one mile to the east. The Hollister Mine is an underground gold exploration and test mining operation that is operating under an exploration permit, which allows for underground exploration and a small amount of production per year for test mining purposes. RCG is in the process of permitting full-scale mining at the Hollister Mine. The permitting process for the Hollister Mine includes the preparation of an Environmental Impact Statement (EIS) by the United States Department of the Interior, Bureau of Land Management (BLM). Results of predictive groundwater model simulations presented in this report are intended to support the EIS for the Hollister Mine.

As a part of the EIS process for permitting the Hollister Mine for full-scale production, groundwater modeling is required to estimate:

- the maximum areal extent of drawdown in the groundwater potentiometric surface resulting from dewatering;
- the timing of the occurrence of the maximum extent of drawdown;
- the post-mining rebound, or recovery, of the potentiometric surface; and
- the relationship of the Hollister Mine-related groundwater drawdown to the hydrologic cumulative effects area created by major mine dewatering activities located to the southeast along the Carlin Trend.
- future rates of groundwater pumping that will be necessary to achieve dewatered conditions in the underground workings.

The remainder of Section 1 describes the location, physical and climatic setting, and background of the Hollister Mine. Section 2 presents the hydrogeologic conceptual model of the Hollister Mine and surrounding areas. Section 3 presents the model development, including the modeling approach, model domain and boundary conditions, and hydraulic parameterization. Section 4 presents the model calibration to observed groundwater conditions and sensitivity analyses of model parameters. Section 5 presents the predictive simulations, results, and analyses, including the cumulative effects assessment. Section 6 presents predictive simulations for the No Action Alternative. Section 7 presents conclusions. Section 8 presents cited references.

1.1 Location

The Hollister Mine is located in north-central Nevada, within Elko County and Section 4 of Township 37 North, Range 48 East, MDB&M (Figure 1-1). The Hollister Mine is approximately 38 miles northeast of the town of Battle Mountain and can be reached from Interstate 80 in Battle Mountain by way of the Silver Cloud Road, or by the Dunphy Road exit to the east. Year-round access is from State Route 18, which can be reached from the Golconda exit on Interstate 80 (approximately 61 miles to the intersection with the Ivanhoe Access Road, and then approximately 10 miles southeast to the Project site).

Use of contents on this sheet is subject to the limitations specified at the end of this document.
HollisterMineEIS_GWModelingReport_FINAL.docx

1.2 Physical and Climatic Setting

The Hollister Mine is located in the Butte Creek Range within the northern Great Basin, part of the Basin-and-Range physiographic province. Elevations in the Butte Creek Range, on the western flank of the Tuscarora Mountains, approach 7,000 feet above mean sea level (amsl) and in the vicinity of the Hollister Mine vary from 5,500 to 5,900 feet amsl. The Butte Creek Range is bounded on the north by Willow Creek, and on the south by Antelope Creek. Little Antelope Creek, a tributary of Antelope Creek, is located east and south of the Project site. These creeks are within the Humboldt River drainage basin.

The site elevation and location results in a wide range of daily and seasonal temperatures, typical of the high desert climate within the northern Great Basin. High temperatures occur in late July and early August, and the coldest temperatures typically occur in January. Measured temperatures from nearby weather stations in Elko and Beowawe range from 104°F in the summer to -38°F in the winter (BLM, 1988).

The average annual precipitation in the region is about 10 inches, as a combination of snow during the winter months and rain in the late spring (May and June) and during summer thunderstorms. Pan evaporation, as measured at the Beowawe weather station, averages 44 inches per year.

1.3 Project Background

U.S. Steel Corporation (USX) initially explored the Hollister Mine area in the 1980's. Cornucopia Resources purchased what was then called the Ivanhoe property from USX in 1987, and teamed with Galactic Resources to permit and mine by open pit methods an epithermal oxide ore body hosted by Tertiary volcanic rocks. The first gold from the open pit mining operation was poured in 1990. Two pits were developed during this operation, known as the West and East Pits. Hollister Mine operations infrastructure facilities, including the portal for the exploration decline, are located within the East Pit.

Newmont purchased the majority share of the property in 1992, and subsequently determined that the open pit resource was mined out. However, Newmont continued heap leaching operations of the mined ore through 1997.

Great Basin Gold Limited (GBG) acquired Newmont's interest in the 504 claims of the Ivanhoe/Hollister claim block in 1998. GBG conducted several years of surface-based exploration for precious metal-bearing vein deposits hosted by the Ordovician Vinini Formation, which unconformably underlies the Tertiary volcanic rocks. Because of the narrow vein character of the mineralization and the depth to the deposit, exploration from underground workings was eventually determined to be the best method for delineating the deposit and determining its viability for full-scale production. GBG formed a joint venture with Hecla Mining Company (Hecla) known as Hecla Ventures, Inc. to facilitate underground exploration within a subset of the Ivanhoe/Hollister claims known as the Hollister Development Block (HDB).

Underground exploration of the HDB began with the driving of an exploration decline in 2004 from the East Pit area of the previously-mined open pit operations. After five years of site development, Hecla opted out of the agreement in 2007. GBG subsequently formed RCG as a wholly owned subsidiary to continue development of the Hollister Mine.

Inflows of groundwater to the exploration decline first occurred in March 2005 (at approximately five gallons per minute [gpm]) as the underground workings progressed below the water table. The inflow rate increased as the exploration decline progressed to deeper levels, and current inflow rates average approximately 450 gpm. These passive inflows to the underground mine workings are collected in underground sumps, and pumped to surface de-silting facilities before discharge to three rapid infiltration basins (RIBs) located approximately 4-1/2 miles south of the Hollister Mine.

Use of contents on this sheet is subject to the limitations specified at the end of this document.
HollisterMineEIS_GWModelingReport_FINAL.docx

Active dewatering using underground wells is planned for the Hollister Mine to allow mining to greater depths. Groundwater produced by these wells will remain separate from mine water (i.e., passive inflows), and will be pumped to the surface via a dedicated pipeline where it will be discharged to Little Antelope Creek or some alternative disposal method. RCG anticipates active mine dewatering for the duration of the approximate 20-year mine life (S. Godden & Associates, 2009; RCG, 2009a).

Other mining operations along the Carlin Trend to the southeast of the Hollister Mine produce gold from carbonate rock formations that underlie the Ordovician host rock at the Hollister Mine. The regional aquifer within the carbonate formations is far more transmissive than the ore-hosting formation at the Hollister Mine, resulting in much larger mine dewatering rates. Combined Barrick and Newmont dewatering rates along the Carlin Trend change with time as operations are modified, but have been reported to be in excess of 115,000 gpm (BLM, 2000a).

1.4 Project Approach

The primary objective of the groundwater flow modeling for the Hollister Mine is to provide an estimate of the areal extent, magnitude, and timing of drawdown in the Ordovician Vinini Formation-hosted aquifer resulting from the dewatering of the underground mine workings of the Hollister Mine, including the Hatter Expansion area. Other objectives include providing an updated estimate of the rate of groundwater pumping that will be necessary to achieve dewatered conditions in the underground workings for safe and efficient mining.

Model simulations were used to compare the extent of the simulated 10-foot groundwater surface drawdown resulting from dewatering at the Hollister Mine with the cumulative drawdown prediction resulting from combined dewatering efforts within the Carlin Trend. The cumulative drawdown predictions are provided by Barrick Goldstrike (Barrick, 2010) from groundwater modeling results conducted by Barrick Goldstrike for the *Betze Pit Expansion Project Draft Supplemental Environmental Impact Statement* (BLM, 2008). The extent of the 10-foot drawdown contour presented in the *Betze Pit Expansion Project Draft Environmental Impact Statement* is presented on Figure 1-2 and represents the cumulative impacts area (CIA) relative to groundwater for the combined dewatering efforts within the Carlin Trend, excluding planned efforts at the Hollister Mine.

Use of contents on this sheet is subject to the limitations specified at the end of this document.
HollisterMineEIS_GWModelingReport_FINAL.docx

2. CONCEPTUAL MODEL

2.1 Geologic Setting

The gold-bearing vein deposits of the Hollister Mine and the adjacent Hatter Expansion area are hosted in the Ordovician Vinini Formation, which comprises repeating, coarsening-upwards sequences of orthoquartzite, muddy quartzite, siltite and bedded to laminated argillite (RCG, 2009a). The Vinini Formation sediments have undergone a very low grade metamorphism to sub-greenschist facies, and in the Hatter Expansion area the Vinini Formation has been hornfelsed by the heat of one or both of two Tertiary intrusive bodies. Hornfelsing has changed the character of the Vinini Formation argillites to a hard rock that exhibits brittle deformation (RCG, 2009b).

Vinini Formation rocks overlie younger Devonian rocks of the Rodeo Creek Formation as a result of compressional tectonic forces associated with the Late Devonian to Early Missippian Antler Orogeny, which caused large-scale, eastward thrusting of western-facies eugeoclinal (siliciclastic) rocks, including the Vinini Formation, over eastern facies miogeoclinal units (shelf carbonates) along the Roberts Mountains thrust fault system. Lithologic data from a deep borehole completed in the Hollister Mine area indicate that the Roberts Mountain Thrust, and therefore the lower contact of the Vinini Formation, is approximately 6,500 feet below the surface (RCG, 2010a).

The Rodeo Creek Formation underlies the Vinini Formation and comprises a thick sequence of sedimentary rocks consisting of interbedded mudstones, quartzites and muddy carbonates. Underlying the Rodeo Creek Formation are later Silurian/early Devonian Popovich Formation and/or Roberts Mountains Formation carbonates (S. Godden & Associates, 2009).

The Vinini Formation is unconformably overlain by a succession of Tertiary volcanic rocks that range in thickness from 200 to 600 feet thick in the Hollister Mine/Hatter Expansion area. Widespread Tertiary volcanic activity began in the region approximately 43 to 41 million years ago (Ma), during the late Eocene epoch, when ash flow tuffs and lacustrine deposits were laid down on the Paleozoic and Mesozoic basement rocks. In the area of the Hollister Mine and Hatter Expansion, clays and re-worked quartzite characterize the contact between the Vinini Formation and the Tertiary volcanic units (HSI, 1989). Zones of re-worked quartzite ("fanglomerate") are discontinuous at the contact and vary in thickness between two and 50 feet, generally thinning to the west (HCI, 1997).

Regional-scale plutonic activity occurred across the entire Great Basin of Nevada, from the Late Triassic to the Cretaceous. Most of the intrusive bodies are intermediate in composition and tend to be stock size, although dykes and sills of this age are also common. Many of the intrusive bodies have a strong spatial, if not genetic, relationship to several of the region's precious metal districts and deposits (S. Godden & Associates, 2009). A small, altered, multi-phase rhyodacite to granodiorite pluton was emplaced into Paleozoic sedimentary rocks in the eastern portion of the Hollister Mine and Hatter Expansion area at about 39 Ma. The pluton, known informally as the Hatter stock, is one of many intrusive bodies along the northwest-trending Carlin trend (Wallace, 2003). Several other intrusive bodies are present in the Hatter Expansion area, indicated by borehole lithologic data and geophysical surveys (RCG 2010a).

Abundant high-angle faults cut the Tertiary volcanic and sedimentary rocks (Wallace, 2003). The principal orientations are north-northwest, north-northeast, and east-northeast. Movement along the faults was

Use of contents on this sheet is subject to the limitations specified at the end of this document.
HollisterMineEIS_GWModelingReport_FINAL.docx

normal, and offset along individual faults is less than 100 meters (330 feet) and more commonly less than 50 meters (150 feet).

Four sets of faults have dissected stratigraphy at Hollister. A group of near-vertical faults and fissures that trend west-northwest to east-west host the deeper epithermal gold veins found in the Vinini Formation at the Hollister Mine. The amount of displacement across these faults is small and their strike continuity varies between 30 meters and over a thousand meters (one hundred to several thousand feet). Most of the structures are pre-Tertiary in age. Few of these structures appear to penetrate the lower section of Tertiary volcanic rocks. A second set of faults, that trend northwest to southeast, intersect Tertiary volcanic rocks and mineralized veins at depth. A third group of faults trends north-northwest to south-southeast; this group of faults may be related to a regional "Basin and Range" trend. The youngest set of faults trends northeast to southwest (Wallace, 2003). The offsets observed in these faults (in underground workings) are approximately 45 to 60 meters (150 to 200 feet) with downthrows to the northwest with possibly left-lateral movements (RCG, 2010b).

A northeast to southwest fault, known as the Little Antelope Creek Fault, lies between the Hollister Mine and the Hatter Expansion area (Figure 2-1). Exploration boreholes that have penetrated the Little Antelope Creek Fault indicate that rocks in the structural zone are a mixture of shattered areas and ductile deformation areas (RCG, 2009b), and as such are not anticipated to significantly influence groundwater flow. A graben, known as the Hatter Graben, is formed on the east side of the structure (Figure 2-2) where the stratigraphic sequence is down-dropped by at least 200 feet (possibly as much as 500 feet).

Mineralization at the Hollister Mine consists of epithermal banded quartz veins with electrum and silver selenides (Goldstrand and Schmidt, 2000). Veins in the Hatter Expansion area occur in a wide east-west trending structural zone containing several sub-parallel bonanza-grade veins similar to the vein systems within the adjacent Hollister Mine area.

2.2 Conceptual Hydrogeologic Model

The two hydrogeologic units of interest for development of the Hollister Mine and the Hatter Expansion are the Vinini Formation and Tertiary volcanic rocks. The more transmissive carbonate hydrogeologic units, described in Sections 1.3 and 2.1, are not included in the conceptual hydrogeologic model because of the approximately 4,500-foot vertical separation between the planned lower-most extent of the Hollister Mine workings and the Roberts Mountain Thrust, which separates the Vinini Formation from these deeper carbonate units.

The Vinini Formation forms a part of the regional aquifer, and is the unit that will be locally dewatered to accommodate subsurface mining activities at the Hollister Mine. An overlying, shallow aquifer within the Tertiary volcanic rocks is separated from the regional aquifer in the Vinini Formation in the vicinity of Hollister by an aquitard consisting of clays found at the unconformity between the Vinini Formation and the Tertiary volcanic rocks. Hydrographs from monitor wells completed in both the Vinini Formation and the Tertiary volcanic rocks, presented on Figure 2-3, show that water levels have declined by up to 300 feet locally in the Vinini Formation as a result of dewatering at Hollister, whereas water levels in the Tertiary volcanic rocks have exhibited only minor seasonal fluctuation and no long-term changes. The locations of these monitor wells are presented on Figure 2-4.

Groundwater flow directions in the regional aquifer are presented on Figure 2-5, reproduced from the cumulative impact analysis conducted by the BLM (2000a) for large-scale mine dewatering operations conducted by Newmont and Barrick along the Carlin Trend. This map is based on 1990-1991 unconfined groundwater conditions, and depicts a resultant flow direction to the southwest in the Hollister area. This general direction of groundwater flow reflects the influence of a major regional recharge area along the

Use of contents on this sheet is subject to the limitations specified at the end of this document.
HollisterMineEIS_GWModelingReport_FINAL.docx

Tuscarora Mountains located up-gradient, east and northeast, of the Hollister Mine/Hatter Expansion area (BLM, 2000a). Areal recharge of the regional aquifer in the Vinini Formation may also occur in areas where hydrogeologic conditions allow (i.e., where downward flow is not impeded by aquitards). However, areal recharge is not considered in the numerical groundwater model presented in this report.

Groundwater flow directions in the Tertiary volcanic aquifer at the Hollister Mine are to the south-southeast (Figure 2-6). The orientation of groundwater flow direction for the Tertiary aquifer differs from that of the regional aquifer (Figure 2-5) due primarily to local topographic influences on groundwater flow. Big Butte, located approximately two miles north-northwest of Hollister at an elevation of 6,890 feet amsl, is the major topographic high in the Hollister area, and groundwater flow directions in the volcanic and overlying unconsolidated rocks emanate from it (Brown and Caldwell, 2003). The absence of water level response in the Tertiary volcanic aquifer, despite significant dewatering in the Ordovician Vinini Formation in the vicinity of the Hollister Mine, combined with the divergent groundwater flow directions for both aquifers indicate that there is a general lack of hydraulic communication between the aquifers.

Observations of inflows to the exploration decline and laterals indicate that lithology is a major influence on groundwater movement within the Vinini Formation (RCG, 2007). Most of the groundwater flow through the Hollister underground workings occurs in fractures or along bedding planes of the quartzites of the Vinini Formation; however, large-scale open fractures have not been observed. The argillites, siltstones and mudstones within the Vinini Formation display a very low permeability, evidenced by the very limited groundwater inflow to segments of underground development completed within these lithologic types (RCG, 2007).

Geologic structures that may act as hydraulic barriers within the Vinini Formation aquifer have not been identified. A constant-rate aquifer test of water supply WW-4 (Figure 2-6) was halted when the water level in the well fell abruptly approximately 1,000 minutes into the test (HSI, 1989). This sudden decline in water level would suggest either the dewatering of a fracture system or that the drawdown cone from WW-4 encountered a low-permeability region or a low-permeability fault (i.e., aquifer boundary condition). However, a sudden decrease in inflows to the underground mine workings has not been observed, suggesting that the observed water level decline during the constant-rate aquifer test of WW-4 was related to fracture dewatering. The mixture of shattered areas and ductile deformation areas observed in the Little Antelope Creek Fault (see Section 2.1) together with the absence of sudden decreases in inflows to the underground mine workings indicate that this fault zone has little effect on groundwater flow between the Hollister Mine and the Hatter Expansion area.

Hydraulic conductivity values for the Vinini Formation in the Hollister vicinity have previously been estimated from two constant-discharge aquifer tests (aquifer tests) conducted in two water supply wells (HSI, 1989) and from air lift aquifer testing conducted as part of the hydrogeologic investigation of the mine site (Brown and Caldwell, 2003). An aquifer test conducted in WW-1 (Figure 2-6) yielded an estimated hydraulic conductivity of 0.10 feet per day (ft/d), and an aquifer test conducted in WW-4 yielded an estimated hydraulic conductivity of 0.11 ft/d. The airlift aquifer testing yielded estimated hydraulic conductivity values ranging from 0.002 ft/d to 2.4 ft/d.

The aquifer test at WW-4 yielded an estimated aquifer storativity of 0.008 (HSI, 1989). This value is comparable with the range of confined storativity of 0.0001 to 0.004 for marine clastic rocks above the Roberts Mountain Thrust, which would include the Vinini Formation, presented in BLM (2000b).

The hydrogeologic conceptualization, geologic data, hydraulic parameters derived from previous aquifer testing, as well as from the previous cumulative effects groundwater modeling conducted by Barrick, were all used in the development of the Hollister numerical groundwater model, as discussed in the following sections.

Use of contents on this sheet is subject to the limitations specified at the end of this document.
HollisterMineEIS_GWModelingReport_FINAL.docx

3. MODEL DEVELOPMENT

3.1 Previous Groundwater Modeling

Several groundwater modeling efforts have been previously performed for the Hollister Mine site to estimate likely passive groundwater inflows to the mine as well as potential regional drawdown. The data used in the simplified, precursor modeling, as well as the model results, were used as a starting point in the development of the updated Hollister Mine model. Two of these modeling efforts are discussed below.

3.1.1 Exploration Decline Modeling

Groundwater modeling for the Hollister Mine was first conducted in 2003 to estimate the passive groundwater inflow to a then-proposed exploration decline, and the results were presented in the *Hydrogeologic Report for the Hollister Development Block, Revision I* (Brown and Caldwell, 2003). A spreadsheet model was used for this initial modeling effort. The spreadsheet model utilized aquifer hydraulic data generated from airlift recovery aquifer testing of four boreholes (Figure 3-1) that were part of a hydrogeologic investigation conducted to support permitting of the exploration decline. The equation upon which the spreadsheet modeling was based considered the rate of mining, the depth of the decline below the initial potentiometric surface, the hydraulic conductivity of the geologic unit being penetrated, the specific yield of the aquifer, and time. Although hydraulic conductivity estimates and water levels were available from site data, specific yield was estimated from tests conducted in the same geologic unit at the Turquoise Ridge Mine, located approximately 35 miles west of the Hollister Mine.

Hydraulic conductivity estimates from the airlift recovery aquifer testing ranged from 0.002 ft/d to 2.4 ft/d. Two hydraulic conductivity values were assumed for the spreadsheet model; 0.1 ft/d for decline segments distal from the targeted mineralized veins, and 1.12 ft/d for decline segments proximal to the veins. A specific yield value of 0.01 was used to model all decline segments.

Maximum model-estimated inflow rates to the decline ranged from 335 gpm to 385 gpm, for mining rates of 15 ft/d and 20 ft/d, respectively. The predicted inflow rates compared very favorably with the observed inflow rates.

3.1.2 Drawdown Extents Modeling

An analytic element groundwater flow model was developed to estimate the likely extent of aquifer drawdown created by the pumping of passive inflows into the decline during the initial underground exploration effort (Brown and Caldwell, 2003). The analytic element model was used to simulate the decline as a well located at the site of borehole BH-04 (Figure 3-1) drilled for the hydrogeologic investigation, with groundwater extraction equal to the estimated maximum inflow rate of 385 gpm (i.e., the predicted inflow rate from the spreadsheet model) for a period of 300 days. Aquifer parameters for the analytic element model were set at the same values as those used for the inflow calculations, with the addition of a northeast to southwest hydraulic gradient of 0.01. The model considered drawdown in the Vinini Formation only, which is consistent with evidence that an overlying shallow aquifer hosted in tuffaceous Tertiary volcanic rocks is not hydraulically connected with the Vinini-hosted aquifer. The model simulation indicated that the 10-foot drawdown contour would have an approximate radius of 4,500 feet.

Use of contents on this sheet is subject to the limitations specified at the end of this document.
HollisterMineEIS_GWModelingReport_FINAL.docx

3.2 Screening-Level Model Development and Results

A two-dimensional (2-D), simplified, screening-level model ("screening model") was developed using MODFLOW-2000 to assess the sufficiency of the model domain and any anticipated model boundary interference (Harbaugh et al., 2000). The screening model consists of a single layer composed of 750 rows by 740 columns with 100 foot by 100 foot spacings. The areal extent of the model domain totals approximately 200 square miles and was generally centered up on the Hollister Mine location. Constant head boundary condition cells were used to represent underflow coming into the model from the northeast as well as the underflow leaving the model to the southwest. The constant head values representing inflow to the model were set at a uniform elevation of 5,650 ft amsl, and the constant heads representing outflow were set to a uniform elevation of 4,800 ft amsl. These head values were based upon a review of regional water levels presented by the BLM (2000a). The top elevation of the model represents the approximate upper contact of the Vinini Formation in the vicinity of the mine workings, at an elevation of approximately 5,420 ft amsl. The bottom elevation was set at a uniform elevation of 3,700 ft amsl to ensure that the model had sufficient thickness to adequately represent the full depth of planned mine dewatering. The resultant thickness of Vinini Formation included in the screening model was approximately 1,720 feet. All hydraulic parameters were assumed homogeneous and isotropic, with hydraulic conductivity set at 0.08 ft/day, storativity (or storage coefficient) set at 0.008, and specific yield set to 0.01 percent. The magnitudes of these parameters were based upon calibrated values from previously analytical element dewatering modeling as well as interpretations from local aquifer testing.

The model was set up as a combined steady state/transient model with the first stress period set to produce a steady state solution that was calibrated to approximate regional groundwater gradients and elevations prior to simulating dewatering. The second stress period was set to produce a transient solution that covering 20 years of mine dewatering and associated groundwater drawdown in the vicinity of the mine workings. The remaining transient stress periods account for 100 years of simulated post-mining groundwater recovery.

Numerical "drains" were used to simulate mine dewatering and were placed parallel to the current distribution of mine laterals (Harbaugh and McDonald, 1996; Harbaugh et al., 2000). Drains will remove or "pump" water from the groundwater model over time in order to draw down water levels to an elevation specified for each drain cell. Drain cell width and length were each set to 100 feet. The thickness of the drain bed was set at one foot and drain hydraulic conductivity was set to 0.08 ft/d, or the same value as that used for the surrounding Vinini Formation. Prescribed head values for the drains were set to draw down water levels to the elevation of the deepest mine workings planned for the Hollister Mine, or 4,570 ft amsl, by the end of the 20-year mine dewatering period.

After 20 years of mine dewatering, simulated drawdown at the workings was approximately 800 ft. The extent of the future, estimated 10-foot drawdown contour over time was then used to refine the model domain extent, approach, and overall model design for the more refined and expanded flow model to be used to more accurately estimate impacts of proposed and future dewatering activities at the Hollister Mine.

3.3 Refined MODFLOW Model Development

3.3.1 Approach

Following the development and review of the results of the 2-D screening model, a refined three-dimensional (3-D) numerical flow was constructed using MODFLOW-2000 to simulate and estimate 1) previous mine dewatering activities, 2) the extent and magnitude of future groundwater drawdown associated with planned full scale and No Action Alternative mining scenarios, and 3) the timing of future water level recovery at the mine site. A summary of the specifications of the 3-D numerical flow model (Hollister Model) are presented below in Table 3-1.

Use of contents on this sheet is subject to the limitations specified at the end of this document.
HollisterMineEIS_GWModelingReport_FINAL.docx

Although the Hollister Model contains multiple layers bounded by three-dimensional surfaces (or geologic contacts), it is intended to serve primarily as a tool to assess the regional impacts attributable solely to mine dewatering at the Hollister Mine. It is not designed to reflect detailed or refined hydrogeologic heterogeneity in either the lateral or vertical dimensions, nor does it include other regional groundwater sources or sinks other than underflow within the Ordivician Vinini aquifer. However, previous modeling efforts by Barrick Goldstrike were considered during model development and were used in the development of layer elevations and initial hydraulic parameter estimates (BLM, 2008).

Table 3-1. Specifications of the Hollister Model

Model Characteristics	Specifications
Active Model Domain	~590 square miles
Units	Time: Day Length: Feet
Coordinate System	Adjusted State Plane Nevada East NAD 1927 (See Section 3.3.3)
Model Grid	825 rows by 815 Columns; 2,689,500 Total Cells; 2,010,618 Active Cells; Origin: X:218248 Y: 223041 Rotation: 41° counterclockwise
Cell SIze	100 ft by 100 ft telescoping mesh, increasing to a maximum of 2,000 ft by 2,000 ft at model edges.
Layering – 4 Layers	Layer 1: No Flow – Tertiary Volcanic Aquifer Layers 2, 3 and 4: Vinini Formation, Layer Type: Confined/Unconfined convertible unit with variable transmissivity (LAYCON = 3)
Hydraulic Parameters (Calibrated)	Layer 2: K: 0.2 Kx:Kz: 100:1 Ss = 5e-6 Sy = 0.03 Layer 3: K: 0.15 Kx:Kz: 100:1 Ss = 5e-6 Sy = 0.02 Layer 4: K: 0.15 Kx:Kz: 100:1 Ss = 5e-6 Sy = 0.02 Hatter Graben (Layer 2, 3, and 4): K: 0.003 Kx:Kz: 10:1 Storage parameters the same as those listed above.
MODFLOW-SURFACT Packages	Basic, BCF4, ATO4, PCG5, OC, Well, Drain, GHB
Stress Periods	Transient Calibration: 29 Stress Periods of 60.8 days each (March 2005 through December 2009) Predictive Simulation: 24 Stress Periods ranging from 365 days to 3,650 days through stress period 23 (January 2010 through December 2109). Stress period 24 covers 54,750 days (through December 2249)
Dewatering Wells/Drains	54 Wells simulated as analytic elements in the calibrated transient simulation; 1146 Drains used to simulate dewatering in the predictive simulation
Boundary Conditions	General Head Boundaries were simulated on all 4 sides of the model where the flow gradient was not perpendicular to the model boundary. Reference heads located approximately 2 miles away from model boundaries.
Initial Conditions	Heads from calibrated, steady-state, pre-dewatering simulation used as initial conditions for the transient calibration Head values for the final stress period of the transient calibration used for initial conditions for the predictive simulation
Solution Method	PCG5 using Newton-Raphson solution technique

Use of contents on this sheet is subject to the limitations specified at the end of this document.
HollisterMineEIS_GWModelingReport_FINAL.docx

3.3.2 Computer Code Description

The Hollister Model was developed with MODFLOW-SURFACT version 3 (Hydro-Geologic, 1996). Groundwater Vistas™ (version 5.43) was utilized as the pre- and post-processing software, fully coupled with ESRI® ArcGIS™ (version 9.3) and associated standard GIS format datasets (ESI, 2010; ESRI, 2009).

3.3.3 Units and Coordinate System

The Hollister Model has linear units of feet, temporal units of days, and all model features georeferenced to mine site coordinates, which are a variant of the State Plane Nevada East NAD27 projection. Site coordinates can be adjusted to State Plane by adding a 2,000,000 foot adjustment to the northing values. GIS files associated with the modeling efforts are also georeferenced to the mine site coordinate system.

3.3.4 Model Domain and Boundary Conditions

As shown on Figure 3-2, the full active model domain of the refined Hollister Model is approximately 590 square miles; centered upon the location of the Hollister Mine workings. The model domain was expanded relative to the 2-D, screening-level model in order to limit boundary effects on predicted dewatering impacts from no-flow model boundaries during subsequent predictive model simulations.

General head boundary conditions (GHB's) were assigned to layers 2, 3 and 4 along all edges of the model where groundwater was interpreted to be entering or exiting the model domain; however, where the groundwater flow paths were approximately perpendicular to the edge of the model, no flow boundaries were used (Figure 3-2). Reference heads for the GHB's were set to approximated groundwater elevations 2 miles away from the model domain, based upon the water level contours shown on Figure 2-5 (BLM, 2000a). GHB cell widths, lengths, and thicknesses correspond exactly to individual grid cell dimensions. Hydraulic conductivity for all GHB's was set to the calibrated hydraulic conductivity values for each model layer of the Vinini Formation. During steady-state model calibration, GHB reference heads were adjusted to produce a groundwater flow regime representative of regional water level elevations and gradients prior to mine-dewatering (Figure 2-5). Post-calibration, fluxes at GHB cells were examined to verify that they were feasible and not likely to bias dewatering impact estimates.

3.3.5 Model Discretization and Layering

The Hollister Model consists of four layers and has a cell discretization of 100 by 100 feet in the center of the model, telescoping out to 2,000 by 2,000 feet along the model periphery. Layer 1 extends vertically from ground surface to the upper contact of the Vinini Formation and encompasses the overlying Tertiary volcanics. This layer was represented completely by no flow cells so that only groundwater conditions within the underlying Vinini formation were considered; however, it was included in the model construction to three-dimensionally represent the location of land surface, surficial hydrology features, and the thickness of the Tertiary volcanics within the model framework. Layers 2, 3 and 4 represent the Vinini Formation (at increasing depths) and were all simulated as convertible confined/unconfined aquifer units (or "layer type 3"), which allows the storage properties and transmissivities of the Vinini to vary and shift from unconfined to confined conditions as water levels decline during dewatering and refilling.

The upper contact of the Vinini Formation in the immediate vicinity of the Hollister Mine was provided by RCG. Because the model domain extends approximately 11 miles away from the mine workings, the bottom of the 1997 Barrick Goldstrike groundwater model layer 1 was utilized to represent the upper contact of the Vinini at distances greater than 2 to 3 miles away from the active mine workings (BLM, 2000b). These two data sources were combined using a kriging interpolation scheme to produce a smooth Vinini surface, shown on Figure 3-3, that completely defines the bottom of layer 1, which also corresponds to the top of model

Use of contents on this sheet is subject to the limitations specified at the end of this document.
HollisterMineEIS_GWModelingReport_FINAL.docx

layer 2. Additionally, in a portion of the model domain approximately one mile southeast of the mine site, the elevation of the Vinini was set to a uniform elevation of 5,000 ft amsl. This localized adjustment to the upper contact of the Vinini formation was performed due to the presence of intrusive geologic units in this area that have replaced or highly altered the typical geologic units that comprise the Vinini Formation. In this area, as well as in the area surrounding it, the presence of the intrusive units was represented by changes in hydraulic properties rather than explicit changes in layering elevations. The bottom of layer 2 was set at a uniform thickness of 450 feet below the Vinini contact to represent the upper portion of the Vinini Formation that is currently being mined at the Hollister Mine. Layers 3 and 4 were set at constant thicknesses of 500 feet thick each and represent depths of mining proposed at the Hollister Mine and neighboring Hatter Graben in the future.

3.3.6 Temporal Discretization and Initial Conditions

Both steady-state and transient models were developed and calibrated prior to performing predictive dewatering simulations. A discussion of the calibration and simulation results for these models is presented in Section 4.0. The steady-state model was developed to approximate groundwater conditions in early 2005, prior to dewatering activities at the Hollister Mine. Initial heads for the steady-state model were based upon the head distribution presented by the BLM (2000a) and shown on Figure 2-5. Simulated water levels from the steady-state model were used as initial conditions for the transient, calibrated model. The transient simulation period begins in March 2005 and extends through December 2009. It is comprised of 29 stress periods of 60.8 days each, or approximately two months, with variable and adaptive time stepping to improve model convergence and stability.

3.3.7 Hydraulic Parameterization

Initial estimates of bulk aquifer hydraulic conductivity, specific storage, and specific yield were based upon previous modeling efforts, hydrogeologic investigations, and literature values presented in Section 2.0. However, hydraulic parameters were adjusted and refined during the model calibration process to produce final values. Hydraulic properties were assumed to be homogenous and isotropic within each model layer of the Vinini Formation and intrusive zone east of the Hollister Mine (Figure 3-4). All final, calibrated values fall within appropriate ranges for the observed lithology of the Vinini Formation and neighboring intrusive bodies (BLM, 2000b).

3.3.7.1 Hydraulic Conductivity

With the exception of the zone of intrusive geologic features immediately east of the Hollister Mine, the Vinini Formation in the Hollister Model was simulated as a homogeneous medium. Both the low conductivity intrusive zone and bulk Vinini Formation were conceptualized and simulated as "equivalent porous media". This simplifying assumption means that this fractured and locally complex geology can be simulated as porous media with bulk aquifer hydraulic properties at the scale of the model. Given previous modeling work performed by Barrick Goldstrike, this assumption appears to be validated and appropriate for application to the Hollister Mine dewatering modeling (BLM, 2000b; BLM, 2008).

Hydraulic conductivity for the Vinini Formation in model layer 2 was calibrated to 0.2 ft/day. Upon review of site dewatering rates, water level trends, and regional geologic conditions, it appears that the formation may have a lower fracture density and correspondingly lower permeabilities at greater depths. Therefore, a slightly lower hydraulic conductivity of 0.15 was assigned to model layers 3 and 4 during the calibration process to represent this conceptualization. The horizontal to vertical hydraulic conductivity ratio (or anisotropy ratio) was assumed to be 100:1, reflective of the presence of low permeability argillites and siltstones within the model layers representing the bulk Vinini Formation. These units are conceptualized as

Use of contents on this sheet is subject to the limitations specified at the end of this document.
HollisterMineEIS_GWModelingReport_FINAL.docx

limiting the vertical flow and drainage of water within the Vinini Formation when dewatering hundreds of feet of aquifer at the mine site.

Additionally, the area of intrusives within the adjacent Hatter Graben complex was depicted in the model as a low hydraulic conductivity zone (Figure 3-2). This area was assigned a horizontal conductivity value of 0.003 ft/day in all model layers. This same value was used in the 1997 Barrick Goldstrike model for the intrusive unit directly south of the Barrick Goldstrike mine (BLM, 2000b). The horizontal to vertical hydraulic conductivity anisotropy ratio was assumed to be 10:1 for this low permeability zone; reflective of non-layered intrusive features.

3.3.7.2 Storage

A uniform specific storage value of 5e-6 ft^{-1} was assumed for the entire model. A value of this magnitude is typical of competent yet fractured, hardrock aquifers (Schwartz and Zhang, 2003). Specific yield was calibrated to a uniform value of 0.03 for model layer 2. Similar to the vertical reduction in hydraulic conductivity values, specific yield was set to a uniform value of 0.02 for model layers 2 and 3, representing more competent material and decreasing fracture porosity at depth.

3.3.8 Wells and Mine Dewatering

During the transient calibration simulation, wells were used to simulate dewatering operations associated with the mine workings. No other groundwater pumping or demands were considered or included in the model construction. Total well pumping was based upon historical inflow volumes to the mine decline. Estimated inflows to the mine workings are based upon decline pumping records. Theoretical dewatering wells were placed along the mine decline and laterals according to the temporal locations of mine advance, elevations of the mine workings, and timing of mining activities. Throughout the transient model time period, the total bi-monthly and annual volumes of dewatering pumping matched the recorded volumes, presented in Table 3-2.

The assignment of pumping rates at individual wells was based upon the additional amount of total mine dewatering that occurred during each two-month stress period. The additional amount of total pumping was applied to theoretical wells located in areas of the mine workings that were actively being expanded during that time period. During times when the total dewatering rate declined, pumping was decreased uniformly at all well locations to account for the overall reduction. When the total dewatering rate declined but the mine workings were still being advanced, additional wells were still placed in the new portions of the mine, and the reduction in pumping was again accounted for by reductions in pumping for other wells in the model.

Additionally, as mining progressed it was assumed that the subsurface near shallower portions of the mine were essentially dewatered and no longer required significant dewatering activities. After confirming that simulated water levels were approaching or below the elevations of the mine workings, the simulated pumping for these areas was turned off, and the bi-monthly pumping volume was distributed over the remaining active, theoretical wells.

Table 3-2. Hollister Mine Stress Periods and Pumping Rates

Stress Period	Months-Year	Pumped Volume (Gallons)	Pumped Volume (Acre-feet)
1	March-April 2005	88,920	0.27
2	May-June 2005	455,240	1.40
3	July-August 2005	1,953,000	5.99

Use of contents on this sheet is subject to the limitations specified at the end of this document.
HollisterMineEIS_GWModelingReport_FINAL.docx

Table 3-2. Hollister Mine Stress Periods and Pumping Rates

Stress Period	Months-Year	Pumped Volume (Gallons)	Pumped Volume (Acre-feet)
4	September-October 2005	5,086,800	15.61
5	November-December 2005	7,318,800	22.46
6	January-February 2006	10,410,000	31.95
7	March-April 2006	14,750,000	45.27
8	May-June 2006	21,230,000	65.15
9	July-August 2006	24,080,000	73.90
10	September-October 2006	32,020,400	98.27
11	November-December 2006	30,960,000	95.01
12	January-February 2007	24,983,264	76.67
13	March-April 2007	25,158,256	77.21
14	May-June 2007	22,666,320	69.56
15	July-August 2007	21,099,000	64.75
16	September-October 2007	19,566,510	60.05
17	November-December 2007	18,007,805	55.26
18	January-February 2008	20,950,746	64.30
19	March-April 2008	26,305,420	80.73
20	May-June 2008	33,278,670	102.13
21	July-August 2008	41,420,388	127.11
22	September-October 2008	33,877,238	104.0
23	November-December 2008	27,733,666	85.1
24	January-February 2009	25,570,000	78.5
25	March-April 2009	30,569,000	93.8
26	May-June 2009	35,918,000	110.2
27	July-August 2009	35,241,000	108.2
28	September-October 2009	34,843,143	106.9
29	November-December 2009	36,648,000	112.5
Totals	1763 Days / 4.8 Years	662,189,586	2032.19

Sources: RCG records

Use of contents on this sheet is subject to the limitations specified at the end of this document.

4. MODEL CALIBRATION RESULTS AND SENSITIVITY ANALYSIS

4.1 Calibration Approach

Calibration is the process of adjusting model parameters to achieve a good match between the simulated and observed hydraulic heads, hydraulic gradients, water level trends, or other relevant hydrologic data such as water budget components. These observed data are called calibration "targets". Initial estimates for hydrogeologic parameters are varied within a reasonable range of values, based upon observed or literature-derived estimates, to improve the model's ability to simulate these targets. The calibration exercise provides confidence that the model is capable of simulating the historical, observed groundwater conditions, and it was completed for both the steady-state and historical transient model simulations prior to performing the future, predictive dewatering simulations.

4.2 Model Calibration

The Hollister model was calibrated over the time period of historical dewatering: March 2005 through December 2009. Water levels from two, transient calibration targets were primarily utilized during calibration, monitor wells BH-01 and BH-02 (Figure 3-1) The key model variables that were varied during the transient model calibration process included hydraulic conductivity, specific storage, and specific yield. Reference heads for the general head boundary cells were also adjusted during steady-state calibration, but were primarily used to mimic regional flow gradients and pre-dewatering groundwater elevations at the mine site.

The target criteria for the steady-state calibration were to match the general groundwater elevation at the mine site, or approximately 5,400 ft amsl, and qualitatively match the magnitude and resultant flow direction of the regional groundwater gradient, which is generally directed from the northeast to the southwest. Once a calibrated steady-state simulation was achieved, calibration then focused on matching the transient, time-series water level data at BH-01 and BH-02 by varying the hydraulic properties of the Vinini Formation. The goal of the transient model calibration was to generally reproduce: 1) starting water levels, 2) water levels in 2010, 3) the general trends in observed water level declines, 4) the overall magnitude of drawdown at the two key monitoring locations, and 5) simulated water levels within 100 feet of the three-dimensional distribution of all current mine workings. Given the absence of reliable, observational water level data, other than those from BH-01 and BH-02, the final calibration criterion was critical in ensuring that the model was adequately simulating dewatering conditions over a significantly larger spatial extent than the two viable borehole monitoring locations. Additional calibration information, including comparisons of simulated versus observed values (or model residuals) and standard statistics are provide in Appendix A (Figure A-1 and Figure A-2).

To produce a better calibration and better represent aquifer properties at various depths within the model domain, the Vinini Formation was divided into three separate layers during calibration: model layers 2, 3, and 4. This model refinement improved model calibration by allowing slight adjustment to hydraulic parameters with depth as well as allowing dewatering pumping and associated simulated water levels to be representative of much smaller vertical intervals, thereby improving model resolution and substantially decreasing the degree of averaging of parameters over large thicknesses of aquifer material. Additionally, the additional model

Use of contents on this sheet is subject to the limitations specified at the end of this document.

layers allowed both past and future dewatering activities to be more accurately placed with respect to the elevations of the portions of the mine workings being advanced, removing the limitations associated with a 2-D model representation of aquifer conditions.

Hydraulic conductivity, specific storage and specific yield were all varied to calibrate the transient groundwater flow model. In model layer 2, the calibrated hydraulic conductivity estimate for the bulk of the Vinini Formation was adjusted upwards to 0.2 ft/day, and the calibrated specific yield was also raised to a value of 0.03. Both of these values represent increases from the initial, conceptual estimates for hydraulic conductivity and specific yield of 0.08 ft/day and 0.02, respectively. In order to better match observed trends, the calibrated specific storage was determined to be approximately 5×10^{-6}, a reasonable value for a fractured rock aquifer (Schwartz and Zhang, 2003). For model layer 3 and layer 4, hydraulic conductivity was calibrated to a lower value of approximately 0.15 ft/day, and specific yield was estimated to be approximately 0.02. Specific storage was kept at the same value as that calibrated for model layer 2.

Figure 4-1 and Figure 4-2 present simulated versus observed water levels at monitoring locations BH-01 and BH-02, respectively. Overall, simulated water levels match the pre-dewatering groundwater elevations, observed water levels in 2010, the overall trend of declining water levels, and magnitude of total decline. A comparison of simulated water levels in 2010 versus existing mine workings performed using GIS also show that simulated water levels fall close to the elevations of all dewatered portions of the mine.

There are some variations between simulated and observed water levels over time due to uncertainty regarding placement of theoretical dewatering wells and the simplifying assumptions of horizontal and vertical homogeneity for the bulk of the model. Simulated water levels in late 2006 and throughout 2007 are generally lower than those observed at the two calibration target locations (Figures 4-1 and 4-2). This is likely due to a lack of information on the exact portions of the mine that were producing water. However, by the end of the transient simulation, simulated groundwater elevations and water level trends match observed values. Additionally, the steeper drop in water levels at BH-02 near the end of the transient simulation is due to the effects of dewatering of deeper mine workings laterally adjacent to the location of the monitor well. Because both the 5190 and 5050 mine levels fall within model layer 2, the simulated water level response at BH-02 is reflective of dewatering activities and pumping at both mine elevations. This produces a "hybrid" water level hydrograph at later time periods with a steeper rate of water level decline reflective of deeper dewatering activities occurring below the level that BH-02 was intended to monitor. Still, the overall response at BH-02 was deemed to be a suitably accurate representation of water level declines at the scale of the mine site.

4.3 Results

The results from the calibrated, transient model simulation are discussed below. Results include the simulated spatial and temporal distribution of water levels, simulated water budget estimates, and model sensitivity to key hydraulic parameter estimates.

4.3.1 Simulated Water Levels

Figure 4-3 and Figure 4-4 show simulated water level contours for the Vinini Ordivician aquifer from the steady-state and end of the transient dewatering simulations. Although, these water levels are not anticipated to match actual water level conditions within every part of the model domain, they are deemed to be an adequate representation of regional groundwater elevations and gradients at both the scale of the mine site as well as the scale of the regional aquifer. Generally, the primary groundwater flow direction is from the northeast to the southwest in both simulations, although water levels are significantly lower at the Hollister Mine due to approximately five years of dewatering activities. By 2010, there is a localized deflection of flow gradients toward the mine; however, this alteration in the regional flow regime is only persistent within one to

Use of contents on this sheet is subject to the limitations specified at the end of this document.
HollisterMineEIS_GWModelingReport_FINAL.docx

two miles of the mine workings. Within approximately four miles of the mine, groundwater flow gradients are very similar to pre-dewatering conditions.

4.3.2 Simulated Water Budget

The simulated water budget was reviewed for both the calibrated steady-state and transient models, and is presented below in Table 4-1. Overall water budgets are within reasonable estimates given the hydrogeologic characterization of the regional, fractured rock aquifer system. Note that no recharge or leakage from overlying units was included in either simulation, a conservative assumption taken to not allow an underestimation of future mine-related drawdown during the predictive simulation. The overall water budget increases by approximately 700 acre-feet per year (AFY) from pre-dewatering conditions to 2010, reflective of the magnitude of dewatering pumping recorded in late 2009 (approximately 675 AFY). Mine dewatering is counterbalanced solely by removal of water from storage, and there was a negligible change in fluxes at the general head boundaries. These results demonstrate that no additional water was captured from model boundary conditions during the simulation time period, and there are no boundary effects biasing model results or calibration. Numerical error in the total water budgets was negligible for both simulations.

Table 4-1. Simulated Water budget

Water Budget Components	Steady-State Model Pre-Dewatering March 2005 (Stress Period 1)	Calibrated Model January 2010 (Stress Period 29)
Inflows in AFY (gpm)		
Storage	-	706 (438)
General Head Boundaries	2,892 (1,793)	2,893 (1,793)
Total	2,892 (1,793)	3,599 (2,231)
Outflows in AFY (gpm)		
Storage	-	negligible
Wells	-	675 (419)
General Head Boundaries	2,922 (1,812)	2,922 (1,812)
Total	2,922 (1,812)	3,598 (2,231)

AFY = acre-feet per year
gpm = gallons per minute

4.4 Sensitivity Analysis

A sensitivity analysis was performed on the primary model hydraulic parameters of hydraulic conductivity and storage properties. Figures 4-5 through 4-8 present the results of these analyses as simulated hydrographs at calibration target locations BH-01 and BH-02. Simulated head values from the calibrated model are also included on the figures for comparison purposes. On Figure 4-5 and Figure 4-6, the references to "Main K" and "Low K" refer to the hydraulic conductivity of the Vinini Ordivician aquifer and Hatter intrusive area immediately east of the Hollister Mine, respectively (Figure 3-4).

Model sensitivity to variations in hydraulic conductivity is presented on Figure 4-5 and Figure 4-6. The model is very sensitive to the magnitude of estimated hydraulic conductivity for the bulk Vinini Formation and highly insensitive to changes in assumed hydraulic conductivity for the Hatter intrusive area. This is a positive response because the limited amount of information and high uncertainty for the hydraulic properties of the intrusive area does not significantly effect model calibration or results. A doubling of the hydraulic

Use of contents on this sheet is subject to the limitations specified at the end of this document.
HollisterMineEIS_GWModelingReport_FINAL.docx

conductivity for the Vinini Formation caused simulated water levels to be simulated approximately 100 feet and 70 feet above observed conditions at BH-01 and BH-02, respectively. In contrast, halving the hydraulic conductivity caused water levels to decline too quickly over the calibration time period, and "dried up" the simulated dewatering wells with simulated water levels approximately 120 feet and 80 feet below observed conditions at BH-01 and BH-02, respectively, by June 2008.

Model sensitivity to variations in storage parameters is presented on Figures 4-7 and 4-8. The model is significantly less sensitive to estimated storage values relative to hydraulic conductivity, with variations in simulated head values typically within 20 to 30 feet. However, the model is moderately sensitive to variations in specific yield across a fairly narrow range. The model is also moderately sensitive to specific storage values greater than the calibrated magnitude; however, it is not sensitive to specific storage estimates less than the calibrated value of 5×10^{-6}.

Overall, the results of the sensitivity analysis support the appropriateness of the final calibrated hydraulic parameters, as no significant improvement to model calibration was observed over the range of simulations. Additionally, simulated head responses at BH-01 and BH-02 show similar trends over time regardless of the magnitude of the parameters that were used; highlighting the fact that the model is accurately simulating groundwater conditions given the simplifying assumptions of homogeneity, equivalent porous media, and generalized dewatering locations. Although there is some non-uniqueness and uncertainty associated with the magnitude of the storage parameters used in the model, the sensitivity analysis demonstrated that the range of these values is likely constrained to a fairly narrow range.

Use of contents on this sheet is subject to the limitations specified at the end of this document.
HollisterMineEIS_GWModelingReport_FINAL.docx

5. PREDICTIVE SIMULATIONS AND ANALYSIS

Following the model calibration process and review of the results of the historical transient conditions simulation, a predictive simulation was developed to estimate the future drawdown associated with dewatering to support full scale mining at the current Hollister Mine, future Hollister Mine workings, and planned mining activities within the Hatter Graben just east of the Hollister Mine (Figure 5-1). The development, construction, and results of the predictive model and associated simulations are described below.

5.1 Predictive Simulation Development

Future mine dewatering was simulated for approximately 240 years past present day conditions, or through the year 2250. This simulation time frame assumes a 20-year mine life, through 2030, and dewatering activities at both the Hollister Mine as well as the planned Hatter Expansion location. Because future dewatering requirements and pumping rates are uncertain, the simulated distribution of dewatering locations was based upon the 3-D plan of proposed, future mine workings at Hollister and the general footprint of potential mine workings at the Hatter Expansion site (Figure 5-1). Additional details of the development of the predictive model simulations are provided below along with a discussion of the maximum predicted lateral extent of 10-foot drawdown and simulated future recovery of water levels at both the Hollister and Hatter Expansion areas.

5.1.1 Stress Periods and Initial Conditions

The predictive Hollister model consists of 24 stress periods of varying time intervals that were selected to improve model run times and performance and match key changes in planned future mining activities. Details of the temporal setup of the predictive model are provided below in Table 5-1. The model simulation begins in January 2010 and continues through 2250. Initial water level conditions were imported from the head distribution for each model layer from the calibrated transient model at the end of 2009 (end of calibrated model simulation).

Table 5-1. Hollister Model Stress Period Setup

Stress Period	Length (days)	Elapsed Days	Year Start	Year End
1	365	365	2010	2010
2	365	730	2011	2011
3	365	1,095	2012	2012
4	365	1,460	2013	2013
5	365	1,825	2014	2014
6	365	2,190	2015	2015
7	365	2,555	2016	2016
8	365	2,920	2017	2017
9	365	3,285	2018	2018
10	365	3,650	2019	2019

Use of contents on this sheet is subject to the limitations specified at the end of this document.
HollisterMineEIS_GWModelingReport_FINAL.docx

Table 5-1. Hollister Model Stress Period Setup

Stress Period	Length (days)	Elapsed Days	Year Start	Year End
11	365	4,015	2020	2020
12	365	4,380	2021	2021
13	365	4,745	2022	2022
14	1,095	5,840	2025	2025
15	1,460	7,300	2029	2029
16	365	7,665	2030	2030
17	3,650	11,315	2031	2040
18	3,650	14,965	2041	2050
19	3,650	18,615	2051	2060
20	3,650	22,265	2061	2070
21	3,650	25,915	2071	2080
22	3,650	29,565	2081	2090
23	3,650	33,215	2091	2100
24	54,750	87,965	2101	2250

5.1.2 Simulated Dewatering

Because specific pumping rates required for future dewatering are unknown and highly uncertain, a different dewatering simulation approach was taken relative to the calibrated transient model. The MODFLOW "drain package" was used, which allows future dewatering rates to be calculated based upon the specified elevations of future active mining activities and the calibrated model hydraulic parameters (Harbaugh and McDonald, 1996). The drain package allows water levels to decline to the prescribed elevations of future mine workings coincident with the time when it is anticipated that they will be excavated and advanced.

Table 5-2 presents a time schedule and elevations for future mine development at each site. Drain properties were set to a length of 100 feet (matching model cell size), a width of 20 feet (matching a general width of the mine workings), and a 1-foot drain thickness. The hydraulic conductivity values for the drains were set to that of the surrounding aquifer unit, or 0.2 feet/day and 0.003 feet/day for the Vinini Formation in Layer 2 and Hatter intrusives, respectively. In Layers 3 and 4, the hydraulic conductivity of the drains in the Vinini Formation was set to 0.15 feet/day (i.e., equal to that of the surrounding aquifer unit in that layer). Drain elevations for the Hollister Mine were set to the active mine levels at any given time period by spatially joining the specific elevations of future mine workings from a CAD file provided by Rodeo Creek Gold to Brown and Caldwell (Table 5-2). Drains were assigned to specific model layers based upon their elevations. When mining activities were anticipated to be complete in a given area, drain elevations were reset for that model time period to a level above the pre-existing water table, effectively turning off model dewatering.

Table 5-2. Hollister Mine Drain Setup Schedule

Year	Hollister Mine Level (Generalized)	Hatter Expansion Level	Comments
2010	4,979	-	Based upon future Hollister Mine plan
2011	4,930	-	Based upon future Hollister Mine plan
2012	4,810	-	Based upon future Hollister Mine plan

Use of contents on this sheet is subject to the limitations specified at the end of this document.
HollisterMineEIS_GWModelingReport_FINAL.docx

Year	Hollister Mine Level (Generalized)	Hatter Expansion Level	Comments
2013	4,690	-	Based upon future Hollister Mine plan
2014	4,570	5,200 – 4,800	Subsurface drive over to Hatter, ending at 4,800 elevation at Hatter
2015	4,570	4,800	Hatter Expansion dewatering begins
2016	5,050	4,800	Deep mining stops at Hollister Mine
2017	5,050	4,400	Mine workings advanced downwards
2018	5,050	4,400	-
2019 through 2029	5,050	4,000	Mine workings advanced downwards to final elevation of 4,000 feet
2030 through 2250	-	-	Water level recovery period

5.2 Results of Predictive Simulation

After completion of the predictive simulation, estimated water levels, drawdown, dewatering rates, model water budgets, and water level recoveries were assessed for the entire model domain at a maximum of 10-year intervals to ensure that the model performed appropriately and to ensure that there were no significant boundary effects that biased model results. When appropriate, results for specific years were also assessed to evaluate the maximum extent of drawdown. Given the scope of this work and the modeling approach, the most attention was given to assessing changes from pre-dewatering conditions as opposed to absolute values of water levels or water budget features. However, all model results fall within anticipated magnitudes, given observed mine hydrogeologic conditions and the conceptual model for the mine site and surrounding area, and predicted drawdown can be superimposed upon observed, existing conditions or model results from the Barrick Goldstrike model as a means of assessing future potential impacts of dewatering at the Hollister Mine and future Hatter Expansion (BLM, 2000b). Predicted drawdown, water budget, and water level recoveries are discussed in the sections below.

5.2.1 Predicted Drawdown and Cumulative Effects

The simulated maximum lateral extent of 10-foot drawdown that is attributable to past, current, and future dewatering activities at the Hollister Mine and the Hatter Expansion area is presented on Figure 5-2. The estimated area of 10-foot or greater drawdown has a radial extent of approximately 8 miles away from the Hollister and Hatter Expansion areas. The low conductivity zone, while significant to predicted drawdown and anticipated dewatering rates at the scale of the current and planned mine workings, did not significantly affect the shape of the 10-foot contour, although it is based upon the predicted dewatering rates for the planned Hatter Expansion. The maximum extent of 10-foot drawdown is predicted to occur in approximately 2070, or approximately 40 years after the cessation of mine dewatering. Given the shape of the drawdown contours together with the lack of significant changes in inflows and outflows at the model general head boundaries, there appears to be no significant deflections that would indicate model boundary effects impacting estimated regional water level declines.

Use of contents on this sheet is subject to the limitations specified at the end of this document.
HollisterMineEIS_GWModelingReport_FINAL.docx

The maximum extent of the cumulative 10-foot drawdown contour from the 2007 Barrick groundwater model is also displayed on Figure 5-2. The maximum extent of drawdown greater than 10 feet attributable to dewatering at the Hollister Mine and Hatter Expansion overlaps the extreme northwestern portion of the cumulative impact area, reaching a maximum overlap of approximately 6 miles directly southeast of the Hollister Mine site. Although there is an apparent overlap, dewatering at mines in the Carlin Trend that are southeast of the Hollister Mine occurs in the deeper carbonate aquifer, which is previously discussed in Section 1.3 and Section 2.2 of this report. Elsewhere in the Carlin Trend, water levels in low permeability units overlying the deeper carbonates have declined at a lower rate or have remained relatively constant with respect to water level declines in the deeper carbonates (Maurer, et. al, 1996). Therefore, water level declines indicated by the Barrick groundwater model may be expressed at a lesser magnitude in the overlying, less transmissive Vinini Formation. This lack of communication between the Vinini Formation and underlying carbonate aquifer means that the maximum extent of 10-foot drawdown predicted by the Hollister Model may not be directly summed with the drawdown from the Barrick Model to produce a revised cumulative extent of maximum impact. Also, it may be appropriate to compare the simulated drawdown extents from both the Hollister and Barrick groundwater models at the specific simulation times at which both models reach their respective maximum 10-foot drawdown extents in order to adequately assess cumulative dewatering impact and its relationship to dewatering at the Hollister Mine and Hatter Expansion sites.

Cross sectional views of the vertical change in piezometric surface and associated water level drawdown in 2015 and 2029, which represent the last year of dewatering at the deepest Hollister and Hatter Expansion areas, respectively, are presented on Figure 5-3 through Figure 5-6. Location maps for each cross section are included on each figure; generally, two perpendicularly oriented cross sections were developed for both the main portion of the Hollister Mine as well as the Hatter Expansion area. Also shown on the cross sections are the contact between the Tertiary Volcanics and underlying Ordivician Vinini Formation, as represented in the numerical model construction, and the model simulated full recovered groundwater level. Simulated water levels and associated drawdown over time at the Hollister and Hatter Expansion areas can also be viewed on the hydrographs presented on Figure 5-7. Additional information regarding simulated future water level and drawdown distributions can be found in Appendix A (Figures A-3, A-4, A-5, A-6, and A-7).

An analysis was also performed to assess the sensitivity of the estimated maximum extent of 10-foot drawdown to uncertainty associated with the hydraulic conductivity for the model's low permeability area and specific yield. These parameters were selected for the analysis because the transient model calibration was not found to be sensitive to them, meaning that these values were not highly constrained during the calibration process. Predictions of the maximum extent of the 10-foot drawdown were found to be essentially insensitive to reasonable variations in the hydraulic conductivity of the low permeability area as well as specific yield estimates.

5.2.2 Predicted Water Budget and Dewatering Rates

The simulated water budget components for both the calibrated transient simulation and predictive simulation are presented below in Table 5-3. The overall simulated water budget increased by approximately 300 AFY from 2010 to 2030, in response to an estimated increase in dewatering pumping of approximately the same magnitude (309 AFY). Changes in inflows and outflows at the upgradient and downgradient general head boundaries are negligible, indicating minimal impact or bias on drawdown from these water budget features. By 2110, the total simulated water budget is within approximately 60 AFY of that for the steady-state simulation, indicating that regional groundwater flow conditions are no longer significantly influenced by mining activity. Numerical error in the simulation water budget was negligible for the predictive simulation.

Use of contents on this sheet is subject to the limitations specified at the end of this document.
HollisterMineEIS_GWModelingReport_FINAL.docx

Table 5-3. Simulated Water Budgets – Predictive Simulation			
Water Budget Components	Calibrated Model January 2010 (Stress Period 29)	Predictive Model End of Dewatering Activities January 2030 (Stress Period 15)	Predictive Model End of Simulation January 2110 (Stress Period 24)
Inflows in AFY (gpm)			
Storage	706 (438)	1004 (622)	negligible
General Head Boundaries (GHB's)	2,893 (1,793)	2,898 (1,797)	2,974 (1,843)
Totals	*3,599 (2,231)*	*3,902 (2,419)*	*2,975 (1,844)*
Outflows in AFY (gpm)			
Storage	-	-	133 (82)
Wells / Drains	675 (419)	984* (610*)	-
General Head Boundaries (GHB's)	2,922 (1,812)	2,919 (1,810)	2,841 (1,761)
Totals	*3,598 (2,231)*	*3,902 (2,419)*	*2,974 (1,844)*

AFY = acre-feet per year
gpm = gallons per minute
** Drains used to simulate dewatering.*

Total mine dewatering for both mine sites in 2030 was estimated to stabilize at approximately 610 gpm (~1,000 AFY) by the end of planned mining activities, an increase from the approximately 420 gpm (~675 AFY) of pumping recorded in early 2010 (Table 5-3). Figure 5-8 presents the recorded and estimated future groundwater dewatering rates at the Hollister Mine and Hatter Expansion over time. Note that wells were used to simulate recorded dewatering activities, while drains were used to estimate future potential dewatering rates with the beginning of the predictive simulation time period in 2010. During the predictive simulation, estimated future average annual dewatering rates vary substantially in magnitude in response to mining activities and are almost always greater than those previously observed. This trend is due to the greater depth of mining at the Hollister Mine and additional deep mining activities at the Hatter Expansion. As seen in Table 5-2, the driving of underground workings to the Hatter mine are simulated to begin in 2014 with simulated dewatering at that site beginning in 2015. Contrastingly, deep dewatering at the Hollister Mine ceases in 2016. As seen on Figure 5-8, there are corresponding increases and decreases in pumping rates (of hundreds of gallons per minute) in response to these planned changes in mining activities. Overall, future annualized dewatering estimates range from approximately 450 gpm to over 1,100 gpm; however, beyond year 2020, in response to a planned consistent, active mine working elevation at Hatter, estimated dewatering rates asymptotically decline and ultimately approach 600 gpm. These future dewatering estimates are dependent upon current understand of hydrogeologic conditions at depth at both the Hollister and Hatter Expansion locations and are simulated using numerical, passive drain boundary conditions. Due to local variations in hydrogeologic conditions, lithology, and required dewatering techniques, actual pumping and dewatering rates may vary depending upon conditions encountered in the field.

5.3 Water Level Recovery

The simulated water level elevations, declines, and recoveries for both the Hollister Mine and Hatter Expansion are presented on Figure 5-7. Simulated water levels at the Hatter Expansion were taken from a theoretical monitoring location in the center of the planned Hatter Expansion area. Simulated water levels for BH-02 were compiled from both the historical transient and predictive simulation in order to show a representative hydrograph of dewatering and recovery at the Hollister Mine in the vicinity of current mine

Use of contents on this sheet is subject to the limitations specified at the end of this document.
HollisterMineEIS_GWModelingReport_FINAL.docx

workings. Additionally, a theoretical monitoring location was also placed where future, deeper mining is planned at the Hollister Mine. Water level declines reach the planned depths of mine workings at both sites, indicating that the use of numerical drains adequately dropped water levels to planned mining elevations (Table 5-2). The predictive simulation time period was also expanded to year 2250 to evaluate how close simulated water levels get to pre-dewatering conditions and to assess the sensitivity of predicted recovery times given various water level recovery criteria, discussed below.

Simulated mine dewatering ceases in 2030, and water levels rapidly rebound, coming within 100 feet of pre-dewatering conditions by 2050 for the Hollister Mine and 2060 for the Hatter Expansion. The minimum, simulated water level elevation of 4,000 feet amsl occurs at the Hatter Expansion beginning in 2019, identical to the planned future mine maximum depth presented in Table 5-2. This corresponds to a maximum simulated drawdown of approximately 1,420 feet (at the theoretical Hatter underground workings). The maximum simulated drawdown at the Hollister Mine is approximately 820 feet (an elevation of ~4570 ft amsl). Note that the model does not include sources of recharge or inflows to the aquifer system from overlying or underlying aquifers, nor infiltration from precipitation where the Ordivician Vinini Formation is exposed at land surface. Given these conservative model assumptions, it is likely that simulated water levels will take an unrealistically long time period to reach 100 percent recovery. Therefore, water level recoveries of 95 percent and 99 percent of maximum simulated drawdowns at both the Hollister Mine and Hatter Expansion were evaluated. These drawdown recovery criteria were used to estimate when "fully recovered" conditions occur in the predictive simulation.

Table 5-4 presents simulated water level recovery times based upon the criteria discussed above, and summarizes the information contained in Figures 5-9 and 5-10, which show the refilling curves for the Hollister Mine and planned Hatter Expansion area, respectively. The refilling curves present the percentage of groundwater recovery for each area with respect to the time elapsed after the assumed cessation of mining activities. Note that given the resolution, simplifying assumptions, and data available for the Hollister model construction, estimates of water level recoveries greater than 95 percent are likely beyond the ability of the model to predict with a high degree of confidence. Additionally, simulated groundwater conditions decades into the future are subject to a large amount of uncertainty due to a lack of knowledge about future groundwater inflows and outflows and future groundwater pumping and dewatering demands within the Carlin Trend.

Table 5-4. Simulated Water Level Recovery Times

Drawdown Recovery Percentage	Approximate Recovery Year (years after cessation of mining)		
	Hollister Mine (at BH-02)	Planned Deep Hollister Mine Area	Hatter Expansion Area
95%	2070 (~40 years)	2060 (~30 years)	2065 (~35 years)
99%	2160 (~130 years)	2109 (~79 years)	2118 (~88 years)

Water levels at the Hollister Mine generally recover slower at the location of BH-02 due to the longer period of mine dewatering that has occurred in the vicinity of this well. Relative to the current extent of the Hollister Mine (represented by the BH-02 hydrograph on Figure 5-7), water levels generally recover faster at the Hatter Expansion due to the much shorter duration of simulated dewatering. The shortest water level recovery times are estimated for the aquifer in the immediate vicinity of the planned deep Hollister Mine workings (Table 5-4). This is due in part to the much greater depth of mining at the Hatter Expansion as well as its more distal location to previous dewatering activities near BH-02 (Table 5-2).

Use of contents on this sheet is subject to the limitations specified at the end of this document.
HollisterMineEIS_GWModelingReport_FINAL.docx

6. NO ACTION ALTERNATIVE SIMULATION AND ANALYSIS

The Hollister Model was used to simulate the extent and magnitude of groundwater drawdown and subsequent groundwater level recovery associated with Hollister Mine dewatering under the No Action Alternative. The No Action Alternative is defined as a continuation of underground test mining and exploration activities at current rates through the end of 2011. Under the No Action Alternative, groundwater pumping is permitted for up to 700 gpm, and test mining is permitted at a rate of up to 400 tons per day. At the end of 2011, test mining, exploration activities, and dewatering would cease, and the open stopes of the Hollister Mine would be backfilled in accordance with the plans for full-scale mining. Additionally, the underground workings of the Hollister Mine will refill with groundwater, beginning in 2012.

6.1 Development of No Action Alternative Simulation

The No Action Alternative simulation was created by modifying the predictive model used to simulate dewatering associated with full scale mining conditions over the next 20 years. All model construction details are the same as described in Section 5, with the exception of two modifications to the model drain package. First, the numerical drains used to simulate current and future dewatering at the Hollister Mine as well as the Hatter Expansion area were deactivated after the end of 2011. This represents the end of test mining and dewatering activities under the No Action Alternative scenario. Secondly, the spatial extent of additional dewatering activities in 2011 was reduced from the full scale mining plan by approximately 62 percent to appropriate future No Action Alternative conditions during that year (RCG, October 2010b). To achieve this, drain cells located in the deepest portions of the planned mine workings were removed first. The remaining active drain locations in 2011 correspond to the depths and lateral extent of theoretical test mining occurring in 2011, pursuant to the specifications of the No Action Alternative scenario and the current test mining permit. Simulated groundwater levels were allowed to recover from 2012 through 2250, although they approach pre-mining conditions much more rapidly than the simulation reflecting full scale mining conditions.

6.2 Results of No Action Alternative Simulation

The simulated maximum lateral extent of 10-foot drawdown that is attributable to past, current, and future No Action Alternative dewatering activities at the Hollister Mine is presented on Figure 6-1. The estimated area of 10-foot or greater drawdown has a radial extent of approximately 2 to 2.5 miles away from the Hollister and Hatter Expansion areas, and is estimated to occur between 2020 and 2025, depending upon the direction away from the mine site. This corresponds to approximately 18 to 23 years after the cessation of test mining activities under the No Action Alternative.

The maximum extent of the cumulative 10-foot drawdown contour from the 2007 Barrick groundwater model is also displayed on Figure 6-1. The maximum extent of drawdown greater than 10 feet attributable to dewatering at the Hollister Mine under the No Action Alternative does not overlap the cumulative impact area. See Section 5.2.1 for a discussion of the limitations of comparing drawdown estimates with those from the 2007 Barrick groundwater model.

The average dewatering rate predicted by the model for 2010 and 2011 was approximately 590 gpm. Simulated water levels declined to a maximum depth of approximately 500 feet below predevelopment conditions by the end of 2011. Beginning in 2012, water levels rapidly rebound, as seen on the No Action

Use of contents on this sheet is subject to the limitations specified at the end of this document.
HollisterMineEIS_GWModelingReport_FINAL.docx

Scenario refilling curve shown on Figure 6-2. The refilling curve presents the estimated percentage of groundwater recovery under the No Action Scenario with respect to the time elapsed after the assumed cessation of mining activities in 2012. Groundwater levels are simulated to be recovered to within 95% and 99% of pre-mining conditions by 2023 and 2034, respectively.

Use of contents on this sheet is subject to the limitations specified at the end of this document.
HollisterMineEIS_GWModelingReport_FINAL.docx

7. CONCLUSIONS

The Hollister Mine groundwater model presented in this report was developed to perform simulations of proposed current and future dewatering of the Ordovician Vinini Formation at the Hollister Mine workings in order to assess the maximum extent of the 10-foot drawdown contour, the cumulative groundwater impacts induced by other mining operations in the Carlin Trend, and the timing of groundwater recovery once dewatering operations at the Hollister Mine cease. The Hollister Mine groundwater model is consistent with the conceptual hydrogeologic model presented in Section 2.2 and incorporates geologic and hydrogeologic data that are both site-specific and derived from the Barrick Goldstrike groundwater model (BLM, 2000b). Calibration of the Hollister Mine groundwater model is based on the observed Ordovician Vinini Formation aquifer response to nearly four years of dewatering activities at the Hollister Mine (2005 through 2009), providing a high level of confidence in the model's ability to predict future groundwater conditions. Simulations of future dewatering activities at the Hollister Mine are based on actual conceptual mine plans, and thus present a realistic progression of target dewatering elevations through the life of the Hollister Mine.

Historical water level data from Hollister Mine monitor wells indicate that the past dewatering in the Ordovician Vinini Formation is not affecting water levels in the overlying Tertiary volcanic aquifer, indicating that the two aquifers are not in hydraulic communication. Therefore, significant impacts to the Tertiary volcanic aquifer and its related hydrology are not anticipated to occur as a result of future simulated Hollister Mine dewatering.

Predictive simulations of future full scale mining with the Hollister Mine groundwater model indicate that the maximum extent of the 10-foot drawdown contour will extend radially approximately eight miles from the Hollister Mine, with the maximum extent of impact occurring approximately 40 years post-mining, or approximately in the year 2070. The maximum extent of the 10-foot drawdown contour spatially overlaps a portion of the predicted cumulative effects drawdown induced by other mining/dewatering operations along the Carlin Trend (Figure 5-2). However, the cumulative effects drawdown depicted on Figure 5-2 may be greater than what will be experienced in the overlying low-permeability Vinini Formation being dewatered for Hollister Mine operations. Drawdown from Hollister Mine operations will also temporally precede the occurrence of the cumulative effects drawdown by approximately 40 years (i.e., 2070 versus approximately 2115 for the cumulative effects drawdown).

Water level recovery is simulated to initially be rapid following cessation of mining and dewatering activities at the Hollister Mine and Hatter Expansion, and then will slow with time. For the Hollister Mine, the predictive simulation estimates an asymptotic approach to full recovery, with 95 percent and 99 percent water level recovery estimated to occur approximately a maximum of 40 years and 130 years, respectively, after the cessation of mining activities (corresponding to the years 2070 and 2160). For the Hatter Expansion area, the predictive simulation also estimates an asymptotic water level recovery, with 95 percent and 99 percent recovery simulated to occur approximately 35 and 88 years, respectively, after cessation of mining activities (corresponding to years 2065 and 2118).

Modeling of future potential groundwater conditions under the No Action Alternative scenario was also performed. The No Action Alternative is defined as a continuation of underground test mining and exploration activities at current rates through the end of 2011 with groundwater recovery beginning in 2012.

Use of contents on this sheet is subject to the limitations specified at the end of this document.
HollisterMineEIS_GWModelingReport_FINAL.docx

A predictive simulation of the No Action Alternative scenario with the Hollister Mine groundwater model estimates that the maximum extent of the 10-foot drawdown contour will extend radially approximately 2 to 2.5 miles from the Hollister Mine, with the maximum extent of impact occurring approximately between the years 2020 and 2025. Water levels rapidly rise following the simulated cessation of mining activities at the Hollister Mine, and are estimated to recover to 95 percent and 99 percent of pre-mining conditions by approximately 2023 and 2034, respectively.

Use of contents on this sheet is subject to the limitations specified at the end of this document.

8. REFERENCES

Barrick Goldstrike, 2010, Data transmittal from Johnny Zahn on the 2007 Betze groundwater model. June 14, 2010.

BLM, 1988, *Proposed Ivanhoe/USX Project: Final Environmental Assessment*, United States Bureau of Land Management (BLM), September 1988.

BLM, 2000a, *Cumulative Impact Analysis of Dewatering and Water Management Operations for the Betze Project, South Operations Area Project Amendment, and Leeville Project*, United States Bureau of Land Management (BLM), April 2000.

BLM, 2000b, *Draft Supplemental Environmental Impact Statement, Betze Project, Barrick Goldstrike Mines Inc*., United States Bureau of Land Management (BLM), September 2000.

BLM, 2008, *Betze Pit Expansion Project Draft Supplemental Environmental Impact Statement*, United States Bureau of Land Management (BLM), August 21, 2008.

Brown and Caldwell, 2003, *Hydrogeologic Report for the Hollister Development Block, Revision I, Prepared for Hecla Ventures Corp.*, June 18, 2003.

Environmental Simulations, Inc. (ESI), 2010. Guide to Using Groundwater Vistas, Software Version 5.43.

ESRI, 2009. Arc GIS™ software, version 9.3.

Goldstrand, P.M., and Schmidt, K.W., 2000, *Geology, mineralization, and ore controls at the Ken Snyder gold-silver mine, Elko County, Nevada*, in Cluer, J.K., Price, J.G., Struhsacker, E.M., Hardyman, R.F., and Morris, C.S., eds., Geology and Ore Deposits 2000: the Great Basin and beyond: Geological Socitety of Nevada Symposium Proceedings, May 15-18, 2000, p. 265-287.

Harbaugh, A.W. and McDonald, M.G., 1996. User's Documentation for MODFLOW-96, An Update to the U.S. Geological Survey Modular Finite-Difference Ground-Water Flow Model. United States Geological Survey Open-File Report 96-485.

Harbaugh, A.W., Banta, E.R., Hill, M.C., and McDonald, M.G., 2000. MODFLOW-2000, The U.S. Geological Survey Modular Ground-water Model – User Guide to Modularization Concepts and the Ground-water Flow Process: U.S. Geological Survey Open-File Report 00-92.

Hydro-Geologic, Inc., 1996, MODFLOW-SURFACT™, Version 2.2, Herndon, Va., 1996

Hydrologic Consultants, Inc. (HCI), 1997, West Pit Hydrologic Characterization, Hollister Operations.

Hydro-Search, Inc. (HSI), 1989, *Ground-water Supply Evaluation and Development: Ivanhoe Project, Elko County, Nevada*, Prepared for Galactic Services, Inc.

Maurer, D.K., Plume, R.W., Thomas, J.M., and Johnson, A.K., 1996, *Water Resources and Effects of Changes in Ground-Water Use Along the Carlin Trend, North-Central Nevada*, U.S. Geological Survey Water-Resources Investigations Report 96-4134.

Rodeo Creek Gold (RCG) 2007, Personal communication with Dennis Lang, Hollister Mine Geologist, 2009.

Rodeo Creek Gold (RCG), 2009a, *Plan of Operations Amendment N-76802, Transition from Underground Development and Exploration to Full Underground Mine Production, Hollister Mine Project, Elko County, Nevada*, June 2009.

Rodeo Creek Gold (RCG) 2009b, Personal communication with Brian Morris, Hollister Mine Geologist, 2009.

Rodeo Creek Gold (RCG), 2010a, Correspondence with Robert Thomason, Hollister Exploration Manager, June 29, 2010.

Rodeo Creek Gold (RCG), 2010b, Correspondence with Steve Konieczki, Technical Manager, October 4, 2010.

S. Godden & Associates, 2009, *Revised Technical Report on the June 2009 Update of the Mineral Resource Estimate for Hollister Gold Mine, Elko County, Nevada*, prepared for Great Basin Gold Limited, October 30, 2009.

Schwartz, Franklin W. and Zhang, Hubao, *Fundamentals of Groundwater*, John Wiley & Sons, Inc., New York, NY, 2003

Wallace, A.R., 2003, *Geology of the Ivanhoe Hg-Au District, Northern Nevada: Influence of Miocene Volcanism, Lakes, and Active Faulting on Epithermal Mineralization*, Economic Geology, Vol. 98, 2003, pp. 409-424.

Use of contents on this sheet is subject to the limitations specified at the end of this document.
HollisterMineEIS_GWModelingReport_FINAL.docx

FIGURES

Figure 1-1. Hollister Mine Location
Figure 1-2. Predicted Maximum Extent of the Cumulative 10-Foot Drawdown Contour from Carlin Trend Dewatering Operations
Figure 2-1. Location of the Little Antelope Creek Fault and the Hatter Graben
Figure 2-2. Cross-Section Showing Offset Across the Little Antelope Creek Fault
Figure 2-3. Hydrographs of Ordovician Vinini Aquifer and Tertiary Volcanoics Aquifer Monitor Wells
Figure 2-4. Locations of Ordovician Vinini Aquifer and Tertiary Volcanics Aquifer Monitor Wells
Figure 2-5. Regional Groundwater Elevation Contours
Figure 2-6. Tertiary Volcanics Aquifer Groundwater Elevation Contours
Figure 3-1. 2002 Hydrogeologic Investigation Piezometer and Borehole Location Map
Figure 3-2. Model Domain and Boundary Conditions
Figure 3-3. Surface of Vinini Formation
Figure 3-4. Mine Workings with Theoretical Dewatering Locations
Figure 4-1. BH-01 Observed Versus Simulated Water Levels
Figure 4-2. BH-02 Observed Versus Simulated Water Levels
Figure 4-3. Steady-State Simulated Water Levels
Figure 4-4. Transient Water Levels – 2010
Figure 4-5. BH-01 Hydraulic Conductivity Sensitivity Plot
Figure 4-6. BH-02 Hydraulic Conductivity Sensitivity Plot
Figure 4-7. BH-01 Storage Values Sensitivity Plot
Figure 4-8. BH-02 Storage Values Sensitivity Plot
Figure 5-1. Drain Locations - Predictive Simulation
Figure 5-2. Simulated Maximum Extent of 10-Foot Drawdown (2070)
Figure 5-3. Hollister Mine Cross Sections - 2015
Figure 5-4. Hollister Mine Cross Sections - 2029
Figure 5-5. Hatter Expansion Area Cross Section - 2029, A-A'
Figure 5-6. Hatter Expansion Area Cross Section - 2029, B-B'
Figure 5-7. Simulated Water Level Drawdown and Recoveries
Figure 5-8. Simulated Mine Dewatering – Observed and Predicted Pumping Rates
Figure 5-9 Hollister Mine Workings Refilling Curve
Figure 5-10 Hatter Expansion Area Refilling Curve
Figure 6-1 No Action Alternative Simulation - Maximum Extent of 10 Foot Drawdown (2020)
Figure 6-2 No Action Alternative Simulation - Hollister Mine Water Level Recovery

Use of contents on this sheet is subject to the limitations specified at the end of this document.

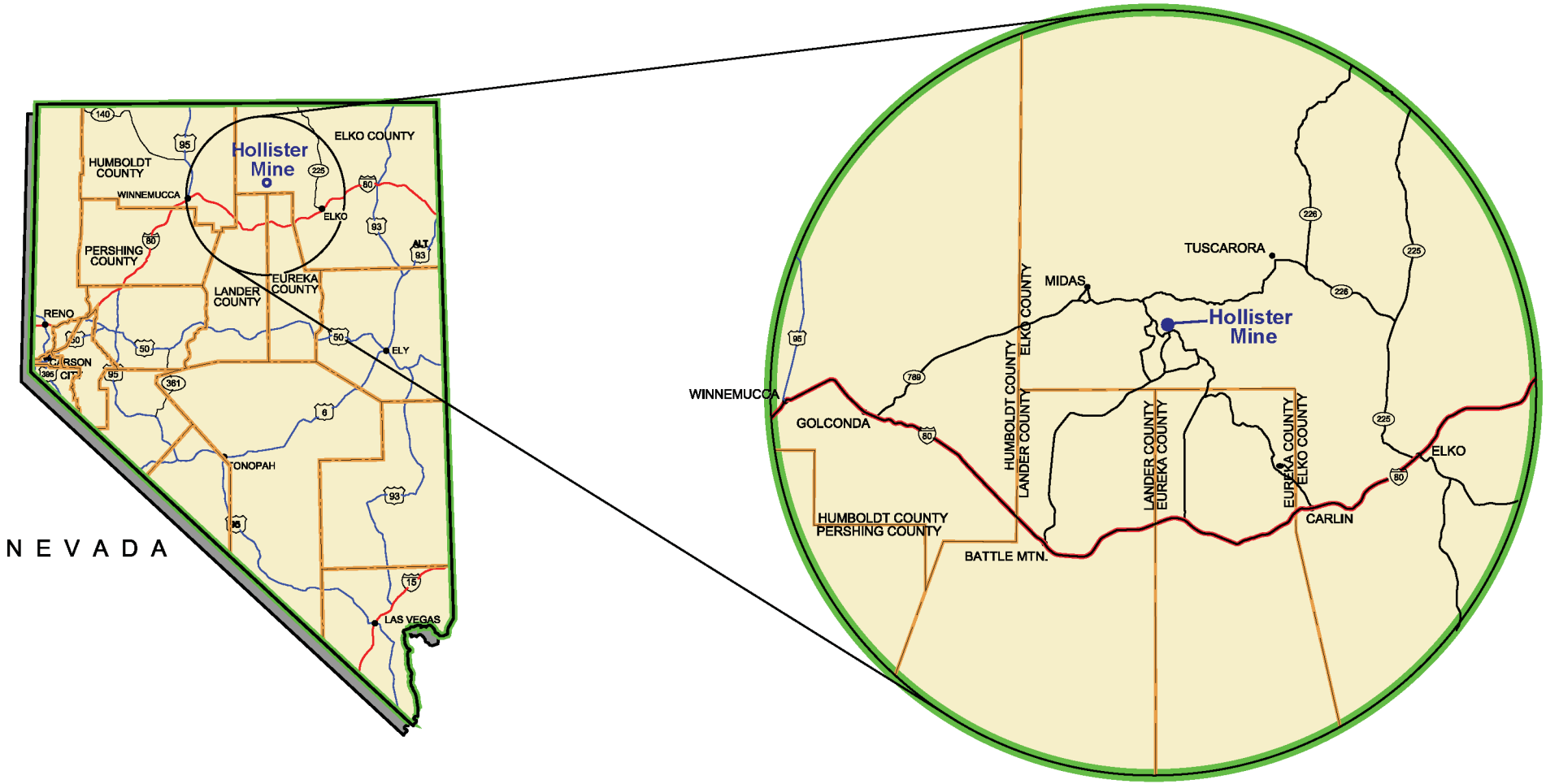

Source: AECOM

BROWN AND CALDWELL	PROJECT 138301	SITE Rodeo Creek Gold - Hollister Mine	Figure 1-1
	DATE 7-7-10	TITLE Hollister Mine Location	

P:\BC_CAR\138301_Hollister_Mine_EIS\GIS\GRAPHICS

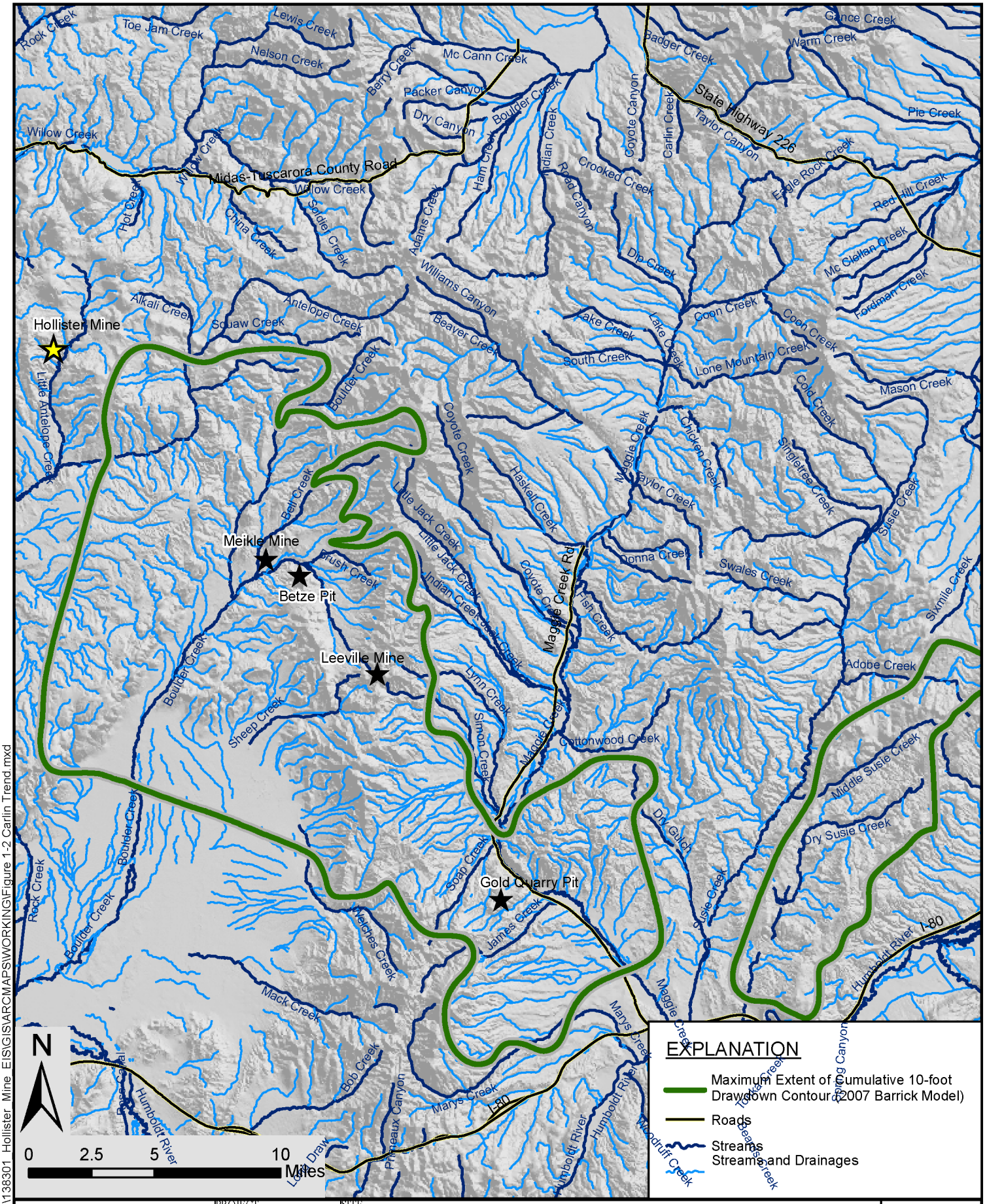

FILE: P:\BC_CAR\138301_Hollister_Mine_EIS\GIS\ARCMAPS\WORKING\Figure 1-2 Carlin Trend.mxd

BROWN AND CALDWELL	PROJECT 138301	SITE Rodeo Creek Gold - Hollister Mine	Figure 1-2
	DATE 6/30/10	TITLE Predicted Maximum Extent of the Cumulative 10-Foot Drawdown Contour from Carlin Trend Dewatering Operations	

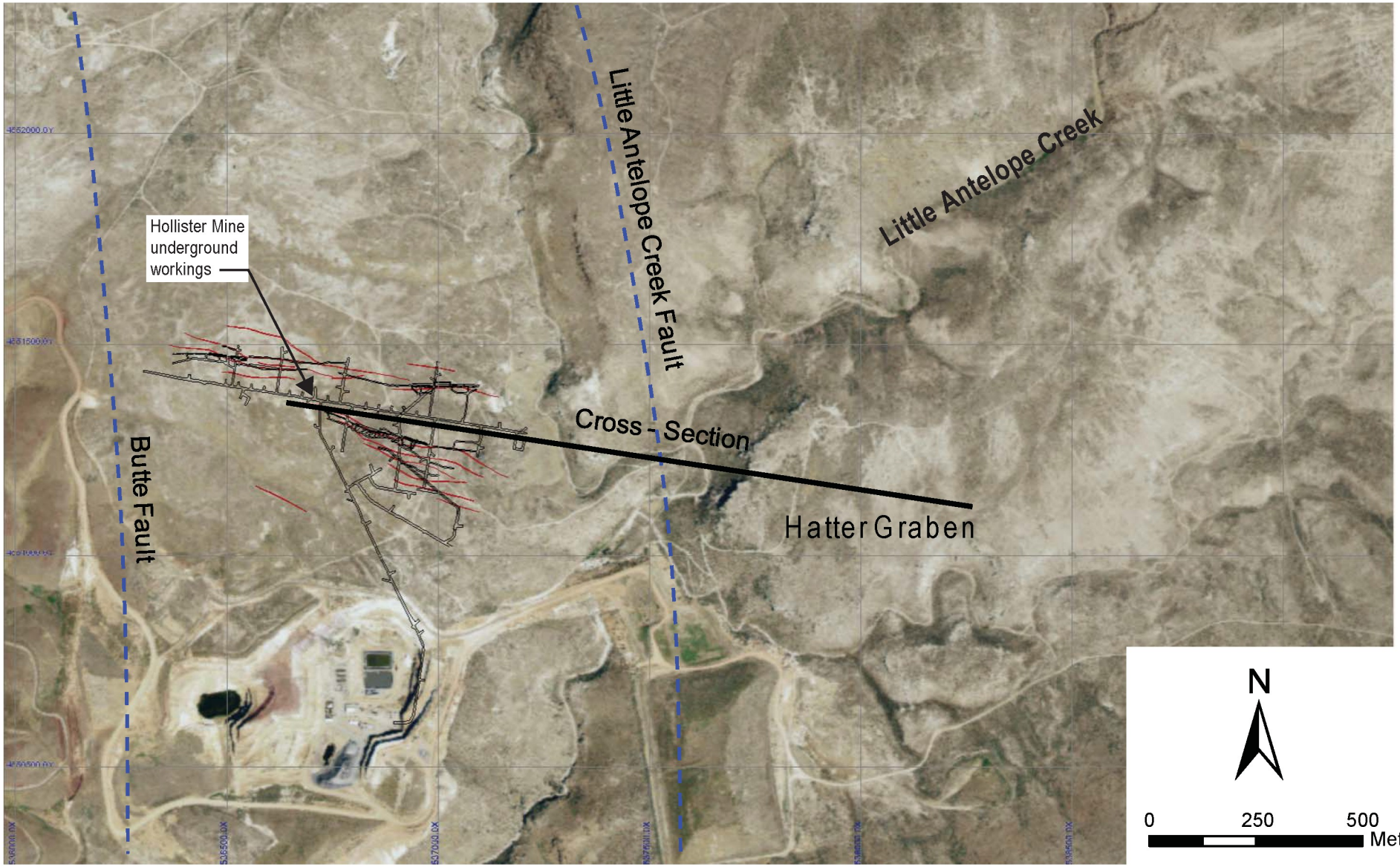

Source: Rodeo Creek Gold

BROWN AND CALDWELL	PROJECT 138301	SITE Rodeo Creek Gold - Hollister Mine	Figure 2-1
	DATE 7-7-10	TITLE Location of the Little Antelope Creek Fault and the Hatter Graben	

P:\BC_CAR\138301_Hollister_Mine_EIS\GIS\GRAPHICS

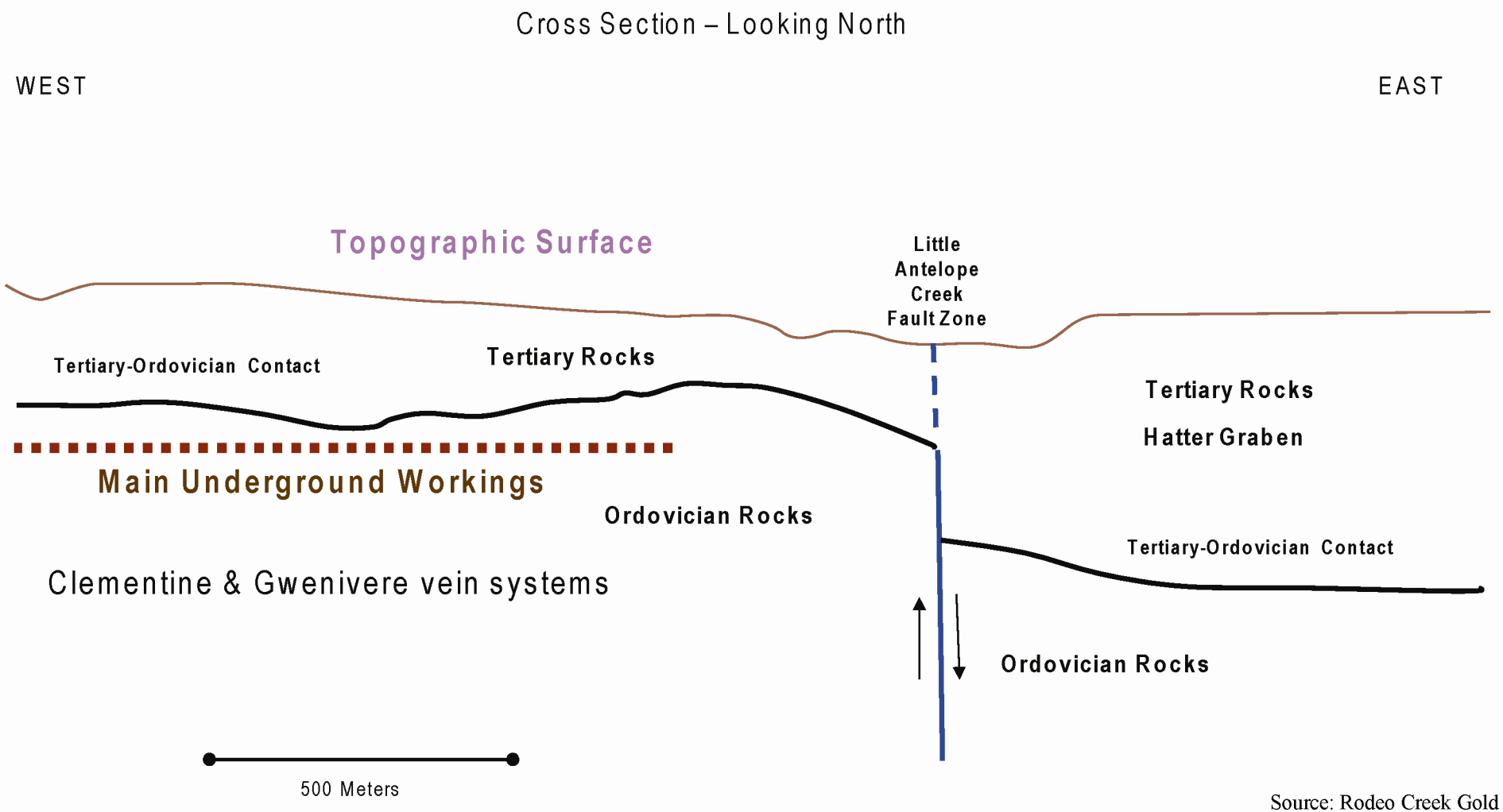

Source: Rodeo Creek Gold

P:\BC_CAR\138301_Hollister_Mine_EIS\GIS\GRAPHICS

BROWN AND CALDWELL	PROJECT 138301	SITE Rodeo Creek Gold - Hollister Mine	Figure 2-2
	DATE 10-28-10	TITLE Cross-Section Showing Offset Across the Little Antelope Creek Fault	

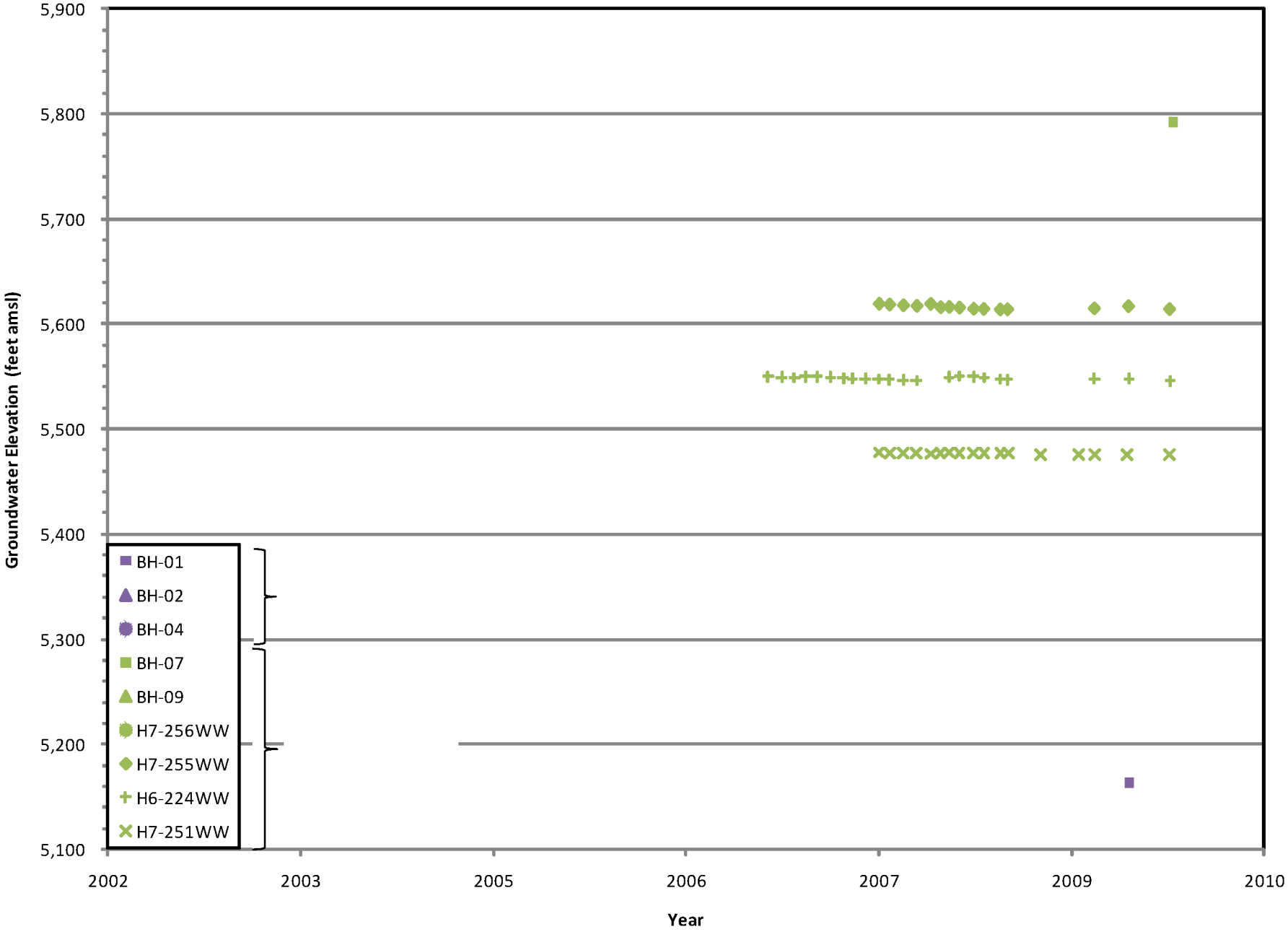

BROWN AND CALDWELL

PROJECT	SITE	
138301	Rodeo Creek Gold - Hollister Mine	Figure
DATE 6/30/10	TITLE Hydrographs of Ordovician Vinini Aquifer and Tertiary Volcanics Aquifer Monitor Wells	2-3

FILE: P:\BC_CAR\138301_Hollister_Mine_EIS\GIS\ARCMAPS\WORKING\Figure 2-3 Hydrographs.mxd

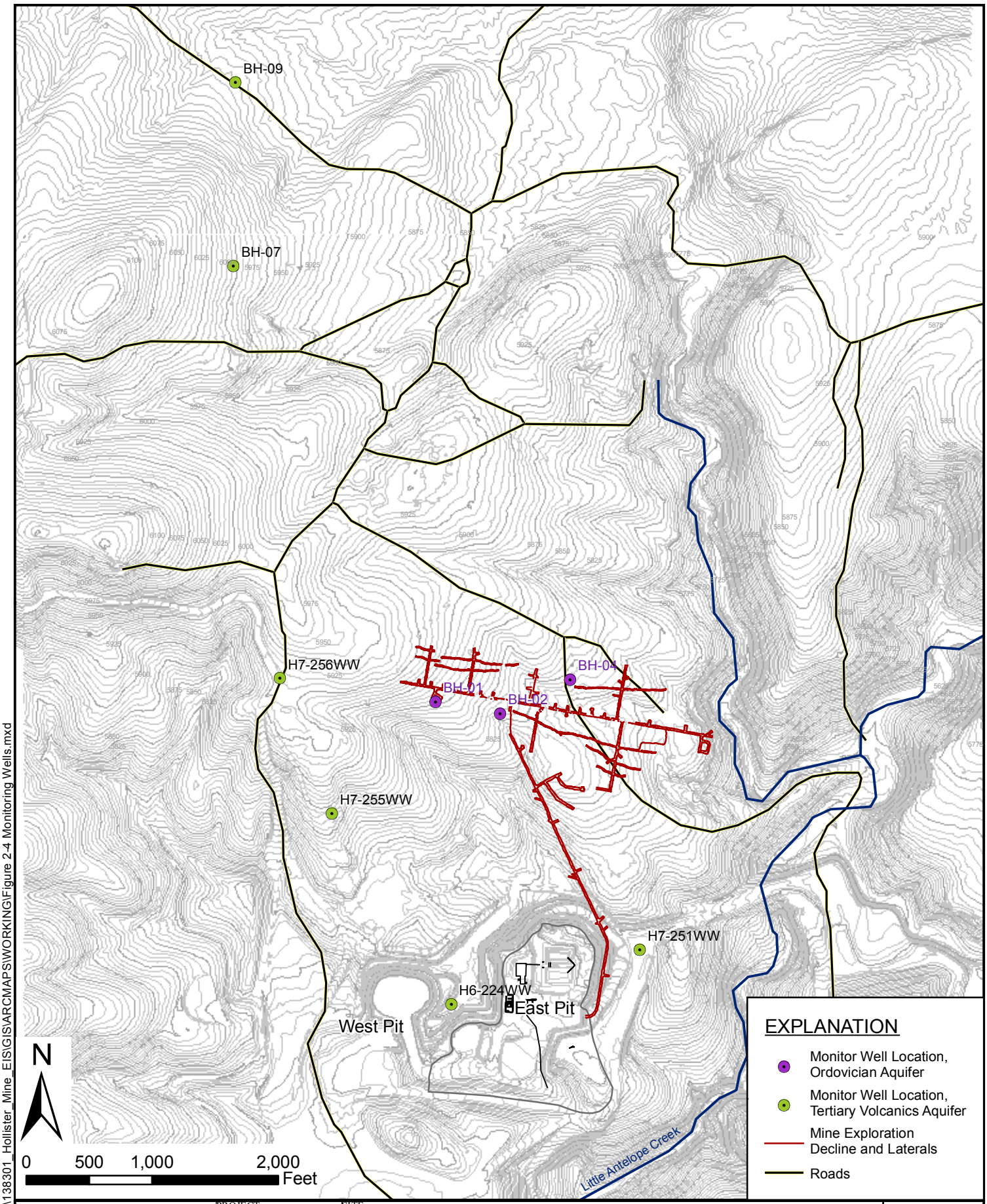

FILE: P:\BC_CAR\138301_Hollister_Mine_EIS\GIS\ARCMAPS\WORKING\Figure 2-4 Monitoring Wells.mxd

BROWN AND CALDWELL

PROJECT	SITE	
138301	Rodeo Creek Gold - Hollister Mine	Figure
DATE	TITLE	
6/30/10	Locations of Ordovician Vinini Aquifer and Tertiary Volcanics Aquifer Monitor Wells	2-4

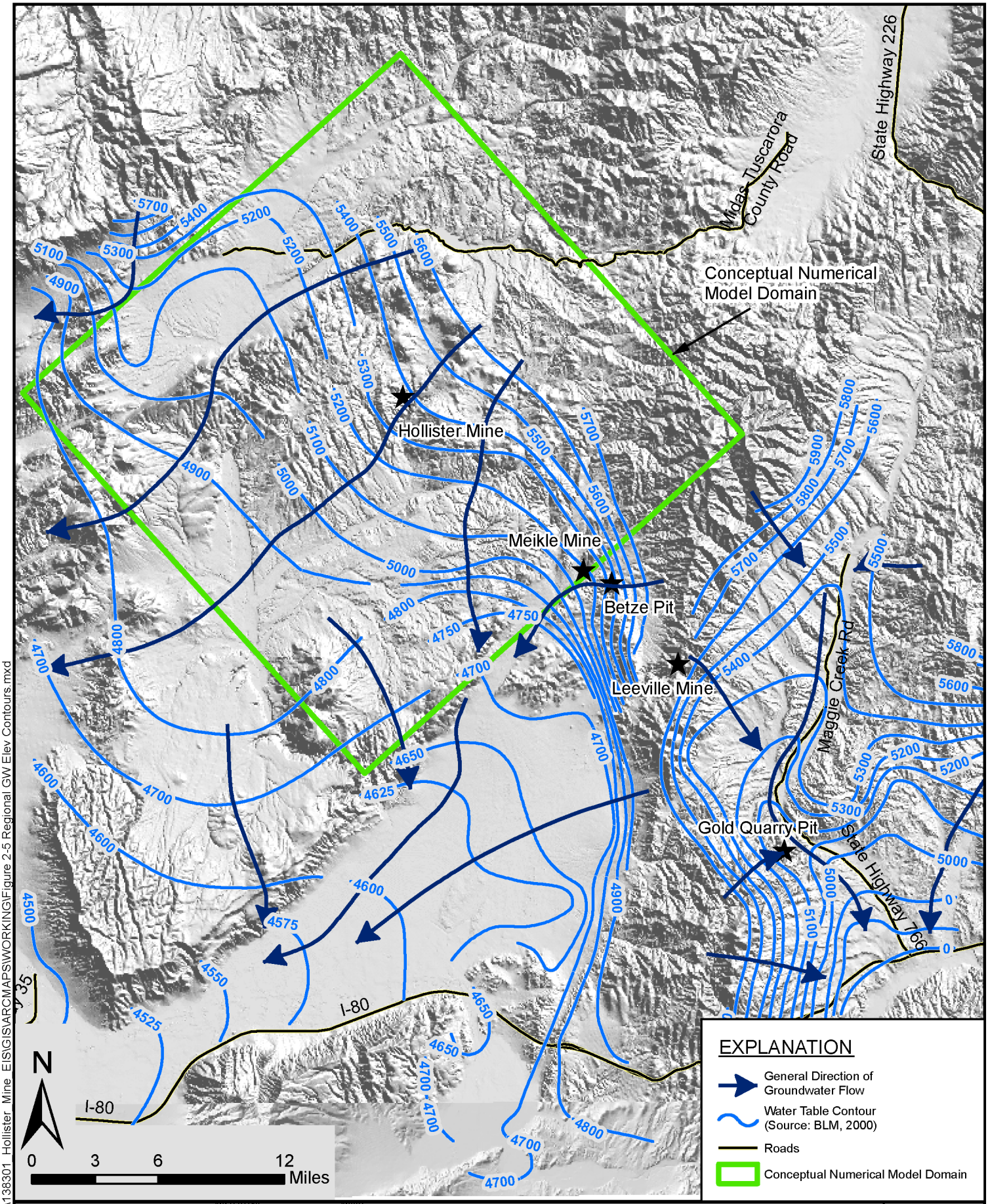

FILE: P:\BC_CAR\138301_Hollister_Mine_EIS\GIS\ARCMAPS\WORKING\Figure 2-5 Regional GW Elev Contours.mxd

BROWN AND CALDWELL

PROJECT	SITE	
138301	Rodeo Creek Gold - Hollister Mine	Figure
DATE	TITLE	
6/30/10	Regional Groundwater Elevation Contours	2-5

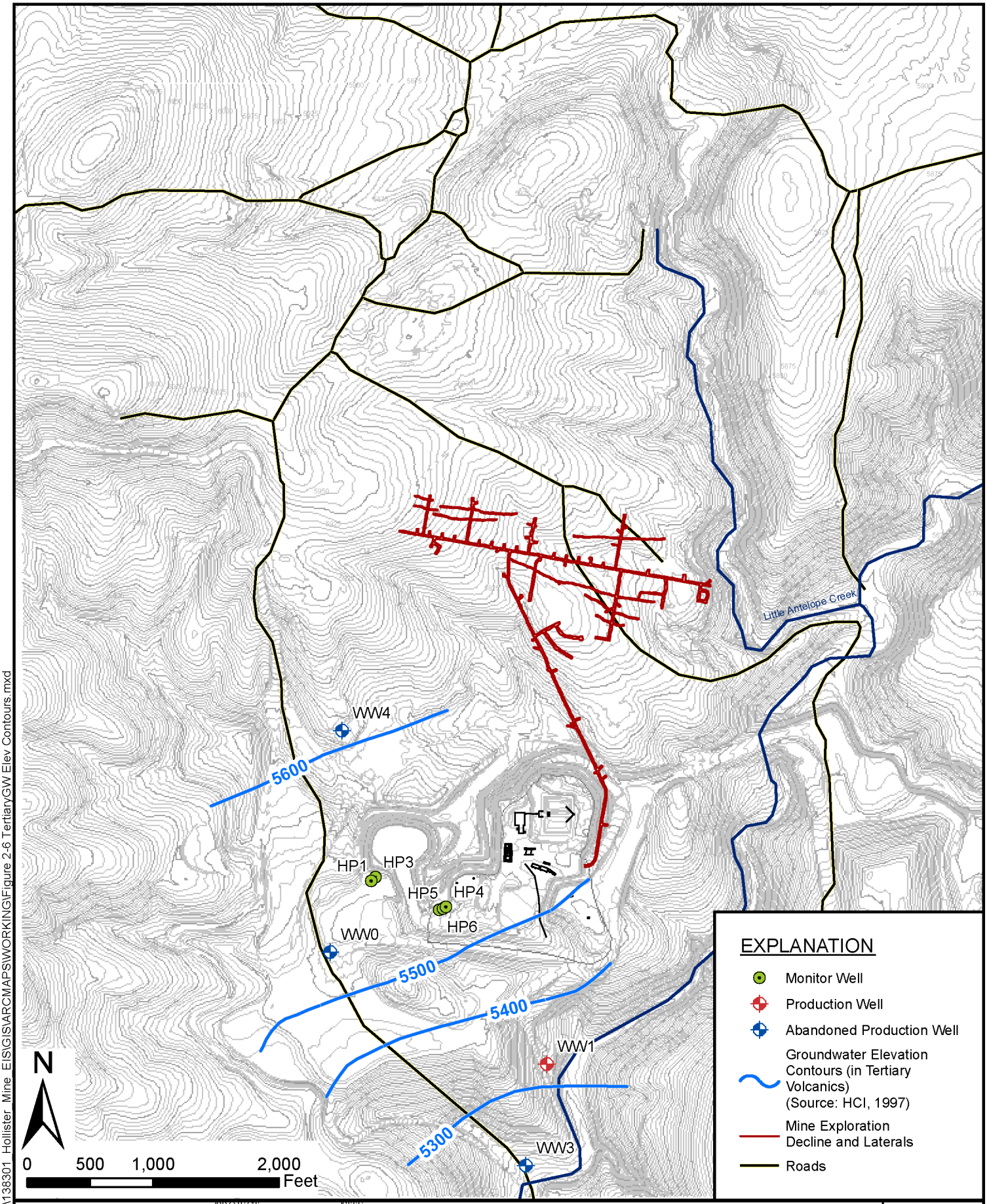

FILE: P:\BC_CAR\138301_Hollister_Mine_EIS\GIS\ARCMAPS\WORKING\Figure 2-6 TertiaryGW Elev Contours.mxd

BROWN AND CALDWELL

PROJECT	SITE	
138301	Rodeo Creek Gold - Hollister Mine	Figure
DATE	TITLE	
6/30/10	Generalized Tertiary Volcanics Aquifer Groundwater Elevation Contours	2-6

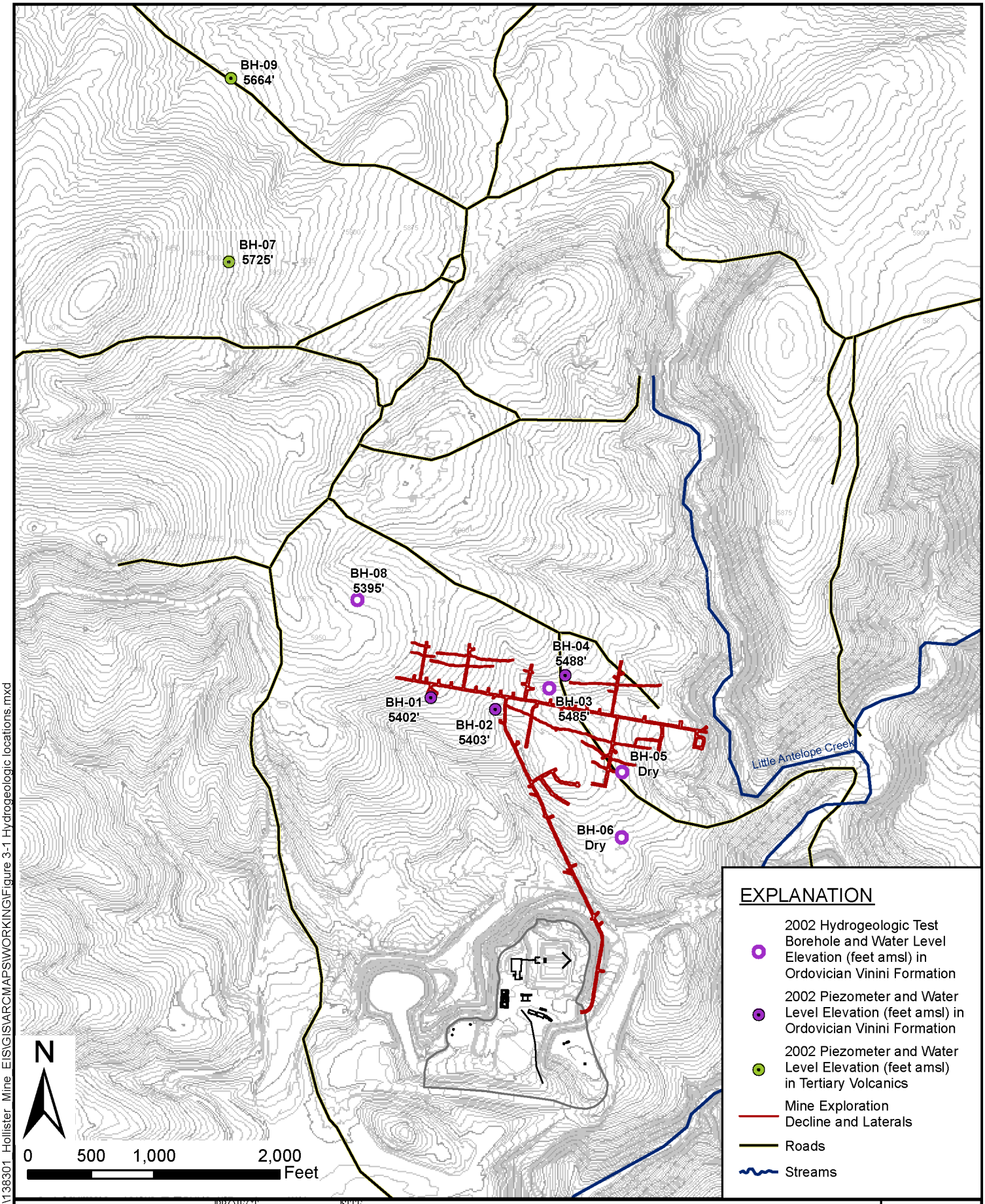

FILE: P:\BC_CAR\138301_Hollister_Mine_EIS\GIS\ARCMAPS\WORKING\Figure 3-1 Hydrogeologic locations.mxd

BROWN AND CALDWELL

PROJECT	SITE	
138301	Rodeo Creek Gold - Hollister Mine	Figure
DATE	TITLE	
6/30/10	2002 Hydrogeologic Investigation Piezometer and Borehole Location Map	3-1

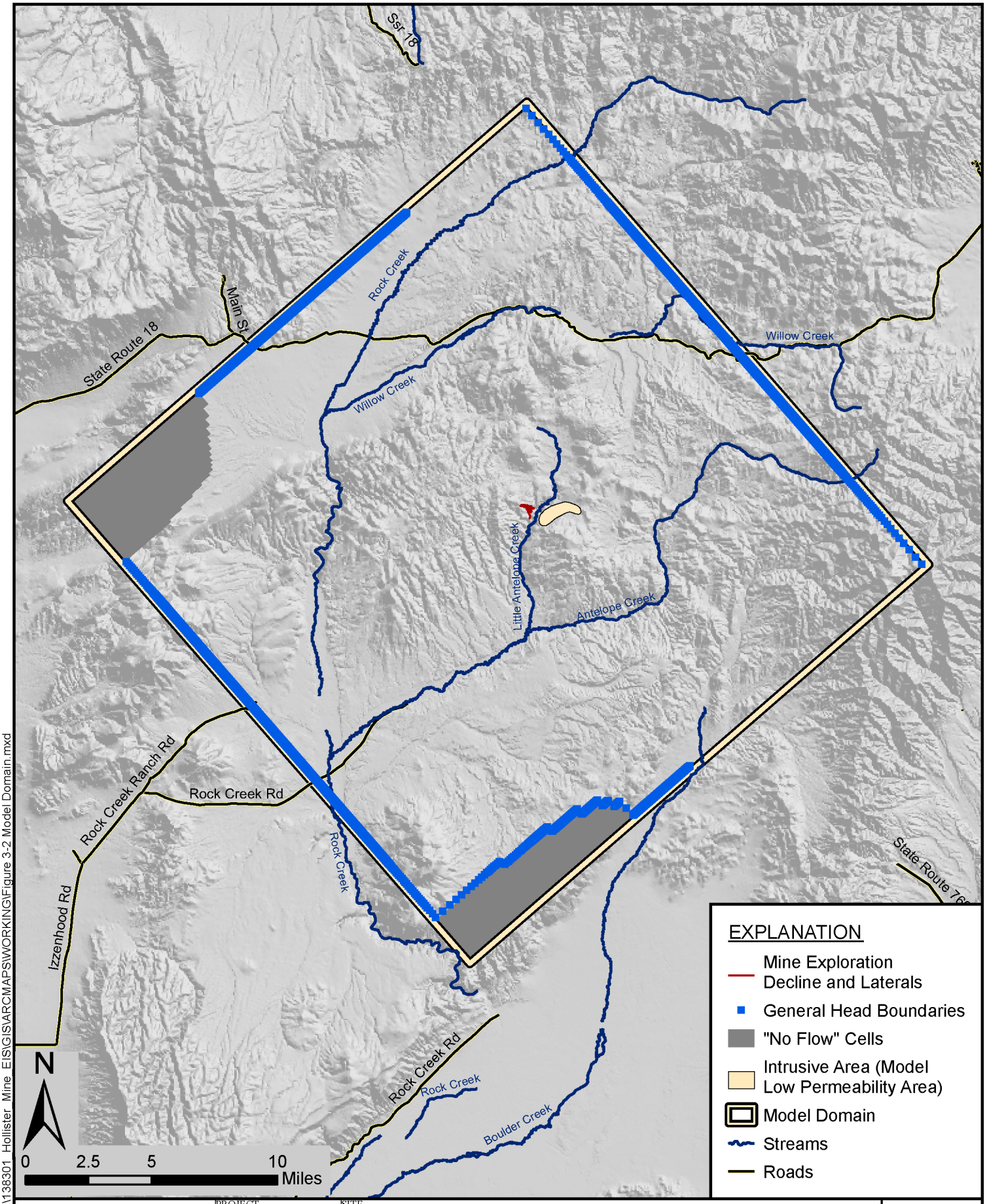

FILE: P:\BC_CAR\138301_Hollister_Mine_EIS\GIS\ARCMAPS\WORKING\Figure 3-2 Model Domain.mxd

BROWN AND CALDWELL

PROJECT	SITE	
138301	Rodeo Creek Gold - Hollister Mine	Figure
DATE	TITLE	
6/16/10	Model Domain and Boundary Conditions	3-2

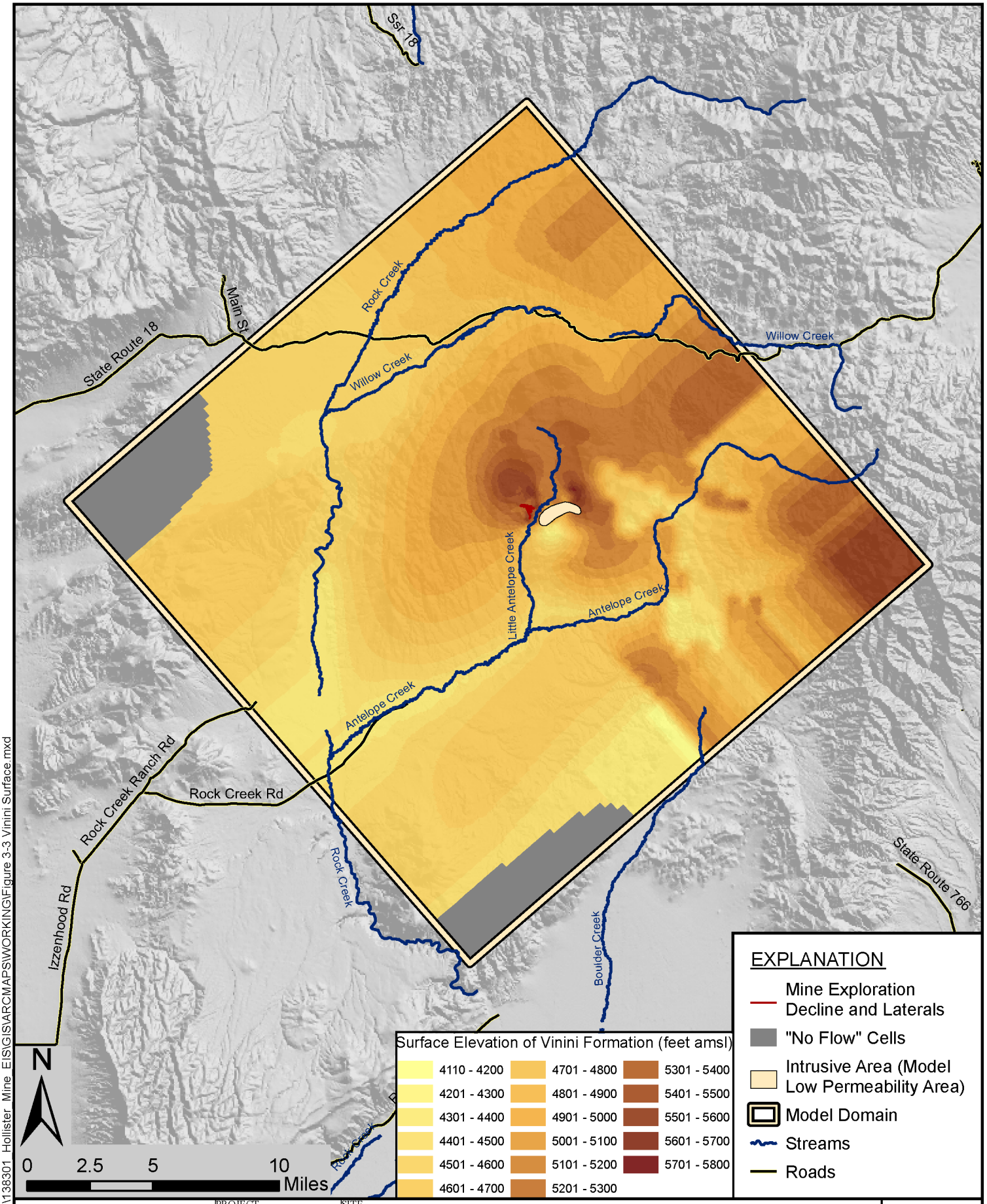

FILE: P:\BC_CAR\138301_Hollister_Mine_EIS\GIS\ARCMAPS\WORKING\Figure 3-3 Vinini Surface.mxd

BROWN AND CALDWELL

PROJECT	SITE	
138301	Rodeo Creek Gold - Hollister Mine	Figure
DATE	TITLE	
6/16/10	Surface of Vinini Formation	3-3

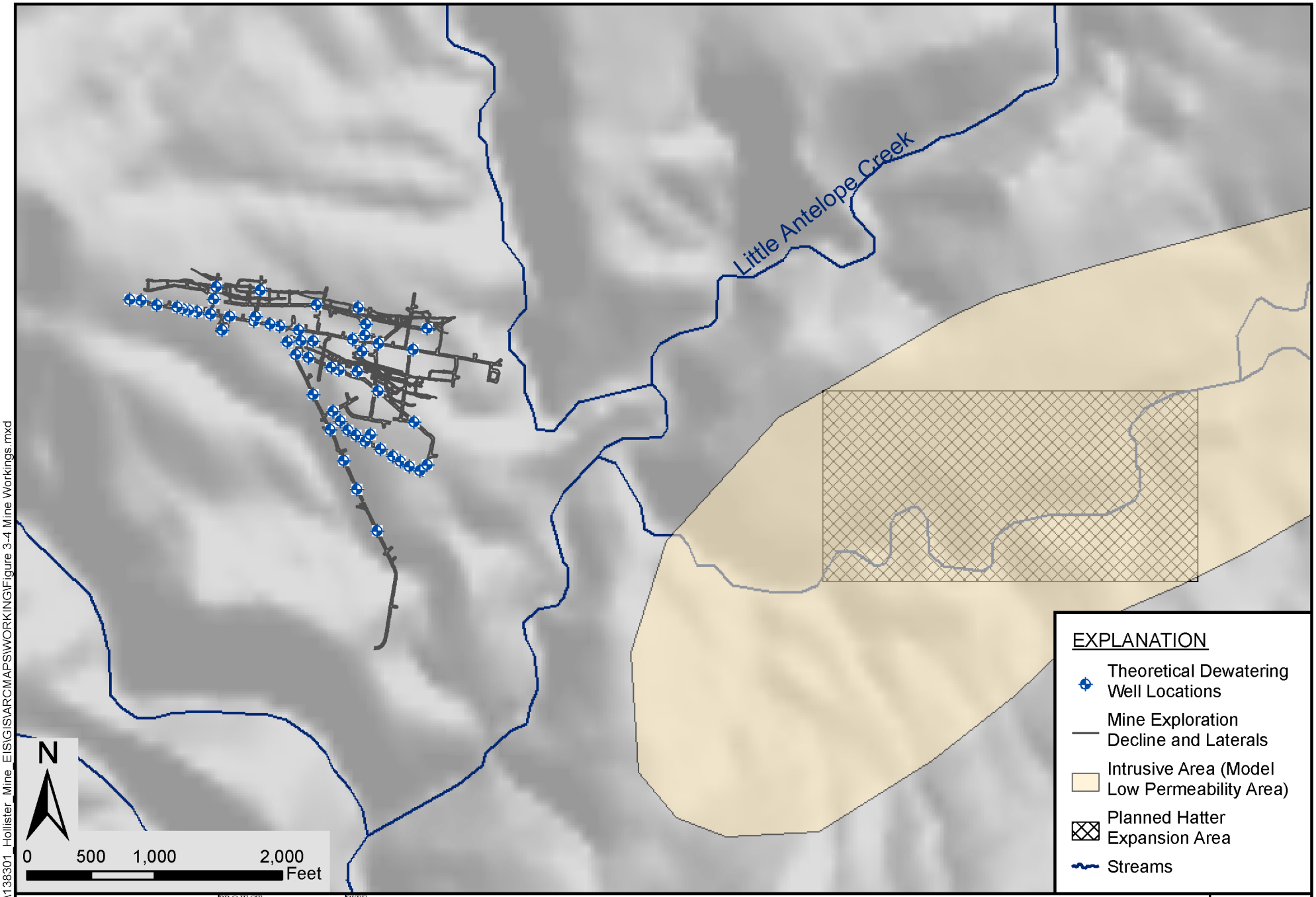

BROWN AND CALDWELL

PROJECT	SITE	
138301	Rodeo Creek Gold - Hollister Mine	Figure
DATE	TITLE	
6/16/10	Mine Workings with Theoretical Dewatering Locations	3-4

FILE: P:\BC_CAR\138301_Hollister_Mine_EIS\GIS\ARCMAPS\WORKING\Figure 3-4 Mine Workings.mxd

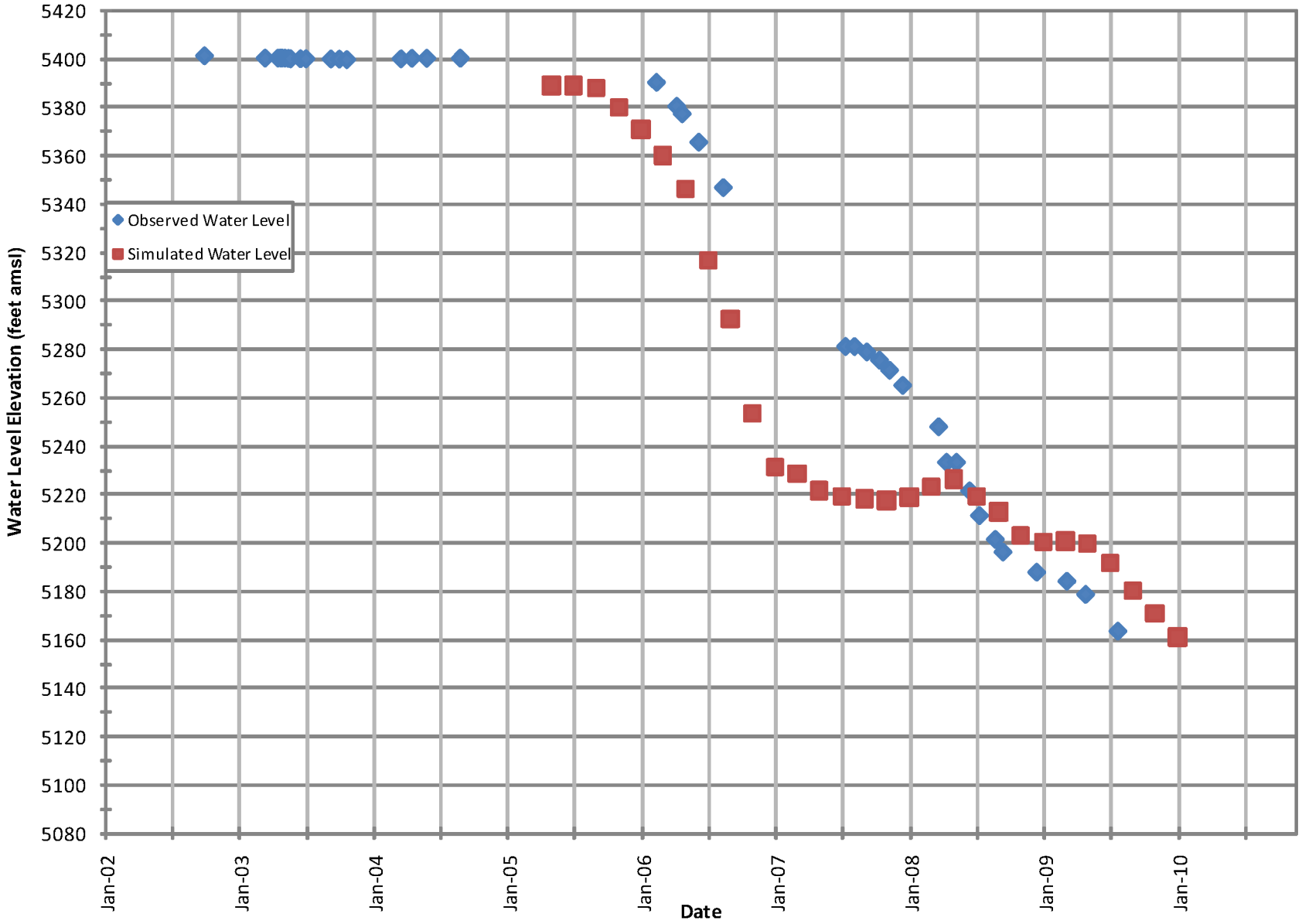

BROWN AND CALDWELL

PROJECT	SITE	
138301	Rodeo Creek Gold - Hollister Mine	Figure
DATE 6/30/10	TITLE BH-01 Observed Versus Simulated Water Levels	4-1

FILE: P:\BC_CAR\138301_Hollister_Mine_EIS\GIS\ARCMAPS\WORKING\Figure 4-1 BH-1 Calibration Plot.mxd

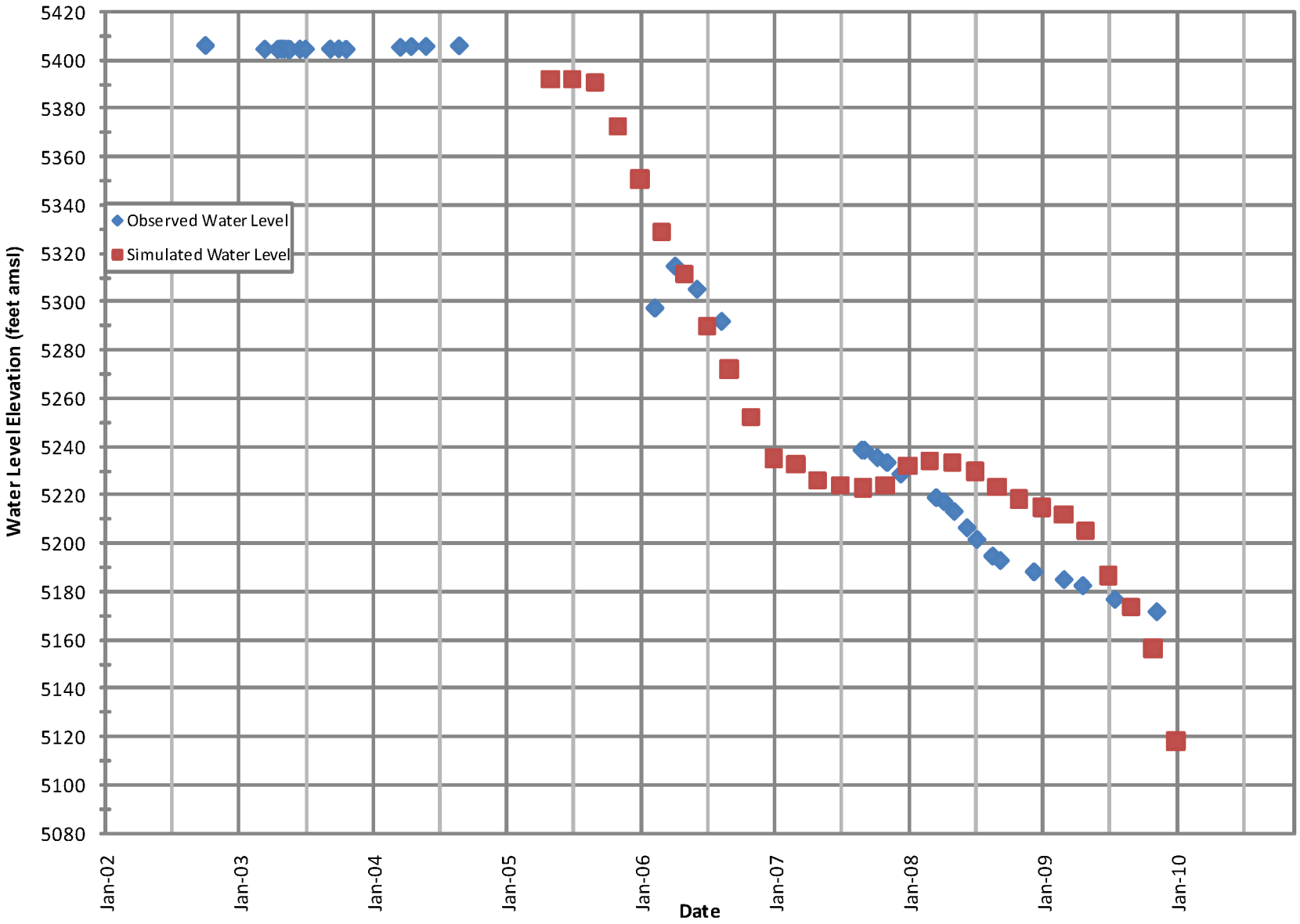

FILE: P:\BC_CAR\138301_Hollister_Mine_EIS\GIS\ARCMAPS\WORKING\Figure 4-2 BH-2 Calibration Plot.mxd

BROWN AND CALDWELL

PROJECT	SITE	
138301	Rodeo Creek Gold - Hollister Mine	Figure
DATE	TITLE	
6/30/10	BH-02 Observed Versus Simulated Water Levels	4-2

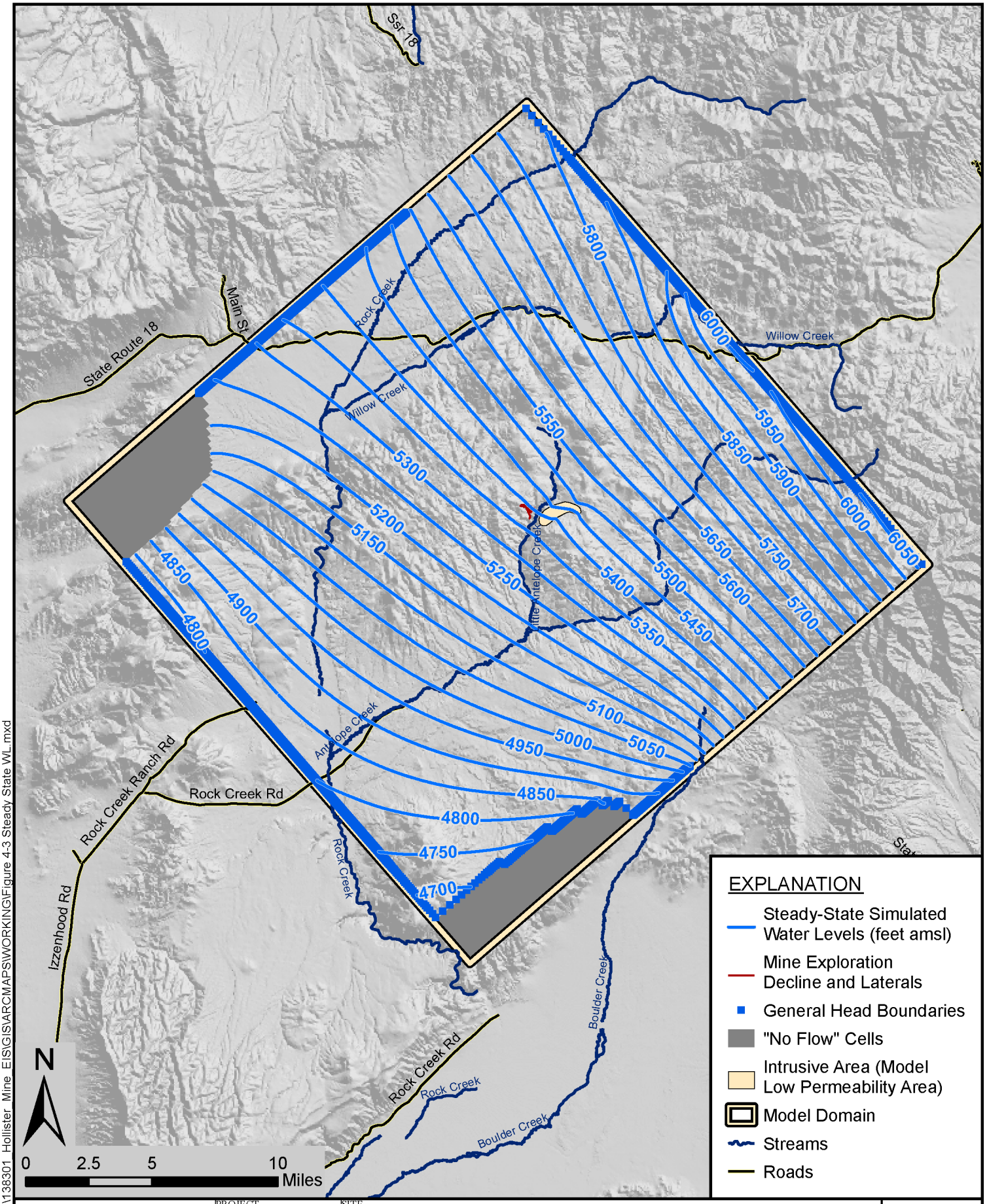

FILE: P:\BC_CAR\138301_Hollister_Mine_EIS\GIS\ARCMAPS\WORKING\Figure 4-3 Steady State WL.mxd

BROWN AND CALDWELL	PROJECT 138301	SITE Rodeo Creek Gold - Hollister Mine	Figure 4-3
	DATE 6/16/10	TITLE Steady-State Simulated Water Levels	

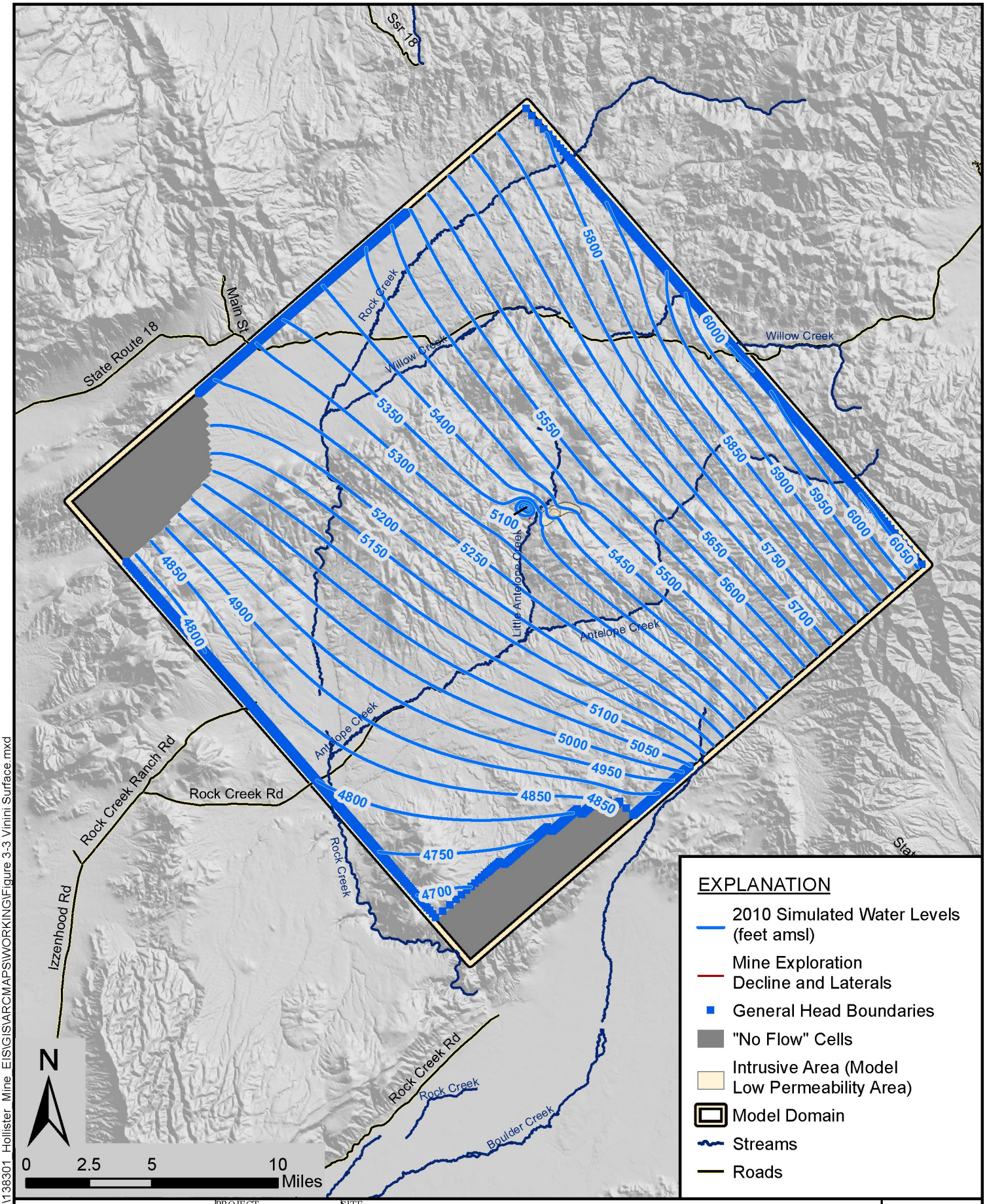

FILE: P:\BC_CAR\138301_Hollister_Mine_EIS\GIS\ARCMAPS\WORKING\Figure 3-3 Vinini Surface.mxd

BROWN AND CALDWELL

PROJECT	SITE	
138301	Rodeo Creek Gold - Hollister Mine	Figure
DATE	TITLE	
6/16/10	Transient Water Levels - 2010	4-4

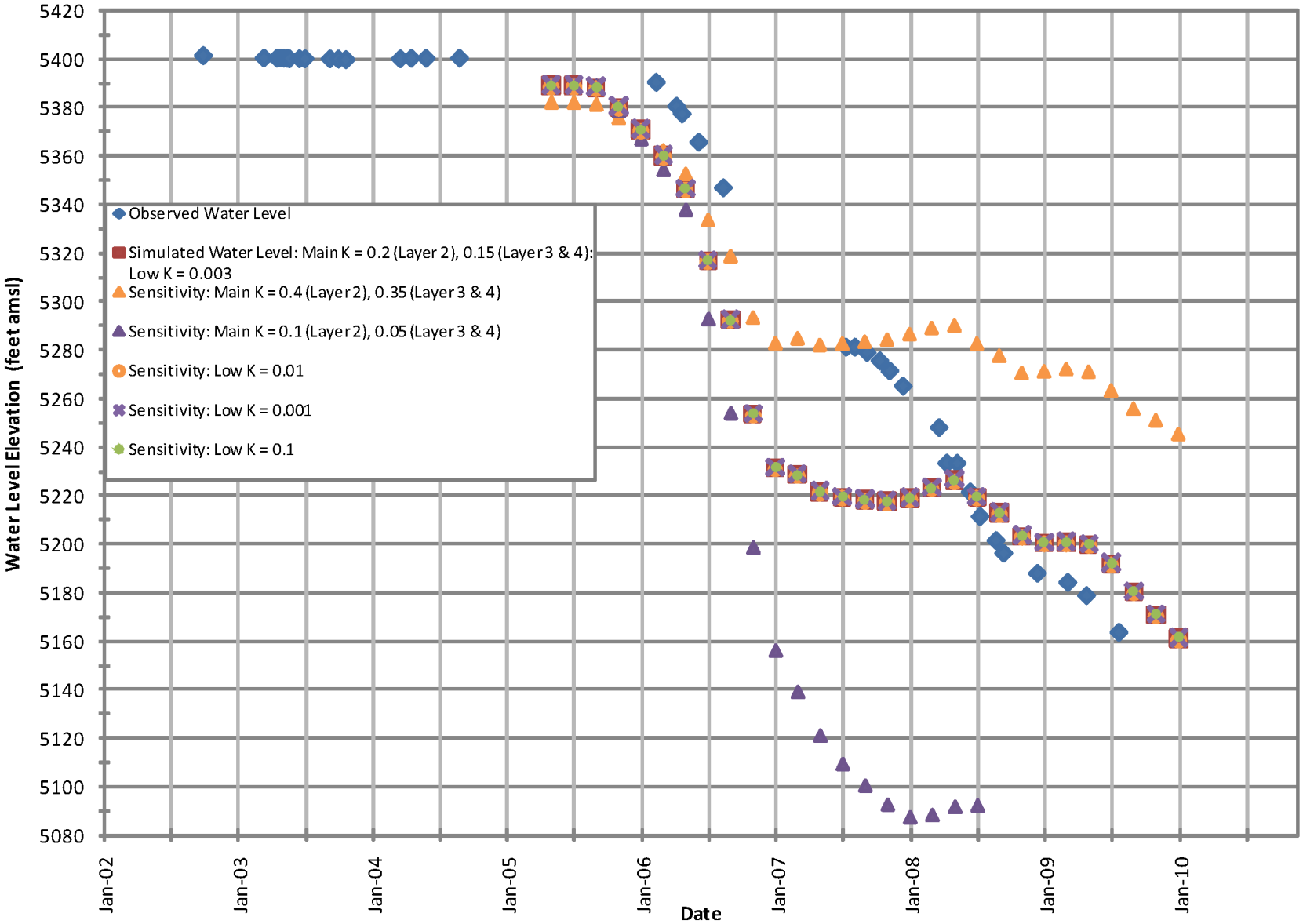

Note: K = Horizontal Hydraulic Conductivity (values in feet per day)
Low K = Horizontal Hydraulic Conductivity in Hatter low permeability area

BROWN AND CALDWELL

PROJECT	SITE	
138301	Rodeo Creek Gold - Hollister Mine	Figure
DATE 6/30/10	TITLE BH-01 Hydraulic Conductivity Sensitivity Plot	4-5

FILE: P:\BC_CAR\138301_Hollister_Mine_EIS\GIS\ARCMAPS\WORKING\Figure 4-5 BH-1 Sens K Chart.mxd

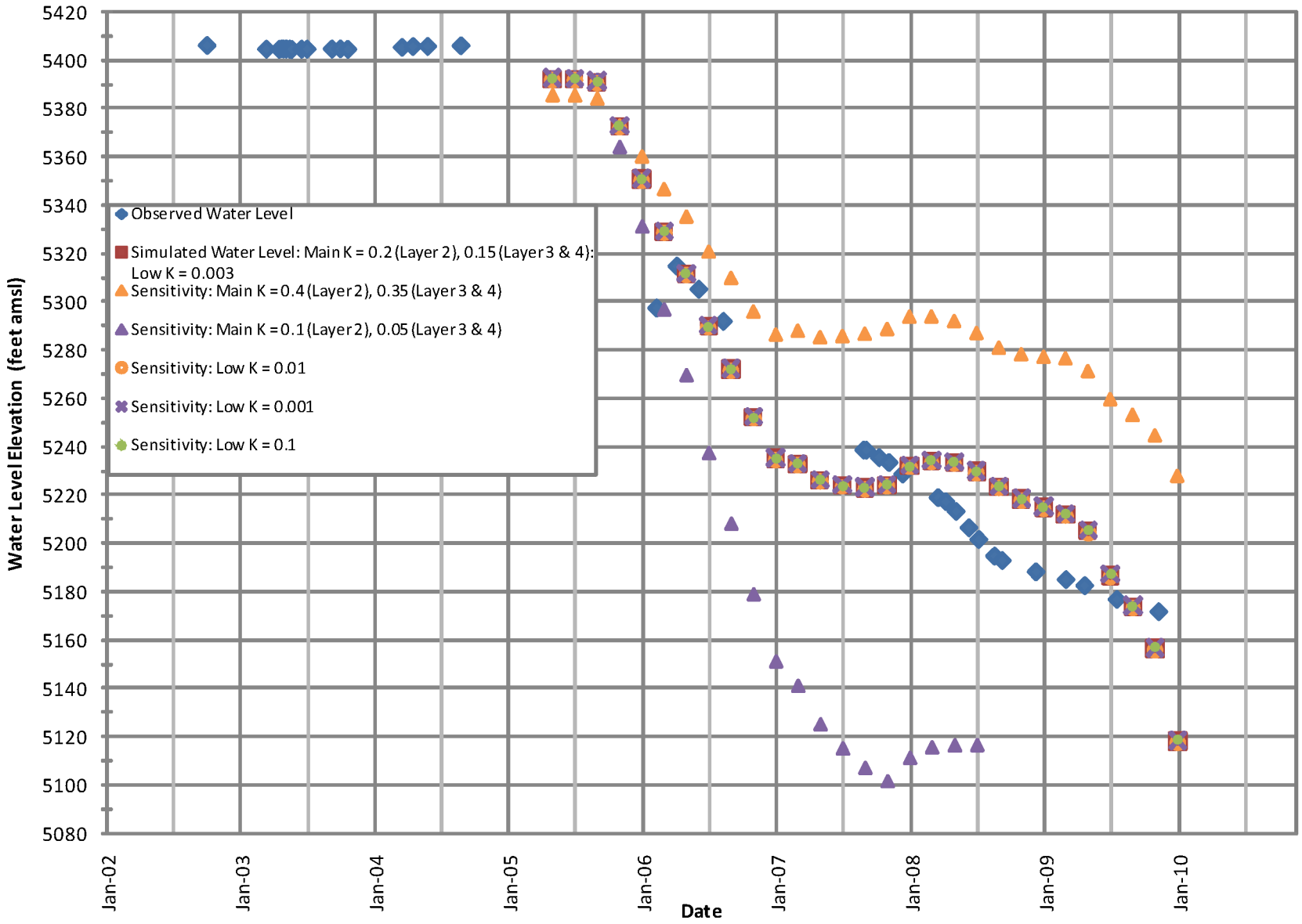

Note: K = Horizontal Hydraulic Conductivity (values in feet per day)
Low K = Horizontal Hydraulic Conductivity in Hatter low permeability area

BROWN AND CALDWELL	PROJECT 138301	SITE Rodeo Creek Gold - Hollister Mine	Figure 4-6
	DATE 6/30/10	TITLE BH-02 Hydraulic Conductivity Sensitivity Plot	

FILE: P:\BC_CAR\138301_Hollister_Mine_EIS\GIS\ARCMAPS\WORKING\Figure 4-6 BH-2 Sens K Chart.mxd

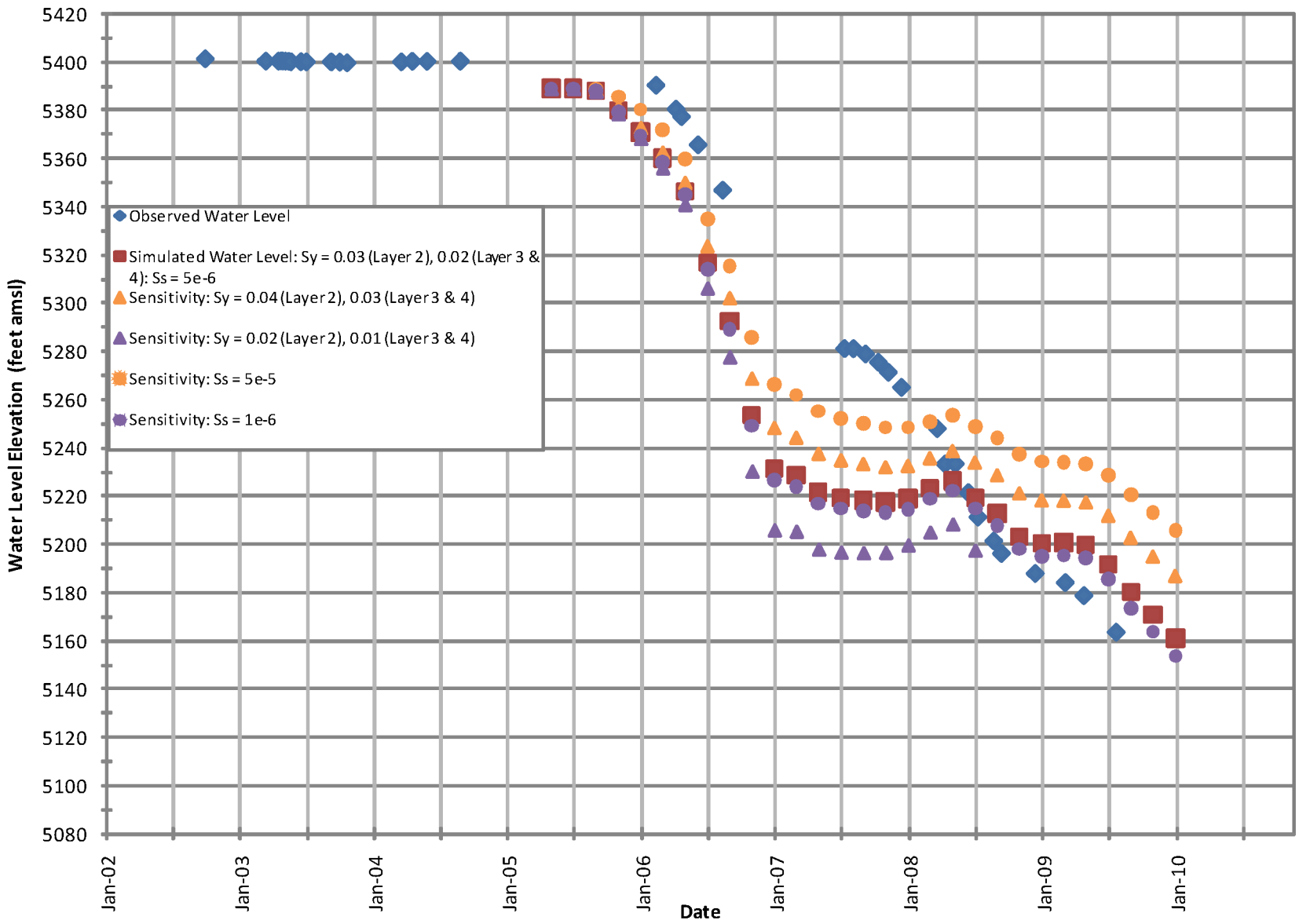

Note: Sy = Specific yield, Ss = Specific Storage

FILE: P:\BC_CAR\138301_Hollister_Mine_EIS\GIS\ARCMAPS\WORKING\Figure 4-7 BH-1 Sens Storage Chart.mxd

BROWN AND CALDWELL	PROJECT 138301	SITE Rodeo Creek Gold - Hollister Mine	Figure 4-7
	DATE 6/30/10	TITLE BH-01 Storage Values Sensitivity Plot	

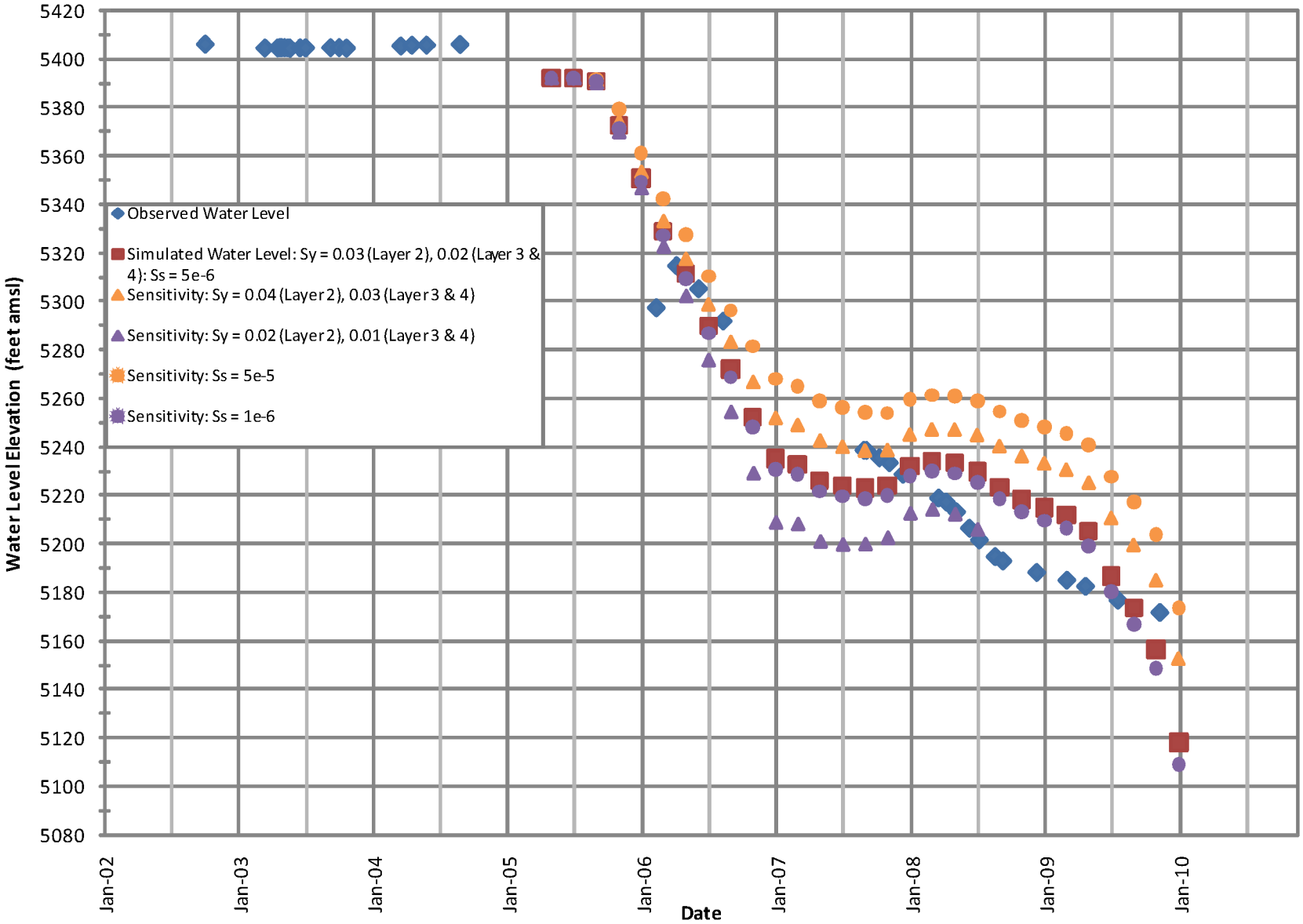

Note: Sy = Specific yield, Ss = Specific Storage

FILE: P:\BC_CAR\138301_Hollister_Mine_EIS\GIS\ARCMAPS\WORKING\Figure 4-8 BH-2 Sens Storage Chart.mxd

BROWN AND CALDWELL	PROJECT 138301	SITE Rodeo Creek Gold - Hollister Mine	Figure 4-8
	DATE 6/30/10	TITLE BH-02 Storage Values Sensitivity Plot	

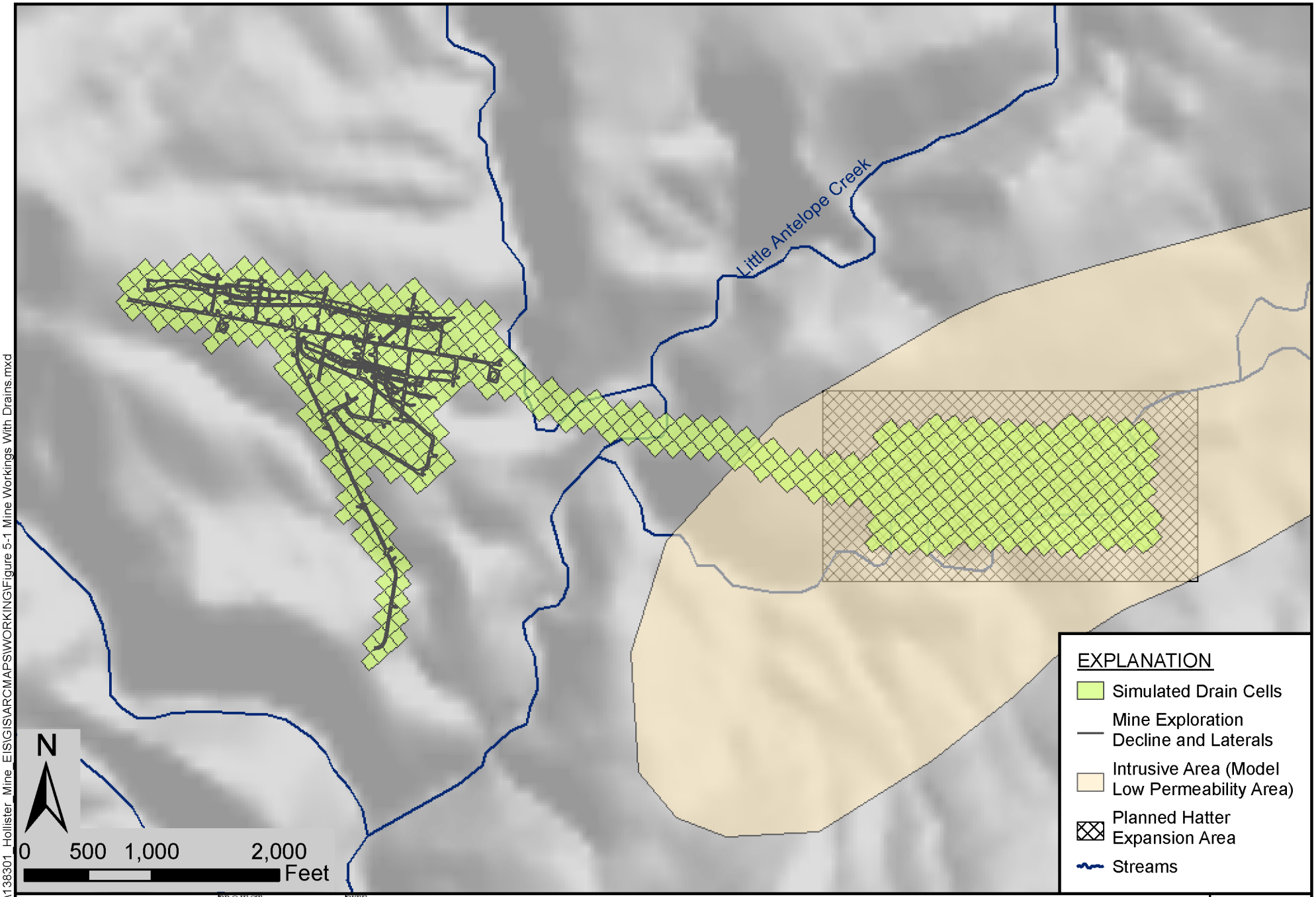

BROWN AND CALDWELL

PROJECT	SITE	
138301	Rodeo Creek Gold - Hollister Mine	Figure
DATE 6/16/10	TITLE Drain Locations - Predictive Simulation	5-1

FILE: P:\BC_CAR\138301_Hollister_Mine_EIS\GIS\ARCMAPS\WORKING\Figure 5-1 Mine Workings With Drains.mxd

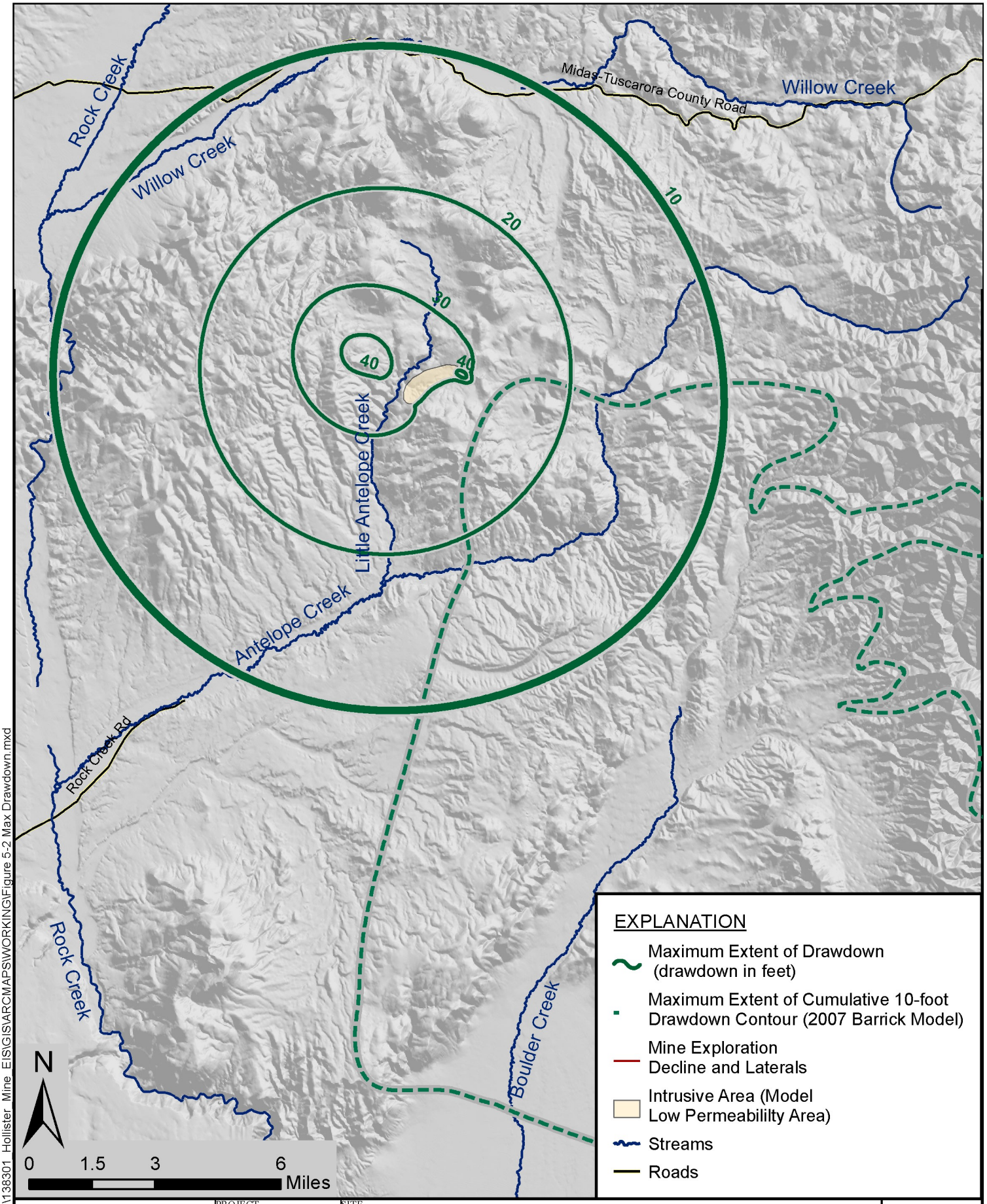

FILE: P:\BC_CAR\138301_Hollister_Mine_EIS\GIS\ARCMAPS\WORKING\Figure 5-2 Max Drawdown.mxd

BROWN AND CALDWELL

PROJECT	SITE	
138301	Rodeo Creek Gold - Hollister Mine	Figure
DATE	TITLE	
6/16/10	Simulated Maximum Extent of 10-Foot Drawdown (2070)	5-2

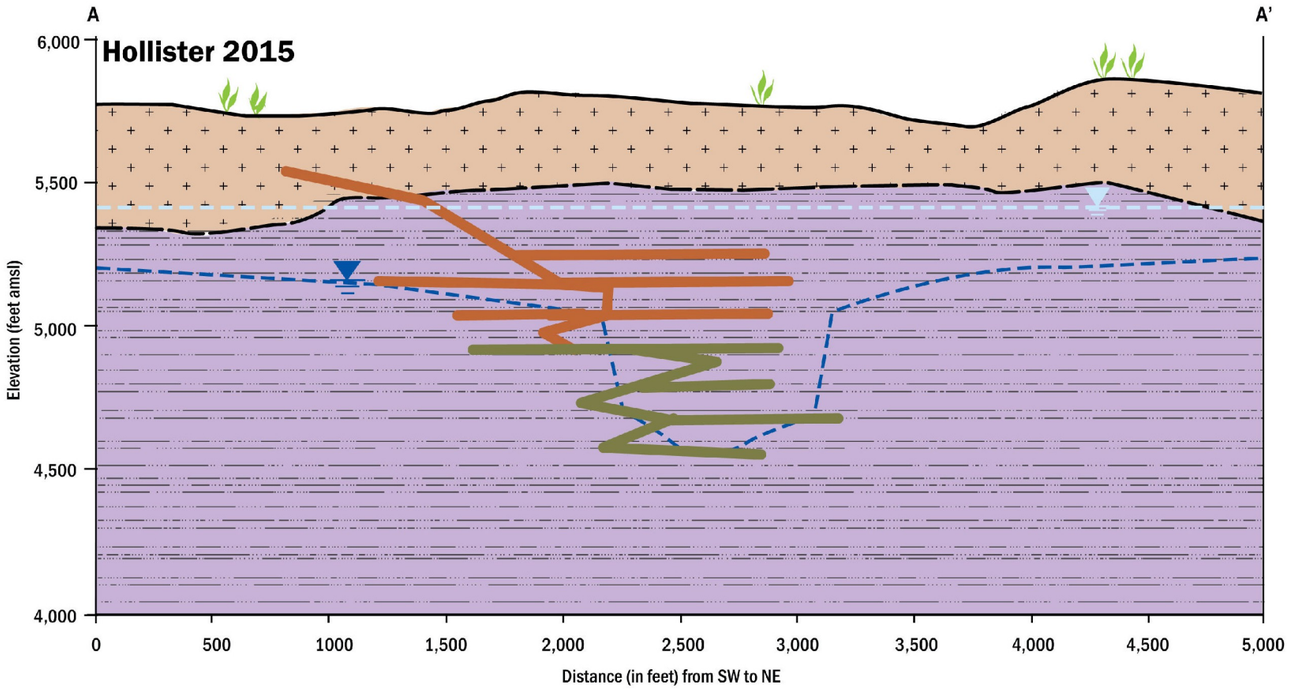

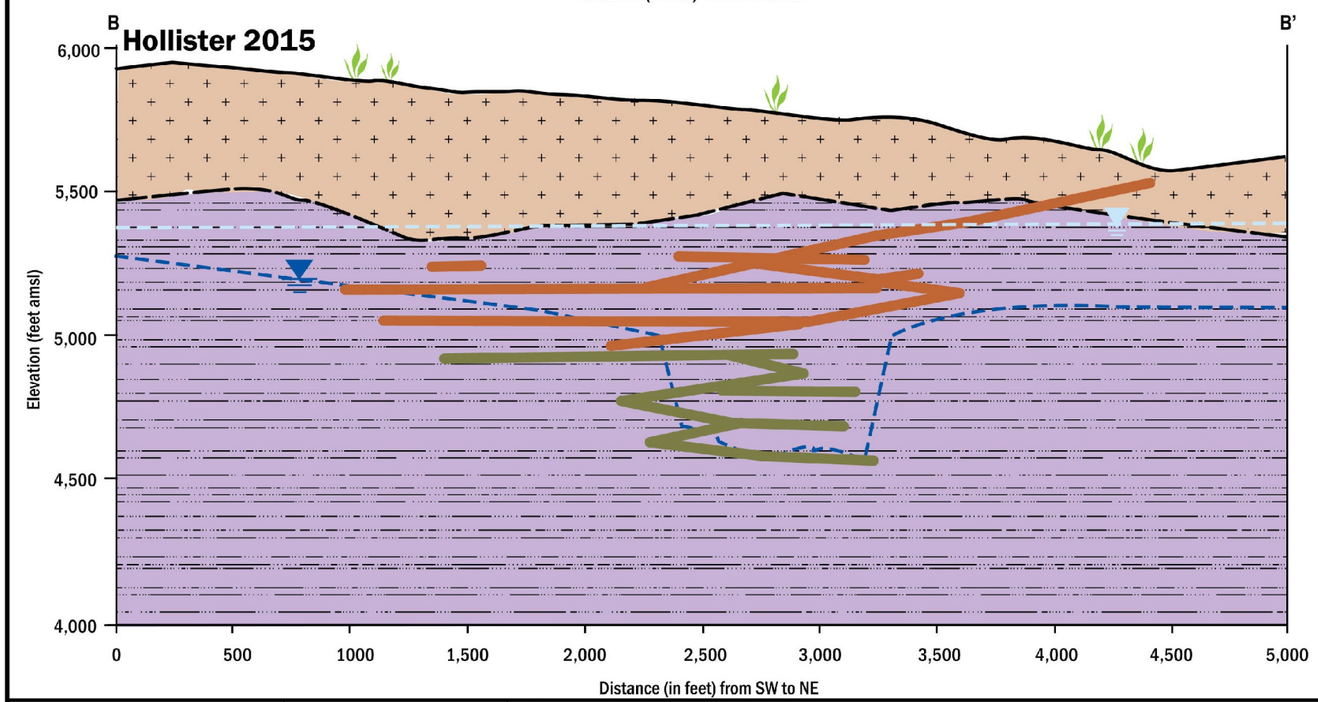

EXPLANATION

- Land Surface
- Simulated Groundwater Piezometric Surface (Confined)
- Simulated Recovered Piezometric Surface (Confined)
- Tertiary-Ordovician Contact
- Tertiary Volcanics
- Ordovician Vinini Formation
- Mine Workings, March 2010
- Future Mine Workings

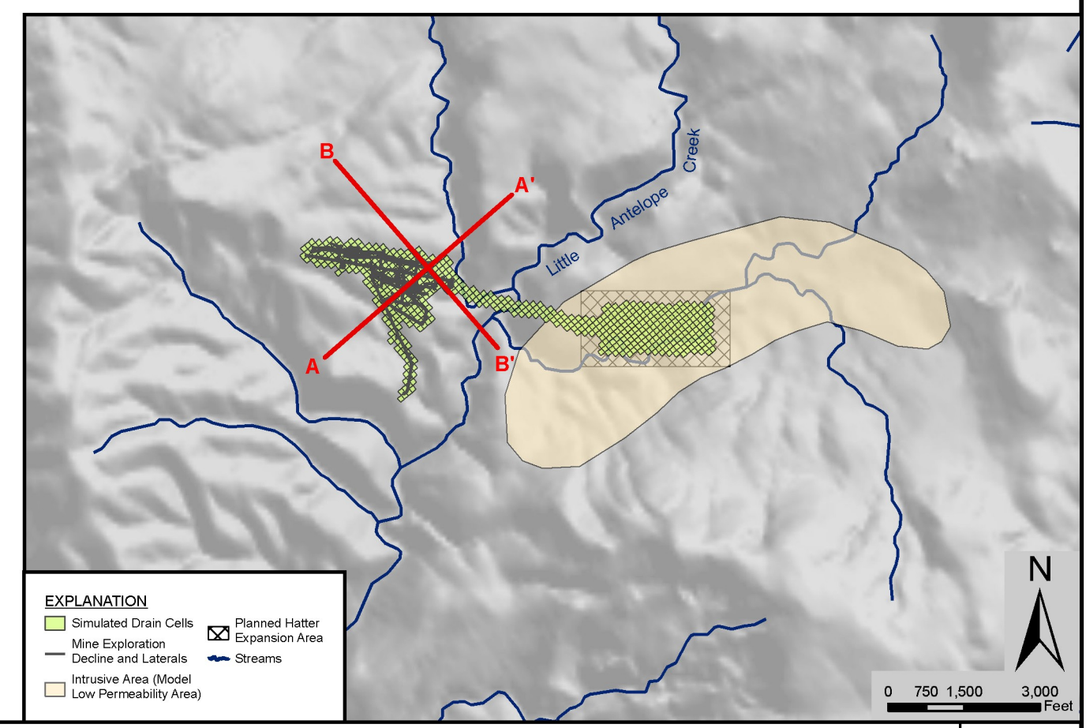

BROWN AND CALDWELL

PROJECT	SITE	
138301	Rodeo Creek Gold - Hollister Mine	Figure
DATE 6/16/10	TITLE Hollister Mine Cross Sections - 2015	5-3

FILE: P:\BC_CAR\138301_Hollister_Mine_EIS\GIS\ARCMAPS\WORKING\Figure 5-3 Hollister Cross Sections.mxd

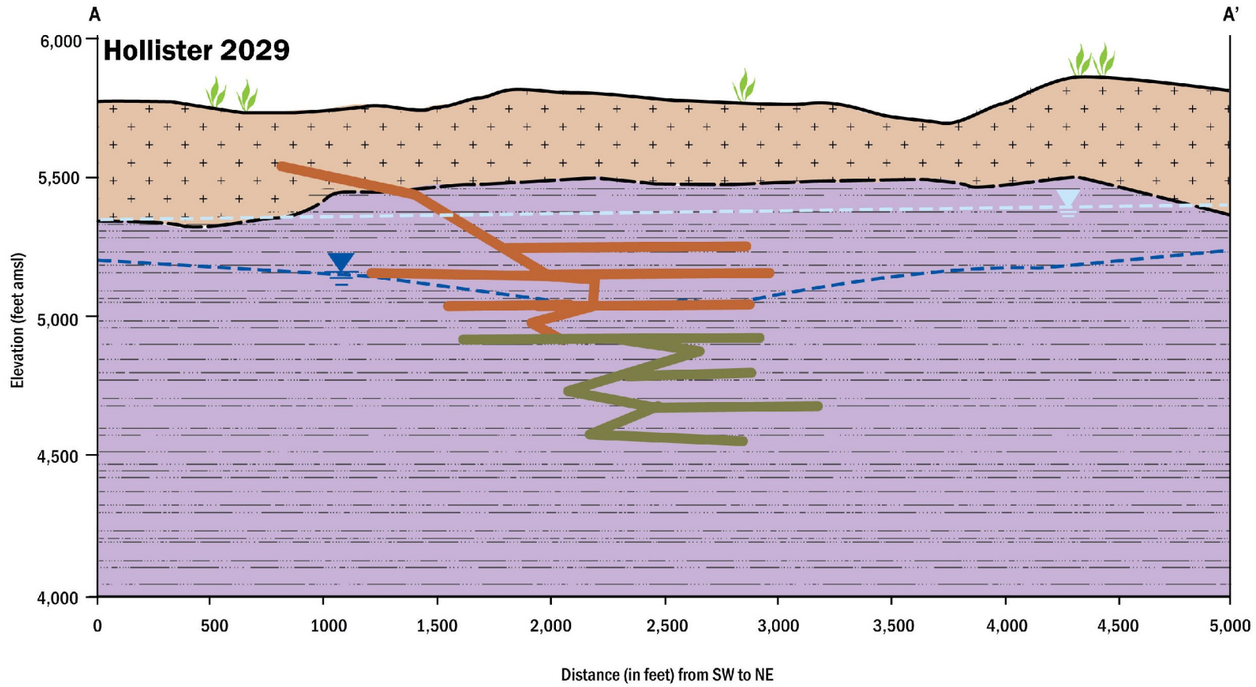

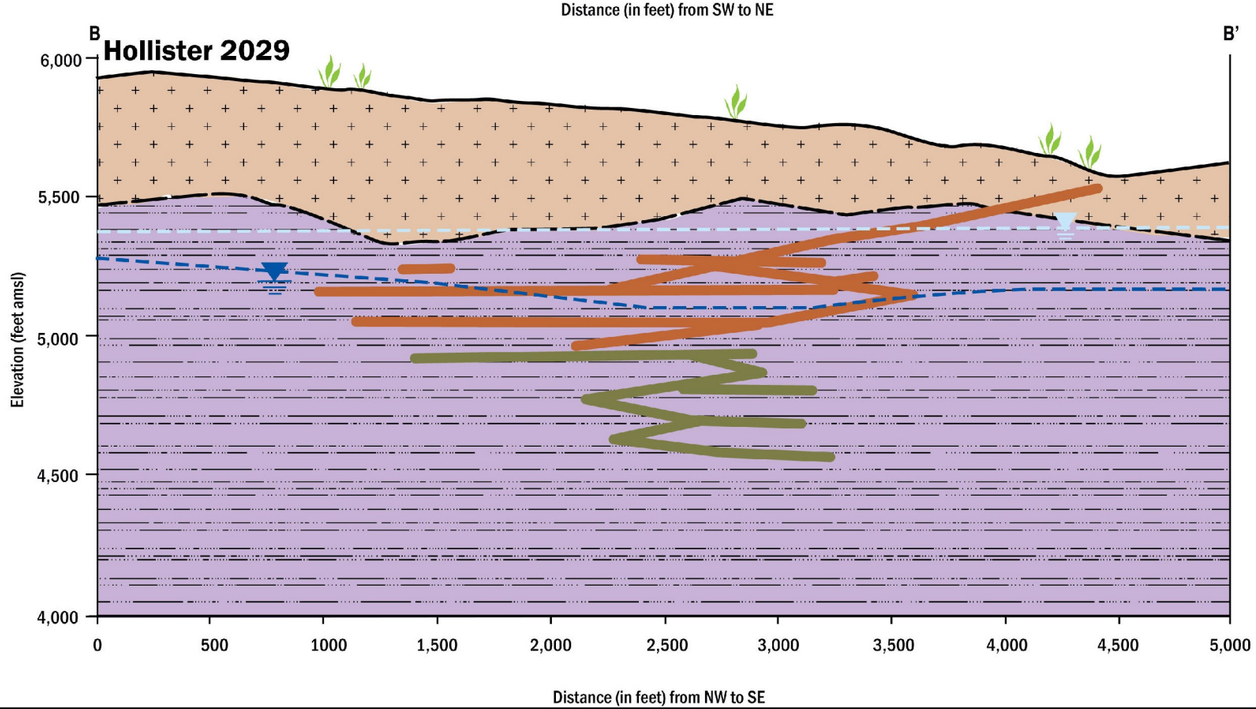

EXPLANATION

- Land Surface
- Simulated Groundwater Piezometric Surface (Confined)
- Simulated Recovered Piezometric Surface (Confined)
- Tertiary-Ordovician Contact
- Tertiary Volcanics
- Ordovician Vinini Formation
- Mine Workings, March 2010
- Future Mine Workings

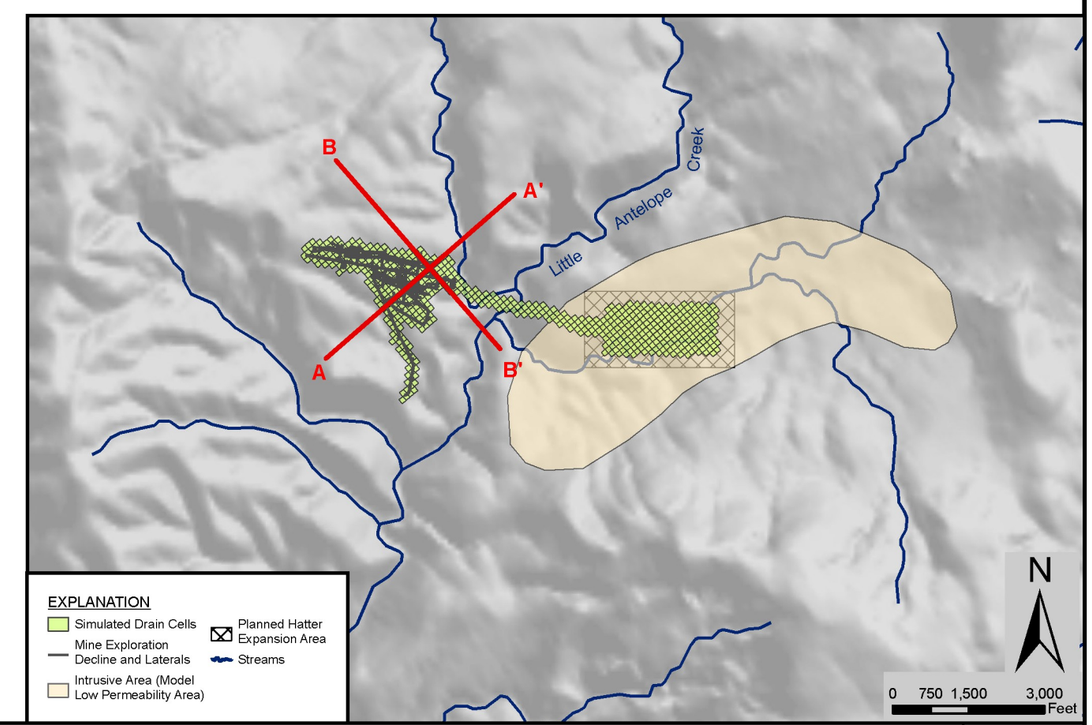

BROWN AND CALDWELL

PROJECT	SITE	
138301	Rodeo Creek Gold - Hollister Mine	Figure
DATE 6/16/10	TITLE Hollister Mine Cross Sections - 2029	5-4

FILE: P:\BC_CAR\138301_Hollister_Mine_EIS\GIS\ARCMAPS\WORKING\Figure 5-3 Hollister Cross Sections 2.mxd

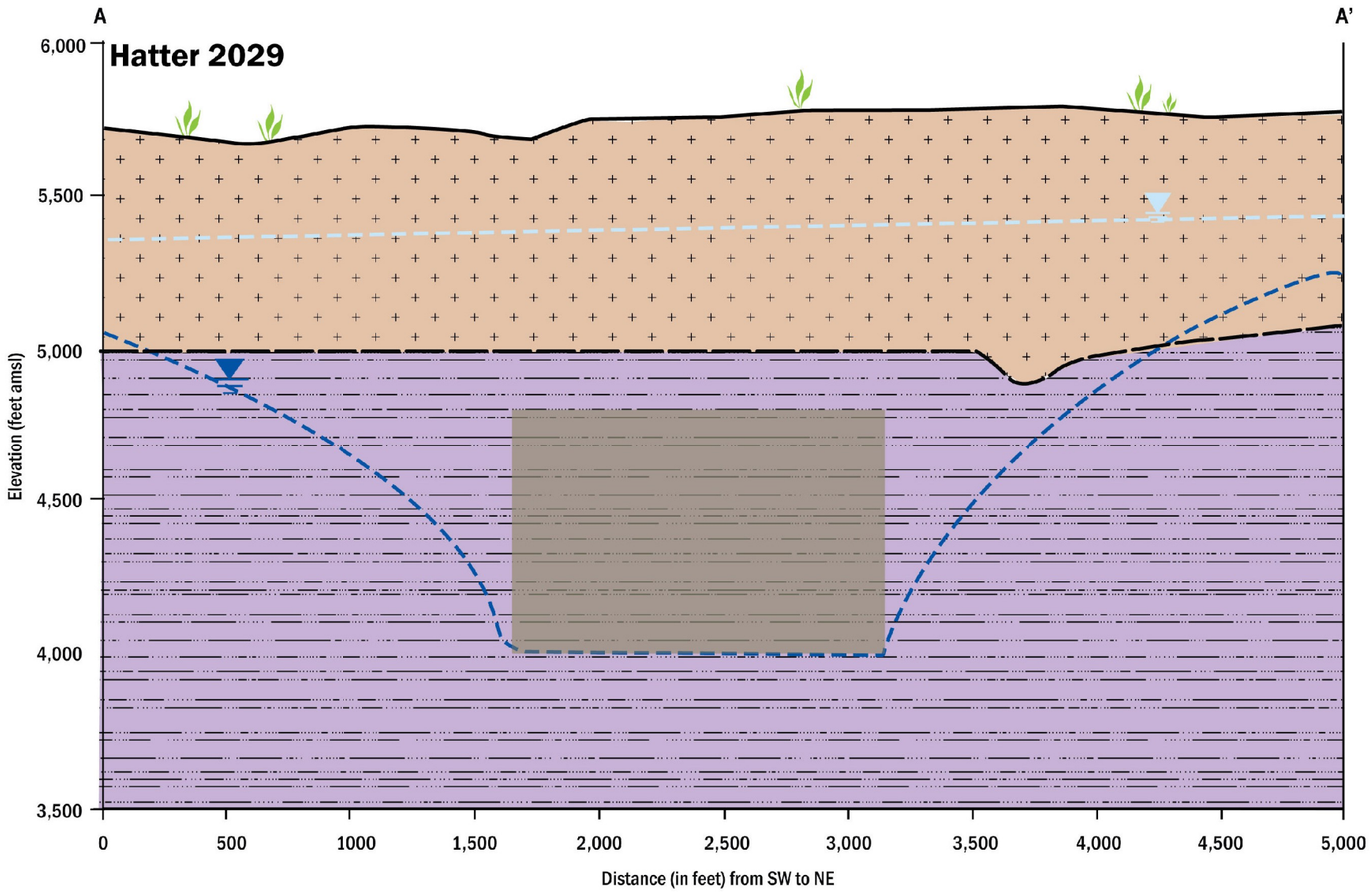

EXPLANATION

- Land Surface
- Simulated Groundwater Piezometric Surface (Confined)
- Simulated Recovered Piezometric Surface (Confined)
- Tertiary-Ordovician Contact
- Tertiary Volcanics
- Ordovician Vinini Formation
- Hatter Expansion Mine Workings (generalized)

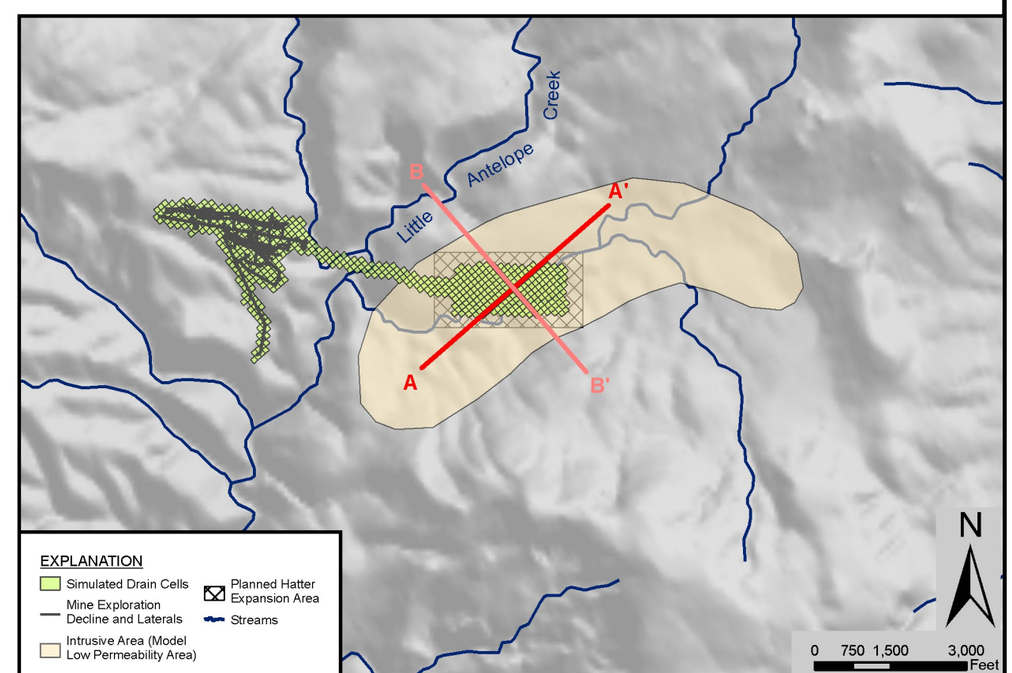

FILE: P:\BC_CAR\138301_Hollister_Mine_EIS\GIS\ARCMAPS\WORKING\Figure 5-5 Hatter Cross Section.mxd

BROWN AND CALDWELL

PROJECT	SITE	
138301	Rodeo Creek Gold - Hollister Mine	Figure
DATE	TITLE	
6/16/10	Hatter Expansion Area Cross Section - 2029, A-A'	5-5

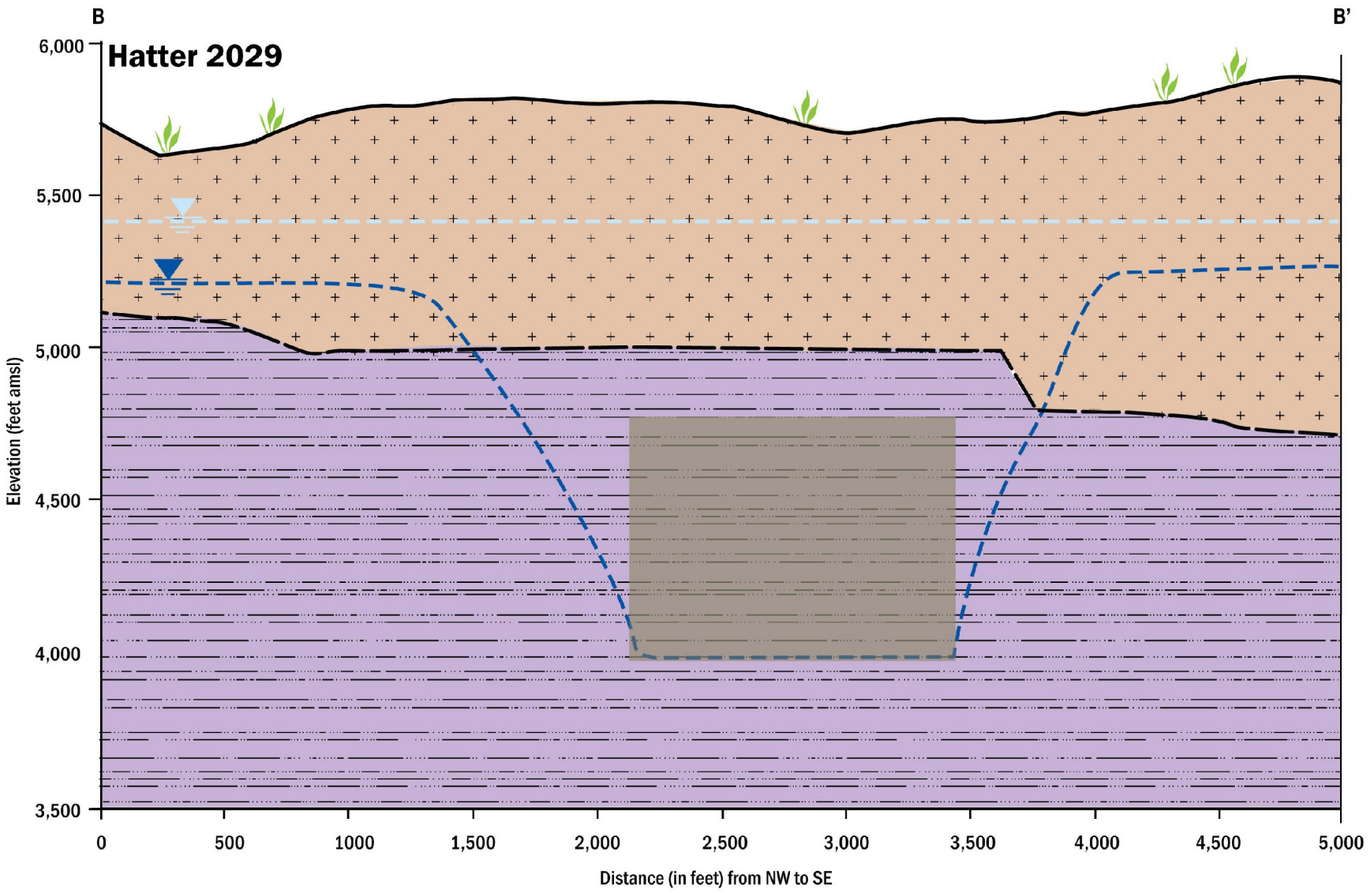

EXPLANATION

- Land Surface
- Simulated Groundwater Piezometric Surface (Confined)
- Simulated Recovered Piezometric Surface (Confined)
- Tertiary-Ordovician Contact
- Tertiary Volcanics
- Ordovician Vinini Formation
- Hatter Expansion Mine Workings (generalized)

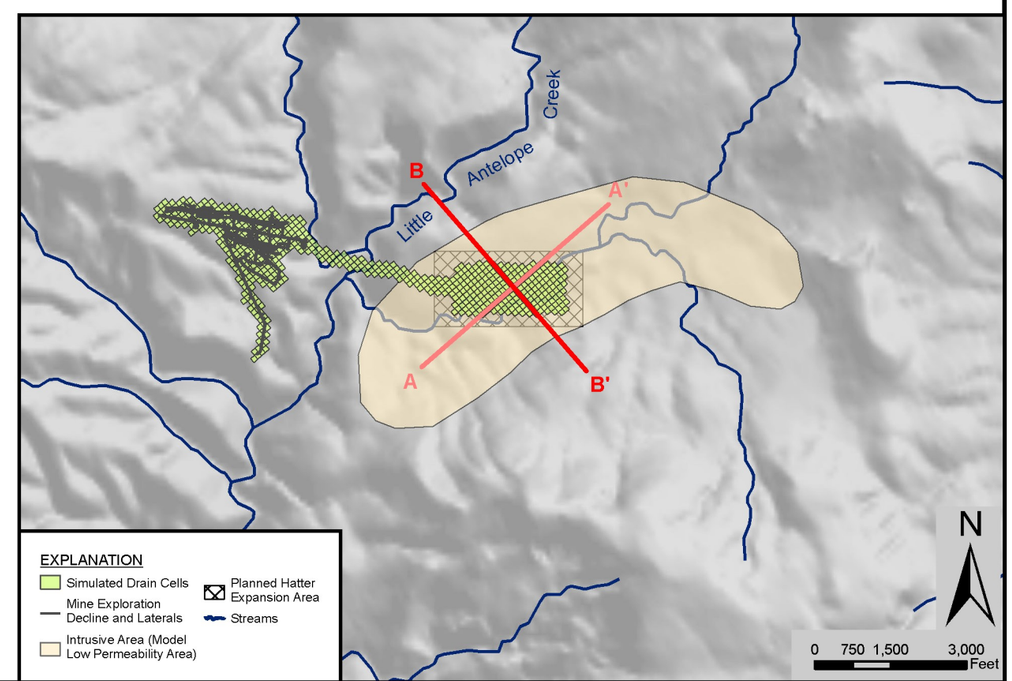

BROWN AND CALDWELL

PROJECT	SITE
138301	Rodeo Creek Gold - Hollister Mine
DATE	TITLE
6/16/10	Hatter Expansion Area Cross Section - 2029, B-B'

Figure 5-6

FILE: P:\BC_CAR\138301_Hollister_Mine_EIS\GIS\ARCMAPS\WORKING\Figure 5-5 Hatter Cross Section 2.mxd

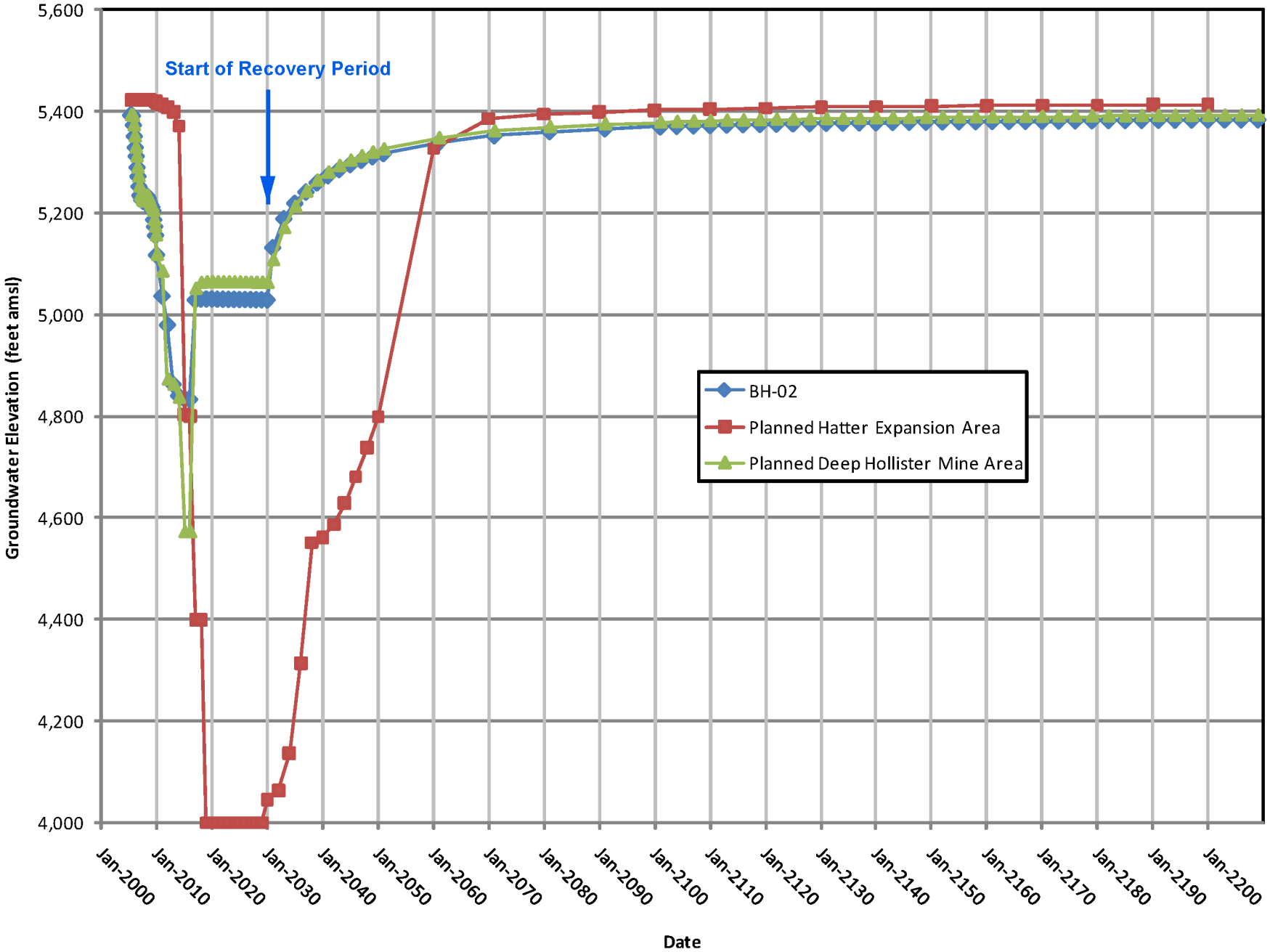

FILE: P:\BC_CAR\138301_Hollister_Mine_EIS\GIS\ARCMAPS\WORKING\Figure 5-7 WL Recoveries.mxd

BROWN AND CALDWELL

PROJECT	SITE	
138301	Rodeo Creek Gold - Hollister Mine	Figure
DATE	TITLE	
6/30/10	Simulated Water Level Drawdown and Recoveries	5-7

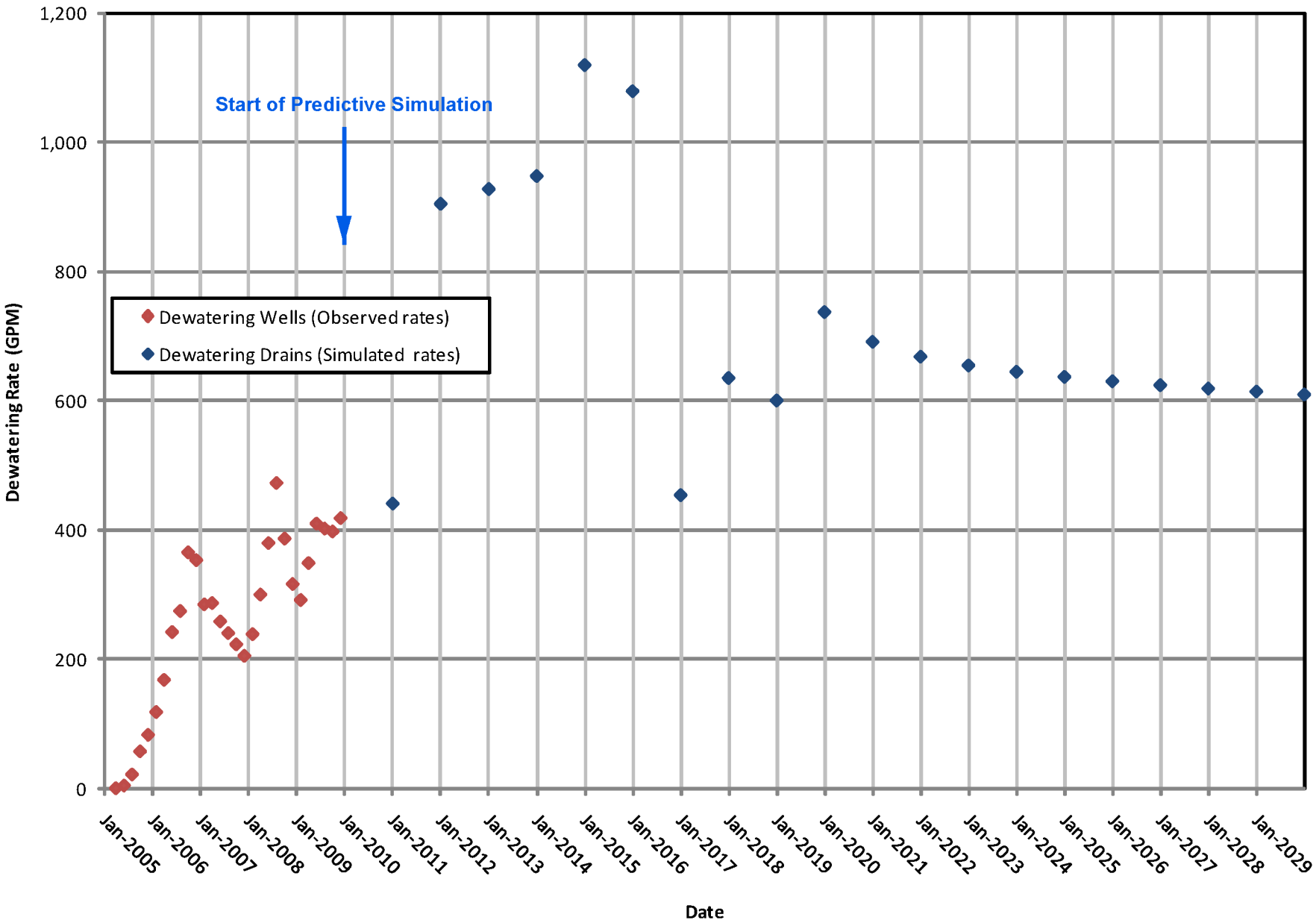

BROWN AND CALDWELL

PROJECT	SITE	
138301	Rodeo Creek Gold - Hollister Mine	Figure
DATE 6/30/10	TITLE Simulated Mine Dewatering – Observed and Predicted Pumping Rates	5-8

FILE: P:\BC_CAR\138301_Hollister_Mine_EIS\GIS\ARCMAPS\WORKING\Figure 5-8 Simulated Dewatering.mxd

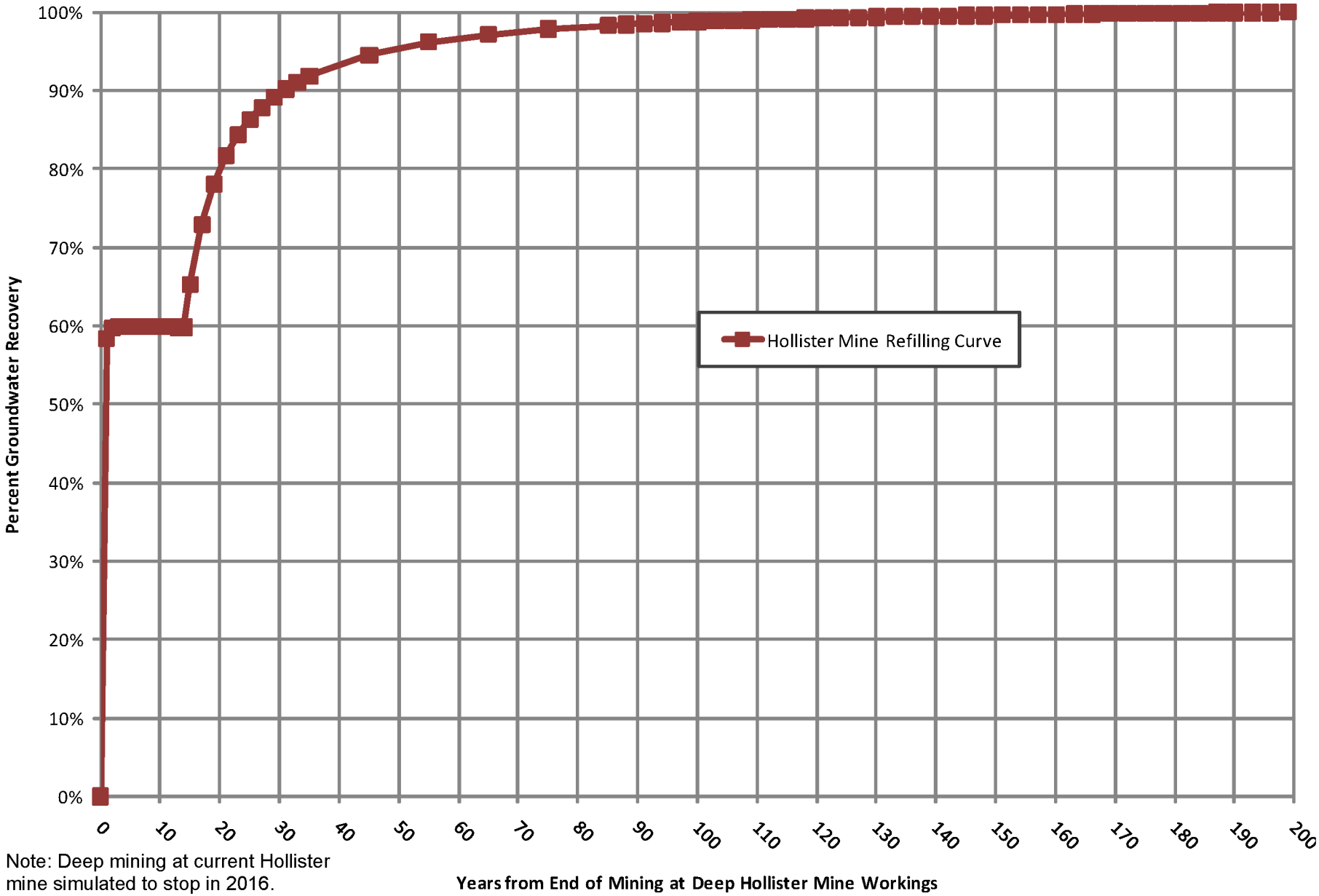

Note: Deep mining at current Hollister mine simulated to stop in 2016.

BROWN AND CALDWELL	PROJECT 138301	SITE Rodeo Creek Gold - Hollister Mine	Figure 5-9
	DATE 8/26/2010	TITLE Hollister Mine Workings Refilling Curve	

FILE: P:\BC_CAR\138301_Hollister_Mine_EIS\GIS\ARCMAPS\WORKING\Figure 5-9 Hollister Refilling Curve.mxd

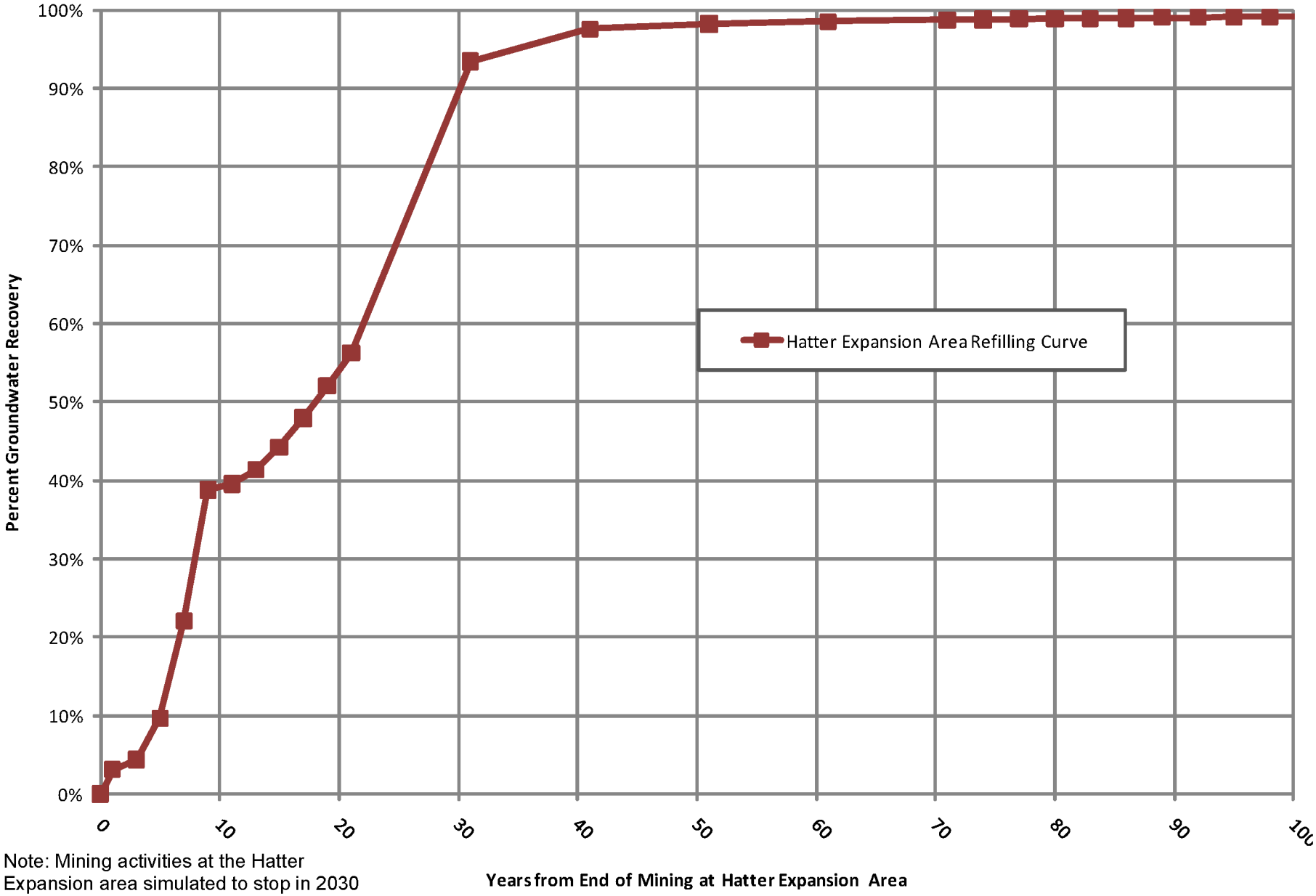

Note: Mining activities at the Hatter Expansion area simulated to stop in 2030

BROWN AND CALDWELL	PROJECT 138301	SITE Rodeo Creek Gold - Hollister Mine	Figure
	DATE 8/26/2010	TITLE Hatter Expansion Area Refilling Curve	5-10

FILE: P:\BC_CAR\138301_Hollister_Mine_EIS\GIS\ARCMAPS\WORKING\Figure 5-10 Hatter Refilling Curve.mxd

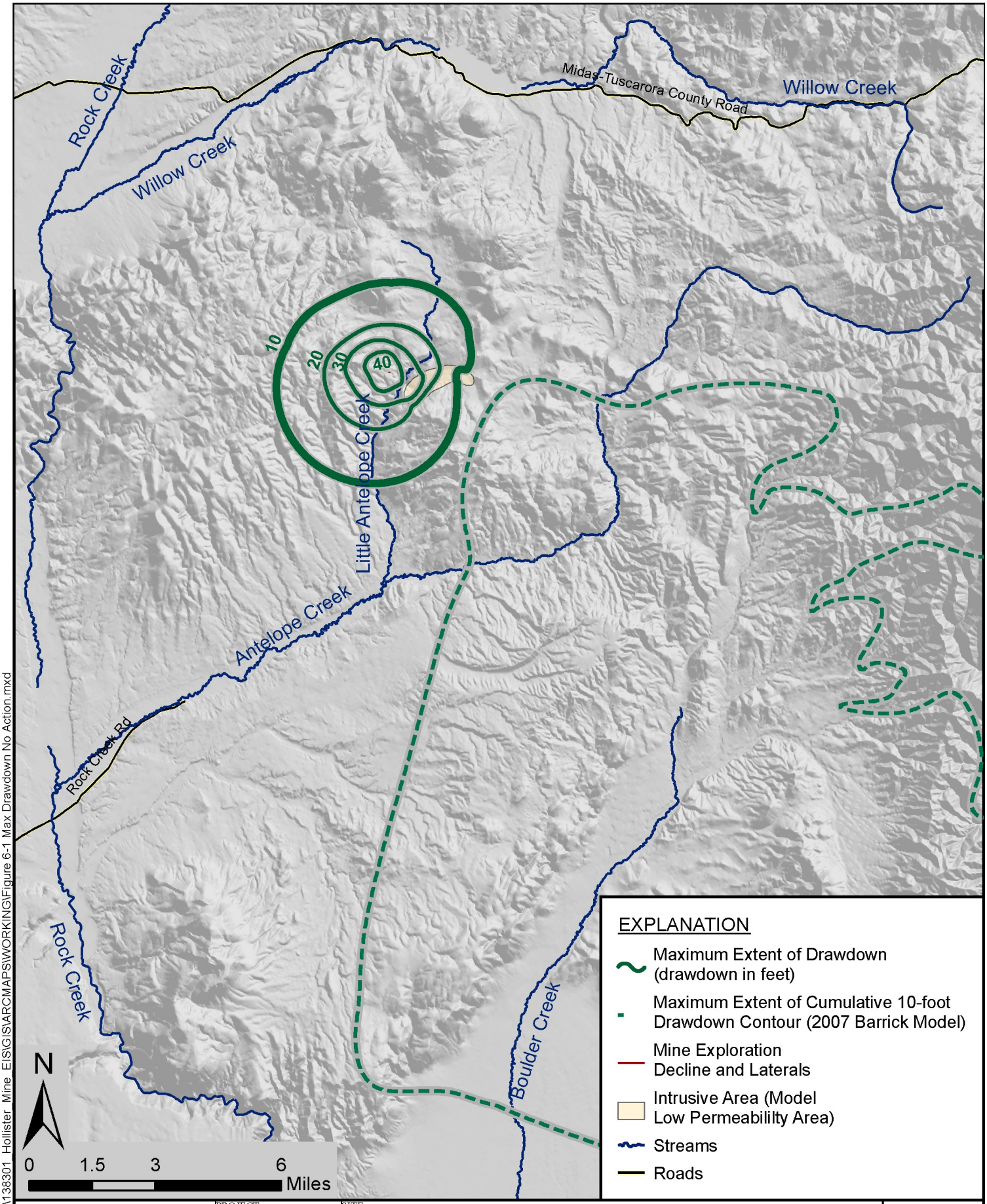

FILE: P:\BC_CAR\138301_Hollister_Mine_EIS\GIS\ARCMAPS\WORKING\Figure 6-1 Max Drawdown No Action.mxd

BROWN AND CALDWELL

PROJECT	SITE	
138301	Rodeo Creek Gold - Hollister Mine	Figure
DATE	TITLE	
10/7/10	No Action Alternative Simulation - Maximum Extent of 10-Foot Drawdown (2020)	6-1

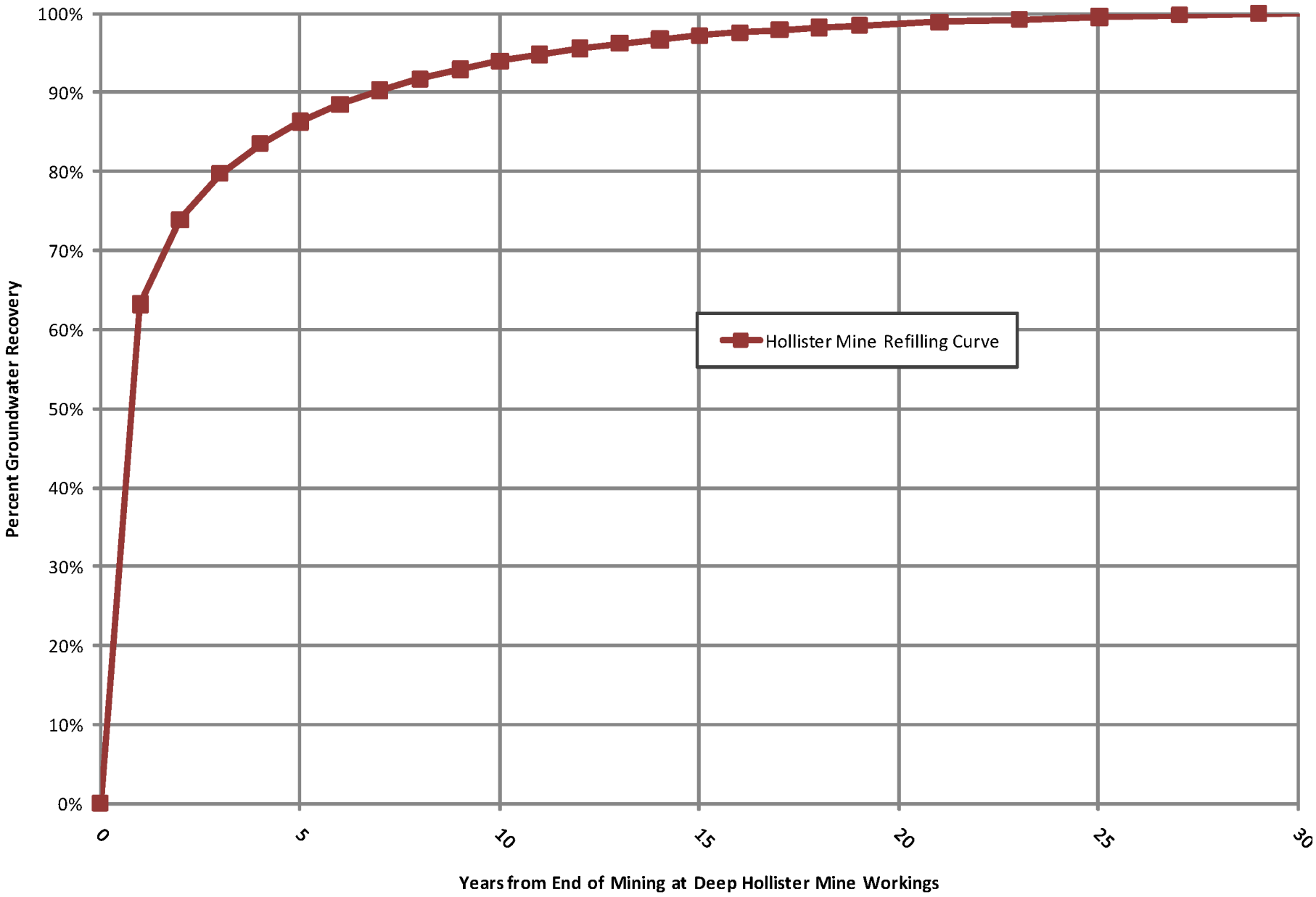

BROWN AND CALDWELL	PROJECT 138301	SITE Rodeo Creek Gold - Hollister Mine	Figure 6-2
	DATE 10/7/10	TITLE No Action Alternative Simulation - Hollister Mine Water Level Recovery	

FILE: P:\BC_CAR\138301_Hollister_Mine_EIS\GIS\ARCMAPS\WORKING\Figure 6-2 WL Recoveries No Action.mxd

APPENDIX A: SUPPORTING GROUNDWATER MODEL INFORMATION

Figure A-1. Steady State Model Water Level Residuals
Figure A-2. BH-01 & BH-02 Calibrations Plot of Observed versus Simulated Water Levels
Figure A-3. Simulated Water Levels in Vinini Formation in 2016
Figure A-4. Simulated Water Levels in Vinini Formation in 2030
Figure A-5. Simulated Water Levels in Vinini Formation at Time of Maximum Extent of Drawdown (2070)
Figure A-6. Simulated Drawdown in Vinini Formation in 2016
Figure A-7. Simulated Drawdown in Vinini Formation in 2030

Use of contents on this sheet is subject to the limitations specified at the end of this document.

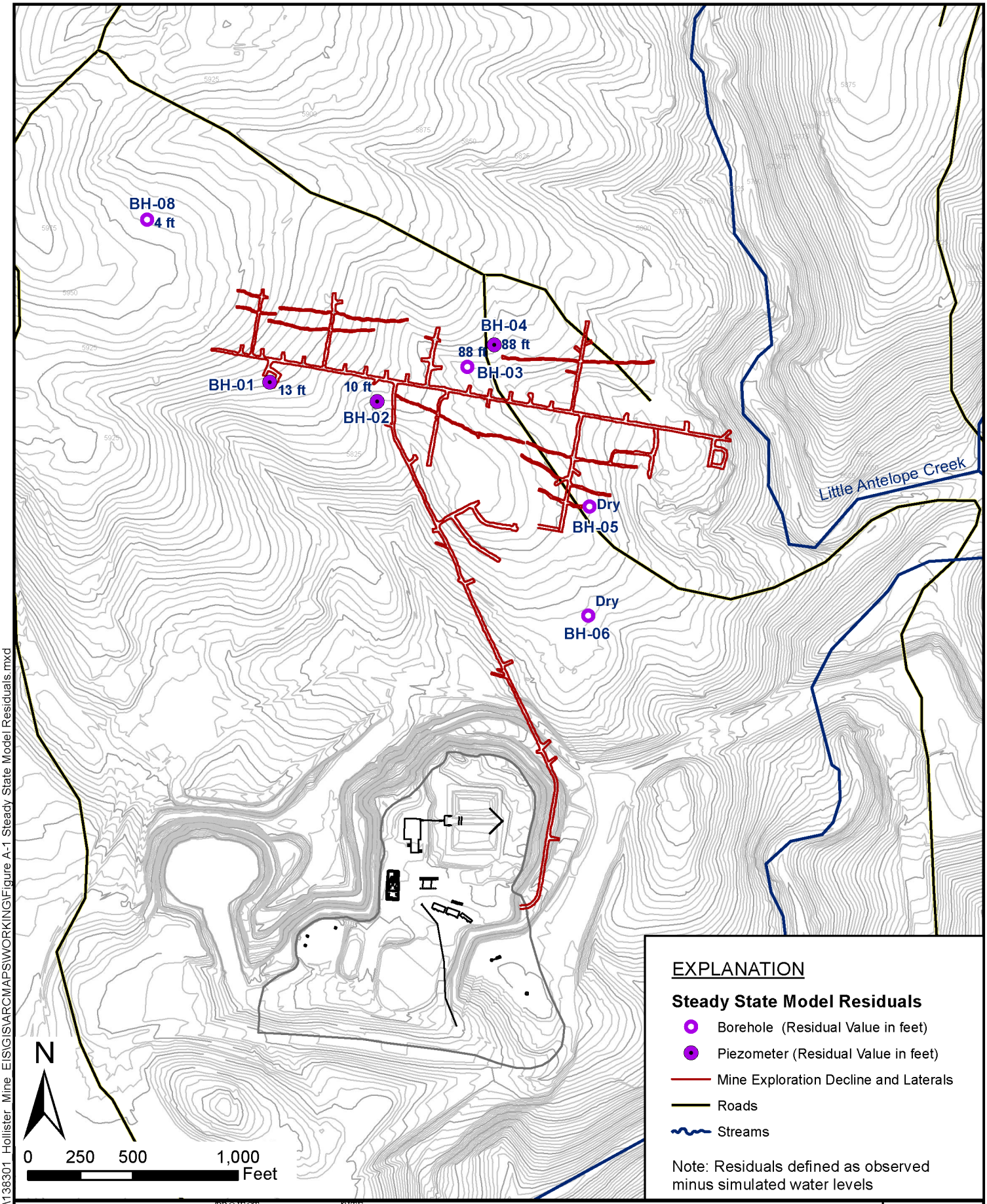

FILE: P:\BC_CAR\138301_Hollister_Mine_EIS\GIS\ARCMAPS\WORKING\Figure A-1 Steady State Model Residuals.mxd

BROWN AND CALDWELL	PROJECT 138301	SITE Rodeo Creek Gold - Hollister Mine	Figure A-1
	DATE 6/30/10	TITLE Steady State Model Water Level Residuals	

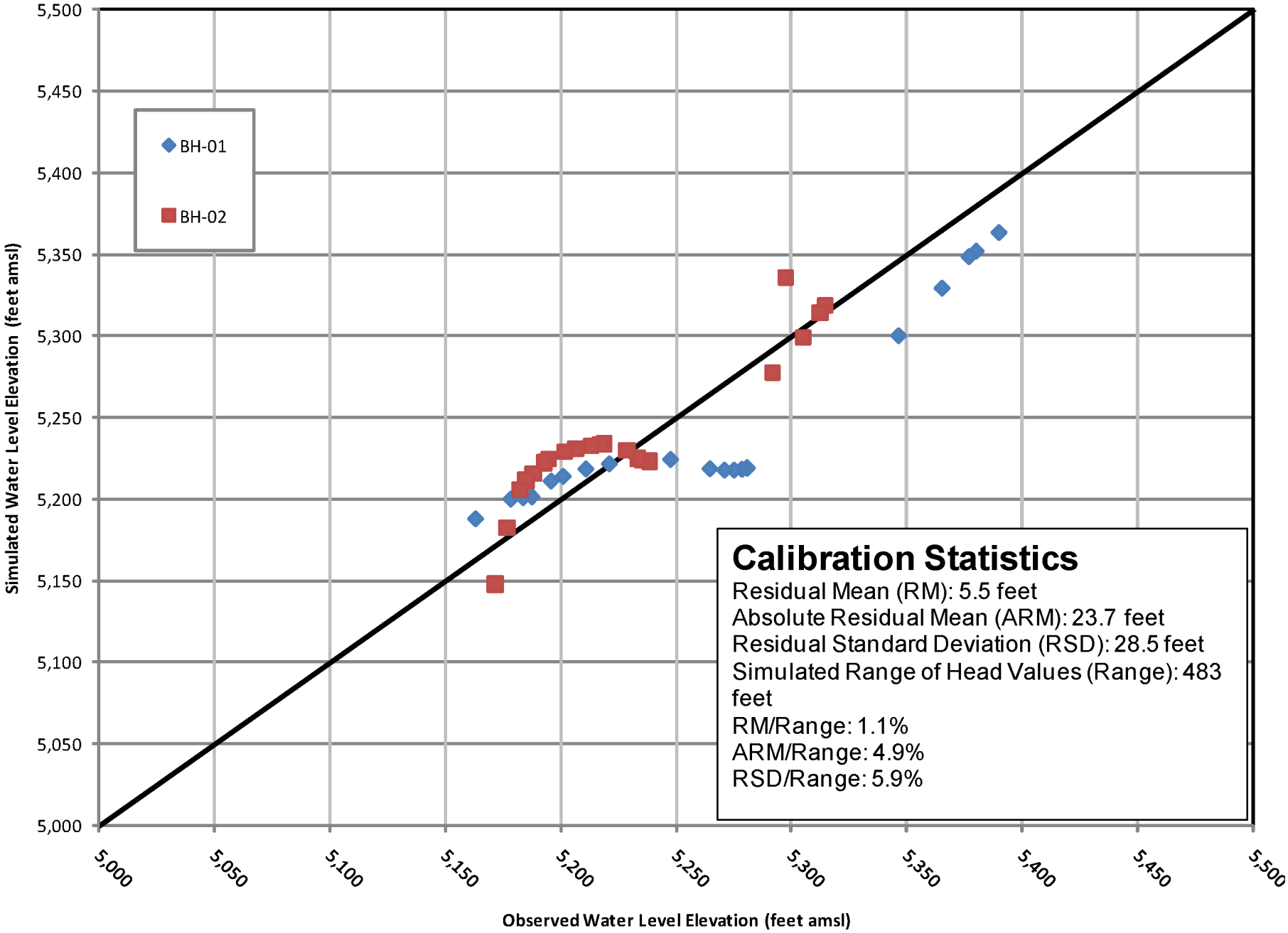

FILE: P:\BC_CAR\138301_Hollister_Mine_EIS\GIS\ARCMAPS\WORKING\Figure A-2 BH-01 & BH-02 Calibration Plot.mxd

BROWN AND CALDWELL

PROJECT	SITE	
138301	Rodeo Creek Gold - Hollister Mine	Figure
DATE 8/26/2010	TITLE BH-01 & BH-02 Calibrations Plot of Observed versus Simulated Water Levels	A-2

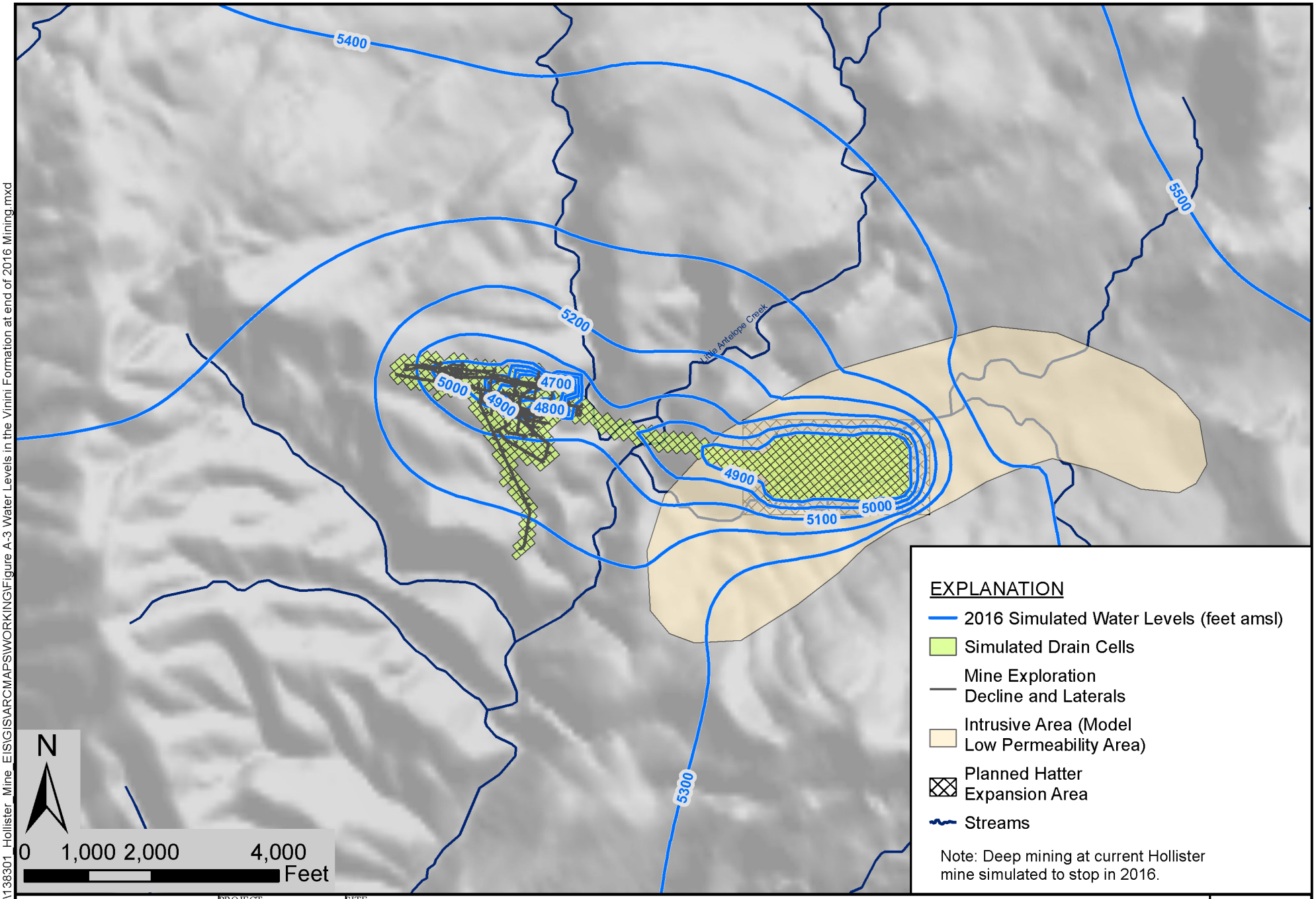

FILE: P:\BC_CAR\138301_Hollister_Mine_EIS\GIS\ARCMAPS\WORKING\Figure A-3 Water Levels in the Vinini Formation at end of 2016 Mining.mxd

BROWN AND CALDWELL

PROJECT	SITE	
138301	Rodeo Creek Gold - Hollister Mine	Figure
DATE	TITLE	
8/26/2010	Simulated Water Levels in Vinini Formation in 2016	A-3

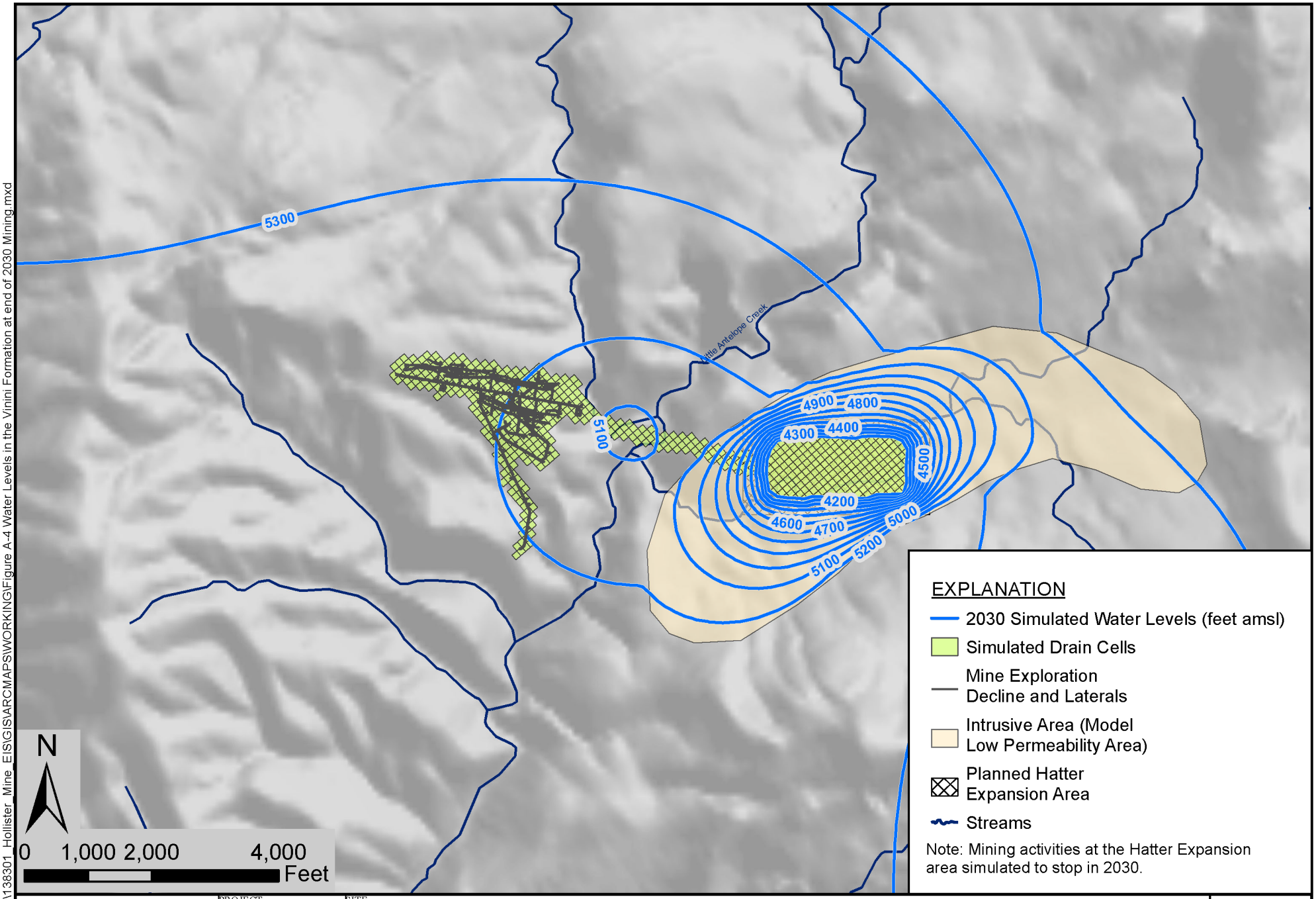

FILE: P:\BC_CAR\138301_Hollister_Mine_EIS\GIS\ARCMAPS\WORKING\Figure A-4 Water Levels in the Vinini Formation at end of 2030 Mining.mxd

BROWN AND CALDWELL

PROJECT	SITE	
138301	Rodeo Creek Gold - Hollister Mine, Hatter Expansion	Figure
DATE	TITLE	
8/26/2010	Simulated Water Levels in Vinini Formation in 2030	A-4

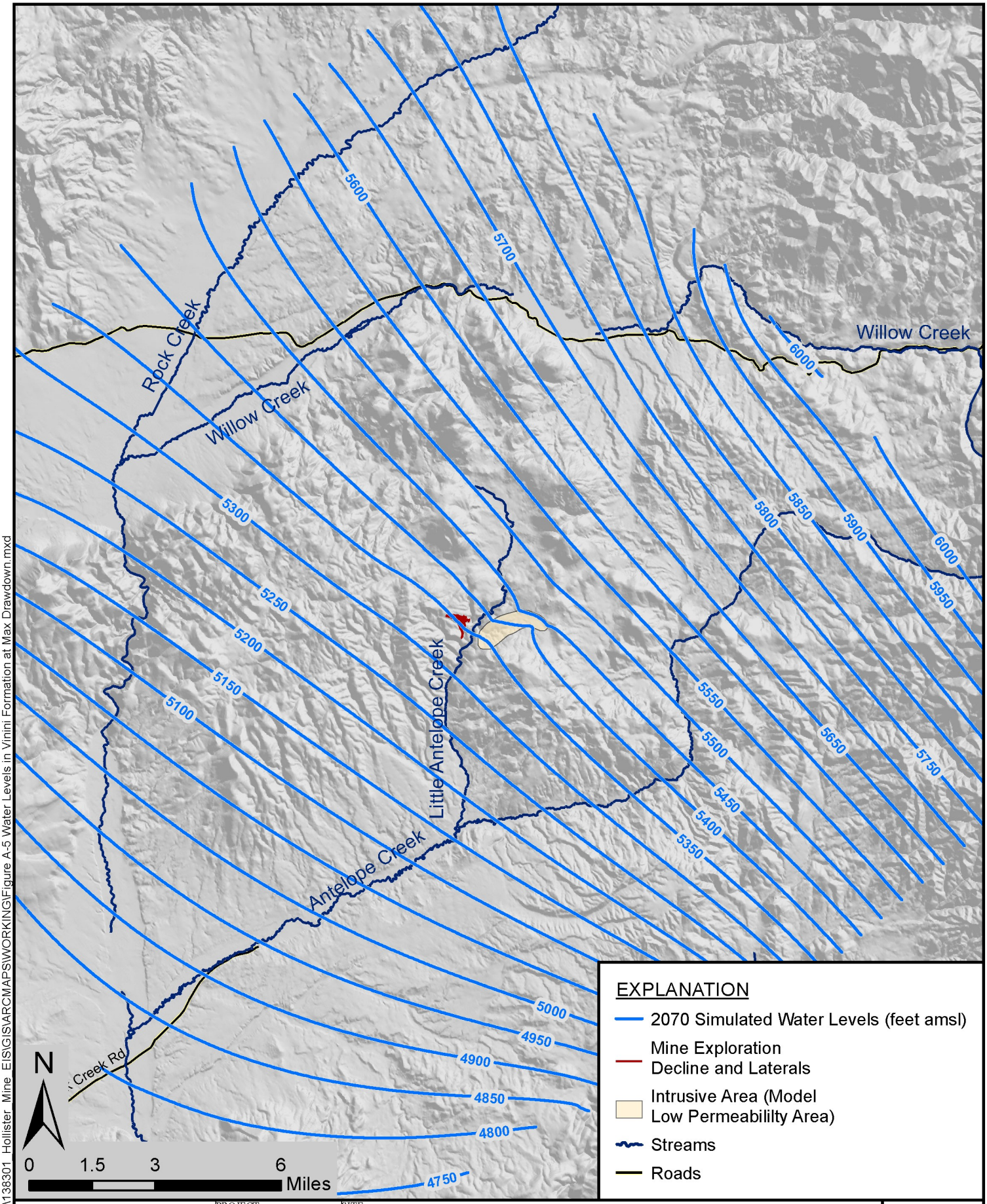

BROWN AND CALDWELL

PROJECT	SITE	
138301	Rodeo Creek Gold - Hollister Mine	Figure
DATE	TITLE	
8/26/2010	Simulated Water Levels in the Vinini Formation at Time of Maximum Extent of Drawdown (2070)	A-5

FILE: P:\BC_CAR\138301_Hollister_Mine_EIS\GIS\ARCMAPS\WORKING\Figure A-5 Water Levels in Vinini Formation at Max Drawdown.mxd

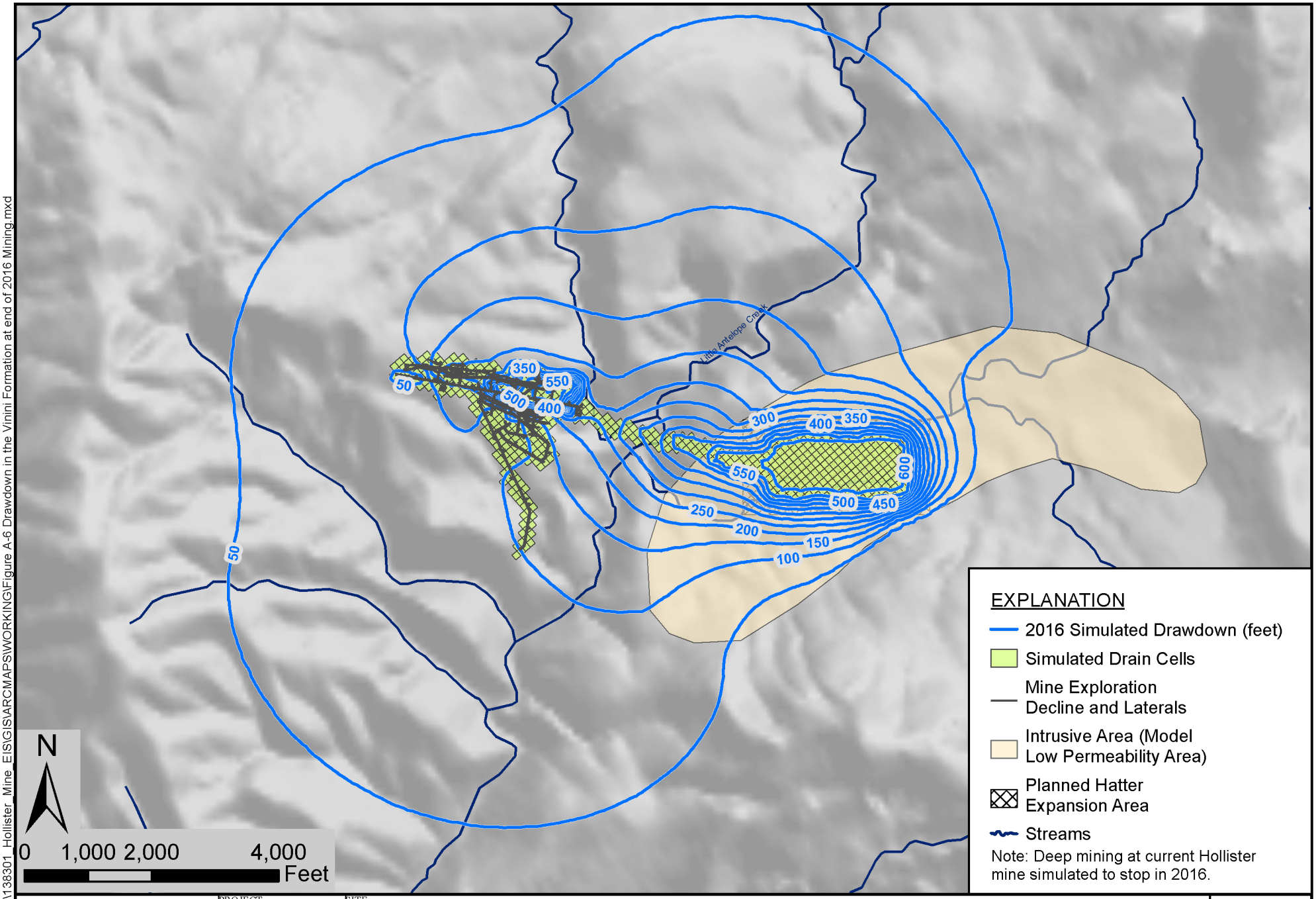

FILE: P:\BC_CAR\138301_Hollister_Mine_EIS\GIS\ARCMAPS\WORKING\Figure A-6 Drawdown in the Vinini Formation at end of 2016 Mining.mxd

BROWN AND CALDWELL

PROJECT	SITE	
138301	Rodeo Creek Gold - Hollister Mine	Figure
DATE	TITLE	
8/26/2010	Simulated Drawdown in Vinini Formation in 2016	A-6

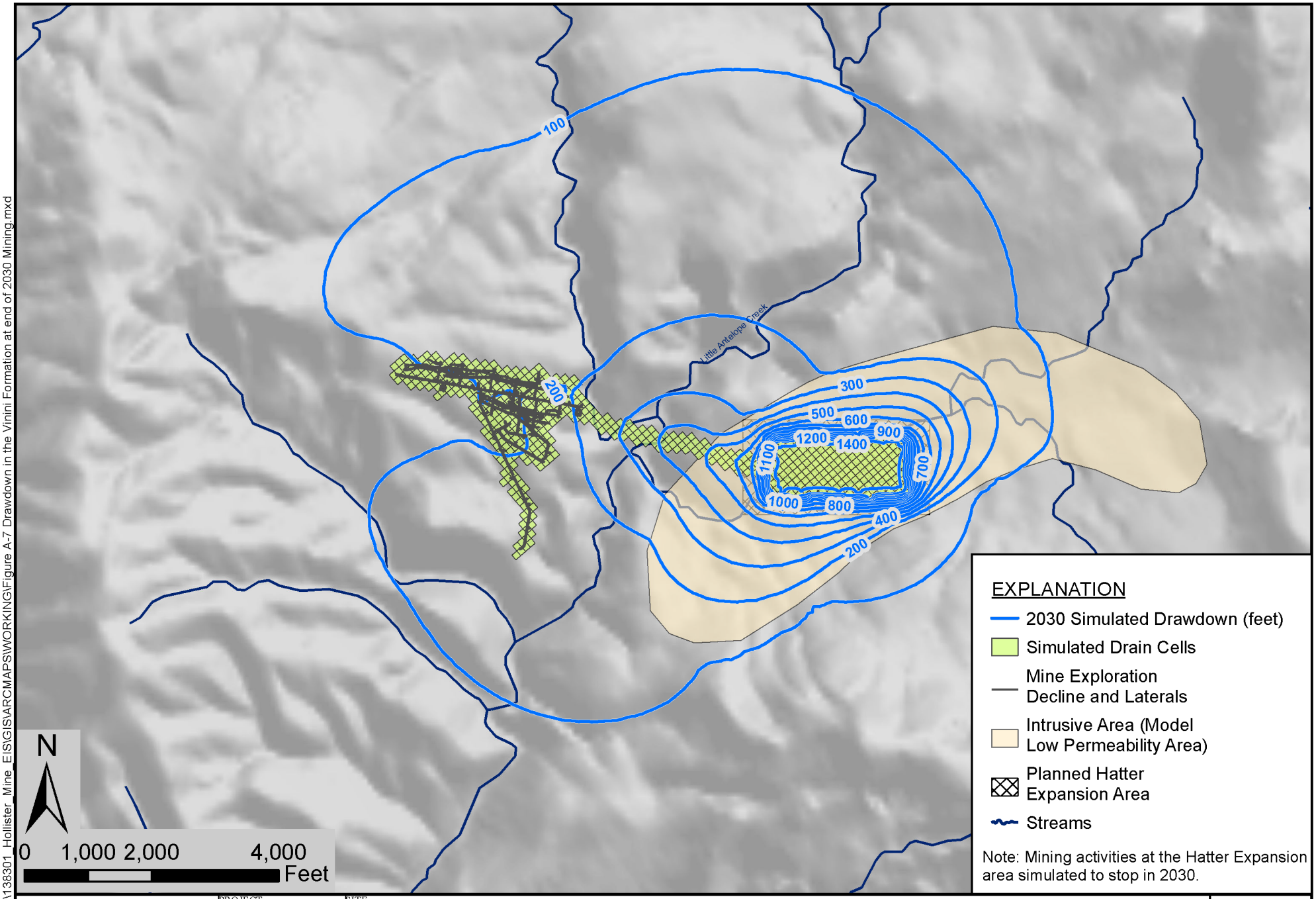

FILE: P:\BC_CAR\138301_Hollister_Mine_EIS\GIS\ARCMAPS\WORKING\Figure A-7 Drawdown in the Vinini Formation at end of 2030 Mining.mxd

BROWN AND CALDWELL

PROJECT	SITE	
138301	Rodeo Creek Gold - Hollister Mine, Hatter Expansion	Figure
DATE	TITLE	
8/26/2010	Simulated Drawdown in Vinini Formation in 2030	A-7

B3 Geochemical Model Report

RODEO CREEK HOLLISTER MINE
UNDERGROUND WORKINGS WATER QUALITY PREDICTION

October 13, 2010

Prepared for:

Brown and Caldwell
3264 Goni Road
Suite 153
Carson City, Nevada 89706

Prepared by:

Enchemica LLC
2335 Buckingham Circle
Loveland, Colorado 80538
(970) 203-0179

TABLE OF CONTENTS

List of Tables ii
List of Figures ii
List of Appendices ii
Executive Summary iii
1.0 Introduction 1
2.0 Site Data 2
2.1 Geologic Setting 2
2.2 Mine Plan Data 3
2.3 Hydrologic Data 9
2.4 Groundwater Quality Data 9
2.5 Waste Rock Testing Data 9
3.0 Geochemical Modeling Code and Database 17
4.0 Conceptual Model 19
4.1 Hydrogeologic Data and Assumptions 19
4.2 Leaching of Mine Wall Rock and Waste Rock 20
4.3 Cementitious Material Leaching 20
4.4 Sources of Nitrogen Compounds 21
4.5 Chemical Constituents and Reactions Included in Geochemical Model 21
5.0 Geochemical Modeling Results 25
6.0 Summary and Conclusions 30
7.0 References 31

LIST OF TABLES

Table 2-1. Parameters Used to Calculate Mine Water Quality

Table 2-2. Particle Size Gradation

Table 2-3. Calculation of Geometric Surface Area for Waste Rock Size Fractions

Table 2-4. Chemical Composition of Portland Type II Cement

Table 2-5. Hollister Mine and Hatter Expansion Mine Drain Setup Schedule

Table 2-6. Predicted Percent Water Level Recovery or Saturated Percentage of the Vertical Extent of Mine Workings, Hollister Mine and Hatter Expansion

Table 2-7. Vinini Formation Borehole Water Quality

Table 2-8. Underground Discharge Water Quality Summary

Table 2-9. Statistical Summary of Concentrations in First Four-Week Humidity Cell Composite Samples

Table 2-10. Mean Constituent Releases from First Four-Week Composite Humidity Cell Samples

Table 3-1. Potential Constituents of Concern Included in Modeling Calculations

Table 3-2. Solubility Data Added to the MINTEQ.v4 Database

Table 4-1. Potential Secondary Mineral Phases

Table 5-1. Solid Phase Changes

Table 5-2. Predicted Aqueous Concentrations

Table 5-3. Surface Species

LIST OF FIGURES

Figure 4-1. Potential Sources and Sinks of Constituents in Underground Workings Water

LIST OF APPENDICES

Appendix A. Underground Drainage Water Quality Data and Waste Rock Humidity Cell Data

Appendix B. Geochemical Modeling Calculations

EXECUTIVE SUMMARY

Rodeo Creek Gold Inc. (Rodeo Creek) is constructing an exploration decline and performing test drilling at their Hollister Mine site in Elko County, Nevada. Full scale mining will involve both the Hollister Mine workings and the planned Hatter Expansion. After mining is complete, dewatering will be discontinued and the underground workings will fill with groundwater. An investigation was carried out to predict the water quality in the underground workings after the mine is completely filled.

Available site information, including the geologic setting, mine plan, water quality data, waste rock testing data and hydrologic data were used to develop a geochemical conceptual model of processes at the site. This conceptual model and site data were used to formulate PHREEQC geochemical modeling calculations to predict steady-state water quality in the underground workings.

The geochemical conceptual model includes the assumption that the results of waste rock testing can be extrapolated to the mine wall rock and backfilled waste rock based on the surface areas of the materials. It is also assumed that the first four-week composite from waste rock humidity cell testing is representative of the mine wall rock and waste rock leaching. Because information regarding the distribution of the mine workings, waste rock and cement as a function of depth is unavailable, it is assumed that the mine workings, waste rock and cement will be uniformly distributed over the depth of the workings. Because of the long time period required for groundwater to fill the underground workings and the high sulfate content of the underground workings water, cementitious materials in the concrete are assumed to be completely available for reaction. It is also assumed that the composition of inflowing groundwater can be represented by available borehole water samples, the entire flooded underground workings can be approximated as a single, well-mixed system and the rate of outflow of water from the workings during mine filling will be negligible.

The important chemical processes included in the geochemical conceptual model are: leaching of acidity, metals and other constituents from the mine wall rock and backfilled waste rock; leaching of alkalinity, calcium and silica from the cementitious phases in concrete; influx of dissolved constituents in the groundwater; precipitation/dissolution reactions; and constituent adsorption on precipitated iron hydroxide. The solid phases allowed to precipitate in the geochemical modeling calculations are phases that have been identified in the literature as those that form readily under the relatively low-temperature conditions anticipated in the underground workings.

PHREEQC geochemical modeling calculations were performed assuming two different surface areas for the mine wall rock and backfilled waste rock. For both sets of calculations, redox conditions were relatively oxidizing and the pH of the solution was controlled at approximately 10.2 by precipitation of tobermorite [$(Ca(OH)_2)_2(SiO_2)_{2.4}\bullet 2H_2O(s)$]. This alkaline pH is

consistent with the relatively large neutralizing potential in the cement (10,269 ton $CaCO_3$) compared to the acid-base potential in the waste rock backfill (-3,032 ton $CaCO_3$). Because the neutralizing potential in the cement exceeds the acid-base potential in the waste rock by more than a factor of three, the alkalinity in the cement is more than sufficient to neutralize the acidity released by the waste rock and mine wall rock.

For both mine wall rock and waste rock surface areas used in the calculations, the concentrations of arsenic, barium, cadmium, chloride, copper, fluoride, iron, lead, magnesium, manganese, nickel, nitrate and zinc are less than the NDEP Profile I reference values. The predicted pH value of approximately 10.2 exceeds the Profile I reference value. The predicted concentrations for both mine wall rock and waste rock surface areas exceed the Profile I reference values for aluminum, antimony, chromium, selenium, sulfate, thallium and total dissolved solids. The predicted beryllium concentration exceeds its Profile I reference value for the higher mine wall rock and waste rock surface area, but is below its reference value for the lower surface area.

1.0 INTRODUCTION

Rodeo Creek Gold Inc. (Rodeo Creek) is constructing an exploration decline and performing test drilling at their Hollister Mine site in Elko County, Nevada. Full scale mining will involve both the Hollister Mine workings and the planned Hatter Expansion. After mining is complete, dewatering will be discontinued and the underground workings will eventually fill with groundwater. An investigation was carried out to predict the water quality in the underground workings after the mine is completely filled.

Section 2.0 summarizes the available site data, including the geologic setting, mine plan, water quality data, waste rock testing data and hydrogeologic data. The PHREEQC geochemical modeling code and database used to perform the water quality calculations are described in Section 3.0 and the conceptual model used to formulate the modeling calculations is summarized in Section 4.0. The results of the calculations are described in Section 5.0.

The results of this investigation are summarized in Section 6.0. The results indicate that the neutralizing potential of the cement in concrete used to stabilize the backfill will be more than sufficient to counteract the acidity released by the mine wall rock and waste rock backfill. As a result, the pH of the underground workings water at steady state will be alkaline and controlled by the precipitation of tobermorite [$(Ca(OH)_2)_2(SiO_2)_{2.4}\bullet 2H_2O(s)$] at approximately 10.2. Aqueous concentrations of arsenic, barium, cadmium, chloride, copper, fluoride, iron, lead, magnesium, manganese, nickel, nitrate and zinc are not predicted to exceed NDEP Profile I reference values. Constituents predicted to exceed NDEP Profile I reference values in the underground workings water include pH, aluminum, antimony, chromium, selenium, sulfate, thallium and total dissolved solids and possibly beryllium.

2.0 SITE DATA

Information required for predicting underground workings water quality after groundwater inflow is complete includes the mineralogy and chemistry of the rocks that will be exposed on the mine walls, the mineralogy and chemistry of waste rock that will be backfilled in the mine, the configuration of the workings, the length of time the mine wall rock and waste rock will be exposed to the atmosphere during mining and reflooding of the workings, the length of time cementitious materials will be submerged in the mine water and the sources and chemistry of inflowing groundwater. Site data used to calculate the underground mine water quality are summarized in Table 2-1. The sources of these data are described in the following sections.

Table 2-1. Parameters Used to Calculate Mine Water Quality

Parameter	Value (SI units)	Value (English Units)	Report Section
Total length of Hollister Mine workings	12,649 m	41,500 ft	2.2
Hollister Mine workings volume	141,018 m^3	4,980,000 ft^3	2.2
Radius of Hollister Mine workings	1.88 m	6.18 ft	2.2.1
Mine wall geometric surface area	149,718 m^2	1,611,550 ft^2	2.2.1
Mine wall reactive surface area	14,971,800 m^2	161,155,000 ft^2	2.2.1
Waste rock field volume	42,305 m^3	1,494,000 ft^3	2.2.2
Waste rock field density	1,560 kg/m^3	97.42 lb/ft^3	2.2.2
Assumed waste rock material density	2,650 kg/m^3	165.4 lb/ft^3	2.2.2
Waste rock total mass	65,985,107 kg	72,736 tons	2.2.2
Waste rock particle volume	24,900 m^3	879,337 ft^3	2.2.2
Waste rock geometric surface area	155,479,964 m^2	1,673,572,408 ft^2	2.2.2
Waste rock reactive surface area	1,088,359,751 m^2	11,715,006,856 ft^2	2.2.2
Mine wall rock and waste rock reactive surface area	1,103,331,535 m^2	11,876,161,806 ft^2	2.2.2
Concrete volume	14,158 m^3	500,000 ft^3	2.2.3
Cement volume	3,540 m^3	125,000 ft^3	2.2.3
Cement density	2,340 kg/m^3	146.1 lb/ft^3	2.2.3
Cement mass	8,282,679 kg	18,260,179 lbs	2.2.3
Underground workings water volume	101,959 m^3	3,600,663 ft^3	2.2.4
Mine wall rock and waste rock reactive surface area per volume of water	10,821 m^2/m^3	3,298 ft^2/ft^3	2.2.4

2.1 Geologic Setting

The Rodeo Creek Hollister Mine site is located at the north end of the Carlin Trend, in Elko County, Nevada. The site geology has been described by Walker (2003a, 2003b). A Tertiary volcanic, intrusive and epiclastic complex of rocks crops out at the surface, except for limited areas of Pliocene and younger sediments on the east side of the project. The Ordovician Vinini

Formation underlies the Tertiary rocks. Ore minerals occur in banded quartz veins in the Vinini Formation. Pyrite may reach 1 to 3% by volume in the alteration halos around the veins.

Three rock types were identified for waste-rock testing from the Vinini Formation (Walker 2003a, 2003b): (1) andesite, (2) quartzite, including quartzite, quartzite/siltite and quartzite/argillite and (3) interbedded argillite/siltite, including argillite, argillite/quartzite, argillite/siltite and siltite. Andesite was encountered only in the initial portion of the decline, and the majority of mine wall rock in the underground workings is likely to consist of quartzite and interbedded argillite/siltite.

2.2 Mine Plan Data

The length of the workings, waste rock density, waste rock volume and concrete volumes were obtained from Rodeo Creek (Taylor 2010a, 2010b, 2010c, 2010d) and Brown and Caldwell (Cain 2010). The total vertical depth of mining beneath the water table at the site will extend from around 5,400 ft to 4,000 ft amsl. The Hollister Mine will have 41,500 ft of open workings and 4,980,000 ft^3 total volume of open workings.

A subsurface drift will be constructed to the planned Hatter Expansion, beginning at 5,200 ft amsl in the Hollister Mine workings and ending at approximately 4,800 ft amsl. The Hatter Expansion will extend to approximately 4,000 ft amsl. The Hatter Expansion is expected to increase the length and volume of open workings, volumes of waste rock backfill and cement by 40%. The water quality prediction calculations depend on the proportions of waste rock backfill volume, mine wall surface area and cement volume to the volume of water in the workings. Because these ratios will not change with the planned Hatter Expansion, all calculations were carried out using data for the Hollister Mine workings, but will also be applicable to the planned Hatter Expansion.

2.2.1 Surface Area of the Underground Workings

The mine wall surface area was approximated using the dimensions of the Hollister Mine workings, assuming a cylindrical shape, with a volume (V) of 4,980,000 ft^3 and length (l) of 41,500 ft. A radius (r) of 6.18 ft was calculated for this cylinder using the equation:

$$\text{—} \qquad (1)$$

The surface area (S) of a cylinder can be calculated from the radius and length:

$$S = 2\pi rl \qquad (2)$$

Using equation (2), the Hollister Mine wall geometric surface area was calculated to be 1,611,550 ft^2. The reactive surface area of the mine wall will be greater than the geometric surface area because of surface irregularity, natural fracturing and faulting and the effects of

blasting. Morin and Hutt (2006) found that these features can result in a reactive surface area that exceeds the geometric surface area by a factor ranging from 27 to 161. Because site-specific data regarding the increase in surface area are unavailable, the geometric surface area was increased by a factor of 100, which falls near the middle of this range. This increase yielded a reactive mine wall surface area of 161,155,000 ft^2.

2.2.2 Waste Rock

The underground workings will be backfilled with waste rock that will occupy an estimated 25% to 30% of the workings volume. The higher estimate of 30% was used in the calculations to maximize the waste rock surface area and minimize the amount of water in the calculations, thereby increasing calculated constituent concentrations in the underground workings water. The total volume of waste rock was calculated to be 1,494,000 ft^3.

The volume occupied by the waste rock includes both the waste rock particles and the void space between the particles. The volume occupied by the waste rock particles is required to calculate the final volume of water in the mine. The total mass of waste rock is 72,736 tons (145,472,000 lbs), based on an inverse field density of 20.53 ft^3/ton (Taylor 2010c) and the total volume of waste rock. Assuming the waste rock particles have a density equal to quartz (165 lb/ft^3), the volume of the waste rock particles is 879,337 ft^3.

The backfilled waste rock will not be crushed or otherwise treated before placement in the underground workings, so the particle size distribution will equal the run-of-mine size distribution. Knowledge of the particle size distribution is necessary for estimating the surface area of the waste rock particles. The waste rock particle size gradation was determined by Knight Piésold (2010). Coarser size fractions (4 inch to 18 inch) were estimated visually in the field and four samples of the finer materials (less than 4 inch) were collected and composited for laboratory size gradation; these results were combined to generate an overall particle size distribution (Table 2-2).

The weight percentages of waste rock in each particle size range (Table 2-3) were calculated using the particle size gradation data (Table 2-2); the mass of each particle size in a cubic meter of waste rock was calculated using these weight percentages and the reported inverse field density of 20.53 ft^3/ton (1,560 kg/m^3). The surface area and volume of the waste rock particles were calculated for each size fraction assuming spherical particles with a diameter equal to the midpoint of the size range using equations (3) and (4), respectively:

$$4 \tag{3}$$

$$\frac{4}{3} \quad 3 \tag{4}$$

Table 2-2. Particle Size Gradation

Sieve Size	Sieve Size (mm)	Field Results (% finer)	Laboratory Results (% finer)	Overall (% finer)
>18 inch	> 457.2	100	--	100
18 inch	457.2	96	--	96
12 inch	304.8	90	--	90
10 inch	254	85	--	85
8 inch	203.2	77	--	77
6 inch	152.4	70	--	70
4 inch	101.6	65	--	65
3 inch	76.2	--	100	65
2 inch	50.8	--	88.1	57
1.5 inch	38.1	--	77.8	51
1 inch	25.4	--	63.2	41
0.75 inch	19.05	--	52.6	34
0.5 inch	12.7	--	39.7	26
0.375 inch	9.525	--	33.6	22
#4	4.75	--	25.9	17
#8	2.38	--	17.8	12
#16	1.20	--	12.3	8
#40	0.422	--	9.7	6
#50	0.297	--	8.4	5
#100	0.152	--	6	4
#200	0.075	--	4.5	3

Source: Knight Piésold (2010)

For example, the maximum size of the waste rock was reported to be 24 inch (Taylor 2010b), so for the largest size fraction, the size range was assumed to be 18 to 24 inch (0.457 to 0.610 m), with an average 21 inch (0.533 m) diameter and an average radius of 10.5 inch (0.267 m). The surface area of a spherical particle of this radius is 9.62 ft^2 (0.894 m^2) and the volume is 2.81 ft^3 (0.0795 m^3); using the particle volume and the assumed waste rock particle density of 165 lb/ft^3 (2,650 kg/m^3), the mass of each particle is calculated to be 464 lb (211 kg). Using the mass of this size fraction per unit volume of 3.89 lb/ft^3 (62.39 kg/m^3, which is 4% of the total 1,560 kg/m^3), the number of particles of this size would be 0.00839 per ft^3 (0.296 per m^3) of waste rock. Multiplying the surface area per particle by the number of particles provides the geometric surface area per unit volume of waste rock for each size fraction. The results of these calculations are provided in Table 2-3. These results show that approximately 75% of the total

geometric surface area is associated with the smallest particle size waste rock (less than 200 mesh or 0.075 mm) even though this material represents only 3 weight % of the waste rock.

The geometric surface area of the waste rock particles was calculated to be 1,120 ft^2/ft^3 (3,675 m^2/m^3), which yields a total geometric surface area of 1,673,580,448 ft^2 (155,479,964 m^2). White and Peterson (1990) determined a roughness factor of seven to account for surface irregularity associated with freshly fractured minerals. Multiplying the geometric surface area by this roughness factor yields an estimated waste rock backfill reactive surface area of 11,715,063,133 ft^2 (1,088,359,751 m^2). The total mine wall rock and waste rock reactive surface area is 11,876,218,084 ft^2 (1,103,331,535 m^2). The reactive surface area of the waste rock backfill constitutes over 98% of the expected total reactive surface area.

2.2.3 Concrete

The backfilled waste rock will be stabilized by the emplacement of concrete every six feet. The estimated total volume of concrete is 500,000 ft^3 (14,158 m^3) (Taylor 2010b). The concrete will be made up of 25% (by volume) Portland Type II cement and 75% cellular foam. It is assumed that the cementitious material in the concrete will react when submerged in the mine water and the cellular foam will remain inert.

Portland Type II cement has moderate sulfate resistance, with a typical composition listed in Table 2-4. The density of Portland cement is about 146 lb/ft^3 (2,340 kg/m^3), so the expected mass of cement in the mine workings is 18,260,179 lb (8,282,679 kg). The neutralizing potential (NP) of the cement was calculated using the chemical composition in Table 2-4, which provides a CaO concentration in the cement of 63.0 wt%. The NP of the cement was calculated to be 1,125 ton $CaCO_3$/kton.

2.2.4 Underground Workings Water Volume and Rock Surface Area to Volume Ratio

The total volume of water present in the underground workings will equal the volume of the underground workings of 4,980,000 ft^3 (141,018 m^3), minus the volumes occupied by the waste rock particles (879,337 ft^3 or 24,900 m^3) and concrete backfill (500,000 ft^3 or 14,158 m^3). The calculated water volume is 3,600,663 ft^3 (101,959 m^3).

The ratio of mine wall rock and waste rock surface area to water volume is required for the underground workings water quality modeling calculations. The total reactive waste rock and mine wall surface area (Section 2.2.2) divided by the water volume is 3,298 ft^2/ft^3 (10,821 m^2/m^3). Because the mine wall rock and waste rock are assumed to be composed of equal amounts of quartzite and argillite/siltite, the surface area to volume ratio for each of these rock types is 1,649 ft^2/ft^3 (5,411 m^2/m^3).

Table 2-3. Calculation of Geometric Surface Area for Waste Rock Size Fractions

Size Range (mm)	Weight percent	Mass per m^3 (kg)	Particle radius (m)	Particle volume (m^3)	Particle surface area (m^2)	Mass per particle (kg)	Number of particles per m^3 waste rock	Geometric Surface Area (m^2/m^3)	Surface area (% of total)
> 457.2	4.00	62.39	0.2667	0.0795	0.894	211	0.296	0.265	0.01%
304.8 to 457.2	6.00	93.58	0.1905	0.0290	0.456	76.7	1.22	0.556	0.02%
254 to 304.8	5.00	77.99	0.1397	0.114	0.245	30.3	2.58	0.632	0.02%
203.2 to 254	8.00	124.8	0.1143	6.25×10^{-3}	0.164	16.6	7.53	1.24	0.03%
152.4 to 203.2	7.00	109.2	0.08890	2.94×10^{-3}	0.0993	7.80	14.0	1.39	0.04%
101.6 to 152.4	5.00	77.99	0.06350	1.07×10^{-3}	0.0507	2.84	27.4	1.39	0.04%
76.2 to 101.6	0.00	0.00	0.04445	3.68×10^{-4}	0.0248	0.975	0.00	0.00	0.00%
50.8 to 76.2	7.74	120.6	0.03175	1.34×10^{-4}	0.0127	0.355	340	4.30	0.12%
38.1 to 50.8	6.70	104.4	0.02223	4.60×10^{-5}	6.21×10^{-3}	0.122	857	5.32	0.14%
25.4 to 38.1	9.49	148.0	0.01588	1.68×10^{-5}	3.17×10^{-3}	0.0444	3,333	10.56	0.29%
19.05 to 25.4	6.89	107.5	0.01111	5.75×10^{-6}	1.55×10^{-3}	0.0152	7,055	10.95	0.30%
12.7 to 19.05	8.39	130.8	7.938×10^{-3}	2.09×10^{-6}	7.92×10^{-4}	5.55×10^{-3}	23,560	18.65	0.51%
9.525 to 12.7	3.97	61.84	5.556×10^{-3}	7.19×10^{-7}	3.88×10^{-4}	1.90×10^{-3}	32,480	12.60	0.34%
4.75 to 9.525	5.01	78.06	3.569×10^{-3}	1.90×10^{-7}	1.60×10^{-4}	5.05×10^{-4}	1.55×10^{5}	24.76	0.67%
2.38 to 4.75	5.27	82.12	1.783×10^{-3}	2.37×10^{-8}	3.99×10^{-5}	6.29×10^{-5}	1.31×10^{6}	52.15	1.42%
1.2 to 2.38	3.58	55.76	8.950×10^{-4}	3.00×10^{-9}	1.01×10^{-5}	7.96×10^{-6}	7.01×10^{6}	70.53	1.92%
0.422 to 1.2	1.69	26.36	4.055×10^{-4}	2.79×10^{-10}	2.07×10^{-6}	7.40×10^{-7}	3.56×10^{7}	73.59	2.00%
0.297 to 0.422	0.84	13.18	1.798×10^{-4}	2.43×10^{-11}	4.06×10^{-7}	6.45×10^{-8}	2.04×10^{8}	83.01	2.26%
0.152 to 0.297	1.56	24.33	1.123×10^{-4}	5.92×10^{-12}	1.58×10^{-7}	1.57×10^{-8}	1.55×10^{9}	245.4	6.68%
0.075 to 0.152	0.98	15.21	5.675×10^{-5}	7.66×10^{-13}	4.05×10^{-8}	2.03×10^{-9}	7.50×10^{9}	303.4	8.25%
< 0.075	2.93	45.62	1.875×10^{-5}	2.76×10^{-14}	4.42×10^{-9}	7.32×10^{-11}	6.24×10^{11}	2,755	74.95%
Total								3,675	100%

Table 2-4. Chemical Composition of Portland Type II Cement

Chemical Name	Chemical Formula	Weight Percent
Tricalcium silicate	$3CaO•SiO_2$	51
Dicalcium silicate	$2CaO•SiO_2$	24
Tricalcium aluminate	$3CaO•Al_2O_3$	6
Tetracalcium aluminoferrite	$4CaO•Al_2O_3•Fe_2O_3$	11
MgO	MgO	2.9
SO_3	SO_3	2.5
Free CaO	CaO	1

2.2.5 Duration of Mine Wall and Waste Rock Exposure

The Hollister Mine and Hatter Expansion mine drain setup schedule (Table 2-5) indicates the length of time mine wall rock and backfilled waste rock will be exposed to the atmosphere. The total vertical extent of mining at the Hollister Mine began at an elevation of approximately 5,400 ft amsl in 2005 and will be advanced to 4,570 ft amsl in 2016 (Cain 2010). A subsurface drift from the Hollister Mine workings will begin at 5,200 ft amsl in 2014 and will end at 4,800 ft amsl at Hatter. Beginning in 2017 and ending in 2029, the Hatter Expansion workings will be advanced downward to a final elevation of 4,000 ft amsl.

Table 2-5. Hollister Mine and Hatter Expansion Mine Drain Setup Schedule

Year	Hollister Mine Level (Generalized, ft)	Hatter Expansion Level (ft)	Comments
2010	4,979	--	Based upon future Hollister Mine plan
2011	4,930	--	Based upon future Hollister Mine plan
2012	4,810	--	Based upon future Hollister Mine plan
2013	4,690	--	Based upon future Hollister Mine plan
2014	4,570	5,200 – 4,800	Subsurface drift over to Hatter, ending at 4,800 ft elevation at Hatter
2015	4,570	4,800	Hatter Expansion dewatering begins
2016	5,050	4,800	Deep mining stops at Hollister Mine
2017	5,050	4,400	Hatter Expansion workings advanced downwards
2018	5,050	4,400	--
2019 through 2029	5,050	4,000	Hatter Expansion workings advanced downwards to final elevation of 4,000 ft
2030 through 2250	--	--	Water level recovery period

Source: Cain (2010)

2.3 Hydrologic Data

The results of hydrologic modeling performed to simulate drawdown and water level recovery at the Hollister Mine and Hatter Expansion are summarized in Table 2-6. For the Hollister Mine workings, water level recovery will begin in 2016 when deep mining ends. Water levels in the Hollister Mine workings are projected to recover relatively quickly to 58.4% of the total vertical extent of the workings by the end of 2016 (Table 2-6). Water levels will be maintained relatively constant at approximately 5,063 ft amsl in the Hollister Mine workings until 2029 when mining is completed in the Hatter Expansion. Water levels then will increase by an amount sufficient to submerge more than 90% of the vertical extent of the Hollister Mine workings by the end of 2050 and more than 95% of the vertical extent of the workings by 2070. Water levels then gradually approach steady state, reaching 99% of water level recovery by 2130.

Water level recovery is predicted to begin in the Hatter Expansion in 2029 after mining is completed. Water levels are predicted to rise and submerge more than 50% of the vertical extent of the Hatter Expansion workings by 2048. More than 90% of the extent of the Hatter Expansion workings will be submerged by 2060 and more than 95% will be submerged by 2070. Water levels in the Hatter Expansion workings will then gradually approach steady state, reaching 99% of water level recovery by 2115.

Exploratory mining began in 2005 at the Hollister Mine and the percentage of water level recovery in the Hollister Mine workings will reach 99% in the year 2130. Consequently, the majority of the mine wall rock and waste rock in the Hollister Mine and Hatter Expansion workings will be exposed to the atmosphere for a maximum of 125 years.

2.4 Groundwater Quality Data

Composition data for the groundwater entering the workings are available from boreholes emplaced in the Vinini Formation and sampled before exploratory mining began at the site (Table 2-7). In addition, water quality data are available for the drainage currently being discharged from the underground workings during exploratory mining (Table 2-8, Appendix A).

2.5 Waste Rock Testing Data

Acid-base accounting (ABA), Meteoric Water Mobility Testing (MWMP) and kinetic testing (BC Humidity Cell Protocol) were carried out to characterize rock samples obtained from drill core and boreholes in the area of the exploration decline (Walker 2003a, 2003b). The waste rock humidity cell results reported by Walker (2003a) can be used to characterize potential releases of constituents from the mine wall rock and waste rock backfill.

Table 2-6. Predicted Percent Water Level Recovery or Saturated Percentage of the Vertical Extent of the Mine Workings, Hollister Mine and Hatter Expansion

Hollister Mine		Hatter Expansion	
Model Time	Percent Water Level Recovery or Saturated Percentage of Vertical Mine Extent	Model Time	Percent Water Level Recovery or Saturated Percentage of Vertical Mine Extent
4/2005	100.0%	2010	99.8%
12/2005	94.9%	2011	99.5%
12/2006	80.8%	2012	99.1%
12/2007	80.4%	2013	98.5%
12/2008	78.3%	2014	96.5%
12/2009	66.5%	2015	56.5%
12/2010	62.5%	2016	56.4%
12/2011	36.6%	2017	28.2%
12/2012	35.4%	2018	28.2%
12/2013	32.3%	2019	0.0%
12/2014	0.0%	2029	0.0%
12/2015	0.0%	2030	3.1%
12/2016	58.4%	2032	4.4%
12/2017	59.8%	2034	9.7%
12/2018	59.9%	2036	22.1%
12/2019	59.9%	2038	38.8%
12/2020	59.9%	2040	39.5%
12/2030	65.2%	2042	41.3%
12/2040	86.3%	2044	44.3%
12/2050	91.8%	2046	47.9%
12/2060	94.5%	2048	52.0%
12/2070	96.2%	2050	56.3%
12/2080	97.2%	2060	93.4%
12/2090	97.8%	2070	97.6%
12/2100	98.3%	2080	98.2%
12/2130	99.1%	2090	98.5%
12/2151	99.4%	2100	98.7%
12/2181	99.7%	2115	99.0%
12/2196	99.9%	2187	99.5%
12/2217	100.0%	2232	99.7%

Source: Cain (2010)

Table 2-7. Vinini Formation Borehole Water Quality

Borehole	BH-01	BH-01	BH-02[a]	BH-02	BH-04[a]	BH-04
Date	9/29/2002	3/13/2003	10/1/2002	3/13/2003	10/11/2002	3/13/2003
Bicarbonate	127	104	54	51	88	62
Aluminum	<0.02	<0.02	<0.02	<0.02	0.099	<0.02
Antimony	0.0743	<0.003	0.0187	<0.003	<0.003	<0.003
Arsenic	0.0306	<0.005	0.0086	<0.005	0.0155	<0.005
Barium	0.134	0.071	0.134	0.196	0.032	0.031
Beryllium	<0.002	<0.002	<0.002	<0.002	<0.002	<0.002
Boron	0.221	0.10	0.143	<0.01	0.068	<0.01
Cadmium	<0.002	<0.002	<0.002	<0.002	<0.002	<0.002
Calcium	45.3	48	20	23	30	28
Chloride	15	15	24	24	26	25
Chromium	<0.005	<0.005	<0.005	<0.005	<0.005	<0.005
Copper	<0.01	<0.01	<0.01	<0.01	<0.01	<0.01
Fluoride	0.94	0.9	1.3	1.3	0.85	0.9
Iron	1	0.038	<0.02	0.036	0.0445	0.021
Lead	<0.007	<0.007	<0.007	<0.007	<0.007	<0.007
Magnesium	14.3	14.8	6	6.2	9.6	7.9
Manganese	0.219	0.375	0.12	0.01	0.039	0.092
Mercury	0.0005	<0.0005	<0.0005	<0.0005	<0.0005	<0.0005
Nickel	<0.02	<0.02	<0.02	<0.02	<0.02	<0.02
Nitrate and Nitrite as N	<1	0	<1	0	<1	0.7
pH, lab (standard units)	8.26	7.29	7.58	7.97	8.27	7.58
Potassium	4.85	4.75	2.58	2.74	2.48	2.29
Selenium	<0.01	<0.01	<0.01	<0.01	<0.01	<0.01
Silver	<0.01	<0.01	<0.01	<0.01	<0.01	<0.01
Sodium	31.4	26	30	68	29.9	32
Sulfate	72	60	50	110	57	58
Thallium	<0.001	<0.001	<0.001	<0.001	<0.001	<0.001
Total Dissolved Solids	280	244	180	183	260	283
Zinc	<0.05	<0.05	<0.05	<0.05	<0.05	<0.05
Speciated Charge Balance (%)	10.6	21.0	4.52	8.84	3.40	8.46

All units mg/L unless otherwise noted

a – water quality analysis used in PHREEQC calculations

Table 2-8. Underground Discharge Water Quality Summary

Constituent	Mean	Maximum	Minimum	Number of Analyses	Nondetects
Bicarbonate	91	150	24	12	0
Aluminum	0.80	5.4	<0.045	12	7
Antimony	0.017	0.026	0.0052	12	0
Arsenic	0.069	0.30	0.006	12	0
Barium	0.054	0.24	0.024	12	0
Beryllium	0.001	0.0017	<0.001	12	9
Boron	0.14	0.38	<0.1	12	5
Cadmium	<0.001	<0.001	<0.001	12	12
Calcium	58	96	30	12	0
Chloride	23	53	7.9	12	0
Chromium	0.006	0.013	<0.005	12	11
Copper	0.055	0.098	<0.05	12	10
Fluoride	1.1	1.6	0.79	12	0
Iron	1.9	17	<0.01	12	2
Lead	<0.01	<0.01	<0.01	12	12
Magnesium	11	16	6.5	12	0
Manganese	0.40	1.5	<0.005	12	1
Mercury	0.0006	0.0017	<0.0001	12	3
Molybdenum	0.010	0.012	<0.01	8	7
Nickel	0.025	0.054	<0.01	12	6
Nitrate + Nitrite as N	1.4	1.7	<0.1	12	6
pH, lab (standard units)	8.3	9.71	6.58	12	0
Potassium	5.9	8.1	4.2	12	0
Selenium	0.0085	0.02	<0.005	12	8
Silver	0.010	0.062	<0.005	12	11
Sodium	30	39	24.00	12	0
Strontium	0.20	0.27	0.14	8	0
Sulfate	164	250	90.00	12	0
Thallium	0.0010	0.0015	<0.001	12	11
Total Dissolved Solids	375	480	240.00	12	0
Vanadium	0.015	0.021	<0.01	8	3
Zinc	0.10	0.35	<0.01	12	6
Conductivity (µS/cm)	594	657	562	4	0
Alkalinity, $CaCO_3$	88	130	40	12	0

All units mg/L unless otherwise noted

The waste rock types identified at the site and tested were andesite, quartzite and interbedded argillite/siltite (Section 2.1). Andesite is only encountered in the first 500 to 600 ft of the decline and does not make up a significant fraction of the mine wall rock or waste rock that will be backfilled in the mine (Walker 2003a). Humidity cell testing of the andesite waste rock also indicates that andesite will not be acid producing. Consequently, the humidity cell test results obtained with andesite were not included in the water quality evaluation. The waste rock and, by extension, the mine wall rock are expected to be 50% quartzite and 50% argillite/siltite (Walker 2003b).

ABA tests were carried out on 40 quartzite rock samples, five argillite rock samples and 15 siltite rock samples (Walker 2003b). The average acid-base potential (ABP) was -29.54 ton $CaCO_3$/kton for quartzite, -35.20 ton $CaCO_3$/kton for argillite and -60.05 ton $CaCO_3$/kton for siltite. Assuming the waste rock and mine wall rock will consist of 50% quartzite, 25% siltite and 25% argillite, the mean ABP is predicted to be -41.69 ton $CaCO_3$/kton.

Humidity cell tests were carried out on 14 quartzite samples and seven argillite/siltite samples representative of the mine waste rock (Walker 2003a, 2003b). The results of the humidity cell tests carried out with quartzite and argillite/siltite were used to predict the release of weathering products from the mine wall rock and waste rock by determining the release of constituents per unit surface area in the humidity cell tests and extrapolating to the predicted surface area of the mine wall rock and waste rock. The mean constituent releases were calculated separately for the quartzite and argillite/siltite samples for input into the geochemical modeling calculations. Constituents of potential concern at the site based on NDEP Profile I analysis of humidity cell effluents appear to be pH, aluminum, antimony, arsenic, barium, beryllium, boron, cadmium, chromium, copper, fluoride, iron, lead, manganese, nickel, selenium, sulfate, thallium and zinc.

Each humidity cell test was carried out using approximately 1.2 kg of waste rock crushed to achieve a particle size of less than 0.25 inch (0.635 cm). The solution volumes used to flush the waste rock were approximately 0.5 L per week. The tests were conducted for a maximum of 20 weeks.

The humidity cell test procedure greatly accelerates the weathering rates of mine wall rock and waste rock compared to rates anticipated under field conditions. For example, Walker (2003a) calculated that 1 week of humidity cell testing is equivalent to 110 years of exposure to air and water at the site. Because the mine walls and waste rock are likely to be exposed to air for a maximum of about 125 years (Section 2.3), it is assumed that the composited water sample collected during the first four weeks of the humidity cell tests would adequately represent potential releases of metals and acidity from the quartzite and argillite/siltite. Analyses of composited water samples collected from the quartzite and argillite/siltite humidity cell tests using during the first four weeks of testing are summarized in Table 2-9, with detailed results provided in Appendix A.

Table 2-9. Statistical Summary of Concentrations in First Four-Week Humidity Cell Composite Samples

Rock Type	Quartzite				Argillite/siltite			
Constituent	Mean	Maximum	Minimum	Median	Mean	Maximum	Minimum	Median
Aluminum	10.4	45.3	0.147	1.44	31.0	65.2	0.588	31.0
Antimony	0.002	0.006	<0.001	0.002	0.003	0.01	<0.001	0.002
Arsenic	0.054	0.14	0.010	0.033	0.17	0.66	<0.01	0.058
Barium	0.0388	0.127	0.0093	0.021	0.02	0.05	0.007	0.020
Beryllium	0.023	0.17	<0.002	0.002	0.06	0.27	0.007	0.017
Boron	0.046	0.101	<0.04	<0.04	0.062	0.13	<0.04	<0.04
Cadmium	0.0313	0.318	<0.002	0.005	0.12	0.31	0.003	0.070
Calcium	26.8	95.10	6.19	20.0	90.4	145	9.47	104
Chloride	1.08	1.57	0.620	1.000	1.16	1.41	0.570	1.24
Chromium	0.09	0.43	<0.006	0.0068	0.20	0.61	<0.006	0.157
Copper	0.44	1.64	0.010	0.297	2.48	7.66	0.188	1.66
Fluoride	1.14	3.50	0.19	0.56	3.45	8.15	<0.20	2.24
Iron	67.3	315	0.392	13.4	134	353	4.310	144
Lead	0.01	0.04	<0.005	0.006	0.02	0.05	0.007	0.014
Magnesium	10.4	65.2	0.766	5.98	30.5	56.9	1.730	31.6
Manganese	1.87	7.94	0.0262	0.887	1.64	2.93	0.787	1.41
Mercury	<0.002	<0.002	0.0013	<0.002	<0.0002	<0.0002	<0.0002	<0.0002
Nickel	0.74	3.27	0.066	0.410	2.59	5.25	0.469	2.60
Nitrate and Nitrite as N	0.07	0.11	0.030	0.060	0.11	0.33	0.040	0.080
pH (standard units)	3.96	5.44	2.810	3.775	3.28	4.12	2.66	3.12
Potassium	4.62	18.3	<1.0	4.45	13.90	41.70	1.00	4.20
Selenium	0.05	0.14	0.010	0.029	0.10	0.25	0.045	0.091
Silver	0.006	0.0139	<0.005	<0.005	<0.005	<0.005	<0.005	<0.005
Sodium	3.80	7.44	1.95	3.29	8.25	12.2	2.34	9.59
Sulfate	331	1,130	39.8	206	886	1,530	301	1,010
Thallium	0.005	0.010	<0.001	0.004	0.009	0.019	0.003	0.009
Total Dissolved Solids	517	1,690	60.0	331	1,373	2,370	477	1,620
Zinc	2.74	17.5	0.074	0.289	8.74	30.8	0.152	5.47

All units mg/L unless otherwise noted

The release of constituents per unit surface area of the waste rock in the humidity cell tests was calculated using the surface area estimated from the grain size. Based on a grain size of 0.635 cm (0.25 inch), the estimated surface area is 6.54×10^{-3} m^2/cm^3 using the correlation provided by White and Peterson (1990) for freshly fractured materials. Assuming the crushed waste rock had a bulk density consistent with sand (1.60 g/cm^3), the specific surface area of the crushed waste rock used in the humidity cell tests is estimated to be 4.08 m^2/kg. Using the average volume of the first four flushes (approximately 2 L) and the average mass of waste rock in the humidity cells (approximately 1.2 kg) (Walker 2003a) with the gram formula weight of each constituent, the constituent concentrations in the humidity cell leachates (mg/L) can be converted to the mass released per m^2 of waste rock surface area:

Mean constituent release (mole/m^2) =
Mean constituent release (mg/L) × solution volume (L)/mass of waste rock (kg) ×
1 kg waste rock/4.08 m^2 ÷ gram formula weight (mg/mole)

The calculated constituent releases are summarized in Table 2-10.

Table 2-10. Mean Constituent Releases from First Four Week Composite Humidity Cell Samples

Constituent	Quartzite (µmoles/m^2)	Argillite/siltite (µmoles/m^2)
Aluminum	156.2	465.2
Antimony	0.007825	0.01142
Arsenic	0.2905	0.907
Barium	0.1141	0.06557
Beryllium	1.032	2.572
Boron	1.725	2.336
Cadmium	0.1124	0.4325
Calcium	270.1	913.7
Chloride	12.29	13.30
Chromium	0.7258	1.545
Copper	2.798	15.85
Fluoride	24.34	73.55
Iron	486.8	970.6
Lead	0.01713	0.04131
Magnesium	173.3	507.9
Manganese	13.78	12.12
Nickel	5.067	17.89
Nitrate and Nitrite (as N)	1.896	3.101
Potassium	47.77	144.1
Selenium	0.2325	0.5185
Sodium	66.73	145.5
Sulfate	1,393	3,738
Thallium	0.01059	0.01757
Zinc	16.95	54.20

3.0 GEOCHEMICAL MODELING CODE AND DATABASE

The PHREEQC geochemical modeling code (version 2.17, Parkhurst and Appelo 1999) was used for this investigation. The MINTEQ.v4 database distributed with the PHREEQC code (USGS 2010) was used because it is well-documented (EPA 1999) and includes aqueous speciation and solid phase solubility data for the potential constituents of concern (Table 3-1). Neither waste rock leachates from the humidity cell tests (Section 2.5) nor groundwater (Section 2.4) had significant concentrations of mercury or silver, so these NDEP Profile I constituents were not included in the modeling calculations.

Table 3-1. Potential Constituents of Concern Included in Modeling Calculations

Constituent	Sources
Aluminum	Waste rock, groundwater
Antimony	Waste rock, groundwater
Arsenic	Waste rock, groundwater
Barium	Waste rock, groundwater
Beryllium	Waste rock
Bicarbonate	Groundwater
Boron	Waste rock, groundwater
Cadmium	Waste rock
Calcium	Waste rock, groundwater
Chloride	Waste rock, groundwater
Chromium	Waste rock
Copper	Waste rock
Fluoride	Waste rock, groundwater
Iron	Waste rock, groundwater
Lead	Waste rock, groundwater
Magnesium	Waste rock, groundwater
Manganese	Waste rock, groundwater
Nickel	Waste rock
Nitrate	Waste rock, groundwater
pH	Waste rock, groundwater
Potassium	Waste rock, groundwater
Selenium	Waste rock
Sodium	Waste rock, groundwater
Sulfate	Waste rock, groundwater
Thallium	Waste rock
Zinc	Waste rock

The MINTEQ.v4 database does not include data for several potentially important solid phases, including hydrozincite [$Zn_5(OH)_6(CO_3)_2$(cr)], which could form as zinc is released by the waste rock. Log K_{sp} data reported for hydrozincite by Eary (1999) were included in the calculations

(Table 3-2). At high pH values that may be caused by dissolution of cementitious materials, the solid phases ettringite [$Ca_6Al_2(SO_4)_3(OH)_{12}$•$26H_2O$(s)], hydrogarnet [$Ca_3Al_2(OH)_{12}$(s)], Fe-hydrogarnet [$Ca_3Fe_2(OH)_{12}$(s)], tobermorite and monosulfate [$(CaO)_3Al_2O_3CaSO_4$•$12H_2O$(s)] may form in the hydrated cement paste or during cement leaching. The log K_{sp} values for these phases reported by Lothenbach and Winnefeld (2006) were included in the calculations (Table 3-2).

Table 3-2. Solubility Data Added to the MINTEQ.v4 Database

Phase	Reaction	Log K_{sp}	Source
Hydrozincite	$Zn_5(OH)_6(CO_3)_2(s) + 6\ H^+ =$ $5\ Zn^{2+} + 6\ H_2O + 2\ CO_3^{2-}$	-12.68	Eary (1999)
Ettringite	$Ca_6Al_2(SO_4)_3(OH)_{12}$•$26H_2O(s) =$ $6\ Ca^{2+} + 2\ Al(OH)_4^- + 3\ SO_4^{2-} + 4\ OH^- + 26\ H_2O$	-45.09	Lothenbach and Winnefeld (2006)
Hydrogarnet	$Ca_3Al_2(OH)_{12}(s) =$ $3\ Ca^{2+} + 2\ Al(OH)_4^- + 4\ OH^-$	-22.46	Lothenbach and Winnefeld (2006)
Fe-hydrogarnet	$Ca_3Fe_2(OH)_{12}(s) =$ $3\ Ca^{2+} + 2\ Fe(OH)_4^- + 4\ OH^-$	-26.78	Lothenbach and Winnefeld (2006)
Tobermorite	$(Ca(OH)_2)_2(SiO_2)_{2.4}$•$2H_2O(s) + 0.4\ H_2O =$ $2\ Ca^{2+} + 2.4\ H_3SiO_4^- + 1.6\ OH^-$	-18.2	Lothenbach and Winnefeld (2006)
Monosulfate	$(CaO)_3Al_2O_3CaSO_4$•$12H_2O(s) =$ $4\ Ca^{2+} + 2\ Al(OH)_4^- + SO_4^{2-} + 4\ OH^- + 6\ H_2O$	-27.7	Lothenbach and Winnefeld (2006)

For calculation of adsorption on precipitated ferrihydrite [$Fe(OH)_3$(s)], the default site densities of 0.005 mol/mol Fe and 0.2 mol/mol Fe reported by Dzombak and Morel (1990) for Type 1 and Type 2 sites, respectively, were used. A surface area of 600 m^2/g was assumed for the precipitated ferrihydrite (Dzombak and Morel 1990).

4.0 CONCEPTUAL MODEL

Prediction of the water quality in the underground mine workings requires the development of a realistic conceptual model. This conceptual model must include all important geochemical and hydrologic processes and features expected to significantly influence water quality. The important processes and features identified for predicting the Hollister Mine underground workings water are:

- Quality of inflowing groundwater
- Rates of groundwater inflow and outflow at steady state
- Amount of mixing within the mine and potential for segregation or stratification
- Leaching from exposed mine wall rock, waste rock backfill and cementitious materials
- Dissolution of nitrogen compounds remaining in the workings from blasting
- Chemical reactions, including precipitation of oversaturated minerals and sorption of minor constituents on iron oxyhydroxides

4.1 Hydrogeologic Data and Assumptions

The underground workings water quality is predicted for the fully developed mine after closure, when steady-state hydrologic conditions have been achieved. Based on the hydrologic modeling data, 99% of the final water level will be achieved in the Hollister Mine workings by the year 2130 (Section 2.3). Because the waste rock will be stabilized by emplacement of concrete every 6 ft, the waste rock and concrete will be in close contact. Because information on the distribution of the mine workings, waste rock and cement with depth was not available, it is assumed that the mine workings, waste rock and cement will be uniformly distributed over the depth of the workings. Because there is no information indicating that waste rock or cement will be stratified within the underground workings, it is assumed that the entire flooded underground workings can be approximated as a single, well-mixed system. It is also assumed that the rate of outflow of water from the workings during filling will be negligible.

The source of water to the mine after closure will be groundwater in the surrounding Vinini Formation that flows into the mine in response to the gradient created by the dewatered mine workings. The quality of the groundwater in the formation surrounding the mine workings is available from borehole water quality data (Table 2-7). These data show that groundwater will not be a significant source of beryllium, cadmium, chromium, copper, lead, mercury, nickel, selenium, silver, thallium or zinc to water in the underground workings.

Aqueous speciation calculations carried out with the data in Table 2-7 resulted in positive charge balances for all borehole samples. Four of the six borehole water samples had charge balances that exceeded the generally acceptable limit of 5% (Table 2-7). Consequently, only the two samples with speciated charge balances of less than 5% (BH-02 10/1/2002 and BH-04 10/11/2002) were used to calculate underground workings water quality.

4.2 Leaching of Mine Wall Rock and Waste Rock

Because the mine wall rock and waste rock backfill will be exposed to air and humidity during mining, oxidation of sulfides in the mine wall rock and waste rock is expected to occur. As a consequence of sulfide mineral oxidation, the mine wall rock and waste rock backfill will be potential sources of acidity and dissolved constituents to the mine water. At the end of mining, the underground workings will flood, and weathering products will be released from the mine wall rock and waste rock to the inflowing groundwater. After the mine wall rock and waste rock are submerged, sulfide oxidation is expected to essentially cease because no atmospheric oxygen will be present and the concentrations of oxygen that can dissolve in water are relatively low. The dissolved oxygen in the mine water was accounted for in the calculations by equilibrating the mine water with atmospheric oxygen during groundwater mixing and reaction of the wall rock and waste rock.

The quantities of chemical constituents released from the humidity cell test results were calculated per unit surface area (μmoles/m^2) (Table 2-10). All calculations in PHREEQC were carried out on the basis of 1 kg of water (essentially 1 L). The total surface area of the mine wall rock and waste rock per liter of water in the underground workings was calculated to be 10,821 m^2/m^3, which is equivalent to 5.411 m^2/L each for quartzite and argillite/siltite (Section 2.2.4). The total amount of each constituent released by mine wall rock and waste rock leaching per liter of solution was calculated by multiplying the concentrations in Table 2-10 for each waste rock type by 5.411 m^2.

4.3 Cementitious Material Leaching

Cementitious materials in the underground workings will include the cement fraction of the concrete used to stabilize the waste rock backfill. These cementitious materials will interact with the mine water, leaching calcium hydroxide [$Ca(OH)_2$(s)], silica and other constituents, neutralizing acidity released by the oxidized mine wall rock and waste rock. The cementitious material in the concrete will be Portland Type II cement. The anhydrous phases in cement (Table 2-4) hydrate to form a variety of minerals. It was assumed that the hydrated phases tobermorite, portlandite, brucite, ettringite, Fe-hydrogarnet and hydrogarnet will be present in the cement, based on the composition in Table 2-4.

The cementitious material in the concrete is unlikely to undergo significant reaction or degradation until submerged in water. The hydrologic data (Section 2.3) indicate that 90% or more of the vertical extent of the Hollister Mine workings and Hatter Expansion workings will be submerged by the year 2060. The water levels in the workings will not reach 99% of the vertical extent until 2115 or later (Table 2-6). Consequently, it was assumed that a substantial majority of the cementitious materials in the mine will be submerged and subjected to leaching by the underground mine water for an extended time period.

Cement dissolution in low-sulfate solutions typically begins with leaching of free lime, followed by long-term dissolution of the calcium silicate minerals (Criscenti et al. 1996, Aviam et al. 2004). However, after the cementitious materials are submerged in the underground workings, reaction between the mine water and the cementitious materials is likely to be influenced by acidity and sulfate leached from the backfilled waste rock and mine wall rock (Attiogbe and Rizkalla 1988, Aviam et al. 2004, Planel et al. 2006, Schmidt et al. 2009). Sulfate created during sulfide oxidation can react with free lime in cement to form gypsum [$CaSO_4 \bullet 2H_2O(s)$]. The volume increase caused by gypsum formation results in cracking of the cement surface. The gypsum further reacts with calcium aluminate in the cement to form ettringite, causing additional volume changes and increased crack formation. Cracking in the cement provides a larger surface area for corrosion to occur, enhancing the degradation rate (Aviam et al. 2004, Planel et al. 2006).

Sulfate attack on cement in the flooded underground workings is expected to initiate cement cracking, increase reactivity, increase the release of calcium to the solution and increase the precipitation of sulfate. Consequently, increased cement degradation in the underground workings after closure is expected to decrease sulfate and TDS through gypsum precipitation and increase solution pH because of the reaction of alkalinity leached from the cement. Because of the length of time available for most cement to react with the mine water and because the sulfate in the mine water is likely to enhance cement leaching rates, it is assumed that the cement will be available to completely react with the underground workings water.

4.4 Sources of Nitrogen Compounds

Relatively low concentrations of nitrate, nitrite and ammonium are likely to remain in the mine wall rock and waste rock because of blasting residues. The majority of these residues will be removed from the underground workings by dewatering during operations. Nitrate plus nitrite-nitrogen concentrations in the underground drainage samples ranged from below detection to 1.7 mg/L (Table 2-8, Appendix A). Because the rock samples used in the humidity cell tests were obtained from cores and boreholes and were collected before exploratory mining began, they were not exposed to blasting residues before testing. Small concentrations of nitrate plus nitrite were released by the waste rock during humidity cell testing, which were used to calculate releases from the waste rock. The mean concentration in the underground discharge (1.4 mg/L) was added to the concentration calculated from waste rock leaching to achieve an estimated nitrate plus nitrate concentration in the underground workings that takes blasting residues into account.

4.5 Chemical Constituents and Reactions Included in Geochemical Model

The modeled constituents include pH and the major elements aluminum, calcium, chloride, iron, magnesium, manganese, nitrate (+ nitrite), potassium, sodium and sulfate. The following minor element metals and metalloids were included in the geochemical modeling calculations based on

reported concentrations in the humidity cell leachates (Walker 2003a): antimony, arsenic, barium, beryllium, boron, cadmium, chromium, copper, fluoride, lead, nickel, selenium, thallium and zinc. Mercury and silver were included in the Profile I analyses of the humidity cell test leachates, but were not included in the modeling calculations because these constituents were present at non-detectable or very low concentrations in the humidity cell test leachates. Although silica was not included in the humidity cell leachate analyses, silica was included in the geochemical modeling calculations because weathering of both the waste rock and cementitious materials would be expected to release silica to the water in the underground workings. Borehole water quality data used to determine the composition of inflowing groundwater to the underground workings are summarized in Table 2-7. Based on these data, inorganic carbon was also included in the modeling calculations.

The possible sources and sinks of constituents to water in the underground workings are illustrated in Figure 4-1. The reactions of potential importance in the underground workings include oxidation of sulfide minerals, mainly pyrite, which will release metals and acidity to water in the underground workings. Acid neutralization reactions will also occur, including those associated with interaction of acidic water with the cementitious materials in the underground workings. Precipitation of secondary minerals will provide upper limits for the concentrations of a number of constituents released by leaching of the mine wall rock, waste rock and cementitious materials in the underground workings. Aqueous constituent concentrations may also be limited by sorption on iron oxides and hydroxides formed by pyrite oxidation.

The MINTEQ.v4 database contains solubility data for a very large number of solid phases. However, because of the slow precipitation kinetics of some phases, many of these phases may not precipitate from solution if oversaturated. The solid phases that might form in the underground workings (Table 4-1) were identified based on the reported likelihood of their formation in mining-affected aqueous systems (Nordstrom et al. 1990, Eary 1999, Nordstrom and Alpers 1999) and in other low-temperature systems affected by metals (Rai et al. 1987). Potential solubility controls were not identified for boron, chromium, nickel and selenium. Concentrations of these constituents may therefore be controlled by mass balance and possibly by adsorption on ferrihydrite. No likely solubility controls or adsorption data were identified for thallium. Consequently, thallium concentrations in the modeled underground workings water are controlled by mass balance. All modeling calculations were carried out assuming a temperature in the underground workings of 25°C.

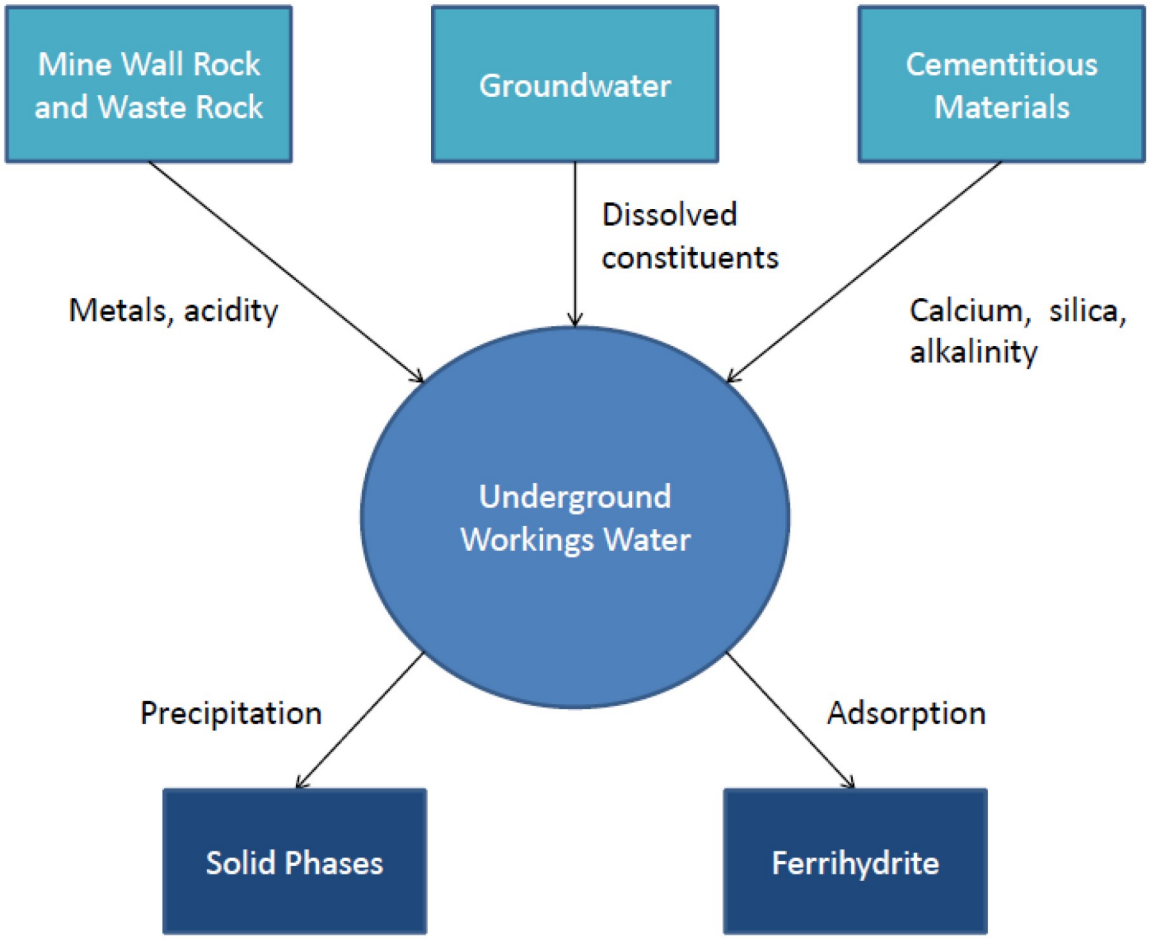

Figure 4-1. Potential Sources and Sinks of Constituents in Underground Workings Water

Table 4-1. Potential Secondary Mineral Phases

Mineral	Formula	Comments	Reference
Gypsum	$CaSO_4 \bullet 2H_2O(s)$	Sulfate concentrations greater than about 2,000 mg/L	Eary (1999), Nordstrom and Alpers (1999)
Calcite	$CaCO_3(s)$	Slightly oversaturated at pH > 7, used saturation index of 0.5	Eary (1999), Nordstrom and Alpers (1999)
Fluorite	$CaF_2(s)$	Fluoride concentrations greater than about 2 mg/L	Eary (1999), Nordstrom and Alpers (1999)
Chalcedony	$SiO_2(s)$	Low-temperature groundwater silica solubility control	Nordstrom et al. (1990)
Alunite	$KAl_3(SO_4)_2(OH)_6(s)$	Reasonable aluminum solubility control for pH < 6	Eary (1999), Nordstrom and Alpers (1999)
Basaluminite	$Al_4(OH)_{10}SO_4(s)$	Reasonable upper bound for aluminum, pH < 6	Eary (1999)
$Al(OH)_3(am)$	$Al(OH)_3(am)$	Reasonable upper bound for aluminum, pH > 6	Eary (1999), Nordstrom and Alpers (1999)
Kaolinite	$Al_2Si_2O_5(OH)_4(s)$	Solubility control for aluminum	Nordstrom and Alpers (1999)
Ferrihydrite	$Fe(OH)_3(s)$	Iron solubility control pH < 5	Eary (1999)
H-jarosite	$HFe_3(SO_4)_2(OH)_6(s)$	Possible iron solubility control	Nordstrom and Alpers (1999)
K-jarosite	$KFe_3(SO_4)_2(OH)_6(s)$	Possible iron solubility control	Nordstrom and Alpers (1999)
Manganite	γ-MnOOH(s)	Upper bound for manganese, pH < 6	Eary (1999), Nordstrom and Alpers (1999)
Birnessite	δ-$MnO_2(s)$	Manganese solubility control, pH < 6	Eary (1999)
Rhodochrosite	$MnCO_3(s)$	Upper bound for manganese, pH > 6	Eary (1999)
$Ba_3(AsO_4)_2(s)$	$Ba_3(AsO_4)_2(s)$	Possible arsenic solubility control in systems with barium ions	Rai et al. (1987)
Barite	$BaSO_4(s)$	Solubility control for barium	Eary (1999), Nordstrom and Alpers (1999)
$Be(OH)_2(am)$	$Be(OH)_2(am)$	Solubility control for beryllium by analogy with aluminum	Fishbein (1981)
Otavite	$CdCO_3(s)$	Solubility control for cadmium, pH 7.5 to 8.5	Eary (1999)
$Cd_4(OH)_6SO_4(s)$	$Cd_4(OH)_6SO_4(s)$	Upper bound for cadmium pH > 9	Eary (1999)
Tenorite	CuO	Solubility control for copper, pH > 7	Eary (1999)
Brochantite	$Cu_4(OH)_6SO_4(s)$	Solubility control pH > 7; upper bound for copper for pH < 7	Eary (1999)
Malachite	$Cu_2(OH)_2CO_3(s)$	Solubility control for copper in carbonate systems, pH > 7	Eary (1999)
Sepiolite	$Mg_2Si_3O_{7.5}OH \bullet 3H_2O$	Solubility control for magnesium	Nordstrom and Alpers (1990)
$Ni(OH)_2(s)$	Ni(OH)(s)	Upper bound for nickel at high pH	Peltier et al. (2006)
Larnakite	$PbO{:}PbSO_4(s)$	Solubility control for lead, pH > 7.5	Eary (1999)
Cerrusite	$PbCO_3(s)$	Upper bound for lead, pH > 6	Eary (1999)
Zincite	ZnO(s)	Solubility control for zinc, pH > 7.5	Eary (1999)
Hydrozincite	$Zn_5(OH)_6(CO_3)_2(s)$	Solubility control for zinc, pH from 4.5 to 7.5	Eary (1999)
Portlandite	$Ca(OH)_2(s)$	Forms at high pH during cement leaching	Criscenti et al. (1996)
Brucite	$Mg(OH)_2(s)$	Forms at high pH during cement leaching	Lothenbach and Winnefeld (2006)
Ettringite	$Ca_6Al_2(SO_4)_3(OH)_{12} \bullet 26H_2O(s)$	Forms at high pH during cement leaching	Lothenbach and Winnefeld (2006)
Monosulfate	$(CaO)_3Al_2O_3CaSO_4 \bullet 12H_2O(s)$	Forms at high pH during cement leaching	Criscenti et al. (1996)

5.0 GEOCHEMICAL MODELING RESULTS

The geochemical modeling calculations were performed using the following steps:

1. Mixing of two borehole water compositions (BH-02 10/1/2002 and BH-04 10/11/2002) in equal proportions to simulate the water quality of the inflowing groundwater
2. Leaching of constituents from the mine wall rock and waste rock and equilibration of the solution with atmospheric oxygen
3. Reaction of the solution with hydrated cement phases and chalcedony [SiO_2(s)], precipitation of solid phases and adsorption of constituents by ferrihydrite

The calculated surface area of the waste rock backfill is much larger than the surface area of the mine wall rock, so it is expected to dominate releases of constituents of potential concern to water in the underground workings. The surface area calculated for the waste rock backfill was approximated based on the particle size distribution and is a somewhat uncertain parameter. The sensitivity of the water quality calculation results to the mine wall rock plus waste rock reactive surface area was evaluated in a second set of calculations by increasing the surface area by a factor of 10, i.e., to 54.11 m^2/L each for quartzite and argillite/siltite.

The calculated changes in the amounts of solid phases for the two mine wall rock and waste rock reactive surface areas are provided in Table 5-1. The aqueous constituent concentrations are summarized in Table 5-2 and the concentrations of adsorbed species are provided in Table 5-3. The initial solid phase assemblage included chalcedony and the cementitious phases brucite, ettringite, Fe-hydrogarnet, hydrogarnet, portlandite and tobermorite. Reaction of the mine wall rock, waste rock and cementitious phases with the groundwater caused brucite, chalcedony, ettringite, Fe-hydrogarnet, hydrogarnet and portlandite to dissolve and $Ba_3(AsO_4)_2$(s), ferrihydrite, fluorite, gypsum, hydrozincite, kaolinite, sepiolite, tenorite and tobermorite to precipitate in the calculations with both surface areas. Precipitation of birnessite and calcite was observed in the calculation with the lower mine wall rock and waste rock surface area but not in the calculation with the higher surface area. The calculation carried out with the higher mine wall rock and waste rock surface area also resulted in the precipitation of manganite, $Ni(OH)_2$(s) and zincite.

For both sets of calculations, the pH of the solution was controlled by precipitation of tobermorite at pH 10.2 to 10.3 via the reaction:

$$(Ca(OH)_2)_2(SiO_2)_{2.4}\bullet 2H_2O(s) + 0.4\ H_2O = 2\ Ca^{2+} + 2.4\ H_3SiO_4^- + 1.6\ OH^- \qquad (5)$$

This pH exceeds the NDEP Profile I reference value. The redox conditions were relatively oxidizing in the calculation with the lower surface area, with slightly lower redox conditions predicted by the calculations with the higher surface area.

Table 5-1. Solid Phase Changes

Mine wall rock and waste rock surface area	5.411 m^2/L		54.11 m^2/L	
Phase	Initial	Final	Initial	Final
$Ba_3(AsO_4)_2(s)$	0.00	5.206×10^{-7}	0.00	3.441×10^{-6}
Birnessite	0.00	1.416×10^{-4}	0.00	0.00
Brucite	0.05844	0.00	0.05844	0.00
Calcite	0.00	9.852×10^{-4}	0.00	0.00
Chalcedony	10.00	9.090	10.00	9.240
Ettringite	0.008455	0.00	0.008455	0.00
Fe-Hydrogarnet	0.01839	0.00	0.01839	0.00
Ferrihydrite	0.00	0.04467	0.00	0.1156
Fluorite	0.00	2.419×10^{-4}	0.00	0.002615
Gypsum	0.00	0.03728	0.00	0.2801
Hydrogarnet	0.02797	0.00	0.02797	0.00
Hydrozincite	0.00	7.700×10^{-5}	0.00	5.819×10^{-4}
Kaolinite	0.00	0.03810	0.00	0.05324
Manganite	0.00	0.00	0.00	0.001403
$Ni(OH)_2(s)$	0.00	0.00	0.00	8.876×10^{-4}
Portlandite	0.4775	0.00	0.4775	0.00
Sepiolite	0.00	0.03122	0.00	0.04781
Tenorite	0.00	9.989×10^{-5}	0.00	0.001007
Tobermorite	0.1228	0.4306	0.1228	0.3349
Zincite	0.00	0.00	0.00	8.919×10^{-4}

All units moles/kg water

The alkaline pH of the solutions is consistent with the relatively large NP of the cement compared to the ABP of the waste rock. Multiplying the NP of 1,125 ton $CaCO_3$/kton cement by the mass of cement (9.130 kton) in the Hollister Mine yields a total NP of 10,269 ton $CaCO_3$. In comparison, the average ABP of the waste rock (-41.69 ton $CaCO_3$/kton) multiplied by the 72.7 kton mass of waste rock yields a total ABP of -3,032 ton $CaCO_3$. This ABP neglects the ABP in the mine wall rock, but the mine wall rock is expected to have relatively little effect because of the much greater surface area associated with the waste rock. Because the NP in the cement (10,269 ton $CaCO_3$) is more than a factor of three greater than the ABP in the waste rock (-3,032 ton $CaCO_3$), the alkalinity in the cement is more than sufficient to neutralize the acidity released by the waste rock and mine wall rock.

Table 5-2. Predicted Aqueous Concentrations

Mine wall rock and waste rock surface area	5.411 m^2/L	54.11 m^2/L	NDEP Profile I reference value
pH (standard units)	10.24	10.32	6.5 to 8.5
pe (dimensionless)	10.32	3.04	--
Aluminum	0.2164	0.2641	0.2
Antimony	0.02222	0.1381	0.006
Arsenic	5.477×10^{-7}	4.100×10^{-6}	0.01
Barium	0.001997	6.134×10^{-4}	2.0
Beryllium	0.002037	0.01684	0.004
Boron	0.3461	2.516	--
Total inorganic carbon (as CO_3^{2-})	1.491	5.111×10^{-9}	--
Cadmium	1.427×10^{-4}	0.001451	0.005
Calcium	638.6	548.8	--
Chloride	30.17	75.12	400
Chromium	0.2253	0.4303	0.1
Copper	2.685×10^{-4}	2.880×10^{-4}	1
Fluoride	1.964	2.367	4
Iron	4.929×10^{-4}	5.948×10^{-4}	0.6
Lead	9.402×10^{-7}	1.055×10^{-5}	0.015
Magnesium	0.004043	0.003428	150
Manganese	3.004×10^{-8}	6.367×10^{-4}	0.1
Nickel	0.02087	0.05370	0.1
Nitrate as N	1.782	5.241	10
Potassium	43.48	414.1	--
Selenium	0.3231	0.08062	0.05
Silica	68.80	80.27	--
Sodium	56.83	298.2	--
Sulfate	1,602	2,277	500
Thallium	0.03141	0.3158	0.002
Zinc	1.935×10^{-5}	0.05634	5
Total Dissolved Solids	2,473	3,736	1,000
Ionic Strength (moles/L)	0.04528	0.06398	--

All units mg/L unless otherwise noted
-- indicates no NDEP Profile I standard

Table 5-3. Surface Species

5.411 m^2/L			54.11 m^2/L		
Species	Mole Fraction	Molality	Species	Mole Fraction	Molality
Hfo_sONi+	0.479	1.079×10^{-4}	Hfo_sONi+	0.424	2.484×10^{-4}
Hfo_sOHCa+2	0.275	6.192×10^{-5}	Hfo_sOCrOH+	0.163	9.565×10^{-5}
Hfo_sO-	0.166	3.729×10^{-5}	Hfo_sOBe+	0.145	8.480×10^{-5}
Hfo_sOBe+	0.059	1.327×10^{-5}	Hfo_sOHCa+2	0.096	5.635×10^{-5}
Hfo_sOCd+	0.013	2.831×10^{-6}	Hfo_sOZn+	0.061	3.587×10^{-5}
Hfo_sOH	0.003	7.695×10^{-7}	Hfo_sO-	0.058	3.411×10^{-5}
Hfo_sOCu+	0.003	6.384×10^{-7}	Hfo_sOCd+	0.045	2.621×10^{-5}
Hfo_sOPb+	0.001	3.173×10^{-7}	Hfo_sOPb+	0.005	3.160×10^{-6}
Hfo_sOHSO4-2	0.001	1.352×10^{-7}	Hfo_sOH	0.001	7.023×10^{-7}
Hfo_sOHCrO4-2	0.000	6.843×10^{-8}	Hfo_sOCu+	0.001	5.817×10^{-7}
Hfo_sOHAsO4-3	0.000	4.796×10^{-8}	Hfo_sOHAsO4-3	0.000	1.784×10^{-7}
Hfo_sOZn+	0.000	1.527×10^{-8}	Hfo_sOHSO4-2	0.000	1.239×10^{-7}
Hfo_sOH2+	0.000	3.638×10^{-10}	Hfo_sOHSeO3-2	0.000	1.217×10^{-7}
Hfo_sOHBa+2	0.000	2.711×10^{-10}	Hfo_sOHCrO4-2	0.000	6.261×10^{-8}
Hfo_sOHSeO4-2	0.000	5.175×10^{-11}	Hfo_sOH2+	0.000	3.313×10^{-10}
Hfo_wOCa+	0.501	4.513×10^{-3}	Hfo_wOCa+	0.495	1.160×10^{-2}
Hfo_wO-	0.483	4.353×10^{-3}	Hfo_wO-	0.479	1.122×10^{-2}
Hfo_wOH	0.010	8.984×10^{-5}	Hfo_wOH	0.010	2.311×10^{-4}
Hfo_wONi+	0.002	1.7005×10^{-5}	Hfo_wOBe+	0.005	1.111×10^{-4}
Hfo_wOHSO4-2	0.002	1.579×10^{-5}	Hfo_wONi+	0.005	1.102×10^{-4}
Hfo_wOHCrO4-2	0.001	7.989×10^{-6}	Hfo_wOHAsO4-3	0.003	5.871×10^{-5}
Hfo_wOBe+	0.001	6.169×10^{-6}	Hfo_wOHSO4-2	0.002	4.077×10^{-5}
Hfo_wOHAsO4-3	0.001	5.559×10^{-6}	Hfo_wOHSeO3-2	0.002	4.003×10^{-5}
Hfo_wOMg+	0.000	8.786×10^{-7}	Hfo_wOHCrO4-2	0.001	2.060×10^{-5}
Hfo_wOCu+	0.000	3.823×10^{-7}	Hfo_wOZn+	0.001	1.236×10^{-5}
Hfo_wOCd+	0.000	1.410×10^{-7}	Hfo_wOCd+	0.000	3.678×10^{-6}
Hfo_wOH2+	0.000	4.247×10^{-8}	Hfo_wOMg+	0.000	2.258×10^{-6}
Hfo_wOHSeO4-2	0.000	6.041×10^{-9}	Hfo_wOCu+	0.000	9.815×10^{-7}
Hfo_wSO4-	0.000	3.743×10^{-9}	Hfo_wOH2+	0.000	1.090×10^{-7}
Hfo_wOZn+	0.000	1.866×10^{-9}	Hfo_wOPb+	0.000	4.645×10^{-8}
Hfo_wCrO4-	0.000	1.727×10^{-9}	Hfo_wSeO3-	0.000	3.210×10^{-8}
Hfo_wOPb+	0.000	1.655×10^{-9}	Hfo_wH2BO3	0.000	1.143×10^{-8}
Hfo_wH2BO3	0.000	7.036×10^{-10}	Hfo_wSO4-	0.000	9.648×10^{-9}
Hfo_wOBa+	0.000	2.855×10^{-10}	Hfo_wCrO4-	0.000	4.446×10^{-9}
Hfo_wSeO4-	0.000	1.247×10^{-12}	Hfo_wOBa+	0.000	2.885×10^{-10}
Hfo_wOHSbO(OH)4-	0.000	7.017×10^{-13}	Hfo_wOHSeO4-2	0.000	1.097×10^{-10}

Hfo_s species represent Type 1 surface site adsorption on ferrihydrite
Hfo_w species represent Type 2 surface site adsorption on ferrihydrite

The predicted aqueous concentrations are compared to the NDEP Profile I reference values in Table 5-2. For both reactive surface areas used in the modeling calculations, the concentrations of arsenic, barium, cadmium, chloride, copper, fluoride, iron, lead, magnesium, manganese, nickel, nitrate and zinc are less than the NDEP Profile I reference values. The predicted concentrations for both the lower and higher mine wall rock and waste rock surface areas exceed the Profile I reference values for aluminum, antimony, chromium, selenium, sulfate, thallium and total dissolved solids. The predicted beryllium concentration exceeds the Profile I reference value for the higher mine wall rock and waste rock surface area, but is below the reference value for the lower surface area.

In both calculations, gypsum precipitation limits sulfate concentrations, and chalcedony, fluorite, kaolinite, sepiolite and tobermorite precipitation control silica, fluoride, aluminum, magnesium and calcium concentrations, respectively. Barium and arsenic aqueous concentrations are controlled by precipitation of $Ba_3(AsO_4)_2(s)$ and copper concentrations are controlled by tenorite precipitation in calculations with both surface areas. Iron concentrations are controlled by the solubility of ferrihydrite, with manganese concentrations controlled by the solubility of birnessite in the lower surface area calculations and by manganite in the higher-surface-area calculations. Aqueous zinc concentrations are controlled by the solubility of hydrozincite in the lower surface area calculations, and by hydrozincite plus zincite in the higher surface area calculations. Total inorganic carbon is precipitated in calcite and hydrozincite in the lower surface area calculations and in hydrozincite in the higher surface area calculations.

The aqueous nickel concentration is controlled by $Ni(OH)_2(s)$ in the higher surface area calculations. There are no predicted solubility-controlling solids for nickel when the lower surface area is used in the calculations and the aqueous nickel concentration is controlled by adsorption.

No solubility-controlling solids are predicted to form based on the calculations carried out using either of the surface areas for antimony, beryllium, boron, cadmium, chloride, chromium, lead, nitrate, potassium, selenium, sodium and thallium. Beryllium, cadmium, chromium and lead concentrations are significantly reduced by adsorption. The selenium concentration is controlled by the quantity leached from the mine wall rock and waste rock for the lower-surface area calculation, but the selenium concentration is controlled by adsorption for the higher-surface-area calculation. Adsorption has no effect on antimony, boron, chloride, nitrate, potassium, sodium or thallium concentrations, which are mainly controlled by the quantities leached from the mine wall rock and waste rock. For the lower-surface-area calculations, antimony, boron, chloride and sodium concentrations are also significantly affected by the concentrations in the inflowing groundwater.

6.0 SUMMARY AND CONCLUSIONS

The water quality in the underground workings of the Hollister Mine and Hatter Expansion will be affected by: the chemical composition of the inflowing groundwater; leaching of metals, acidity and other constituents from oxidized mine wall rock and backfilled waste rock; leaching of alkalinity, calcium and silica from cement in concrete used to stabilize the waste rock backfill; and resulting mineral precipitation and adsorption reactions.

The neutralizing potential of cement in the backfill will exceed the acid-base potential of the mine wall rock and waste rock. Consequently, the pH of the underground workings water will be alkaline and controlled by the precipitation of tobermorite at approximately 10.2, which exceeds the NDEP Profile I reference value. Aqueous concentrations of arsenic, barium, cadmium, chloride, copper, fluoride, iron, lead, magnesium, manganese, nickel, nitrate and zinc are not predicted to exceed NDEP Profile I reference values. Concentrations of aluminum, antimony, chromium, selenium, sulfate, thallium and total dissolved solids are predicted to exceed NDEP Profile I reference values. Beryllium may also exceed its reference value, depending on the reactive surface area of the mine wall rock and waste rock.

Discharge of water from the underground workings directly to the surface will not occur at the Hollister Mine because pre-mining groundwater levels were at a lower elevation than the decline portal, and under any foreseeable conditions the water levels will not recover to a higher elevation. After closure, the underground workings will act as a groundwater sink (i.e., groundwater flow directions will be inward toward the dewatered underground workings) for greater than 200 years until the workings are completely filled and hydrologic conditions return to steady state. Downgradient flow of groundwater following the completed refilling of the underground mine workings is expected to be relatively slow because of the low hydraulic conductivity of the Vinini Formation. The effects of elevated constituent concentrations in the underground workings water on downgradient groundwater are expected to be reduced by the effects of dilution (dispersion) and chemical attenuation.

7.0 REFERENCES

Attiogbe, E.K. and S.H. Rizkalla. 1988. Response of concrete to sulfuric acid attack. *ACI Materials Journal* 84:481-488.

Aviam, O, G. Bar-Nes, Y. Zeiri and A. Sivan. 2004. Accelerated biodegradation of cement by sulfur-oxidizing bacteria as a bioassay for evaluating immobilization of low-level radioactive waste. *Applied and Environmental Microbiology* 70:6031-6036.

Cain, R.B. 2010. Brown and Caldwell, email to J.A. Schramke, Enchemica LLC, July 22, 2010.

Criscenti, L.J., R.J. Serne, K.M. Krupka and M.I. Wood. 1996. *Predictive Calculations to Assess the Long-Term Effect of Cementitious Materials on the pH and Solubility of Uranium (VI) in a Shallow Land Disposal Environment*. Pacific Northwest National Laboratory, PNNL-11182, Richland, Washington.

Dzombak, D.A., and F.M.M. Morel. 1990. *Surface Complexation Modeling, Hydrous Ferric Oxide.* John Wiley & Sons, New York.

Eary, L.E. 1999. Geochemical and equilibrium trends in mine pit lakes. *Applied Geochemistry* 14:963-987.

EPA (U.S. Environmental Protection Agency). 1999. *MINTEQA2/PRODEFA2, A Geochemical Model for Environmental Systems: User Manual Supplement for Version 4.0.* Prepared by HydroGeoLogic Inc., Herndon, Virginia and Allison Geoscience Consultants Inc., Flowery Branch, Georgia, Revised September 1999.

Fishbein, L. 1981. Sources, transport and alterations of metal compounds: an overview. I. Arsenic, beryllium, cadmium, chromium and nickel. *Environmental Health Perspectives* 40:43-64.

Knight Piésold. 2010. *Hollister Mine Waste Rock Gradation Procedure and Results.* Memorandum to Teresa Conner, Environmental Manager, Great Basin Gold Inc., July 6, 2010.

Lothenbach, B. and F. Winnefeld. 2006. Thermodynamic modelling of the hydration of Portland cement. *Cement and Concrete Research* 36:209-226.

Morin, K.A. and N.M. Hutt. 2006. MEND minewall technique: overview and details. *13th Annual BC MEND Workshop, Open Pits and Underground Mine Workings.* Vancouver, British Columbia. November 29-30, 2006.

Nordstrom, D.K., and C.N. Alpers. 1999. Geochemistry of acid mine waters. In *The Environmental Geochemistry of Mineral Deposits, Part A: Processes, Techniques, and Health Issues.* Eds. G.S. Plumlee and M.J. Logsdon. Society of Economic Geologists, Reviews in Economic Geology, 6A:133-160.

Nordstrom, D.K., L.N. Plummer, D. Langmuir, E. Busenberg, H.M. May, B.F. Jones, and D.L. Parkhurst. 1990. Revised chemical equilibrium data for major water-mineral reactions and their limitations. In *Chemical Modeling of Aqueous Systems III*, Eds. D.C. Melchior and R.L. Bassett, American Chemical Society, Washington, DC, ACS Symposium Series 416:398-413.

Parkhurst, D.L., and C.A.J. Appelo. 1999. *User's Guide to PHREEQC (Version 2)–A Computer Program for Speciation, Batch-Reaction, One-Dimensional Transport and Inverse Geochemical Calculations*. Water-Resources Investigations Report 99-4259, United States Geological Survey, Denver, Colorado.

Peltier, E. R. Allada, A. Navrotsky and D.L. Sparks. 2006. Nickel solubility and precipitation in soils: a thermodynamic study. *Clays and Clay Minerals* 54:153-164.

Planel, D., J. Sercombe, P. Le Bescop, F. Adenot and J.M. Torrenti. 2006. Long-term performance of cement paste during combined calcium leaching-sulfate attack: kinetics and size effect. *Cement and Concrete Research* 36:137-143.

Rai, D., C.C. Ainsworth, L.E. Eary, S.V. Mattigod and D.R. Jackson. 1987. *Inorganic and Organic Constituents in Fossil Fuel Combustion Residues. Volume 1: A Critical Review.* EA-5176, Electric Power Research Institute, Palo Alto, California.

Schmidt, T., B. Lothenbach, M. Romer, J. Neuenschwander, and K. Scrivener. 2009. Physical and microstructural aspects of sulfate attack on ordinary and limestone blended Portland cements. *Cement and Concrete Research* 39:1111-1121.

Taylor, F.D. 2010a. Rodeo Creek Gold Inc, email to B. Hart, Brown and Caldwell, May 13, 2010.

Taylor, F.D. 2010b. Rodeo Creek Gold Inc, email to B. Hart, Brown and Caldwell, June 2, 2010.

Taylor, F.D. 2010c. Rodeo Creek Gold Inc, email to B. Hart, Brown and Caldwell, June 3, 2010.

Taylor, F.D. 2010d. Rodeo Creek Gold Inc, email to B. Hart, Brown and Caldwell, June 24, 2010.

USGS (United States Geological Survey). 2010. *PHREEQC (Version 2)--A Computer Program for Speciation, Batch-Reaction, One-Dimensional Transport, and Inverse Geochemical Calculations* http://wwwbrr.cr.usgs.gov/projects/GWC_coupled/phreeqc/ Accessed April 13, 2010.

Walker (Walker & Associates). 2003a. *Waste Rock Characterization Report*. Appendix A in Support of an Application for a Small Scale Facility Water Pollution Control Permit. Prepared for Hecla Ventures Corporation Hollister Development Block, Elko County Nevada, May 5, 2003.

Walker (Walker & Associates). 2003b. *Waste Rock Characterization Report for the Plan of Operations*. Prepared for Hecla Ventures Corporation Hollister Development Block, Elko County Nevada, January 13, 2003.

White, A.F. and M.L. Peterson. 1990. Role of reactive-surface area characterization in geochemical kinetic models. In *Chemical Modeling of Aqueous Systems II*, Eds. D.C. Melchior and R.L. Bassett, American Chemical Society, Washington DC, ACS Symposium Series 416:461-475.

APPENDIX A

UNDERGROUND DRAINAGE WATER QUALITY DATA AND WASTE ROCK HUMIDITY CELL DATA

Table A-1. Underground Drainage Water Quality

Date	2/21/2007	4/4/2007	8/14/2007	12/11/2007	3/6/2008	5/7/2008
Bicarbonate	24	71	85	85	88	88
Aluminum	<0.045	<0.045	1.6	<0.045	<0.045	<0.045
Antimony	0.010	0.016	0.014	0.0052	0.01	0.024
Arsenic	0.021	0.047	0.086	0.0060	0.026	0.065
Barium	0.029	0.026	0.087	0.049	0.029	0.024
Beryllium	<0.001	<0.001	0.0017	<0.001	<0.001	<0.001
Boron	<0.1	<0.1	<0.1	<0.1	<0.1	0.12
Cadmium	<0.001	<0.001	<0.001	<0.001	<0.001	<0.001
Calcium	30	38	61	40	56	84
Chloride	29	7.9	53	16	41	17
Chromium	<0.005	<0.005	<0.005	<0.005	<0.005	<0.005
Copper	<0.05	<0.05	<0.05	<0.05	<0.05	<0.05
Fluoride	0.88	0.96	1.5	1.1	1.4	1.2
Iron	0.015	<0.01	2	0.02	0.22	<0.05
Lead	<0.01	<0.01	<0.01	<0.01	<0.01	<0.01
Magnesium	6.7	8.3	14	12	14	6.5
Manganese	<0.005	0.017	1.1	0.93	1.5	0.0076
Mercury	<0.0001	<0.0001	<0.0001	0.00012	0.00063	0.00024
Molybdenum	<0.01	<0.01	<0.01	<0.01	<0.01	0.012
Nickel	<0.01	<0.01	0.047	0.040	0.034	<0.01
Nitrate + Nitrite as N	<1	<0.1	<1	<1	<1	0.77
pH, lab (standard units)	9.44	9.11	7.30	7.03	7.09	9.71
Potassium	4.4	4.2	5.2	4.5	5.4	5.7
Selenium	<0.005	<0.01	<0.005	<0.005	<0.005	0.0088
Silver	<0.005	<0.005	<0.005	<0.005	<0.005	<0.005
Sodium	24	24	30	26	32	32
Strontium	0.14	0.15	0.22	0.17	0.2	0.27
Sulfate	90	98	200	140	180	250
Thallium	<0.001	<0.001	<0.001	<0.001	<0.001	<0.001
Total Dissolved Solids	240	270	390	310	450	440
Vanadium	0.021	0.012	0.018	<0.01	<0.01	0.021
Zinc	<0.01	<0.01	0.35	0.16	0.11	<0.01
Conductivity (µS)	--[a]	--	--	--	580	562
Alkalinity, $CaCO_3$	40	74	70	70	72	76

All units mg/L unless otherwise noted
-- = not reported

Table A-1. Underground Drainage Water Quality (contd)

Date	8/22/2008	12/2/2008	1/14/2009	4/21/2009	8/25/2009	10/27/2009
Bicarbonate	120	140	150	110	80	45
Aluminum	1.9	<0.045	5.4	<0.045	0.12	0.27
Antimony	0.022	0.011	0.026	0.023	0.02	0.02
Arsenic	0.052	0.036	0.3	0.03	0.07	0.09
Barium	0.035	0.028	0.24	0.04	0.03	0.03
Beryllium	0.0013	<0.001	0.0015	<0.001	<0.001	<0.001
Boron	0.14	0.15	0.38	0.15	0.13	0.12
Cadmium	<0.001	<0.001	<0.001	<0.001	<0.001	<0.001
Calcium	52	63	96	77	48	53
Chloride	17	12	27	17	19	19
Chromium	<0.005	<0.005	0.013	<0.005	<0.005	<0.005
Copper	0.061	<0.05	0.098	<0.05	<0.05	<0.05
Fluoride	1.2	0.79	1.2	1.6	0.84	0.92
Iron	2.9	0.47	17	0.09	0.09	0.09
Lead	<0.01	<0.01	<0.01	<0.01	<0.01	<0.01
Magnesium	12	9.7	15	16	9.9	9.9
Manganese	0.28	0.049	0.38	0.36	0.02	0.1
Mercury	0.00061	0.00087	0.00088	0.00071	0.0017	0.0013
Molybdenum	<0.01	<0.01	--[a]	--	--	--
Nickel	0.054	0.012	0.047	<0.01	<0.01	<0.01
Nitrate + Nitrite as N	1.7	<5.05	1.46	0.42	1.5	1.7
pH, lab (standard units)	8.75	8.37	8.71	6.58	8.73	9.11
Potassium	6.1	5.2	8.1	7.4	7.7	7
Selenium	0.0075	0.0055	0.02	<0.01	<0.01	<0.01
Silver	<0.005	<0.005	0.062	<0.005	<0.005	<0.005
Sodium	26	34	35	30	29	39
Strontium	0.18	0.26	--	--	--	--
Sulfate	160	160	210	210	120	150
Thallium	<0.001	<0.001	0.0015	<0.001	<0.001	<0.001
Total Dissolved Solids	370	480	480	400	320	350
Vanadium	<0.010	0.018	--	--	--	--
Zinc	0.24	0.027	0.3	<0.01	<0.01	<0.01
Conductivity (µS)	578	657	--	--	--	--
Alkalinity, $CaCO_3$	100	120	130	92	90	120

All units mg/L unless otherwise noted
-- = not reported

Table A-2. Concentrations in First Four Week Humidity Cell Composite Samples

	IH020 330-335' Quartzite	IH020 285-295' Quartzite	IH020 340-350' Quartzite	IH208 514-522.4' Quartzite	IH112 308-318' Quartzite	IH057 528-538' Quartzite	IH013 700-710' Quartzite
Alkalinity, CaCO3 (Acidity)	<1.0	338	<1.0	253	53.6	-300	957
CO3, CaCO3	<1.0	NA	<1.0	NA	NA	NA	NA
HCO3	<1.0	NA	<1.0	NA	NA	NA	NA
Aluminum	0.415	8.85	0.159	14.1	0.381	16.6	35.6
Antimony	0.002	<0.002	0.001	0.002	0.006	0.002	0.003
Arsenic	0.02	0.07	0.028	0.033	0.102	0.032	0.14
Barium	0.0192	0.0147	0.0203	0.013	0.0217	0.0114	0.0093
Beryllium	<0.002	<0.002	<0.002	0.0056	<0.002	0.0056	0.0061
Boron	<0.04	<0.04	<0.04	<0.04	<0.04	<0.04	<0.04
Cadmium	<0.002	0.0234	<0.002	0.0052	<0.002	0.024	0.318
Calcium	22.8	25.3	11.5	7.58	22.7	31.5	12.5
Chloride	0.73	<2.0	0.62	0.75	0.79	<1.0	1.34
Chromium	<0.006	0.18	<0.006	0.0807	<0.006	0.103	0.427
Copper	0.0104	0.161	0.0235	0.395	0.0272	0.651	1.52
Fluoride	0.38	<1.0	0.23	2.52	0.32	3.14	0.62
Iron	0.897	131	2.03	63.9	5.35	74	315
Lead	<0.005	0.0149	0.0056	0.0065	0.0075	0.0087	0.0352
Magnesium	6.83	6.49	3.32	1.44	5.72	10	7.36
Manganese	0.0262	1.79	0.545	0.8	0.521	0.456	4.33
Mercury	<0.002	<0.002	0.0013	<0.002	<0.002	<0.002	<0.002
Nickel	0.183	0.535	0.066	0.345	0.094	0.596	2.71
Nitrate and Nitrite as N	0.08	0.03	0.03	0.06	0.08	0.1	0.11
pH (standard units)	4.77	3.38	4.92	3.36	4.14	3.19	2.81
Potassium	5.5	4.6	4.5	1.6	4.4	<1.0	<1.0
Selenium	0.051	0.034	0.015	0.023	0.135	0.03	0.027
Silver	<0.005	0.0139	<0.005	<0.005	<0.005	<0.005	<0.005
Sodium	3.6	3.2	2.65	1.96	4.22	3.14	2.25
Sulfate	99.1	415	57.6	246	109	385	1,010
Thallium	0.003	<0.01	0.002	<0.001	<0.01	<0.01	<0.01
Total Dissolved Solids	159	676	89	400	163	611	1,630
Zinc	0.223	0.231	0.079	0.212	0.656	3.37	17.5
Sample weight (kg)	1.1943	1.1957	1.1871	1.1743	1.1852	1.1869	1.1964
Sample volume (L)	2.007	1.962	1.978	1.960	2.019	1.979	2.056

All units mg/L unless otherwise noted, NA = not analyzed

Table A-2. Concentrations in First Four Week Humidity Cell Composite Samples (contd)

Sample (units mg/L)	IH149 198-206' Quartzite	IH070 695-705' Quartzite	IH083 587-596' Quartzite	BH-02 665' Quartzite	BH-03 605' Quartzite	BH-04 610' Quartzite	Sample BH-06 400' Quartzite
Alkalinity, CaCO3 (Acidity)	(26.9)	(627)	(431)	92.9	<1.0	81.4	3.9
CO3, CaCO3	NA	NA	NA	NA	<1.0	NA	<1.0
HCO3	NA	NA	NA	NA	<1.0	NA	3.9
Aluminum	0.386	45.3	20.4	1.46	0.147	0.806	1.42
Antimony	<0.001	<0.002	0.003	<0.001	<0.001	<0.001	0.006
Arsenic	<0.01	0.13	0.049	0.019	<0.01	<0.01	0.101
Barium	0.105	0.0439	0.0117	0.0241	0.0976	0.0237	0.127
Beryllium	<0.002	0.117	<0.002	0.17	<0.002	<0.002	<0.002
Boron	<0.04	<0.04	<0.04	0.043	0.062	<0.04	0.101
Cadmium	<0.002	0.0326	0.011	0.0061	<0.002	0.0049	0.0023
Calcium	7.22	95.1	6.19	69.2	17.2	30.6	15.6
Chloride	0.84	1.22	1.24	1.05	1	1.57	0.94
Chromium	0.0075	0.216	0.251	<0.006	<0.006	<0.006	<0.006
Copper	0.337	1.64	0.456	0.639	0.0299	0.256	0.0122
Fluoride	0.19	1.13	1.88	0.5	0.3	0.31	3.5
Iron	3.75	162	156	12.4	0.667	14.3	0.392
Lead	<0.005	<0.005	<0.005	0.0081	<0.005	0.0064	<0.005
Magnesium	0.766	65.2	1.3	22.1	4.75	6.24	4.46
Manganese	0.973	1.15	1.12	5.73	0.575	7.94	0.261
Mercury	<0.002	<0.002	<0.002	<0.002	<0.002	<0.002	<0.002
Nickel	0.076	3.27	0.685	0.798	0.329	0.475	0.142
Nitrate and Nitrite as N	0.05	0.08	0.05	0.05	0.05	0.06	0.09
pH (standard units)	4.42	3.14	3.21	3.68	5.13	3.87	5.44
Potassium	<1.0	<1.0	<1.0	18.3	5.9	5	9.9
Selenium	<0.01	0.111	0.085	0.051	0.021	0.021	0.022
Silver	<0.005	<0.005	<0.005	<0.005	<0.005	<0.005	<0.005
Sodium	2.16	4.36	1.95	7.44	5.57	3.38	7.26
Sulfate	39.8	1,130	443	354	84.8	166	94.8
Thallium	0.002	<0.005	0.01	0.004	0.002	0.002	0.004
Total Dissolved Solids	60	1,690	676	545	122	262	154
Zinc	0.0738	13.7	0.132	1.26	0.213	0.347	0.377
Sample weight (kg)	1.1754	1.1917	1.162	1.181	1.2219	1.2341	1.1979
Sample volume (L)	1.904	1.903	1.893	1.981	1.962	2.016	1.921

All units mg/L unless otherwise noted, NA = not analyzed

Table A-2. Concentrations in First Four Week Humidity Cell Composite Samples (contd)

	IH208 530' Argillite	IH059 641' Argillite	IH013 690-700' Siltite	IH083 596-605' Siltite	BH-01 745' Siltite	BH-02 650' Siltite	BH05 510' Siltite
Acidity	678	901	654	(804)	53.2	152	(117)
Aluminum	55.2	50.6	31	65.2	0.588	4.04	10.1
Antimony	0.002	0.002	0.014	0.002	0.001	0.002	<0.001
Arsenic	0.058	0.225	0.66	0.168	<0.01	0.023	0.03
Barium	0.0101	0.0068	0.0082	0.033	0.0197	0.0246	0.0531
Beryllium	0.0166	0.0469	0.0065	0.0112	0.0161	0.268	0.0349
Boron	<0.04	<0.04	<0.04	0.083	<0.04	0.061	0.132
Cadmium	0.248	0.0703	0.165	0.308	0.003	0.0299	0.0153
Calcium	91.6	145	9.47	104	59.4	117	106
Chloride	1.24	1.35	1.06	1.41	1.12	0.57	1.39
Chromium	0.157	0.401	0.61	0.2	<0.006	<0.006	0.007
Copper	1.57	7.66	1.66	2.72	0.188	2.75	0.84
Fluoride	6.21	2.24	<0.50	8.15	<0.20	0.91	5.92
Iron	144	206	353	189	4.31	27	12.7
Lead	0.039	0.0118	0.0144	0.0076	0.0208	0.0071	0.0471
Magnesium	34.6	56.9	1.73	31.6	22.1	36.4	29.9
Manganese	0.963	1.41	1.59	0.787	2.56	2.93	1.26
Mercury	<0.0002	<0.0002	<0.0002	<0.0002	<0.0002	<0.0002	<0.0002
Nickel	3.04	5.25	3.69	2.6	0.469	1.43	1.66
Nitrate and Nitrite as N	0.12	0.08	0.08	0.33	0.05	0.04	0.05
pH (standard units)	3.12	2.66	2.7	3.03	4.12	3.5	3.85
Potassium	2.2	2.5	1.0	4.2	20.6	25.1	41.7
Selenium	0.061	0.247	0.107	0.052	0.045	0.091	0.104
Silver	<0.005	<0.005	<0.005	<0.005	<0.005	<0.005	<0.005
Sodium	5.76	9.59	2.34	10.3	7.66	9.92	12.2
Sulfate	1,010	1,530	1,030	1,160	301	599	570
Thallium	<0.01	<0.01	0.019	0.009	0.003	0.004	0.007
Total Dissolved Solids	1,620	2,370	1,660	1,750	477	922	814
Zinc	10	30.8	5.47	6.58	0.152	4.68	3.5
Sample weight (kg)	1.1835	1.1882	1.1866	1.1872	1.2026	1.2076	1.1933
Sample volume (L)	2.013	2.021	1.995	1.952	1.976	2.003	1.863

All units mg/L unless otherwise noted

APPENDIX B

GEOCHEMICAL MODELING CALCULATIONS

The geochemical modeling calculations are described in detail, including the input file data, constituent concentrations after each modeling step and final results. In addition, example calculations are provided for a conservative constituent that is not adsorbed or precipitated, a constituent with a concentration affected by precipitation and a constituent that is adsorbed but not precipitated. Additional information is also provided for the calculation of the nitrogen (nitrate plus nitrate) concentration.

B.1 Details of Geochemical Modeling Calculations

The first step in the geochemical modeling calculations was to estimate the water quality of the inflowing Vinini Formation groundwater. This was accomplished by using PHREEQC to mix equal amounts of the two groundwater compositions with adequately small charge balances of less than 5% (BH-02 10/1/2002 and BH-04 10/11/2002, Table 2-7). The compositions listed in Table B-1 were calculated using PHREEQC from the data in Table 2-7 using the gram formula weight (mg/mole) for the various species and the mass of water in the mixture (1 kg). The groundwater composition in the final column of Table B-1 was saved in the PHREEQC calculations for use in the subsequent calculation step.

The next step in the PHREEQC calculations was to simulate the changes that will occur as groundwater enters the underground workings, flushes oxidation products from the wall rock and waste rock and equilibrates with atmospheric oxygen. The oxygen concentration in the airspace in the underground workings was assumed to be 0.20 atm. The amount of oxidation products flushed from the humidity cell tests in the first 4-week composite sample are provided in units of mg/L (Walker 2003a). This concentration was converted to moles of each constituent per unit surface area of waste rock in the test using the expression:

Mean constituent release (mole/m^2) =
Mean constituent release (mg/L) × solution volume (L)/mass of waste rock (kg) ×
1 kg waste rock/4.08 m^2 ÷ gram formula weight (mg/mole)

The solution volumes and waste rock masses used in the humidity cell tests are provided in Table B-2. The mean solution volume divided by the mean mass of waste rock for the quartzite and argillite/siltite tests were 1.651 L/kg and 1.656 L/kg, respectively. The 4.08 m^2/kg surface area of the waste rock in the humidity cell tests was determined from the grain size, as described in Section 2.5.

Table B-1. Vinini Formation Borehole Water Quality and Calculated Average Water Quality

Borehole	BH-02	BH-04	Calculated Vinini Formation Water Quality
Date	10/1/2002	10/11/2002	
Bicarbonate	8.851×10^{-4}	1.443×10^{-3}	1.164×10^{-3}
Aluminum	b.d.	3.670×10^{-6}	1.835×10^{-6}
Antimony	1.536×10^{-7}	b.d.	7.681×10^{-8}
Arsenic	1.148×10^{-7}	2.069×10^{-7}	1.609×10^{-7}
Barium	9.759×10^{-7}	2.331×10^{-7}	6.045×10^{-7}
Beryllium	b.d.	b.d.	0.00
Boron	1.323×10^{-5}	6.292×10^{-6}	9.761×10^{-6}
Cadmium	b.d.	b.d.	0.00
Calcium	4.991×10^{-4}	7.487×10^{-4}	6.239×10^{-4}
Chloride	6.771×10^{-4}	7.335×10^{-4}	7.053×10^{-4}
Chromium	b.d.	b.d.	0.00
Copper	b.d.	b.d.	0.00
Fluoride	6.844×10^{-5}	4.475×10^{-5}	5.660×10^{-5}
Iron	b.d.	7.970×10^{-7}	3.985×10^{-7}
Lead	b.d.	b.d.	0.00
Magnesium	2.469×10^{-4}	3.951×10^{-4}	3.210×10^{-4}
Manganese	2.185×10^{-6}	7.101×10^{-7}	1.447×10^{-6}
Mercury	b.d.	b.d.	0.00
Nickel	b.d.	b.d.	0.00
Nitrate and Nitrite as N	b.d.	b.d.	0.00
pH, lab (standard units)	7.58	8.27	7.96
Potassium	6.600×10^{-5}	6.345×10^{-5}	6.472×10^{-5}
Selenium	b.d.	b.d.	0.00
Silver	b.d.	b.d.	0.00
Sodium	1.305×10^{-3}	1.301×10^{-3}	1.303×10^{-3}
Sulfate	5.206×10^{-4}	5.935×10^{-4}	5.570×10^{-4}
Thallium	b.d.	b.d.	0.00
Zinc	b.d.	b.d.	0.00
Speciated Charge Balance (%)	4.52	3.40	3.89

All units moles/kg water (molality) unless otherwise specified
b.d. = below detection

Table B-2. Calculation of Solid Masses and Solution Volumes Used in First 4 Week Composite Samples for Humidity Cell Tests With Quartzite and Argillite/Siltite

Quartzite			Argillite/Siltite		
Sample ID	Sample Mass (kg)	Cumulative Sample Volume (L)	Sample ID	Sample Mass (kg)	Cumulative Sample Volume (L)
IH020 330-335	1.1943	2.007	IH208 (530')	1.1835	2.013
IH020 285-295	1.1957	1.962	IH059 (641')	1.1882	2.021
IH020 340-350	1.1871	1.978	IH013 690-700	1.1866	1.995
IH208 514-522.4	1.1743	1.960	IH083 596-605	1.1872	1.952
IH112 308-318	1.1852	2.019	BH-01 (745')	1.2026	1.976
IH057 528-538	1.1869	1.979	BH-02 (650')	1.2076	2.003
IH013 700-710	1.1964	2.056	BH05 (510')	1.1933	1.863
IH149 198-206	1.1754	1.904	--	--	--
IH070 695-705	1.1917	1.903	--	--	--
IH083 587-596	1.162	1.893	--	--	--
BH-02 (665')	1.181	1.981	--	--	--
BH-03 (605')	1.2219	1.962	--	--	--
BH-04 (610')	1.2341	2.016	--	--	--
Sample BH-06 (400')	1.1979	1.921	--	--	--
Mean	1.1917	1.967	Mean	1.1927	1.975

The calculations used to derive the constituent release in mole/m^2 are summarized in Tables B-3 and B-4. The mean concentration in mg/L was converted to moles/L by dividing by the gram formula weight. The mean release per kilogram was calculated by multiplying by the mean solution volume divided by the mean mass of rock in the humidity cell tests. This value was converted to units of μmoles/m^2 by dividing by the calculated surface area per kg of the rock in the humidity cell tests (4.08 m^2/kg, Section 2.5) and multiplying by 10^6 μmoles/mole. The values in the final columns of Tables B-3 and B-4, multiplied by the surface area per liter of water for each rock type (either 5.411 m^2 or 54.11 m^2), were added to the inflowing groundwater composition as reactant phases in the PHREEQC calculations.

Table B-3. Constituent Release Calculations Using Quartzite Humidity Cell Test Data

Constituent	Mean Concentration (mg/L)	Formula weight (mg/mole)	Mean Concentration (mole/L)	Mean Release (mole/kg)	Mean Release (μmoles/m^2)
Aluminum	10.43	26,981.5	3.866×10^{-4}	6.382×10^{-4}	156.2
Antimony	0.002357	121,750	1.936×10^{-8}	3.196×10^{-8}	0.007825
Arsenic	0.05386	74,921.6	7.188×10^{-7}	1.187×10^{-6}	0.2905
Barium	0.03876	137,340	2.822×10^{-7}	4.659×10^{-7}	0.1141
Beryllium	0.02302	9,012.2	2.554×10^{-6}	4.217×10^{-6}	1.032
Boron	0.04614	10,811	4.268×10^{-6}	7.046×10^{-6}	1.725
Cadmium	0.03125	112,400	2.780×10^{-7}	4.590×10^{-7}	0.1124
Calcium	26.79	40,085	6.682×10^{-4}	1.103×10^{-3}	270.1
Chloride	1.078	35,453	3.040×10^{-5}	5.019×10^{-5}	12.29
Chromium	0.09337	51,996	1.796×10^{-6}	2.965×10^{-6}	0.7258
Copper	0.4399	63,540	6.923×10^{-6}	1.143×10^{-5}	2.798
Fluoride	1.144	18,998.4	6.023×10^{-5}	9.943×10^{-5}	24.34
Iron	67.26	55,847	1.204×10^{-3}	1.988×10^{-3}	486.8
Lead	0.008779	207,190	4.237×10^{-8}	6.995×10^{-8}	0.01713
Magnesium	10.43	24,312	4.289×10^{-4}	7.080×10^{-4}	173.3
Manganese	1.873	54,938	3.409×10^{-5}	5.627×10^{-5}	13.78
Mercury	<0.002	200,590	--	--	--
Nickel	0.7360	58,710	1.254×10^{-5}	2.070×10^{-5}	5.067
Nitrate and Nitrite as N	0.06571	14,006.7	4.692×10^{-6}	7.745×10^{-6}	1.896
pH, standard units	3.961	--	--	--	--
Potassium	4.621	39,102	1.182×10^{-4}	1.951×10^{-4}	47.77
Selenium	0.0454	78,960	5.753×10^{-7}	9.498×10^{-7}	0.2325
Silver	0.00564	107,870	--	--	--
Sodium	3.796	22,989.8	1.651×10^{-4}	2.726×10^{-4}	66.73
Sulfate	331.0	96,061.6	3.446×10^{-3}	5.689×10^{-3}	1,393
Thallium	0.005357	204,370	2.621×10^{-8}	4.327×10^{-8}	0.01059
Total Dissolved Solids	516.9	--	--	--	--
Zinc	2.741	65,370	4.193×10^{-5}	6.922×10^{-5}	16.95

Table B-4. Constituent Release Calculations Using Argillite/Siltite Humidity Cell Test Data

Constituent	Mean Concentration (mg/L)	Formula weight (mg/mole)	Mean Concentration (mole/L)	Mean Release (mole/kg)	Mean Release (μmoles/m^2)
Aluminum	30.96	26,981.5	1.147×10^{-3}	1.900×10^{-3}	465.2
Antimony	0.003429	121,750	2.816×10^{-8}	4.663×10^{-8}	0.01142
Arsenic	0.1677	74,921.6	2.239×10^{-6}	3.706×10^{-6}	0.907
Barium	0.02221	137,340	1.617×10^{-7}	2.678×10^{-7}	0.06557
Beryllium	0.05717	9,012.2	6.344×10^{-6}	1.050×10^{-5}	2.572
Boron	0.06229	10,811	5.761×10^{-6}	9.539×10^{-6}	2.336
Cadmium	0.1199	112,400	1.067×10^{-6}	1.767×10^{-6}	0.4325
Calcium	90.35	40,085	2.254×10^{-3}	3.732×10^{-3}	913.7
Chloride	1.163	35,453	3.280×10^{-5}	5.431×10^{-5}	13.30
Chromium	0.1981	51,996	3.811×10^{-6}	6.310×10^{-6}	1.545
Copper	2.484	63,540	3.909×10^{-5}	6.473×10^{-5}	15.85
Fluoride	3.447	18,998.4	1.814×10^{-4}	3.004×10^{-4}	73.55
Iron	133.7	55,847	2.394×10^{-3}	3.964×10^{-3}	970.6
Lead	0.02111	207,190	1.019×10^{-7}	1.687×10^{-7}	0.04131
Magnesium	30.46	24,312	1.253×10^{-3}	2.075×10^{-3}	507.9
Manganese	1.643	54,938	2.990×10^{-5}	4.951×10^{-5}	12.12
Mercury	<0.0002	200,590	--	--	--
Nickel	2.591	58,710	4.414×10^{-5}	7.308×10^{-5}	17.89
Nitrate and Nitrite as N	0.1071	14,006.7	7.649×10^{-6}	1.267×10^{-5}	3.101
pH, standard units	3.283	--	--	--	--
Potassium	13.90	39,102	3.555×10^{-4}	5.886×10^{-4}	144.1
Selenium	0.1010	78,960	1.279×10^{-6}	2.118×10^{-6}	0.5185
Silver	<0.005	107,870	--	--	--
Sodium	8.253	22,989.8	3.590×10^{-4}	5.944×10^{-4}	145.5
Sulfate	885.7	96,061.6	9.220×10^{-3}	1.527×10^{-2}	3,738
Thallium	0.008857	204,370	4.334×10^{-8}	7.176×10^{-8}	0.01757
Total Dissolved Solids	1,373	--	--	--	--
Zinc	8.740	65,370	1.337×10^{-4}	2.214×10^{-4}	54.20

The underground workings water quality results obtained using PHREEQC after adding the oxidation products released from the wall rock and waste rock and equilibration with atmospheric oxygen are summarized in Table B-5. This solution was saved in the PHREEQC calculations for use in subsequent modeling of the interaction of the water with cement phases. The results summarized in Table B-5 are not representative of the constituent concentrations that would be observed in the underground workings in the absence of cement phases because some phases, such as H-jarosite and barite, were oversaturated in these solutions but were not allowed to precipitate in this calculation step.

The final step in the PHREEQC calculations was equilibration of the underground workings water with the cementitious phases in the concrete, precipitation of oversaturated solid phases that could form under the low temperature conditions in the underground workings and adsorption of constituents on precipitated ferrihydrite.

The total amount of cement in the underground workings was calculated based on a cement volume of 125,000 ft^3 (3,540 m^3), which is 25% of the total concrete volume. The cement density will be 146.1 lb/ft^3 (2,340 kg/m^3), resulting in a total mass of cement of 18,260,179 lbs (8,282,679 kg). The oxide composition of the Portland Type II cement (Table 2-4) is converted to its elemental composition in Table B-6.

The quantities of hydrated cementitious phases in the concrete used in the PHREEQC calculations were calculated from the elemental composition (Table B-6) based on the following data and assumptions:

- The hydrated phases in the cement will be ettringite, hydrogarnet, Fe-hydrogarnet, tobermorite, brucite and portlandite (Table B-7)
- All sulfate in the cement will be contained in ettringite
- All aluminum in the cement that is not in ettringite will be present in the hydrogarnet
- All iron in the cement will be present in Fe-hydrogarnet
- All silica in the cement will be present in tobermorite
- All magnesium in the cement will be present in brucite
- The calcium in the cement in excess of the amount in ettringite, hydrogarnet and Fe-hydrogarnet will be present in portlandite

All calculations in PHREEQC are carried out on the basis of 1 kg of water, which is essentially equal to 1 liter of solution at the conditions of the calculations, i.e., 25°C and low ionic strength. The amounts of each hydrated cement phase in the final column of Table B-7 were calculated by dividing the total moles by the total volume of solution (101,949,448 L) and were added to the solution compositions listed in Table B-5 in the final step of the PHREEQC calculations.

Table B-5. Solution Composition after Release of Constituents from Wall Rock and Waste Rock and Equilibration with Atmospheric Oxygen

Surface Area per kg Water	$5.411\ m^2$	$54.11\ m^2$
Constituent	Concentration (moles/kg water)	Concentration (moles/kg water)
Aluminum	3.364×10^{-3}	0.03366
Antimony	1.810×10^{-7}	1.119×10^{-6}
Arsenic	6.641×10^{-6}	6.502×10^{-5}
Barium	1.577×10^{-6}	1.034×10^{-5}
Beryllium	1.950×10^{-5}	1.952×10^{-4}
Boron	3.174×10^{-5}	2.297×10^{-4}
Cadmium	2.949×10^{-6}	2.951×10^{-5}
Calcium	7.030×10^{-3}	0.06474
Carbon, total inorganic	1.164×10^{-3}	1.165×10^{-3}
Chloride	8.438×10^{-4}	2.092×10^{-3}
Chromium	1.229×10^{-5}	1.230×10^{-4}
Copper	1.009×10^{-4}	1.010×10^{-3}
Fluoride	5.863×10^{-4}	5.359×10^{-3}
Iron	7.887×10^{-3}	0.07894
Lead	3.163×10^{-7}	3.166×10^{-6}
Magnesium	4.007×10^{-3}	0.03722
Manganese	1.416×10^{-4}	1.404×10^{-3}
Nickel	1.242×10^{-4}	1.243×10^{-3}
Nitrate and Nitrite as N	2.704×10^{-5}	2.707×10^{-4}
pe	17.582	18.519
pH, standard units	3.015	2.079
Potassium	1.103×10^{-3}	0.01046
Selenium	4.064×10^{-6}	4.068×10^{-5}
Sodium	2.452×10^{-3}	0.01280
Sulfate	0.02832	0.2785
Thallium	1.524×10^{-7}	1.525×10^{-6}
Zinc	3.850×10^{-4}	3.854×10^{-3}

Table B-6. Total Moles of Cement Constituents in 8,282,679 kg of Portland Type II Cement

Chemical Formula	Percent by Weight	Total (moles)	Calcium (moles)	Silica (moles)	Aluminum (moles)	Iron (moles)	Magnesium (moles)	Sulfate (moles)
$3CaO•SiO_2$	51	18,500,835	55,502,504	18,500,835	0.00	0.00	0.00	0.00
$2CaO•SiO_2$	24	11,540,881	23,081,762	11,540,881	0.00	0.00	0.00	0.00
$3CaO•Al_2O_3$	6	1,839,237	5,517,711	0.00	3,678,474	0.00	0.00	0.00
$4CaO•Al_2O_3•Fe_2O_3$	11	1,874,792	7,499,169	0.00	3,749,584	3,749,584	0.00	0.00
MgO	2.9	5,958,555	0.00	0.00	0.00	0.00	5,958,555	0.00
SO_3	2.5	2,586,326	0.00	0.00	0.00	0.00	0.00	2,586,326
CaO	1	1,476,956	1,476,956	0.00	0.00	0.00	0.00	0.00
Total	98.4	--	93,078,101	30,041,716	7,428,058	3,749,584	0.00	0.00

Table B-7. Calculation of Hydrated Cement Phases

Minerals	Formula	Proportions	Total Amount of Phase in Underground Workings (moles)	Total Amount of Phase per Liter Underground Workings Water (mole/L)
Ettringite	$Ca_6Al_2(SO_4)_3(OH)_{12}•26H_2O(s)$	1 mole ettringite per 3 moles sulfate	862,109	0.008455
Hydrogarnet	$Ca_3Al_2(OH)_{12}(s)$	1 moles hydrogarnet per 2 moles aluminum	2,851,920	0.02797
Fe-hydrogarnet	$Ca_3Fe_2(OH)_{12}(s)$	1 mole Fe-hydrogarnet per 2 moles iron	1,874,792	0.01839
Tobermorite	$(Ca(OH)_2)_2(SiO_2)_{2.4}(H_2O)(s)$	1 mole tobermorite per 2.4 mole silica	12,517,382	0.1228
Brucite	$Mg(OH)_2(s)$	1 mole brucite per mole magnesium	5,958,555	0.05844
Portlandite	$Ca(OH)_2(s)$	1 mole portlandite per mole calcium	48,690,548	0.4775

The final results of the PHREEQC calculations after reaction of the underground workings water with the hydrated cement phases, precipitation of solid phases and adsorption on precipitated ferrihydrite are summarized in Tables 5-1 through 5-3.

B.2 Example Calculations

The PHREEQC calculations are illustrated using chloride as an example of a conservative constituent, fluoride as an example of a constituent with a final solution concentration controlled by precipitation of a solid phase and beryllium as an example of a constituent with a final solution concentration controlled by adsorption. The calculation of the total nitrogen concentration is also explained in detail, because this calculation differed from those carried out for other constituents because of the potential effects of blasting residues on nitrogen concentrations.

B.2.1 Conservative Constituent Example

Because it is not precipitated as a solid phase or significantly sorbed by ferrihydrite, chloride is a conservative constituent in the geochemical modeling calculations of the underground workings water quality. Consequently, chloride concentrations in the underground workings water will be controlled by the concentrations in the inflowing groundwater and the concentrations released by the mine wall rock and backfilled waste rock. The cementitious material in the underground workings will not be a significant source of chloride.

The chloride concentration calculations are summarized in Table B-8. The average chloride concentration in the Vinini Formation groundwater is 7.053×10^{-4} moles/kg (Table B-1). The mean constituent releases from quartzite and argillite/siltite are calculated using the expressions:

Mean chloride release from quartzite (moles/m^2) = 1.229×10^{-5} mole/m^2 =
1.078 mg/L × 1.651 L/kg waste rock × 1 kg waste rock/4.08 m^2 × mole/35,453 mg

Mean chloride release from argillite/siltite (moles/m^2) = 1.330×10^{-5} mole/m^2 =
1.163 mg/L × 1.656 L/kg waste rock × 1 kg waste rock/4.08 m^2 × mole/35,453 mg

These results are converted to moles by multiplying by the surface area of the waste rock per liter of underground workings water, either 5.411 m^2 or 54.11 m^2 (Table B-8). The aqueous concentration (moles/kg water) can be calculated by dividing the concentration by the final calculated mass of water, which is decreased by the modeled reactions because small amounts are consumed by mineral precipitation (Table B-8). The final concentrations, converted to units of mg/L, are summarized in Table B-8. These results illustrate that for the lower mine wall rock and waste rock surface area, the largest source of chloride is the inflowing groundwater. The higher mine wall rock and waste rock surface area, however, results in more significant chloride contributions from the mine wall rock and waste rock.

Table B-8. Chloride Calculations

Mine wall rock and waste rock surface area	5.411 m^2	54.11 m^2	Units
Groundwater concentration	7.05×10^{-4}	7.05×10^{-4}	moles/kg water
Mean release from quartzite	6.65×10^{-5}	6.65×10^{-4}	moles
Mean release from argillite/siltite	7.20×10^{-5}	7.20×10^{-4}	moles
Total chloride	8.44×10^{-4}	2.09×10^{-3}	moles
Total chloride	29.9	74.1	mg
Final mass of water	0.9915	0.9862	kg
Chloride concentration	30.2	75.1	mg/L

B.2.2 Precipitated Constituent Example

The average fluoride concentration in Vinini Formation groundwater is predicted to be 5.660×10^{-5} moles/kg water (Table B-1). Fluoride release from the quartzite and argillite/siltite mine wall rock and waste rock is calculated per m^2 using the expressions:

Mean fluoride release from quartzite (moles/m^2) = 2.434×10^{-5} mole/m^2 =
1.144 mg/L × 1.651 L/kg waste rock × 1 kg waste rock/4.08 m^2 × mole/18,998.4 mg

Mean fluoride release from argillite/siltite (moles/m^2) = 7.364×10^{-5} mole/m^2 =
3.447 mg/L × 1.656 L/kg waste rock × 1 kg waste rock/4.08 m^2 × mole/18,998.4 mg

These results are converted to moles by multiplying by the surface area of the waste rock per liter of underground workings water, either 5.411 m^2 or 54.11 m^2 (Table B-9). Fluoride is removed from solution by the precipitation of fluorite, which consumes two moles of fluoride per mole of fluorite. The aqueous concentration (moles/kg water) can be calculated by dividing the concentration by the final calculated mass of water, which is decreased because small amounts are consumed by mineral precipitation (Table B-9). The final concentrations, converted to units of mg/L, are summarized in Table B-9. The results of these calculations illustrate that fluoride concentrations remain relatively low compared to the NDEP reference value of 4 mg/L because of fluorite precipitation.

Table B-9. Fluoride Calculations

Mine wall rock and waste rock surface area	5.411 m^2	54.11 m^2	Units
Groundwater concentration	5.66×10^{-5}	5.66×10^{-5}	moles/kg water
Mean release from quartzite	1.32×10^{-4}	1.32×10^{-3}	moles
Mean release from argillite/siltite	3.98×10^{-4}	3.98×10^{-3}	moles
Moles precipitated as fluorite	-4.84×10^{-4}	-5.23×10^{-3}	moles
Total aqueous fluoride	1.02×10^{-4}	1.23×10^{-4}	moles
Total aqueous fluoride	1.95	2.34	mg
Final mass of water	0.9915	0.9862	kg
Fluoride concentration	1.96	2.38	mg/L

B.2.3 Adsorbed Constituent Example

Beryllium concentrations were below detection in all Vinini Formation water samples (Table 2-7), so groundwater is not expected to be a source of beryllium to the underground workings water. Beryllium release from the quartzite and argillite/siltite mine wall rock and waste rock is calculated per m^2 using the expressions:

Mean beryllium release from quartzite (moles/m^2) = 1.032×10^{-6} mole/m^2 =
0.02302 mg/L × 1.651 L/kg waste rock × 1 kg waste rock/4.08 m^2 × mole/9,012.2 mg

Mean beryllium release from argillite/siltite (moles/m^2) = 2.572×10^{-6} mole/m^2 =
0.05717 mg/L × 1.656 L/kg waste rock × 1 kg waste rock/4.08 m^2 × mole/9,012.2 mg

These results are converted to moles by multiplying by the surface area of the waste rock per liter of underground workings water, either 5.411 m^2 or 54.11 m^2 (Table B-10). The moles of beryllium removed from solution by adsorption are subtracted to calculate the total moles of beryllium remaining in solution. The aqueous concentration (moles/kg water) can be calculated by dividing the concentration by the final calculated mass of water, which is decreased because small amounts are consumed by mineral precipitation (Table B-10). The final concentrations, converted to units of mg/L, are summarized in Table B-10. These results illustrate that adsorption significantly affects the final calculated aqueous beryllium concentrations.

Table B-10. Beryllium Calculations

Mine wall rock and waste rock surface area	5.411 m^2	54.11 m^2	Units
Groundwater concentration	0.00	0.00	moles/kg water
Mean release from quartzite	5.59×10^{-6}	5.59×10^{-5}	moles
Mean release from argillite/siltite	1.39×10^{-5}	1.39×10^{-4}	moles
Moles Hfo_sOBe+	-1.39×10^{-5}	-8.36×10^{-5}	moles
Moles Hfo_wOBe+	-6.12×10^{-6}	-1.10×10^{-4}	moles
Total aqueous beryllium	2.28×10^{-7}	1.91×10^{-6}	moles
Total aqueous beryllium	0.00205	0.0172	mg
Final mass of water	0.9915	0.9862	kg
Beryllium concentration	0.00207	0.0174	mg/L

B.2.4 Nitrogen

Nitrate-N concentrations ranged from below detection to 0.7 mg/L in the Vinini Formation water samples (Table 2-7), so groundwater is not expected to be a significant source of nitrate-N to the underground workings water. Precipitation of a nitrate-N solid is not predicted to take place and significant adsorption of nitrate-N is not expected to occur. Consequently, the nitrate-N concentration in the underground workings water will be controlled by leaching from the mine wall rock and waste rock and the release of blasting residues.

Nitrate-N concentrations in the Vinini Formation groundwater used in the geochemical modeling calculations were below analytical detection limits (Table B-11). The mean constituent releases from quartzite and argillite/siltite are calculated using the expressions:

Mean nitrate-N release from quartzite (moles/m^2) = 1.896×10^{-6} mole/m^2 =
0.06571 mg/L × 1.651 L/kg waste rock × 1 kg waste rock/4.08 m^2 × mole/14,006.7 mg

Mean nitrate-N release from argillite/siltite (moles/m^2) = 3.101×10^{-6} mole/m^2 =
0.1071 mg/L × 1.656 L/kg waste rock × 1 kg waste rock/4.08 m^2 × mole/14,006.7 mg

These results are converted to moles by multiplying by the surface area of the waste rock per liter of underground workings water, either 5.411 m^2 or 54.11 m^2 (Table B-11). The mass of nitrate-N is calculated by multiplying by the gram formula weight. The aqueous concentration (mg/kg water) can be calculated by dividing the concentration by the final calculated mass of water, which is decreased by the modeled reactions because small amounts are consumed by mineral precipitation (Table B-11). The concentrations leached from the mine wall rock and waste rock, in units of mg/L, are summarized in Table B-11. The mean concentration of nitrate-N in the underground workings water is 1.4 mg/L (Table 2-8). This mean concentration was

added to the nitrate-N concentrations calculated from mine wall rock and waste rock leaching to account for nitrate-N that may be derived from blasting residues (Table B-11).

Table B-11. Nitrate-N Calculations

Mine wall rock and waste rock surface area	5.411 m^2	54.11 m^2	Units
Groundwater concentration	0.00	0.00	moles/kg water
Mean release from quartzite	1.03×10^{-5}	1.03×10^{-4}	moles
Mean release from argillite/siltite	1.68×10^{-5}	1.68×10^{-4}	moles
Total leached nitrate-N	2.71×10^{-5}	2.71×10^{-4}	moles
Total leached nitrate-N	0.380	3.80	mg
Final mass of water	0.9915	0.9862	kg
Nitrate-N concentration from mine wall rock and waste rock leaching	0.383	3.83	mg/L
Mean nitrate-N in underground workings water	1.4	1.4	mg/L
Total nitrate-N	1.78	5.25	mg/L

B4 Hollister Mine West Pit Shallow Groundwater Technical Memorandum

3264 Goni Road, Suite 153
Carson City, Nevada 89706
Tel: 775-883-4118
Fax: 775-883-5108

Technical Memorandum

Prepared for: Rodeo Creek Gold, Inc.

Project Title: Hollister EIS

Project No: 138301

Draft Technical Memorandum No. 1

Subject: Hollister Mine West Pit Shallow Groundwater

Date: October 4, 2010

To: Teresa Conner, Environmental Manager

From: Brad Hart, Principal Hydrogeologist

1. Introduction

Rodeo Creek Gold, Inc. (RCG) is in the process of permitting the Hollister Mine for full-scale production. The Hollister Mine is an underground gold mining operation located in Elko County, Nevada (Figure 1) that is currently operating under an exploration permit, which allows for bulk sampling and limited test mining. Surface mining was conducted in two pits at the Hollister Mine site in the early 1990s by Cornucopia Resources and Galactic Resources. RCG is considering utilizing one of the previously mined pits, known as the West Pit (Figure 2), as a waste rock storage facility in support of future underground mining operations. The West Pit waste rock facility would be lined to keep groundwater from entering the waste rock, and equipped with an under-drain system to control drainage of water from the waste rock.

The gold-bearing vein system of the Hollister Mine is hosted in the Ordovician Vinini Formation, which is comprised of orthoquartzite, siltite and argillite. The Vinini Formation is unconformably overlain by a succession of Tertiary volcanic rocks that range in thickness from 60 to 200 feet thick in the area (HSI, 1989). Clays and re-worked quartzite characterize the contact between the Vinini Formation and the Tertiary volcanic rocks (HCI, 1997). The Vinini Formation hosts the regional aquifer in the Hollister Mine area, and is the unit that will be locally dewatered to accommodate subsurface mining. The Tertiary volcanic rocks host a shallow aquifer that is separated from the regional aquifer in the vicinity of the Hollister Mine by an aquitard, which consists of clay along the unconformity between the Vinini Formation and the Tertiary volcanic rocks.

A shallow pit lake typically occurs for approximately nine months a year (typically November to July) in the bottom of the West Pit (Figure 2) when groundwater levels in the Tertiary volcanic-hosted shallow aquifer in the vicinity of the West Pit rise sufficiently in response to recharge from precipitation (MWH, 2007). Water quality in the pit lake is characterized by high TDS and generally low pH values (pH values have returned to within acceptable limits from August to December 2008 before declining to slightly below the acceptable limits in April 2009; Montgomery, 2010). Previous studies have characterized this pit lake as an evaporative sink that causes groundwater in the Tertiary volcanic-hosted in the immediate vicinity of the pit lake to flow radially inward (HCI, 1997, MWH, 2007), thereby preventing the movement of mine-impacted shallow groundwater away from the West Pit area. Establishment of a waste rock facility in the West Pit is anticipated to locally affect groundwater conditions in the Tertiary volcanic-hosted shallow aquifer by eliminating infiltration of direct precipitation in the area that would be covered by the new waste rock facility, and elimination of evaporation from the pit lake.

This analysis provides a review of previous West Pit studies and an update of current hydrogeologic conditions in the West Pit area. Also included are the results of an analysis of geochemical data from monitoring wells installed in the shallow Tertiary volcanic aquifer. These analyses were conducted to determine whether the construction of the waste rock facility in the West Pit and potential resultant changes to the groundwater flow regime in the Tertiary volcanic aquifer may affect Little Antelope Creek.

The MA-1 seep (Figure 3) has been identified as the monitoring location to identify potential effects to Little Antelope Creek from anticipated changes in West Pit groundwater conditions, The MA-1 seep emanates from the East Overburden Stockpile (Figure 3), and is located hydraulically upgradient of Little Antelope Creek.

DRAFT for review purposes only. Use of contents on this sheet is subject to the limitations specified at the end of this document.
West Pit Tech Memo.docx

2. Background

The shallow groundwater and the West Pit lake were characterized in 1996 (HCI, 1997) and in 2007 (MWH, 2007) to determine the relationship of the pit lake with the shallow Tertiary volcanic aquifer. As previously stated, these reports characterized the West Pit as a groundwater sink (i.e., cone of depression) resulting from the depression of the pit lake surface due to evaporation. Groundwater elevation contours are presented in these reports to demonstrate that the groundwater level in the pit lake is lower than that measured in piezometers located to the south and east of the pit lake, thereby creating a localized groundwater flow field where water in the surrounding shallow aquifer flows toward the pit lake. Figure 4 depicts water level contours from HCI (1997), and Figures 5 and 6 present water level contours from MWH (2007) for December 2006 and April 2007, respectively.

The HCI (1997) and MWH (2007) reports also provide a water balance analysis that considers pit lake inflows and outflows. Inflows to the pit lake include groundwater inflow from up-gradient areas, direct precipitation to the surface of the pit lake, and runoff to the pit lake from the surrounding pit floor and highwall area. The HCI (1997) report considered the pumping of water from the South Overburden Stockpile to the West Pit as an inflow component, and assumed that this pumping would continue, which it did not. Although groundwater outflow from the West Pit was indicated for the short-term analysis, the long-term analysis indicated that, without the pumping of water from the South Overburden Stockpile to the West Pit, groundwater would not flow outward from the cone of depression surrounding the pit lake (HCI, 1997). The MWH report indicates no groundwater outflow from the West Pit. Therefore, both of these analyses indicate that the only outflow component of water from the West Pit is by evaporation.

3. Additional Analyses

In order to further characterize the groundwater conditions in the Tertiary aquifer in the vicinity of the West Pit, additional water level, water budget, and geochemical analyses were conducted. The objectives of these additional analyses were to determine: 1) whether shallow groundwater in the West Pit area has the potential to migrate to surface water in Little Antelope Creek; and 2) whether the construction of a waste rock facility in the West Pit may alter groundwater flow directions such that shallow groundwater beneath the West Pit would migrate to Little Antelope Creek.
Groundwater flow directions presented on Figures 5 and 6 indicate that groundwater flow directions are to the southeast from areas located south of the 5,550-foot elevation contour. The following sections present groundwater elevation contours from 2010, and the geochemical analysis of the West Pit, the MA-1 seep, and groundwater monitoring wells between the pit and the seep (Figure 3).

3.1 Tertiary Aquifer Flow Directions

Although the general direction of groundwater flow in the Tertiary volcanic aquifer is from north to southeast, localized flow directions vary due to past surface mining activities in the area. These activities included diversion and capture of surface water runoff, disturbance of land surfaces leading to enhanced permeability, and collection of storm and process water in unlined pits, ponds and depressions. These disturbances have resulted in enhanced infiltration that produced localized near-surface groundwater accumulation in the vicinity of the open pits (Montgomery, 2010).

DRAFT for review purposes only. Use of contents on this sheet is subject to the limitations specified at the end of this document.
West Pit Tech Memo.docx

Figures 5 and 6 show water level conditions following the unusually high precipitation year of 2005, when water levels in the Tertiary aquifer rose several feet. Groundwater elevation contours based on January 2010 water level data (Figure 7) indicate the same general flow directions across the East and West Pit areas, except that an embayment in the contours occurs along an axis between monitor wells W-E-1 and DGW-2. At the time of collection of the January 2010 water level data, the West Pit had been dry for a period of approximately five months, but the groundwater contours still indicate groundwater flow toward the West Pit from the area approximately defined by a line between the locations of monitor wells P2 and H6-224WW (Figure 7). To the east and southeast of this line, groundwater flows eastward and southeastward, respectively. The southeasterly component of groundwater flow depicted in Figure 7 is aligned with a historic drainage that was buried by the East Waste Dump during previous surface mining activities.

Although the specific hydrogeologic condition that creates the groundwater divide and the steep hydraulic gradient between the West and East pits has not been identified, a fault in the Tertiary volcanics (depicted on Figure 4) has been mapped during previous geologic investigations. Structural influences on groundwater flow in the Tertiary volcanic aquifer within the Hollister Mine area have been observed (e.g., inflows to the exploration decline from the Tertiary volcanic aquifer were noted during the first several months of decline construction, but these inflows eventually ceased, suggesting that the source area responsible for these inflows had been depleted).

3.2 Changes to West Pit Water Budget

Utilizing the West Pit as a waste rock storage facility would affect the groundwater budget of the West Pit area and may influence groundwater flow directions in the immediate vicinity of the West Pit. The West Pit would be lined to accommodate the waste rock storage facility, which would eliminate both the direct precipitation to the pit lake surface and, to some extent, the runoff contribution to West Pit groundwater budget inflow components. A groundwater budget inflow component that was not considered explicitly in either the MWH or HCI studies is the contribution to groundwater from precipitation falling on the floor of the West Pit outside of the pit lake. This infiltrated volume would be a portion of the groundwater inflow component that would be removed from the total groundwater budget if the area were covered with the waste rock facility. Backfilling the West Pit would also eliminate evaporation from the pit lake surface, which is the outflow component of the West Pit groundwater budget.

The MWH (2007) report is based on a more extensive monitor well network and utilizes site-specific precipitation data than the HCI (1997) report. Therefore, groundwater budget values from the MWH report are cited here. Specifically, the groundwater budget components for the West Pit from the MWH (2007) report are:

- Evaporation (outflow): 192,545 cubic feet per year (cu. ft/yr);
- Runoff from the West Pit catchment (inflow): 4,233 cu. ft/yr;
- Direct precipitation (inflow): 74,973 cu. ft/yr; and
- Groundwater inflow (inflow): 130,660 cu. ft/yr;

Elimination of the evaporation outflow component of the water budget and the runoff and direct precipitation components of the inflow budget would leave a net groundwater through-flow of approximately 130,660 cu. ft/yr. As previously discussed, infiltration of precipitation to groundwater

DRAFT for review purposes only. Use of contents on this sheet is subject to the limitations specified at the end of this document.
West Pit Tech Memo.docx

through the floor of the West Pit catchment area was not considered in the MWH report. However, using the 442,000 square foot (ft^2) catchment area and 13.5-inch average annual precipitation for the six years considered in the MWH (2007) study, and assuming that five percent of the precipitation infiltrates to groundwater, approximately 24,750 cu. ft/yr would infiltrate to groundwater. If that area is covered by the waste rock facility, this quantity would be removed from the groundwater budget, yielding a net groundwater through-flow in the West Pit of approximately 106,000 cu. ft/yr.

Changes in the groundwater flow directions in the immediate vicinity of the West Pit resulting from the water balance change can not be predicted with certainty. However, the persistence of lower water levels in the West Pit area several months after the pit lake dried up (Figure 7) suggests groundwater in this area that is west of the groundwater divide depicted in Figure 7 will continue to flow in a westerly direction.

3.3 Geochemical Analyses

Groundwater geochemical data were evaluated to determine whether these data would support the existence of a hydraulic link between the West Pit pit Lake and groundwater emanate from the MA-1 seep. The geochemical analysis, prepared by Geochemical Solutions, LLC (2010), is attached as Appendix A, and is summarized in this technical memorandum. The approach used for this evaluation was to use the sulfate/chloride (SO4/Cl) ratio to fingerprint the West Pit pit Lake, the MA-1 seep, and the monitoring wells completed in the Tertiary volcanic aquifer that lie between these two points (P1, P2, W-E-1, H6-226WW, H6-224WW, DGQ-1R and DGW-2B; Figure 3). Sulfate is a conservative chemical constituent (i.e., not readily attenuated by aquifer solids) that is associated with the weathering of sulfide minerals, and chloride is a largely natural, chemically conservative constituent that was used to normalize the sulfate concentration. The SO4/Cl ratio for the West Pit, the MA-1 seep and the intervening monitoring wells were plotted as a function of the relative distance from the West Pit to the MA-1 seep (Figure 8). The relative distance corresponds to the order in which the monitoring wells occur along a path from the West Pit to MA-1, without regard to absolute distance. Figure 8 shows that the SO4/Cl ratio varies as a function of relative distance from the West Pit, and that the ratio decreases to a value that is lower than MA-1 at a location (P2/H6-226) between the two end points. This suggests that the two end points (i.e., the West Pit and MA-1) are not hydraulically connected unless significant mixing with lower-quality water occurs between the P2/H6-226 and the MA-1 seep.

The analysis of potential relationships among the sampling locations between the West Pit and the MA-1 seep was refined by plotting the SO4/Cl fingerprint as a function of the associated SO4 concentration (Figure 9), which allows for the interpretation of dilution effects. For any sampling location, the position of its plotted points depicted on Figure 9 may only be produced by mixing two or more of the other sampling locations that bound it. For example, the cluster of points associated with the MA-1 seep on Figure 9 may be produced by mixing of the water chemistry of the clusters of points that are on either side of it. Therefore, the MA-1 chemistry can be produced by mixing P2/H6-226 and West Pit area water (either P1, H6-224, or the West Pit) or DGW-1R. While similar to MA-1 with respect to the SO4/Cl fingerprint, W-E-1 has lower sulfate, which by the location of W-E-1 (Figure 3) suggests that there is not a flow path between West Pit and the MA-1 seep that is north of P2 and H6-226.

West Pit values plot on Figure 9 as a generally horizontal line, indicating changes in total composition while maintaining a constant fingerprint. This horizontal alignment characteristic of the West Pit water is consistent with evaporation that does not involve significant, if any, mineral precipitation. MA-1 seep values do not exhibit this behavior, which suggests a lack of connectivity between the MA-1 seep and the West Pit. Although the MA-1 point cluster presented on Figure 9 can be reproduced using either West Pit water or DGW-1R water to mix with an intermediate water (e.g., P2), Figure 8

illustrates that the SO4/Cl ratio at points between West Pit and MA-1 drops below that of MA-1, and Figure 9 illustrates that the sulfate concentration does as well. Therefore, another input of water (e.g. DGW-1R) would be required to boost these parameters at the intervening monitoring well locations to values associated with the MA-1 seep. The higher SO4/Cl ratio at the MA-1 seep relative to P2 cannot be reproduced by evaporation alone (i.e., evaporation that may occur at the MA-1 seep). If a water is evaporated (e.g., West Pit lake), the resulting water chemistry would shift horizontally (i.e., the SO4/Cl ratio would not increase), as both sulfate and chloride would concentrate proportionally and the ratio would not be expected to increase.

The relative proportions of P2 and DGW-1R water required to produce water similar to MA-1 were estimated using a mixing model that calculates the concentrations of sulfate and chloride for a range of mixing proportions between the two waters. The SO4/Cl ratio was then calculated and plotted versus sulfate. Figure 10 illustrates the result of calculations of mixing DGW-1R water with P2 water. The black line on Figure 10 represents the binary mixing of P2 and DGW-1R water, with the points in yellow along the line representing 10 percent mixing increments. The MA-1 seep data points lie at a position along this line that corresponds to a mixing proportion of about 95 percent P2 water and 5 percent DGW-1R water. A similar calculation (Figure 11) indicates that a mixture of 30 percent P1 water to 70 percent P2 water is necessary to achieve the same effect as using 5 percent DGW-1R water. Given the analysis presented in Figure 8 (i.e., the dip in the SO4/Cl ratio), this magnitude of mixing does not appear to be likely.

4. Summary and Conclusions

The following summarizes the current understanding of the flow conditions in the Tertiary volcanics aquifer in the vicinity of the West Pit and between the West Pit and the MA-1 seep.

- Previous studies (HCI, 1997; MWH, 2007) have characterized the West Pit lake as an evaporative groundwater sink (i.e., cone of depression) that causes groundwater in the vicinity of the West Pit to flow radially inward, thereby preventing the migration of this water southeastward along the larger-scale groundwater flow path.
- Groundwater elevation data suggest that there is a groundwater divide located between monitoring well P1and the P2/H6-224WW.
- Recent groundwater elevation data from 2010 suggest groundwater continues to flow toward the West Pit from areas west of the groundwater divide, even after the pit lake disappeared.
- Construction of a waste rock facility in the West Pit would affect the water budget in the West Pit area, which could affect groundwater flow directions.
- Construction of the West Pit waste rock facility would reduce direct precipitation, runoff, and infiltration contributions to the West Pit area by approximately 104,000 cu. ft/yr.
- Geochemical analyses presented here do not support existence of a groundwater flow path from the West Pit to the MA-1 seep.

Evidence presented in this technical memorandum indicates that, although groundwater flow conditions may be altered as a result of the construction of a waste rock facility in the West Pit, it is not likely to affect Little Antelope Creek or other surface waters because the direction of groundwater flow from the West Pit area is not toward Little Antelope Creek with or without the presence of the West Pit lake. Some improvement of groundwater quality in the West Pit vicinity may occur as a result of eliminating infiltration of precipitation through the pit walls and pit floor with construction of the waste rock facility.

DRAFT for review purposes only. Use of contents on this sheet is subject to the limitations specified at the end of this document.
West Pit Tech Memo.docx

References

Geochemical Solutions, 2010, Hollister EIS Evaluation of Connectivity Between West Pit and Seep MA-1, Memorandum prepared by Mark A. Williamson, PhD, prepared for Brown and Caldwell, August 22, 2010.

HCI, 1997, West Pit Hydrologic Characterization, Hollister Operations Area, prepared for Newmont Gold Company, prepared by Hydrologic Consultants, Inc., February 1997.

HSI, 1989, Ground-Water Supply Evaluation and Development, Ivanhoe Project, Elko County, Nevada, prepared for Galactic Services, Inc., prepared by Hydro-Search, Inc., February 15, 1989.

Montgomery, 2010, Hydrogeologic Monitoring Summary 2006-2009, Hollister Mine Area, Elko County, Nevada, Prepared for Rodeo Creek Gold Inc., prepared by Montgomery & Associates, September 17, 2010.

MWH, 2007, Hydrologic Study of the Hollister Reclamation Project, prepared for Newmont Mining Corporation, prepared by MWH Americas, Inc., June 2007.

DRAFT for review purposes only. Use of contents on this sheet is subject to the limitations specified at the end of this document.
West Pit Tech Memo.docx

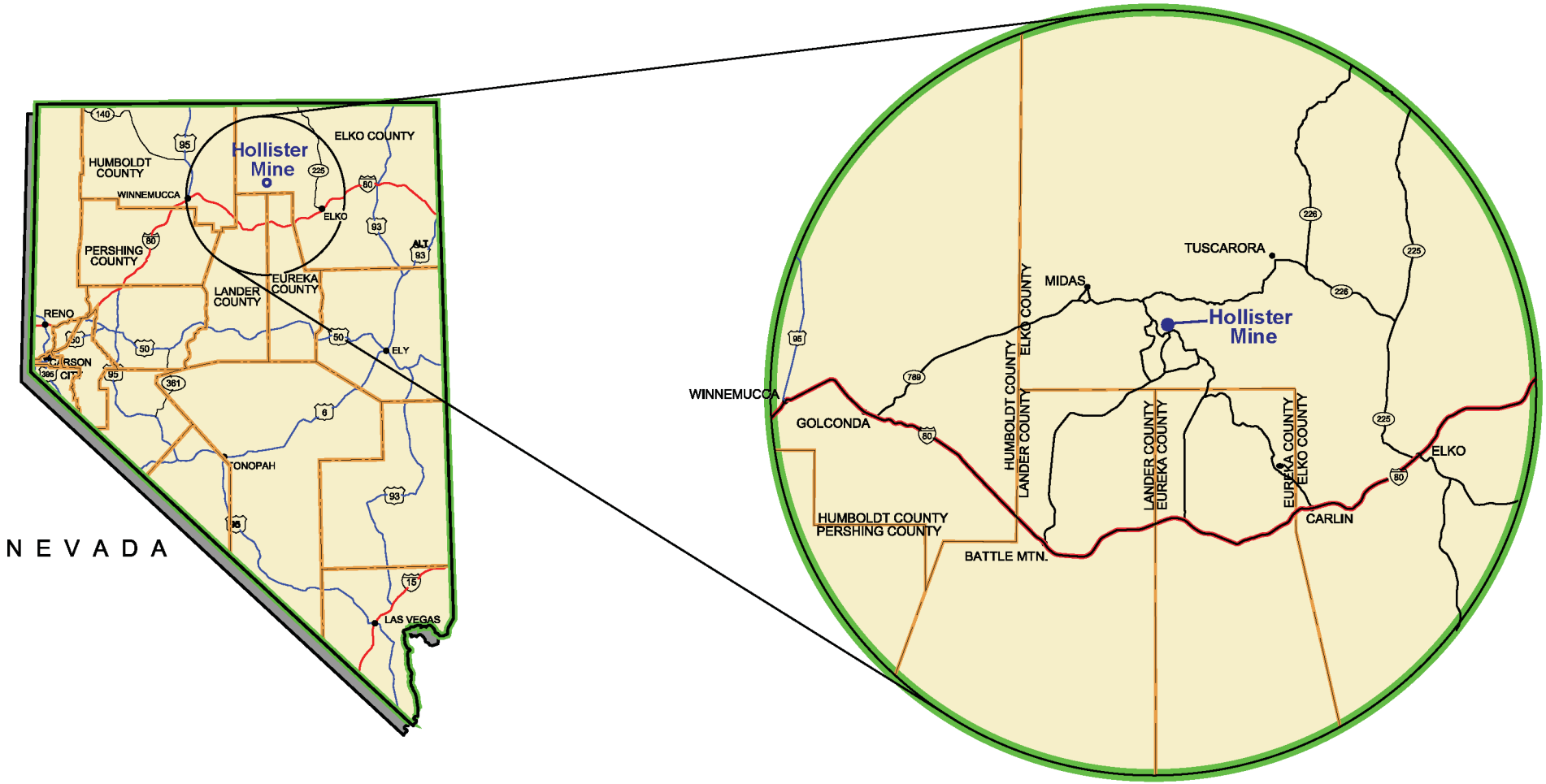

Source: AECOM

BROWN AND CALDWELL	PROJECT 138301	SITE Rodeo Creek Gold - Hollister Mine	Figure 1
	DATE 7-7-10	TITLE Hollister Mine Location	

P:\BC_CAR\138301_Hollister_Mine_EIS\GIS\GRAPHICS

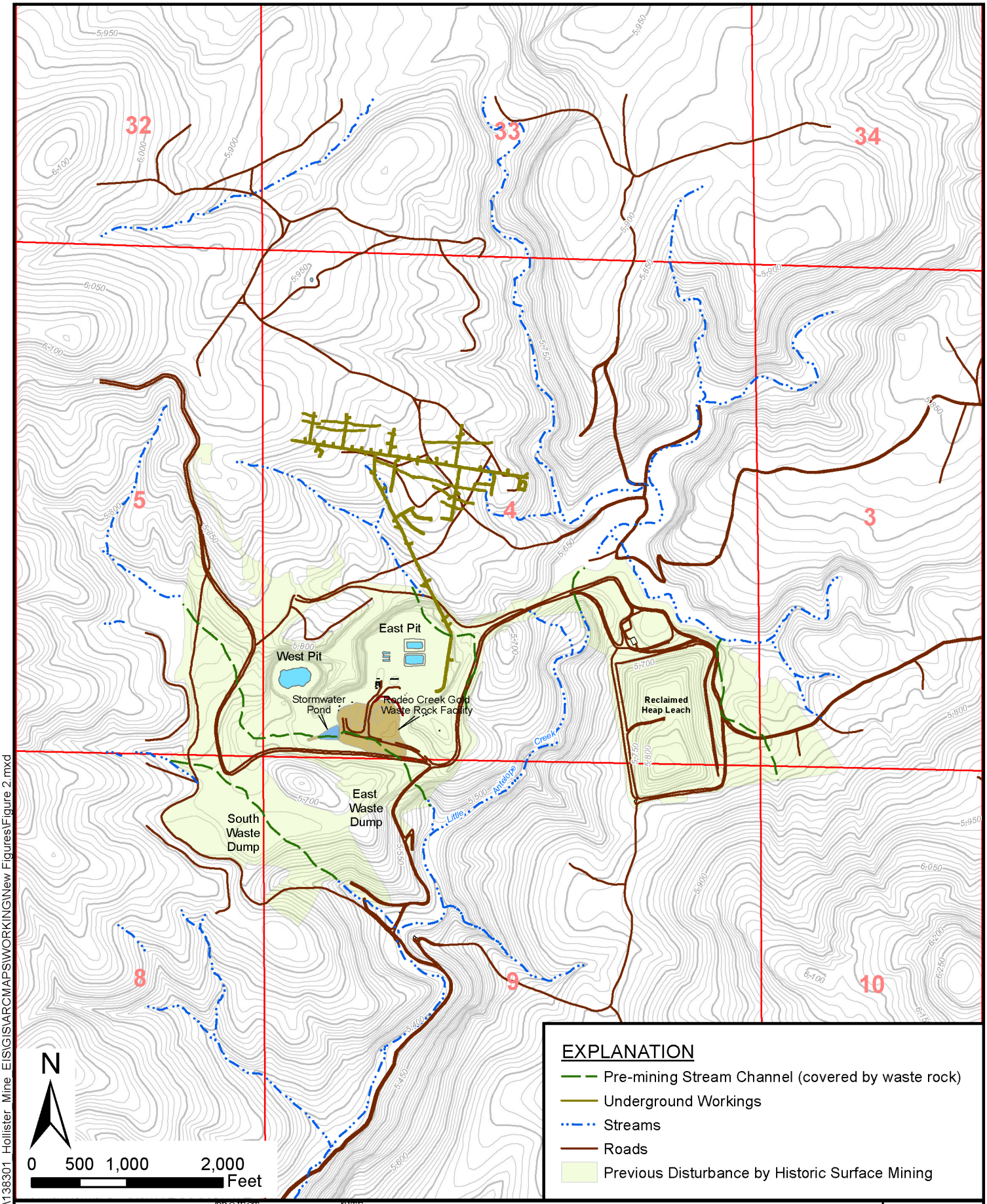

FILE: P:\BC_CAR\138301_Hollister_Mine_EIS\GIS\ARCMAPS\WORKING\New Figures\Figure 2.mxd

BROWN AND CALDWELL

PROJECT	SITE	
138301	Rodeo Creek Gold - Hollister Mine	Figure
DATE	TITLE	
9/24/10	Hollister Mine Site Map	2

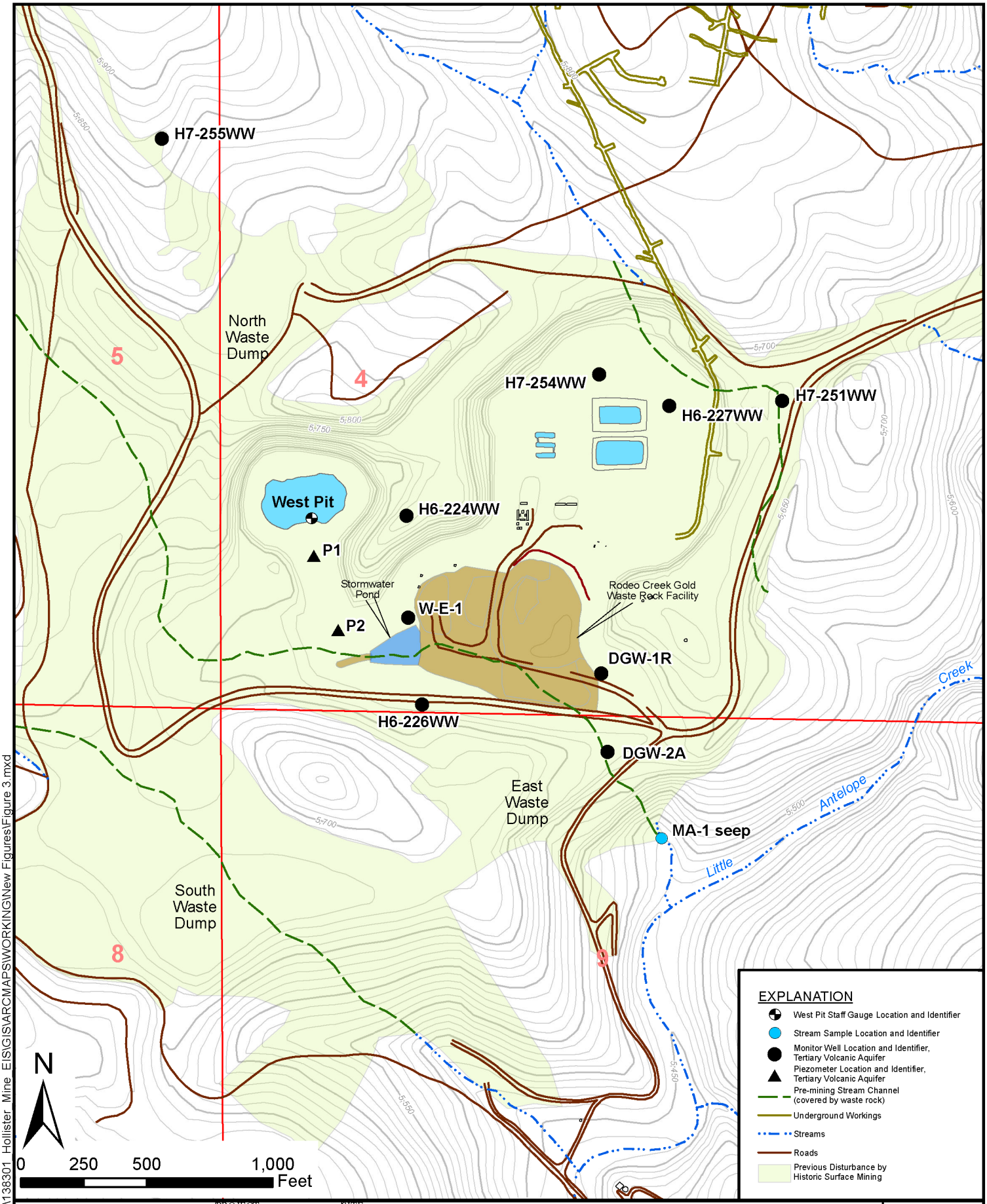

FILE: P:\BC_CAR\138301_Hollister_Mine_EIS\GIS\ARCMAPS\WORKING\New Figures\Figure 3.mxd

BROWN AND CALDWELL

PROJECT	SITE	
138301	Rodeo Creek Gold - Hollister Mine	Figure
DATE	TITLE	
9/24/10	Tertiary Volcanics Monitoring Locations and the MA-1 Seep	3

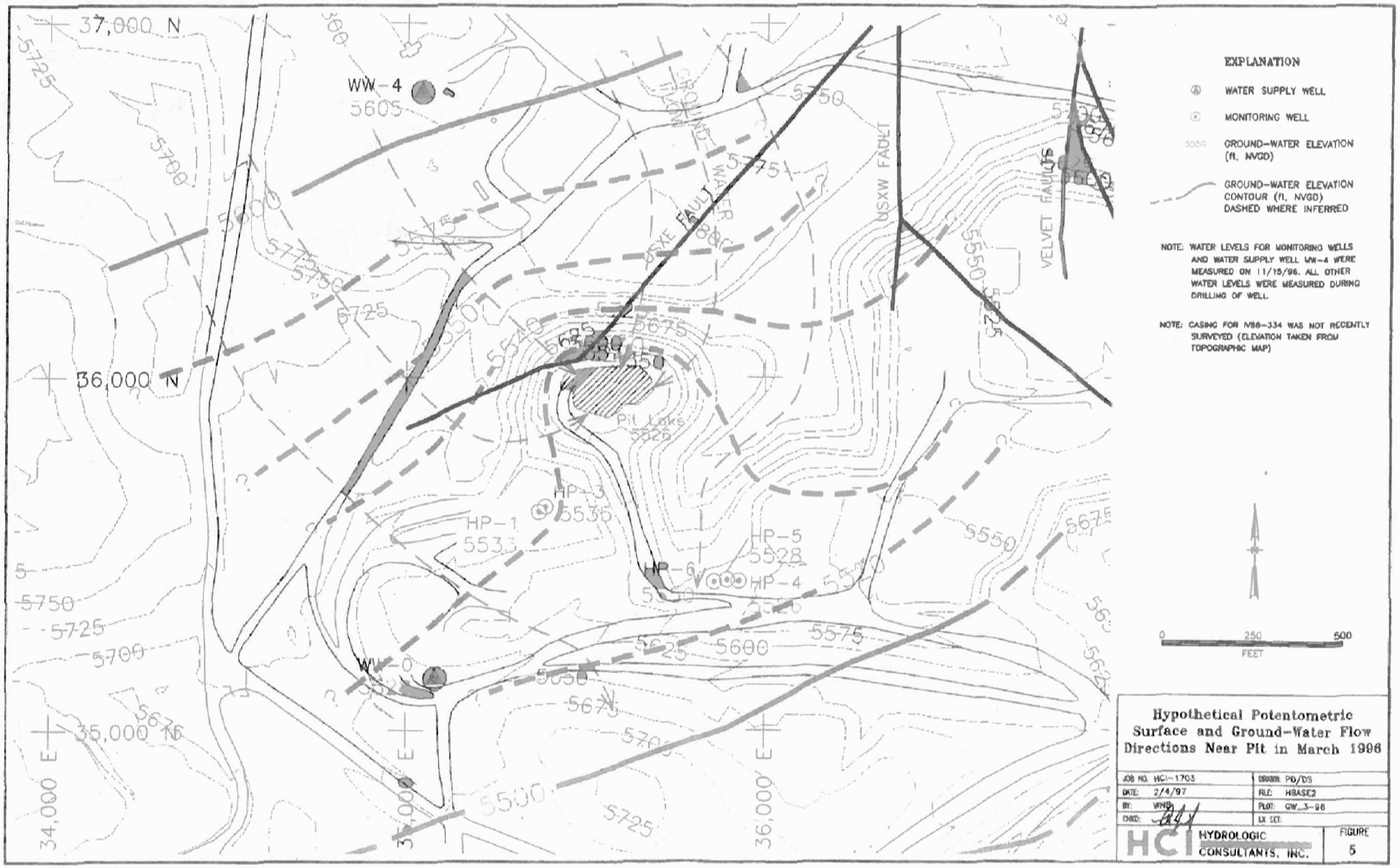

BROWN AND CALDWELL	PROJECT 138301	SITE Rodeo Creek Gold - Hollister Mine	Figure 4
	DATE 9/27/10	TITLE Tertiary Volcanics Aquifer Water Level Contours, 1997	

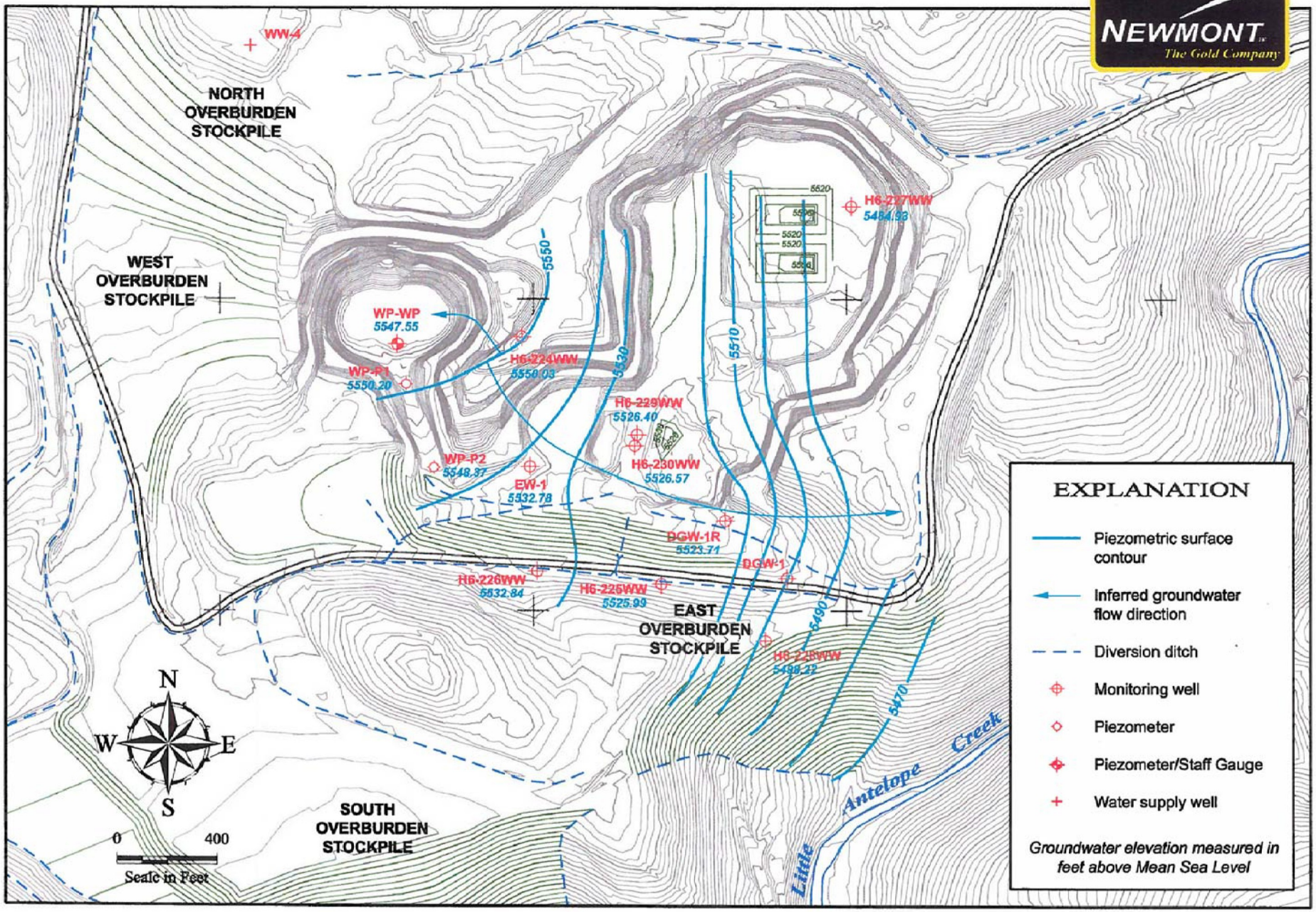

BROWN AND CALDWELL

PROJECT	SITE	Figure
138301	Rodeo Creek Gold - Hollister Mine	5
DATE	TITLE	
9/27/10	Tertiary Volcanics Aquifer Water Level Contours, December 2006	

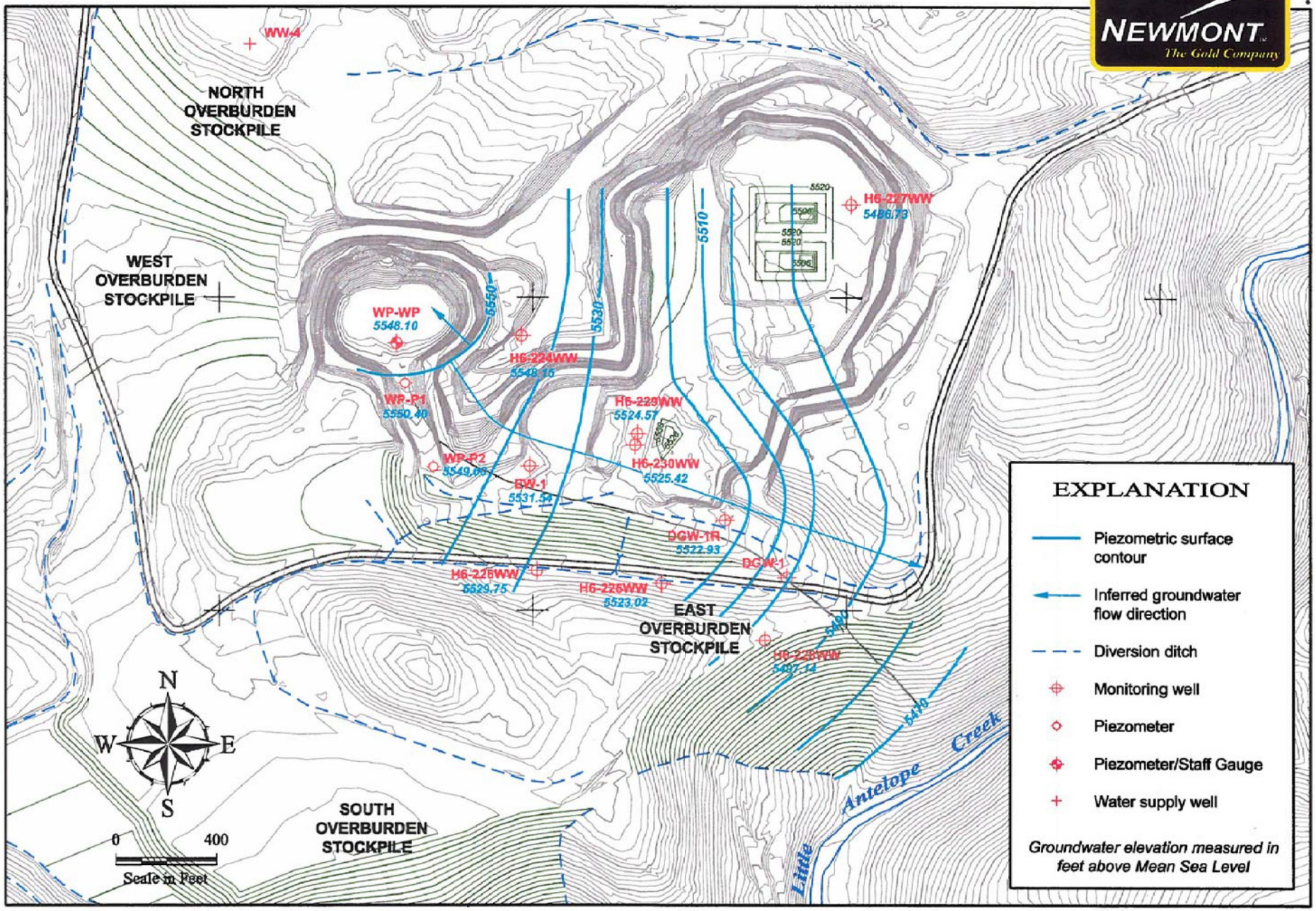

BROWN AND CALDWELL	PROJECT 138301	SITE Rodeo Creek Gold - Hollister Mine	Figure 6
	DATE 9/27/10	TITLE Tertiary Volcanics Aquifer Water Level Contours, April 2007	

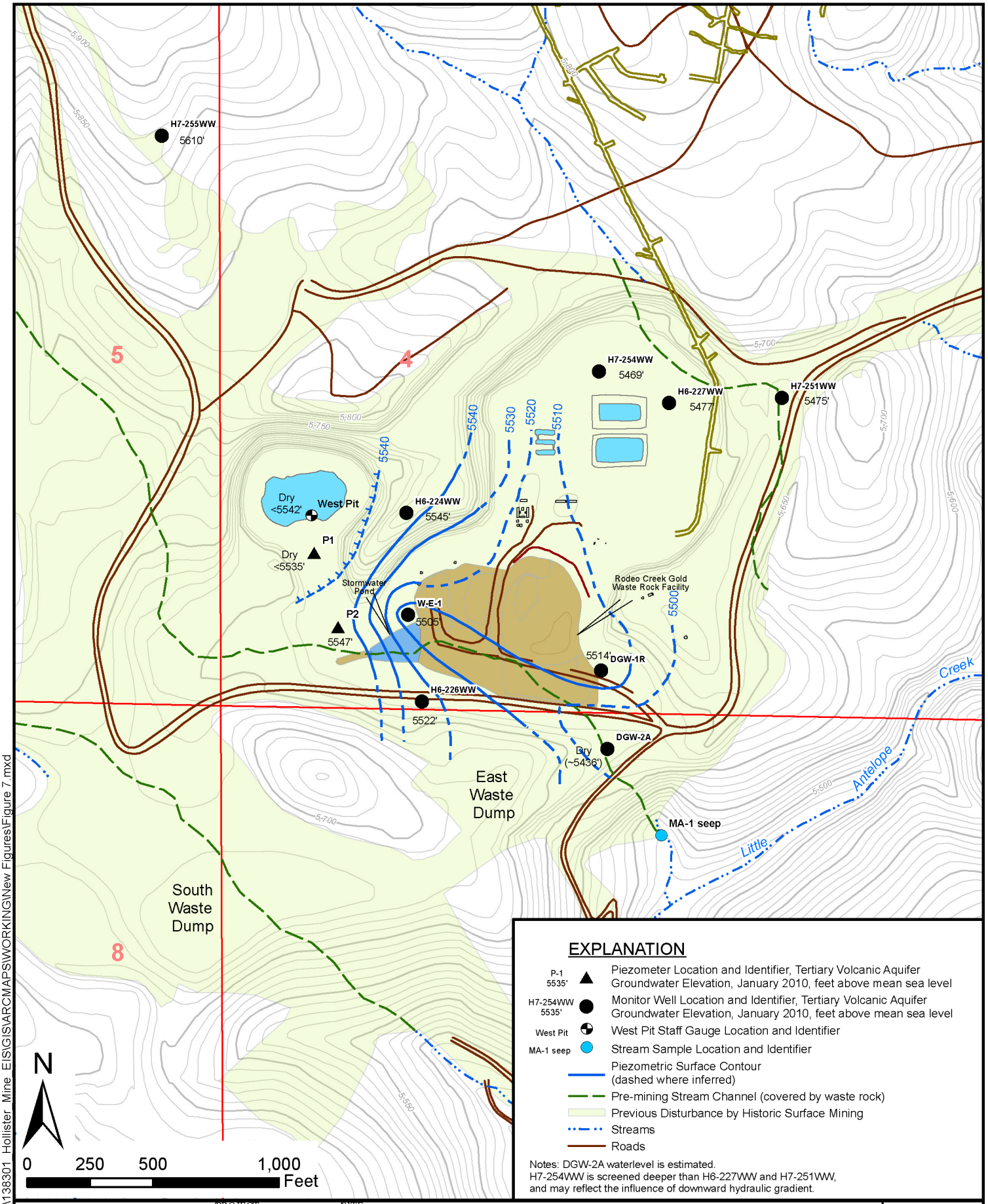

FILE: P:\BC_CAR\138301_Hollister_Mine_EIS\GIS\ARCMAPS\WORKING\New Figures\Figure 7.mxd

BROWN AND CALDWELL

PROJECT	SITE	
138301	Rodeo Creek Gold - Hollister Mine	Figure
DATE	TITLE	
9/24/10	Tertiary Volcanics Aquifer Water Level Contours, January 2010	7

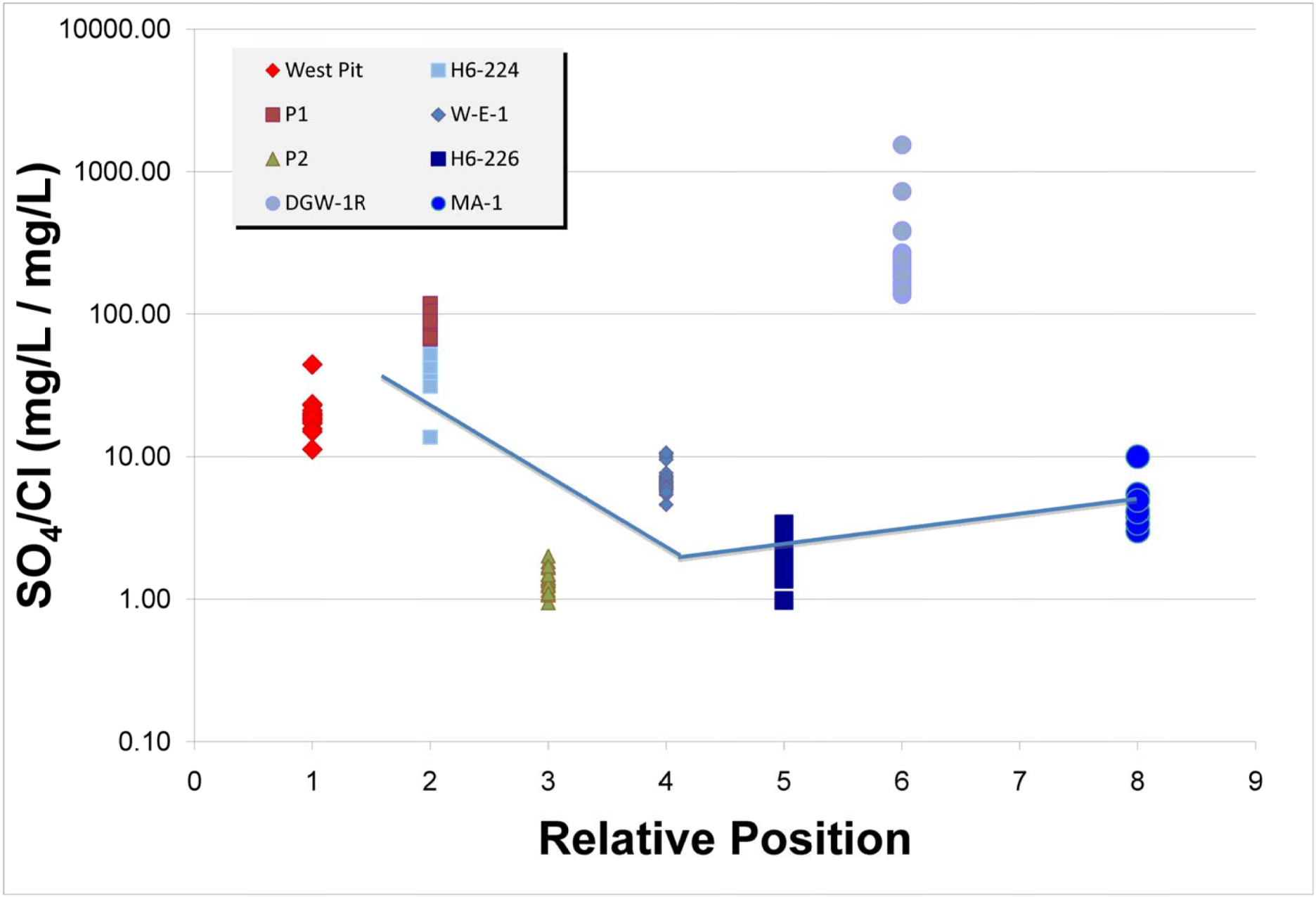

BROWN AND CALDWELL	PROJECT 138301	SITE Rodeo Creek Gold - Hollister Mine	Figure 8
	DATE 9/27/10	TITLE Sulfate/Chloride Ratio as a Function of Relative Position	

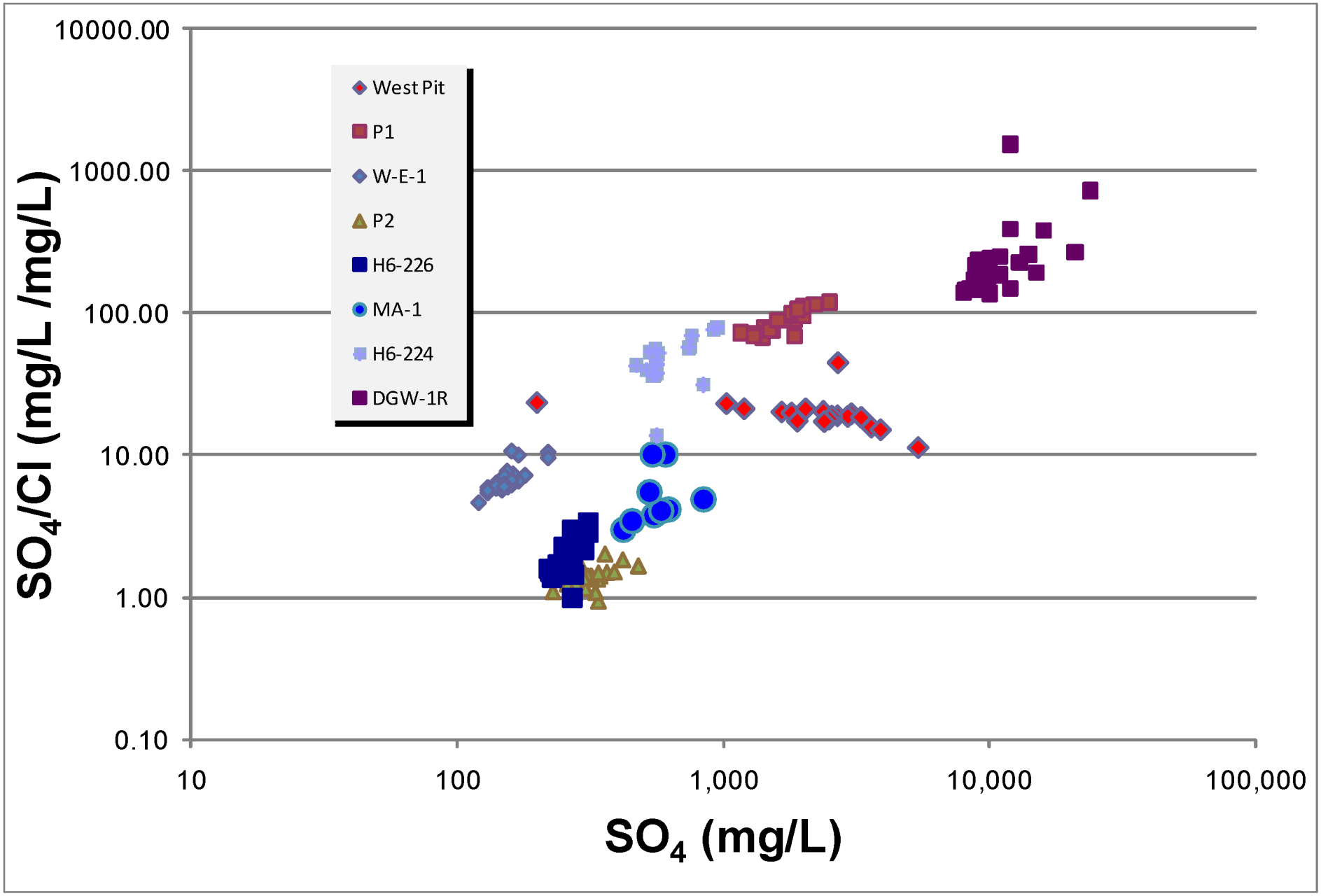

BROWN AND CALDWELL	PROJECT 138301	SITE Rodeo Creek Gold - Hollister Mine	Figure 9
	DATE 9/27/10	TITLE Sulfate/Chloride Ratio as a Function of Sulfate Concentration	

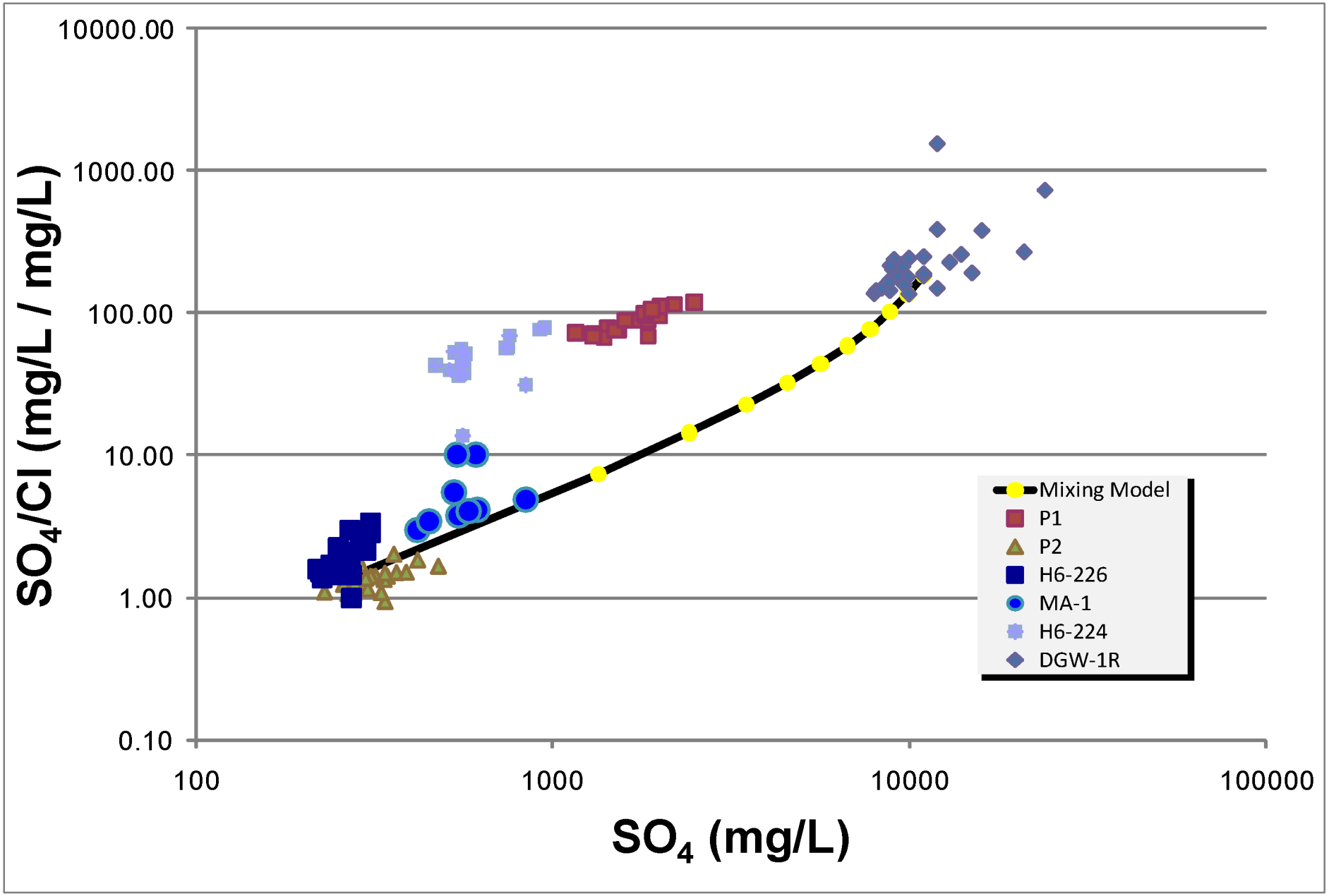

BROWN AND CALDWELL	PROJECT 138301	SITE Rodeo Creek Gold - Hollister Mine	Figure 10
	DATE 9/27/10	TITLE Simple Mixing Model for the Combination of P2 Water and DGW-1R Water	

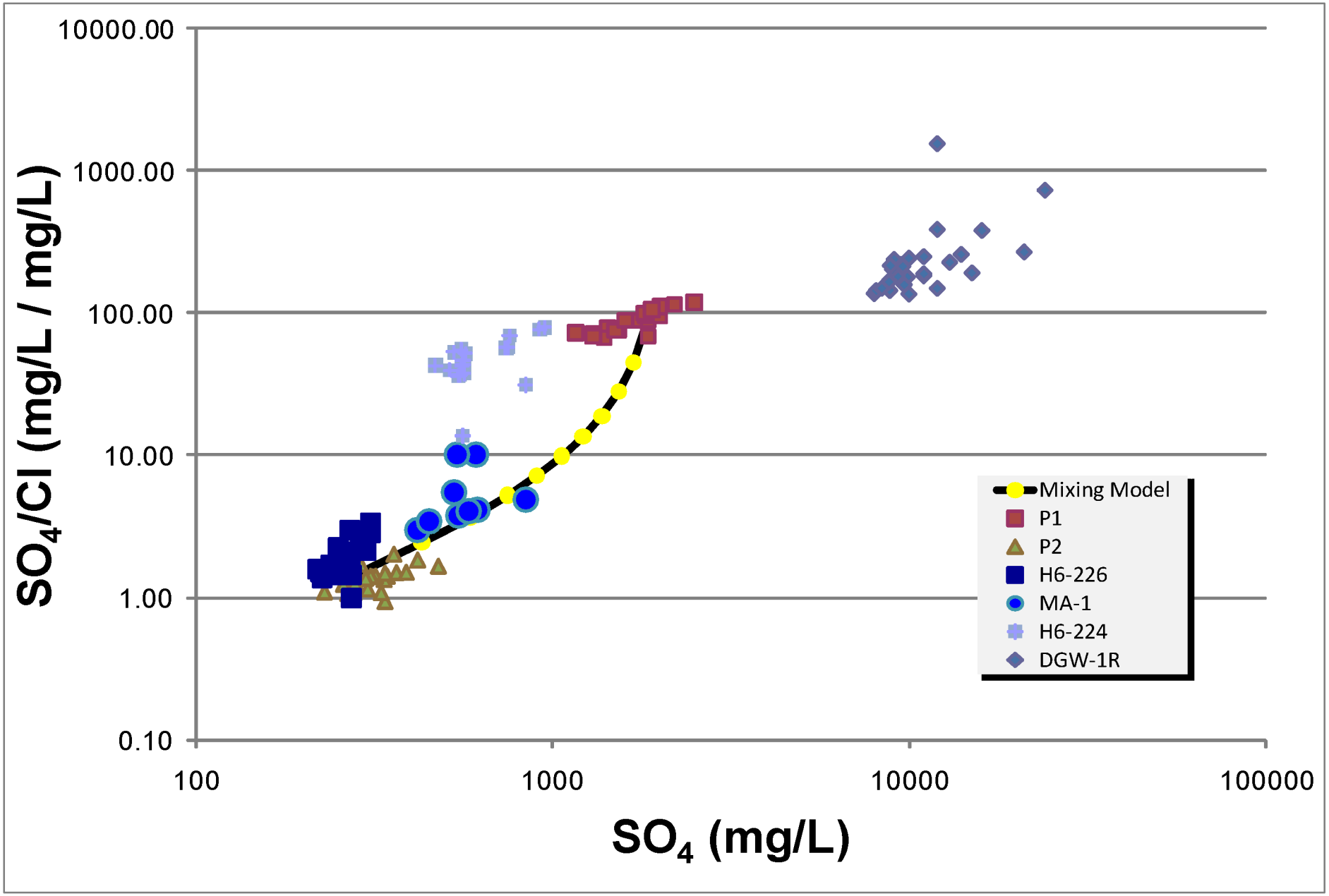

BROWN AND CALDWELL	PROJECT 138301	SITE Rodeo Creek Gold - Hollister Mine	Figure 11
	DATE 9/27/10	TITLE Simple Mixing Model for the Combination of P2 Water and P1 Water	

Attachment A

GEOCHEMICAL SOLUTIONS, LLC
1943 Lakewood Drive Loveland, CO 80538
T 720.373.3714
mark@geochemical-solutions.com
www.geochemical-solutions.com

MEMORANDUM

TO:	Brad Hart	**FROM:**	Mark A. Williamson, PhD
ORGANIZATION:	Brown & Caldwell	**DATE:**	September 27, 2010
CC:	File	**PROJECT:**	1004.10
SUBJECT:	Hollister EIS Evaluation of Connectivity Between West Pit and Seep MA-1		

Summary

Seep MA-1 does not appear to be influenced by groundwater in the vicinity of the West Pit. Although seep MA-1 bears a chemical signature that is consistent with influence by groundwater in the West Pit area (P1, H6-224, West Pit sump), groundwater between the West Pit and MA-1 (P2, H6-226, W-E-1, see Figure 1) does not carry a geochemical fingerprint showing influence from the West Pit. Therefore, it is difficult to link West Pit and MA-1. Alternatively, the groundwater in the vicinity of the waste rock pile in the East Pit (DGW-1R) has a geochemical fingerprint that is consistent with a link to MA-1 while having little or no evidence of intermediate groundwater (groundwater between potential source and MA-1 that appears chemically unaffected). Mixing calculations indicate that about 30% West Pit water mixing with unaffected water is required to reproduce water quality at MA-1. Only 5% groundwater from the DGW-1R area is required to produce the same result.

Approach

The approach used for evaluating a possible hydrologic link between West Pit and MA-1 was to compare the SO_4/Cl (sulfate/chloride) fingerprint for each, as well as for wells that lie between West Pit and MA-1 (intermediate wells). Sulfate is a chemical constituent that is associated with the weathering of sulfide minerals, and chloride is a largely natural, chemically conservative constituent that was used to normalize the sulfate concentration. From late 2005 through early 2009 (Montgomery, 2010) this parameter remained fairly steady and distinct among the various groundwater (and surface water) sampling locations (see Figure 2), which makes it a useful fingerprint for surface and groundwater from various locations at the project site. In the same way that water chemistries are plotted on a standard Piper diagram to illustrate the proportions of three constituents (SO_4, Cl and HCO_3) and illustrate distinct water types, the SO_4/Cl is used to simply distinguish between water types.

The key wells (P1, P2, W-E-1, H6-226WW, H6-224WW, DGQ-1R, and DGW-2B) have samples taken from roughly the same depth below the water table, thus comparison of their chemical compositions is appropriate. Figure 3 shows the depths from which samples are collected. It is noteworthy that DGW-1R and DGW-2b are relatively deep compared with other key wells.

The SO_4/Cl ratio for each key well was plotted as a function of relative distance from the West Pit area (Figure 4). Figure 1 illustrates the positions of the wells. As shown in Figure 4, the SO_4/Cl fingerprint varies as a function of relative distance[1] from the West Pit area, going toward MA-1. The decrease in this parameter to a value that is lower than MA-1 at a point between West Pit and MA-1, highlighted by the line passing through the center of intermediate wells, suggests they are not hydrologically connected. Well W-E-1, which is an intermediate well, appears to have a signature very similar to MA-1. However its SO_4/Cl fingerprint is unique among site wells (see Figure 5) and is not explained by mixing of any observed groundwater compositions.

[1] The relative distance simply corresponds to the order in which wells occur along a path from the West Pit to MA-1, without specific regard to absolute distance (in, say, feet).

Figure 1. Site map showing well locations. The figure is oriented with north to the top.

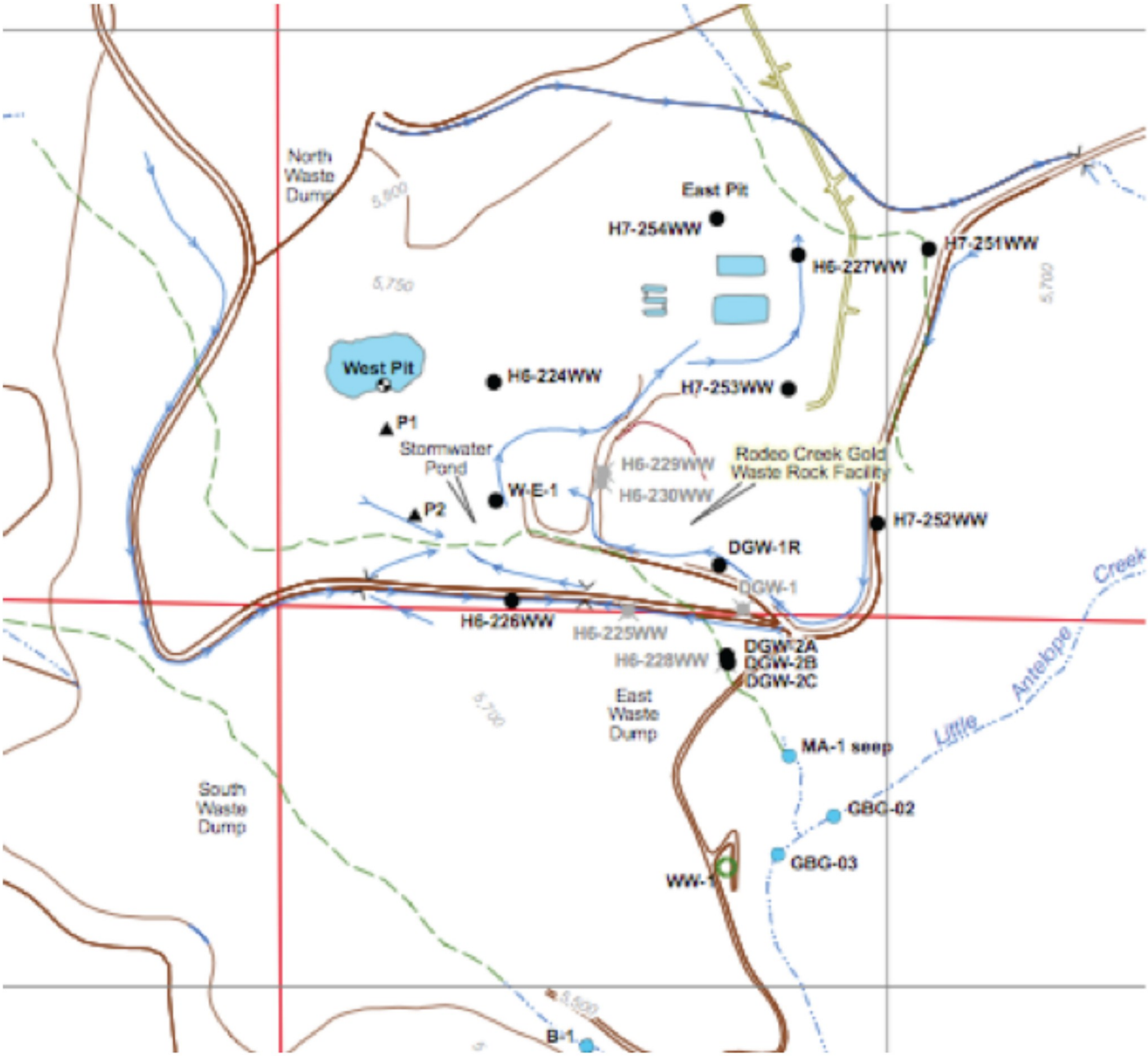

Figure 2. Sulfate/Chloride ratio in key wells over time.

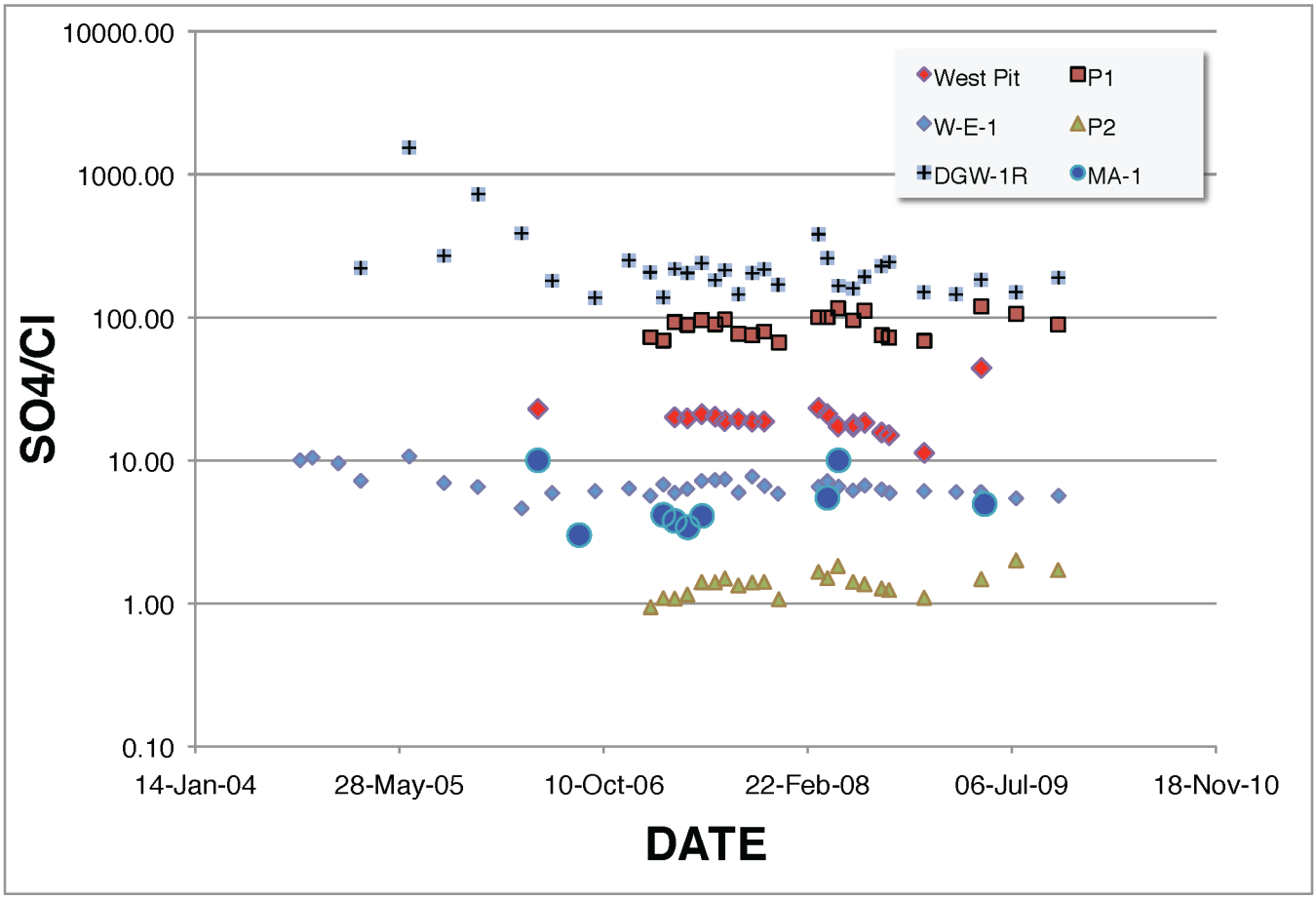

Figure 3. Sampling depths in key wells.

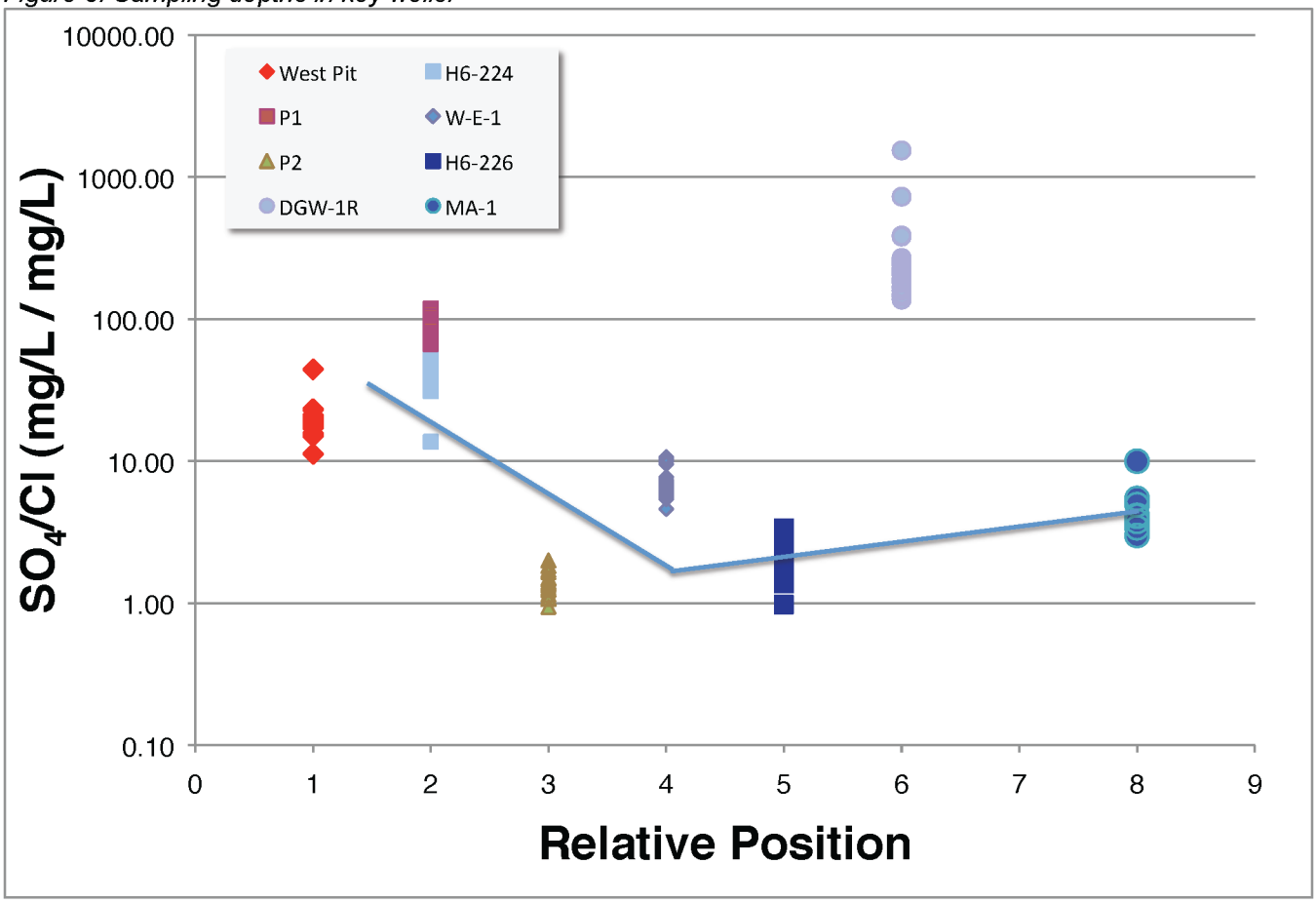

NOTE: WT = Water Table

Figure 4. Sulfate/Chloride ratio with relative distance from West Pit to MA-1.

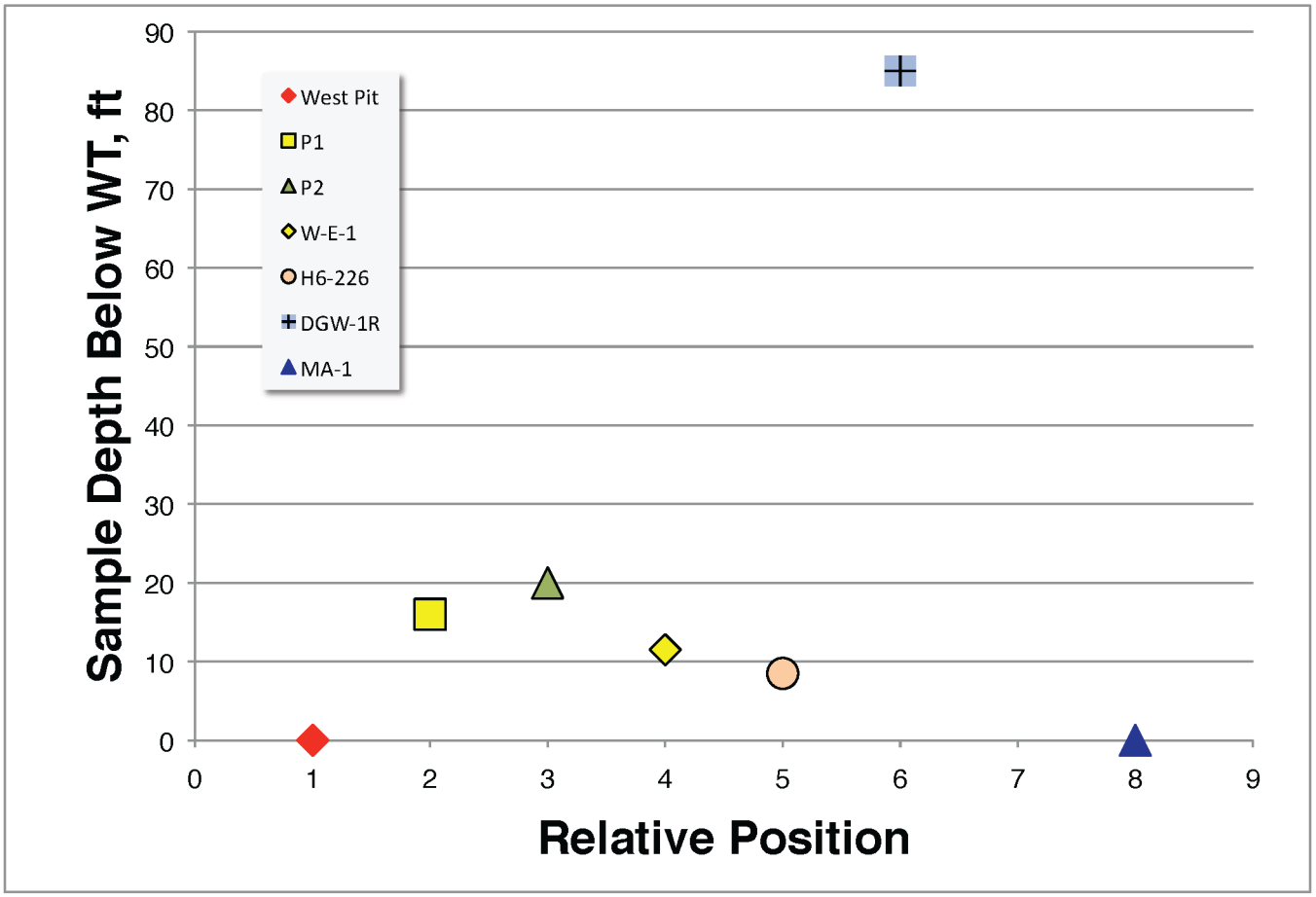

To compliment and refine the potential relationship(s) among the sampling locations with distance (Figure 4), the SO_4/Cl fingerprint is plotted as a function of the associated SO_4 concentration, which is shown in Figure 5. Such a plot directly comparing the fingerprint parameter with total concentration enables interpretation of dilution effects. For any sampling location, the position of its plotted points may only be produced by mixing two (or more) other sampling locations that bound it. In other words, the cluster of points corresponding to MA-1 may be produced by mixing of the (water chemistry) clusters that are on either side of it. MA-1 chemistry can be produced by mixing P2/H6-226 and west pit water (either P1, H6-224, or the West Pit) or DGW-1R. While similar to MA-1 in SO_4/Cl fingerprint, W-E-1 has lower sulfate. This suggests that there is no flow path from the West Pit to MA-1 that travels north of P2 and H6-226. Note that West Pit points plot in Figure 5 as a basically horizontal line, illustrating changes in total composition with a constant fingerprint. This is consistent with evaporation that does not involve significant, if any, mineral precipitation. This flattening effect is not observed at MA-1, suggesting a lack of connectivity between MA-1 and the West Pit.

Figure 5. Sulfate/Chloride as a function of sulfate concentration.

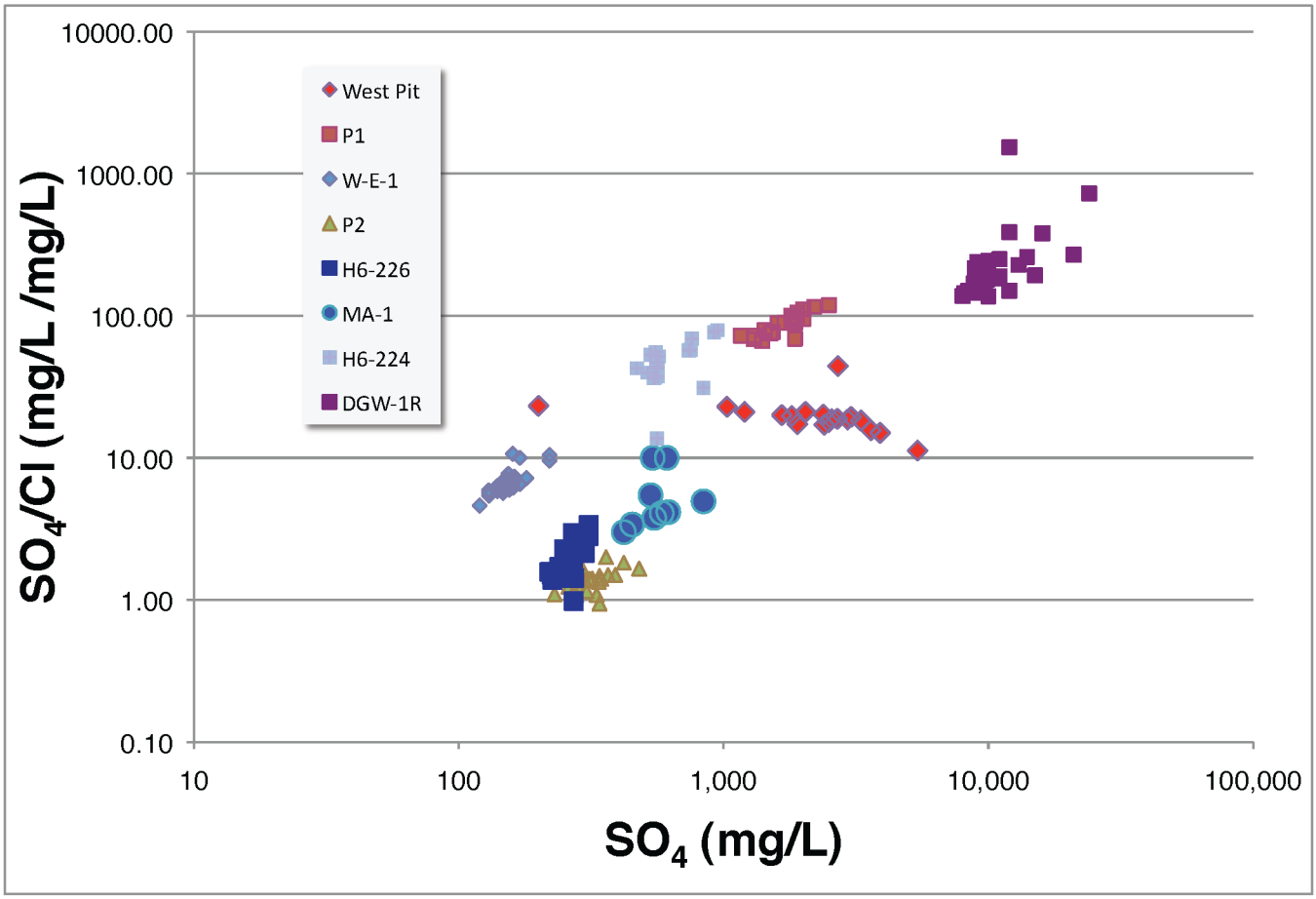

Evaporation does not appear to account for observations at MA-1. Although the MA-1 point cluster can be reproduced using either West Pit water or DGW-1R water to mix with intermediate water (like P2), Figure 4 illustrates that the SO_4/Cl ratio at points between West Pit and MA-1 drops below that of MA-1, and from Figure 5 it can be seen that the sulfate concentration does as well. Thus, another input of water (e.g. DGW-1R) would be required to boost these parameters at mid-point locations to values associated with MA-1. The higher SO_4/Cl ratio at seep MA-1 relative to P2 cannot be reproduced by evaporation alone. If a water is evaporated (for example the West Pit sump), the resulting water chemistry would shift horizontally with SO_4/Cl ratio, not increase, as both sulfate and chloride would concentrate proportionally and the ratio would not be expected to increase.

The relative proportions of P2 type water and DGW-1R water required to produce something that looks like MA-1 can be estimated using a mixing model. The mixing model simply calculates the concentrations of sulfate and chloride for a range of mixing proportions between two waters. The SO_4/Cl ratio is then calculated and plotted versus sulfate. Figure 6 illustrates the result of calculations of mixing DGW-1R water with P2 water. The black line in Figure 6 is the binary mixing of P2 type water and DGW-1R water, and the points along the line are in 10% mixing increments. MA-1 data points lie at a position along this line that correspond to a mixing proportion of about 95% P2 water and 5% DGW-1R water. A similar calculation (Figure 7) indicates that water from P1 must be mixed 30% to 70% P2 to achieve the same effect as 5% DGW-1R. However, given the above analysis (see dip in SO_4/Cl ratio in Figure 4) this magnitude of mixing seems improbable.

Figure 6. Simple mining model for combination of P2 water and DGW-1R water.

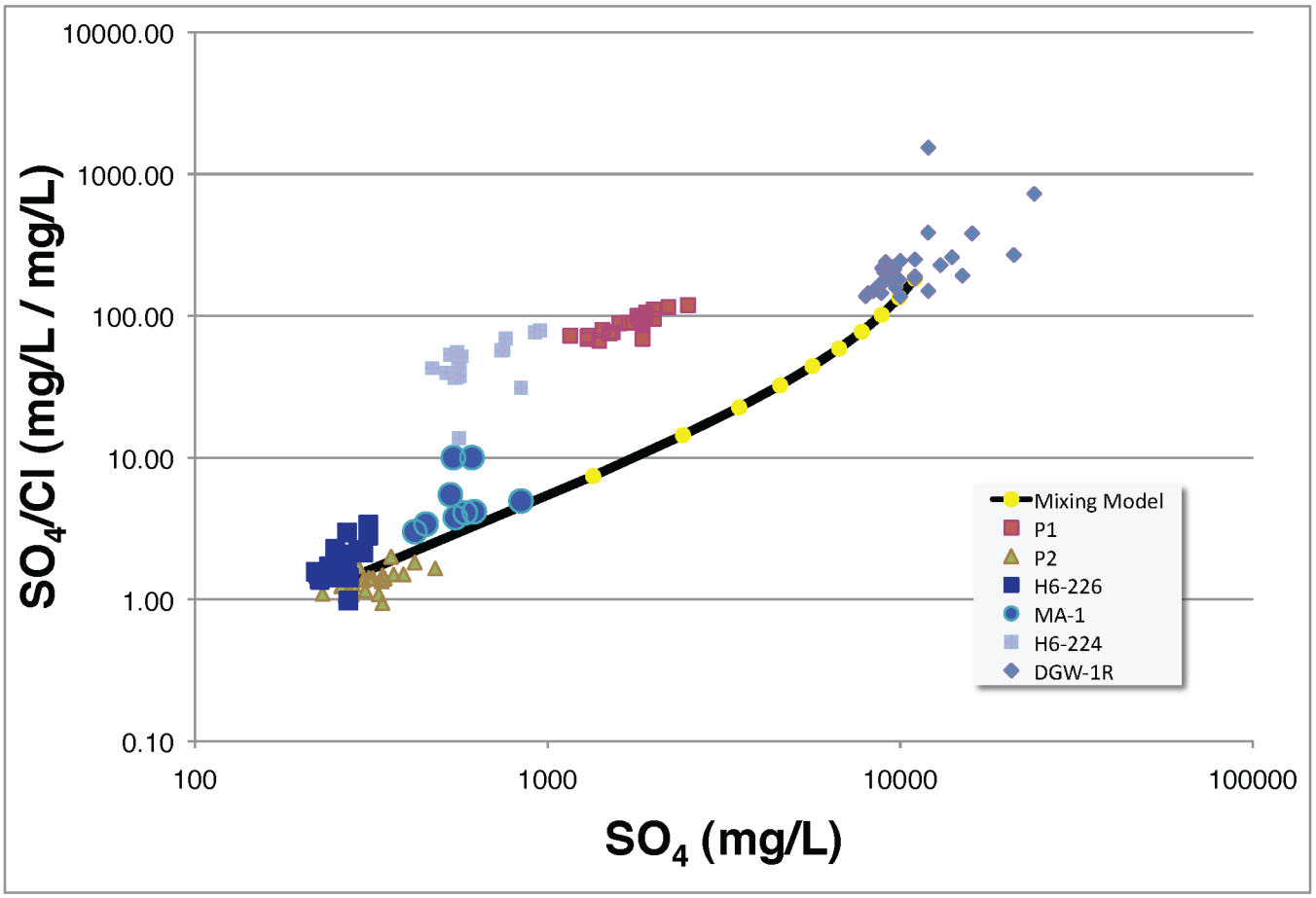

Figure 7. Simple mining model for combination of P2 water and west pit (P1) water.

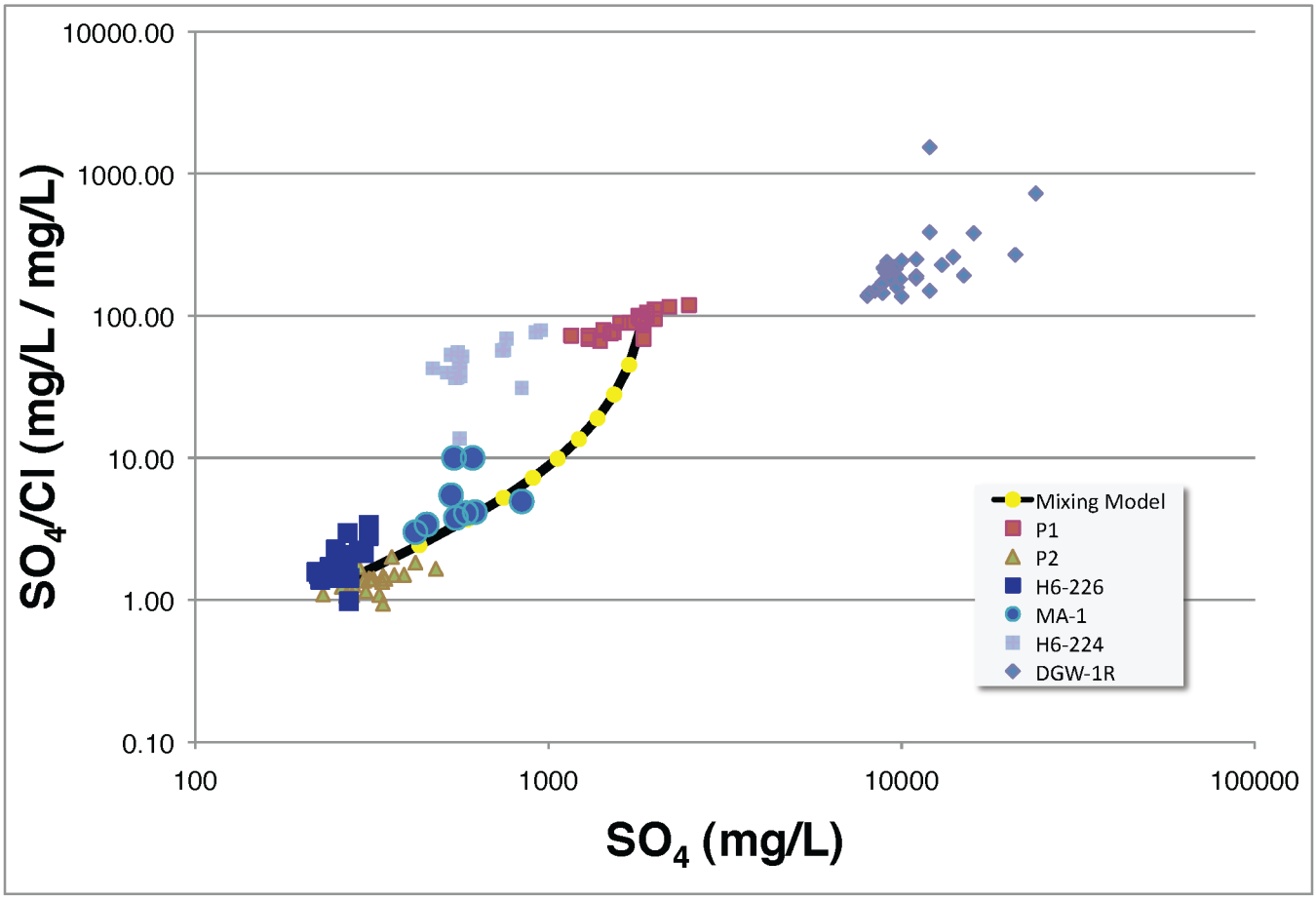

References

Montgomery (2010) Hydrogeologic Monitoring January-December 2009 Hollister Mine Area Elko County, Nevada. Report from Montgomery & Associates to Rodeo Creek Gold, Inc., March 31, 2010.